Editorial

I am glad to be of service to our Academy as well as to the international astronomical community by chairing the Editorial Board of the *Journal of Astrophysics and Astronomy*. With the cooperation of authors, referees and readers, I am confident that the Journal would advance along its intended path of progress. I take this opportunity to make an appeal to the astronomers and astrophysicists over the world for their continued support to the Journal.

J. C. Bhattacharyya
Chairman
Editorial Board

J. Astrophys. Astr. (1988) **9,** 1–5

Thermal-Convective Instability of a Composite Rotating Plasma in a Stellar Atmosphere with Finite Larmor Radius

K. C. Sharma *Department of Mathematics, Himachal Pradesh University, Shimla 171005*

Received 1987 May 28; accepted 1987 November 28

Abstract. Thermal-convective instability of a hydromagnetic, composite, rotating, inviscid and infinitely conducting plasma in a stellar atmosphere has been studied in the presence of finite Larmor radius. It is found that the criterion for monotonic instability holds good in the presence of the effects due to rotation and finite Larmor radius.

Key words: Stellar atmosphere—convective instability, composite plasma

1. Introduction

The instability in which motions of a thermally unstable atmosphere are driven by buoyancy forces, has been termed as 'thermal convective instability'. Defouw (1970) has generalized the Schwarzschild criterion for convection to include departures from adiabatic motion and has shown that a thermally unstable atmosphere is also convectively unstable, irrespective of the atmospheric temperature gradient. He has found that an inviscid stellar atmosphere is unstable if

$$D = \frac{1}{C_p}(L_T - \rho\alpha L_\rho) + \kappa k^2 < 0, \tag{1}$$

where L is the heat-loss function and α, κ, k, L_T, L_ρ denote, respectively, the coefficient of thermal expansion, the coefficient of thermometric conductivity, the wave number of perturbation, the partial derivative of L with respect to temperature T and the partial derivative of L with respect to density ρ, both evaluated in the equilibrium state. C_p is the specific heat at constant pressure.

The effects of uniform rotation and a uniform magnetic field on thermal convective instability of a stellar atmosphere have been studied by Defouw (1970) and independently by Bhatia (1971), Sharma & Prakash (1977) have studied the finite Larmor radius effect on thermal convective instability of a stellar atmosphere. It has been found in the above studies that inequality (1) is a sufficient condition for monotonic instability, for situations of astrophysical interest. In the above studies, a fully ionized plasma has been considered. Quite frequently the plasma is not fully ionized and may, instead, be permeated with neutral atoms. As a reasonably simple approximation the plasma may be idealized as a mixture of a hydromagnetic (ionized) component and a neutral component, the two interacting through mutual collisional effects. Recently, Sharma (1986) has studied the thermal convective instabiity of a composite plasma in a stellar atmosphere with Hall currents.

It may, therefore, be of importance and is the objective of the present paper to study the result of simultaneous inclusion of finite Larmor radius and collisional effects on the thermal convective instability of a composite, inviscid and infinitely conducting plasma in a stellar atmosphere. The effect of a uniform rotation has also been included.

2. Perturbation equations

Here we consider an infinite horizontal composite layer consisting of an inviscid and infinitely conducting, hydromagnetic, incompressible fluid layer of denisty ρ and a neutral gas of density ρ_d, which is in a state of uniform rotation $\mathbf{\Omega} = (0,0, \Omega)$ acted on by a vertical magnetic field $\mathbf{H} = (0, 0, H)$ and gravity force $\mathbf{g} = (0,0, -g)$. This layer is heated from below such that a steady temperature gradient $\beta(= |dT / dz|)$ is maintained. Regarding the model under consideration we assume that both the ionized fluid and the netural gas behave like continuum fluids and that the effects on the neutral component resulting from the presence of gravity and pressure are neglected which is justified in the present context (Hans 1968). The magnetic field interacts with the ionized components only. It is to be noted that in a rotating star which contains a magnetic field, both the axis of rotation and the direction of the magnetic field will differ from that of gravity at an arbitrary point on the star's surface and thus the present investigation may be regarded as a special case of the more general, real, physical situation.

The linearized equations governing the motion of the mixture of the hydromagnetic fluid and a neutral gas are:

$$\rho \frac{\partial \mathbf{u}}{\partial t} = -\nabla \delta p + \frac{1}{4\pi}(\nabla \times \mathbf{h}) \times \mathbf{H} + \mathbf{g}\delta\rho + 2\rho(\mathbf{u} \times \mathbf{\Omega}) + \rho_d v_c(\mathbf{u}_d - \mathbf{u}), \tag{2}$$

$$\frac{\partial \mathbf{u}_d}{\partial t} = -v_c(\mathbf{u}_d - \mathbf{u}), \tag{3}$$

$$\frac{\partial \mathbf{h}}{\partial t} = (H \cdot \nabla) \cdot \mathbf{u}, \tag{4}$$

$$\nabla \cdot \mathbf{u} = 0, \qquad \nabla \cdot \mathbf{h} = 0, \tag{5}$$

Where $\mathbf{u}(u, v, w)$,$\mathbf{h}(h_x, h_y, h_z)$, $\delta\rho$ and $\delta\rho$ denote the perturbations in velocity, magnetic field $\mathbf{H}$, density ρ, and pressure p, respectively; $\mathbf{g}$, u_d, u denote respectively the gravitational acceleration, the velocity of the neutral gas and the collisional frequency between the two components of the composite medium.

For the vertical magnetic field $\mathbf{H}(0, 0, H)$ the stress tensor components $\vec{\vec{\mathbf{P}}}$ taking into account the finite-ion gyration, have the components

$$P_{xx} = -\rho\nu_0\left(\frac{\partial u}{\partial y} + \frac{\partial v}{\partial x}\right), \quad P_{xy} = P_{yx} = \rho\nu_0\left(\frac{\partial u}{\partial x} - \frac{\partial v}{\partial y}\right),$$

$$P_{xz} = P_{zx} = -2\rho\nu_0\left(\frac{\partial v}{\partial z} + \frac{\partial w}{\partial y}\right), \quad P_{yy} = \rho\nu_0\left(\frac{\partial u}{\partial y} + \frac{\partial v}{\partial x}\right),$$

$$P_{yz} = P_{zy} = 2\rho\nu_0\left(\frac{\partial w}{\partial x} + \frac{\partial u}{\partial z}\right), \quad P_{zz} = 0. \tag{6}$$

In Equation (6), $\rho v_0 = NT / 4\omega_H$, where ω_H, is the ion-gyration frequency, while N and T denote, respectively, the number density and the ion temperature.

The first law of thermodynamics may be written as

$$C_v \frac{\mathrm{d}T}{\mathrm{d}t} = -L + \frac{K}{\rho}\nabla^2 T + \frac{p}{\rho^2}\frac{\mathrm{d}\rho}{\mathrm{d}t}, \tag{7}$$

where C_v, K, T, and t denote respectively, the specific heat at constant volume, the thermal conductivity, the temperature, and time.

Following Defouw (1970), the linearized perturbation form of Equation (7) is:

$$\frac{\partial\theta}{\partial t} + \frac{1}{C_p}(L_T - \rho\alpha L_\rho)\theta - \kappa\nabla^2\theta = -\left(\beta + \frac{g}{C_p}\right)w, \tag{8}$$

where θ is the perturbation in temperature. In obtaining (8), use has been made of the Boussinesq equation of state

$$\delta\rho = -\alpha\rho\theta. \tag{9}$$

We consider the case in which both the boundaries are free and the medium adjoining the fluid is non-conducting. The case of two free boundaries is the most appropriate for stellar atmosphere (Spiegel 1965). The boundary conditions appropriate for the problem (*cf.* Chandrasekhar 1961) are

$$w = 0, \quad \theta = 0, \quad \frac{\partial^2 w}{\partial z^2} = 0, \quad \frac{\partial\zeta}{\partial z} = 0, \tag{10}$$

$\xi = 0$ and h_x, h_y, h_z are continuous with an external vacuum field. If the fluid is bounded by an infinitely conducting boundary, no disturbance within it can change the electromagnetic quantities outside. Hence, we have

$$h_z = 0 \tag{11}$$

at a surface bounded by an ideal conductor and, if we further assume that there are no surface charges or surface currents, we may as well take

$$D\xi = 0. \tag{12}$$

The symbols ζ and ξ denote the z-component of vorticity and current density, respectively.

3. Dispersion relation and discussion

Analyzing in terms of normal modes, we seek solutions whose dependence on space and time coordinates is of the form

$$\exp(ik_x x + ik_y y + nt)\sin k_z z, \tag{13}$$

where k_z is an integral multiple of π divided by the thickness of the fluid layer, $k = (k_x^2 + k_y^2 + k_z^2)^{1/2}$ is the wave number of the perturbation and n is the growth rate.

Eliminating u_d between Equations (2) and (3), Equations (8) and (2)–(5) give

$$n'\nabla^2 w = g\alpha\left(\frac{\partial^2\theta}{\partial x^2}+\frac{\partial^2\theta}{\partial y^2}\right)+\frac{H}{4\pi\rho}\frac{\partial}{\partial z}\nabla^2 h_z - 2\Omega\frac{\partial\zeta}{\partial z}+\nu_0\left(\nabla^2-3\frac{\partial^2}{\partial z^2}\right)\frac{\partial\zeta}{\partial z}, \tag{14}$$

$$n'\zeta = \frac{H}{4\pi\rho}\frac{\partial\xi}{\partial z}+2\Omega\frac{\partial w}{\partial z}-\nu_0\left(\nabla^2-3\frac{\partial^2}{\partial z^2}\right)\frac{\partial w}{\partial z}, \tag{15}$$

$$nh_z = H\frac{\partial w}{\partial z}, \tag{16}$$

$$n\xi = H\frac{\partial\zeta}{\partial z}, \tag{17}$$

$$(n+D)\theta = -\left(\beta+\frac{g}{C_p}\right)w, \tag{18}$$

where

$$n' = n\left(1+\frac{\alpha_0\nu_c}{n+\nu_c}\right) \quad \text{and} \quad \alpha_0 = \frac{\rho_d}{\rho}. \tag{19}$$

Eliminating θ, ζ, ξ and h_z from Equations (14)–(18) and using (13), we obtain the dispersion relation in the form

$$n^7 + A_6 n^6 + A_5 n^5 + A_4 n^4 + A_3 n^3 + A_2 n^2 + A_1 n + A_0 = 0, \tag{20}$$

where

$$A_6 = D + 2\nu_c(1+\alpha_0),$$

$$A_5 = 2V_A^2 k_z^2 + 2D\nu_c(1+\alpha_0) + \nu_c^2(1+\alpha_0)^2 + \Gamma\left(\beta+\frac{g}{C_p}\right)+E,$$

$$A_4 = 2V_A^2 k_z^2\{\nu_c(1+\alpha_0)+D+\nu_c\} + D\nu_c^2(1+\alpha_0) + E(D+2\nu_c) + \Gamma\left(\beta+\frac{g}{C_p}\right)\nu_c(2+\alpha_0),$$

$$A_3 = 2V_A^2 k_z^2 D\nu_c + 2\nu_c(1+\alpha_0)V_A^2 k_z^2 D + \nu_c^2(1+\alpha_0)V_A^2 k_z^2 + (V_A^2 k_z^2) + E(2D+\nu_c) + \Gamma\left(\beta+\frac{g}{C_p}\right)\{V_A^2 k_z^2 + \nu_c^2(1+\alpha_0)\},$$

$$A_2 = \nu_c^2(1+\alpha_0)V_A^2 k_z^2 D + (V_A^2 k_z^2)^2(D+2\nu_c) + ED\nu_c^2 + 2\Gamma\left(\beta+\frac{g}{C_p}\right) + V_A^2 k_z^2 \nu_c,$$

$$A_1 = (V_A^2 k_z^2)^2 \nu_c(2D+\nu_c) + \Gamma\left(\beta+\frac{g}{C_p}\right)V_A^2 k_z^2 \nu_c,$$

$$A_0 = (V_A^2 k_z^2)^2 \nu_c^2 D,$$

and

$$\Gamma = \frac{g\alpha(k_x^2+k_y^2)}{k^2}, \quad V_A^2 = \frac{H^2}{4\pi\rho}, \quad E = \frac{k_z^2}{k^2}\{2\Omega+\nu_c(k^2-3k_z^2)\}^2.$$

When $D < 0$, i.e., the inequality (1) is satisfied, the constant term in Equation (20) is negative. This means that Equation (20) has a positive real root leading to monotonic instability. The criterion for instability (1) is, thus, the same in the presence of finite Larmor radius on the thermal convective instabiliity of a composite rotating plasma in a steller atmosphere.

References

Bhatia, P. K. 1971, *Publ. astr. Soc. Japan,* **23**, 181.
Chandrasekhar, S. 1961, *Hydrodynamic and Hydromagnetic Stability*, Clarendon Press, Oxford, p. 162.
Defouw, R. J. 1970, *Astrophys. J.*, **160,** 659.
Hans, H. K. 1968, *Nucl. Fusion,* **8**, 89.
Sharma, K. C. 1986, *Astrophys. Space Sci.,* **125,** 299.
Sharma, R. G, Prakash, K. 1977, *Acta Phys. Hungarica*, **42**, 103.
Spiegel, E. A. 1965, *Astrophys. J.,* **141,** 1068.

J. Astrophys. Astr. (1988) **9,** 7–15

Constraints on the ^{176}Lu Cosmochronometer

J. R. De Laeter *Department of Applied Physics, Curtin University of Technology, Perth, Western Australia, 6001 Australia*
B. J. Allen, G. C. Lowenthal & J. W. Boldeman *Australian Atomic Energy Commission Research Establishment, Lucas Heights, New South Wales, 2232 Australia*

Received 1987 July 15; accepted 1987 December 12

Abstract. In an endeavour to resolve reported discrepancies in the value of the branching ratio of ^{176}Lu at astrophysical energies, a new determineation of the ^{175}Lu ($n\gamma$) ^{176m}Lu capture cross section has been measured as 958 ± 58 mb. This gives a value of the branching ratio of 0.21 ±0.05. This result indicates that some reequilibration of the ground and isomeric states of ^{176}Lu occurs in stellar environments undergoing *s*-process nucleosynthesis, and confirms that ^{176}Lu is not a reliable cosmochronometer. However the very existence of ^{176}Lu in the solar system implies that the ground state of ^{176}Lu was not completely depopulated, and provides the possibility of using this nuclide as a sensitive thermometer for stellar processes.

Key words: *s*-process nucleosynthesis—^{176}Lu cosmochronometer—branching ratio—nuclear reactions

1. Introduction

Neutron capture processes play an important role in astrophysics. The major processes involved in heavy element nucleosynthesis are the slow (*s*) and rapid (*r*) neutron capture processes (Burbidge *et al.* 1957), although the proton (*p*) capture process also plays a role. The site of *s*-process nucleosynthesis is believed to be the red giant phase of stars at temperatures of 2–4 × 10^8 **K**, corresponding to a Maxwellian temperature kT=30 keV. The nuclei are synthesized in a weak neutron flux over a relatively long period of time so that β-decay can occur between successive neutron captures. The *r*-process follows a path on the neutron-rich side of the valley of β-stability, successive neutron captures occurring before the resulting nuclide β-decays.

Of particular significance is the branch in the *s*-process path at ^{176}Lu, because this nuclide is one of the few naturally-occurring radioactive species that has survived from the period of galactic nucleosynthesis. Audouze, Fowler & Schramm (1972) and Arnould (1973) independently suggested that ^{176}Lu could be developed as a cosmochronometer, because the ground state β-decays to ^{176}Hf with a half-life of 3.57 × 10^{10} y. This unique s-process chronometer is therefore of potential value in determining the mean age of nucleosynthesis.

Figure 1 shows the mass region in the vicinity of lutetium, together with the neutron capture and proton capture processes involved in synthesising the various nuclides.

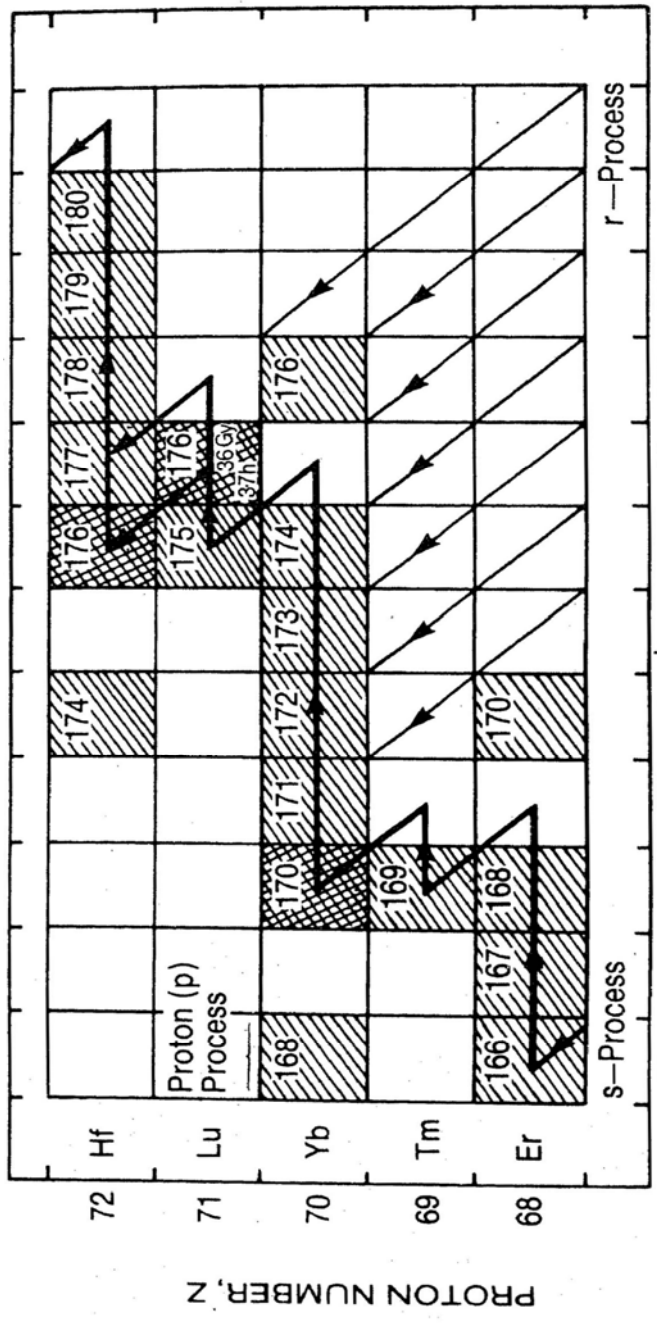

Figure 1. *s*-process path in the rare earth element mass region. *s*-only process nuclides ^{170}Yb, ^{176}Lu and ^{176}Hf are shielded from *r*-process contributions by ^{170}Er and ^{176}Yb respectively. The *s*-process branches at ^{176}Lu if a significant population of the 3.68 h isomeric state occurs.

^{176}Lu and ^{176}Hf are shielded from the r-process by the isobaric nuclide ^{176}Yb and are shown as cross-hatched squares in Fig. 1. The other numbered squares represent stable isotopes. The Lu/Hf chronometer provides the opportunity of using the well-established s-process systematics to determine the production ratios, rather than having to rely on theoretical models, as is the case for *r*-process cosmochronometers. The advantages of the ^{176}Lu chronometer have been discussed by McCulloch, De Laeter & Rosman (1976) and Beer *et al.* (1981).

2. The ^{176}Lu chronometer

Schramm & Wasserburg (1970) developed a nucleochronological formalism for long-lived radionuclides which enables the mean age of nucleosynthesis Δ^{max}, to be determined. Thus a long-lived nuclide, such as ^{176}Lu, is independent of the model of galactic evolution, since it effectively integrates any short-term irregularities which may occur.

The ^{176}Lu chronometer is complicated in that the first excited state of the nucleus is a $J^{\pi} = l^{-}$ level at 127 keV. This isomeric state ^{176m}Lu, β^{-} decays to ^{176}Hf with a half-life of 3.68 h. Thus it is necessary to measure the branching ratio B which is defined as

$$B = \frac{\langle \sigma^{g}_{175} \rangle}{\langle \sigma_{175} \rangle} = 1 - \frac{\langle \sigma^{m}_{175} \rangle}{\langle \sigma_{175} \rangle} = 1 - B^{m} \tag{1}$$

where $\langle \sigma^{g}_{175} \rangle$ and $\langle \sigma^{m}_{175} \rangle$ are the 30keV ^{175}Lu ($n\gamma$) cross-sections to ^{176g} Lu and ^{176m}Lu respectively, and $\langle \sigma_{175} \rangle$ is the total 30 keV cross-section for ^{175}Lu ($n\gamma$) ^{176}Lu. These cross-sections can be measured by irradiating Lu in a neutron flux obtained from the ^{7}Li (p, n) reaction for proton energies just above the reaction threshold.

Figure 2 shows the ^{176}Lu-^{176}Hf decay scheme. Neutron capture on ^{175}Lu leads to the population of two states—the ground state ^{176g}Lu which decays to ^{176}Hf with a long half-life, and the 127 keV isomeric state ^{176m}Lu which decays with a half-life of 3.68 h.

The branching ratio can be determined by measuring $\langle \sigma^{m}_{175} \rangle$ and $\langle \sigma_{175} \rangle$ using neutrons covering an energy spectrum approximating that which would be found in red giant stars. Beer & Käppeler (1980) measured the capture cross-section of ^{175}Lu to the isomeric state in ^{176}Lu to be 809 ± 49 mb. In conjunction with the value Of $\langle \sigma_{175} \rangle$ of 1411 ± 170 mb measured by Macklin & Gibbons (1967), this gave a branching ratio B =0.43 ±0.05. Allen, Lowenthal &De Laeter (1981) independently reported a value for B = 0.21 ±0.04 based on a measurement of 111 1 ± 64mb for $\langle \sigma^{m}_{175} \rangle$.

A number of new determinations of $\langle \sigma_{175} \rangle$ have now been made. Beer *et al.* (1981) obtained a value of 1266 ± 43 mb, and subsequently Beer *et al.* (1984) reported values of 1206 ± 54 mb and 1179 ± 44 mb which were determined at the Oak Ridge linear accelerator (ORELA) and the Karlsruhe 3MV pulsed Van de Graaf accelerator respectively. Since all three measurements agree within experimental errors, a mean value of 1217 mb can be adopted as the best value for $\langle \sigma_{175} \rangle$. This value is in good agreement with earlier determinations of 1240 ± 190 mb (Lepine, Douglas & Maia 1972) and 1208 ± 60 mb (Macklin, Drake & Malanify 1978). If the revised value of 1217 mb is used to calculate B, values of 0.34 ± 0.04 and 0.08 ±0.03 would be derived from the $\langle \sigma^{m}_{175} \rangle$ values of Beer & Käppeler (1980), and Allen, Lowenthal & De Laeter (1981) respectively.

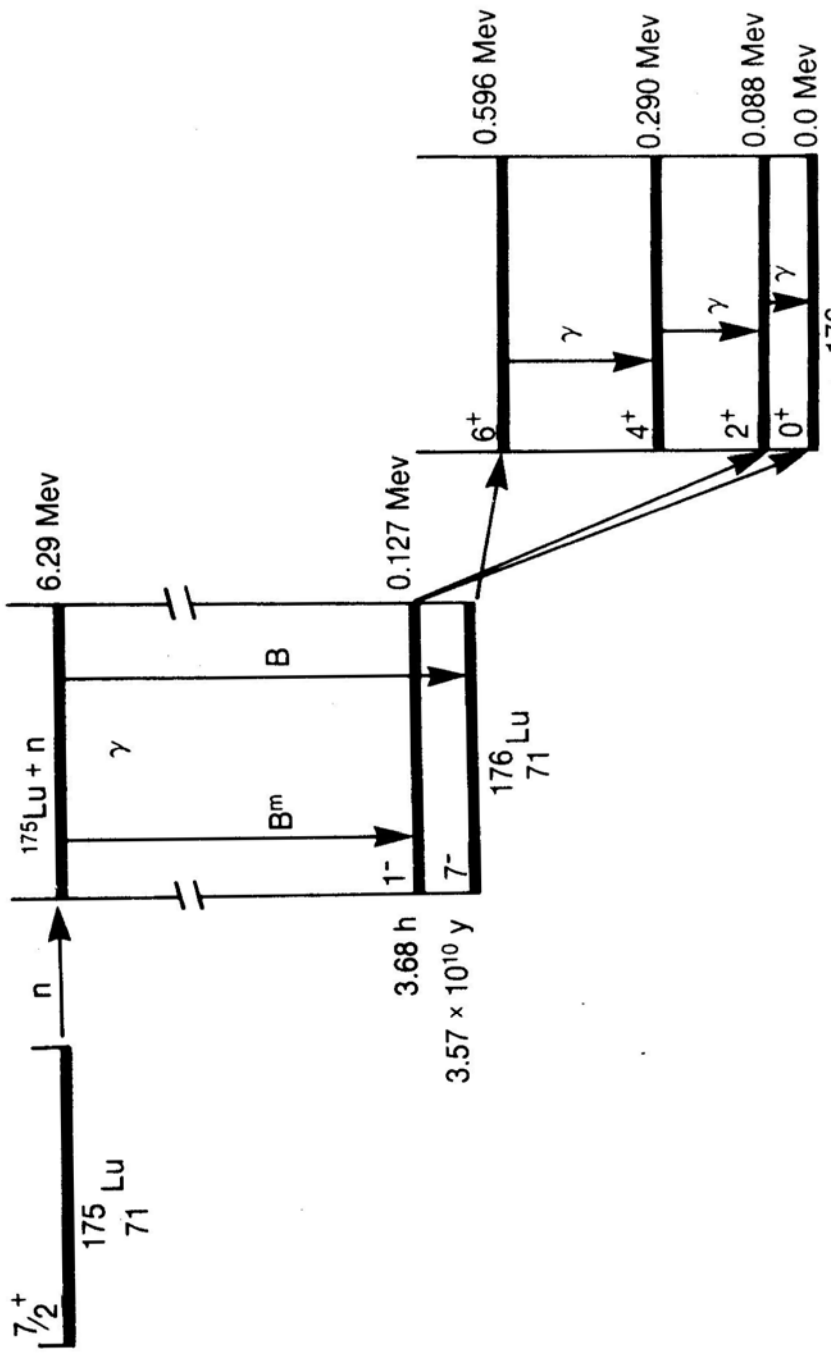

Figure 2. Decay scheme for neutron capture on ^{175}Lu. The isomeric branching ratio B^m is determined by measuring the 88 keV γ yield from ^{176}Hf.

In an endeavour to resolve the discrepancy between these two values for B, we have repeated our measurement of $\langle \sigma^{m}_{175} \rangle$. In the original experiment a Lu_2O_3 powder was used. The powder was enclosed in thin aluminium foil, interleaved with gold foil and the Lu_2O_3/Au sandwich enclosed in a tight-fitting cadmium container to eliminate thermal neutrons. Although care was taken to ensure that the neutron exposures were as uniform as possible, X-ray analyses of the powder sources showed some evidence of aggregation and voiding.

Although essentially the same procedures were used in this experiment as those described by Allen, Lowenthal & De Laeter (1981), Lu metal foil replaced the Lu_2O_3 powder. The Lu/Au sandwich was irradiated in a neutron flux with an energy range up to 105 keV, produced by the Li(*p*, *n)* reaction in the Australian Atomic Energy Commission's 3MV accelerator. The 12.7 mm diameter, 25–60 mg cm $^{-2}$ gold foils were counted in a 4π, β-γ coincidence chamber. The 88 keV γ rays from the ^{176m}Lu activation were measured in a well-calibrated Ge(Li) spectrometer at source-detector distances of 4.5 cm and 9.5 cm. Correction factors and uncertainties are the same as those reported by Allen, Lowenthal & De Laeter (1981). Four separate irradiations were made at a proton energy of 25 keV above the Li(*p*, *n)* threshold. The flux-weighted ratio of the Lu isomer and Au capture cross-sections was found to be $\langle \sigma^{m}_{175} \rangle / \langle \sigma_{197} \rangle = 1.654 \pm 0.076$. A preliminary report of this result was given by Allen *et al.* (1981).

Using the data of Macklin, Halperin & Winters (1975) for the 30 keV Maxwellian average cross section (E_n=0.5–300 keV) of $\langle \sigma_{197} \rangle_{kT=30}$ =624 ± 25mb, the average cross-section at 30±10keV is 579 ± 23 mb. The isomeric cross-section $\langle \sigma^{m}_{175} \rangle_{kT = 30 \pm 10}$ can be calculated to be 958 ±58 mb and the branching ratio is therefore B = 0.21 ±0.05 (using the revised value of 1217 mb for $\langle \sigma_{175} \rangle$). This value is in much closer agreement with the corresponding value of 0.34 ± 0.04 derived from the work of Beer & Käppeler (1980), than our previous value.

Audouze, Fowler & Schramm (1972) derived a simple formalism for determining the mean age of nucleosynthesis Δ^{max}, which can be expressed as

$$\Delta^{max} = \frac{1}{\lambda_{176}} \ln \left[\frac{B \langle N_s \sigma \rangle_{176}}{N_{176} \langle \sigma_{176} \rangle} \right] \qquad (2)$$

where λ_{176} is the decay constant of ^{176}Lu; $\langle N_s \sigma \rangle_{176}$ is the average value of the product of *s*-process abundance and 30 keV average capture cross-section evaluated at mass 176; N_{176} is the abundance of ^{176}Lu at the time of formation of the solar system; $\langle \sigma_{176} \rangle$ is the 30 keV ^{176}Lu ($n\gamma$) ^{177}Lu cross section and B is the branching ratio.

One of the characteristic features of *s*-process systematics is that the product of the abundances of the sonly process nuclides (N_s) and their corresponding capture cross-sections measured at astrophysical energies $\langle \sigma \rangle$ ισ a smooth, slowly varying function of mass number *A,* except for those regions where closed shell effects are dominant (Clayton *et al.* 1961). ^{176}Lu is not in a region of this curve where nuclear shell effects occur, and experimental measurements have confirmed that the 'local approximation' $N_s\sigma$= constant, is valid over a limited mass region (Allen, Gibbons & Macklin 1971).

The data base for the distribution curve has been continually refined. New abundance data by Anders & Ebihara (1982) and Beer *et al.* (1984), and new capture cross-sections by Käppeler *et al.* (1982) have shown that the empirical data is in excellent

agreement with the traditional theoretical model, which assumes a steady neutron flux and an exponential distribution of neutron irradiations. Thus it is possible to estimate a value for $\langle N_s\sigma\rangle_{176}$, based on the assumption that in this region $N_s\sigma$ is a smooth, nearly constant function of mass number.

The values necessary to calculate the mean age of nucleosynthesis using Equation (2), are given in Table 1. A number of determinations for λ_{176}, N_{176} and $\langle\sigma_{176}\rangle$ have been reported, and these parameters no longer represent a limitation in calculating Δ^{max}, although their accuracy needs to be determined to about 1 per cent if a reliable age is to be achieved.

If the value of $B = 0.34$ is used, a mean age of 7.6×10^9 y is derived. On the other hand if $B = 0.21$ is used, the logarithmic term is < 1 and Δ^{max} cannot be calculated. It is therefore apparent that the limiting parameter in obtaining a good assessment of Δ^{max} is the branching ratio.

The essential difference between the values of the branching ratio between this work and that of Beer & Käppeler (1980) arises from the experimental ratio of the energy-averaged neutron capture cross-sections of ^{175m}Lu and ^{197}Au. Other factors relating to the choice of cross-section values and treatment of the neutron energy spectrum may differ, but are not the source of the disagreement. The cross-section ratio is

$$\frac{\langle\sigma_{175m}\rangle}{\langle\sigma_{197}\rangle} = \frac{k_{176m}}{k_{198}} \cdot \frac{n_{197}}{n_{175}}$$

where k and n are expressed per mg of target material in the area defined by the gold foil, and k is the end point abundance of the product nuclei. Our value for this ratio is 1.654±0.076, where the error represents the standard deviation of four separate measurements. Both the Karlsruhe measurements and those at Lucas Heights were measured at $E_p = 25$ keV above threshold. The difference between the two results may be in foil composition, detector calibrations or thickness corrections, but in the light of

Table 1. Parameters relevant to the ^{176}Lu chronometer.

Parameter	Value	Reference
$\langle\sigma^m_{175}\rangle$	809 ± 49 mb	Beer & Käppeler (1980)
	958 ± 58 mb	This work
$\langle\sigma_{175}\rangle$	1266 ± 43 mb	Beer *et al.* (1981)
	1206 ± 54 mb	Beer *et al.* (1984)
	1179 ± 44 mb	Beer *et al.* (1984)
	mean = 1217 mb	
B	0.34 ± 0.04 mb	Beer & Käppeler (1980)
	0.21 ± 0.05 mb	This work
λ_{176}	1.94×10^{-11} y^{-1}	Patchett (1983)
$\langle N_s\sigma\rangle_{176}$	5.47 mb (Si = 10^6 atoms)	Beer (1983)
N_{176}	0.00106	Anders & Ebihara (1982)
$\langle\sigma_{176}\rangle$	1526 ± 69 mb	Beer *et al.* (1984)
	1514 ± 56 mb	Beer *et al.* (1984)
	mean = 1520 mb	

the discrepancy and the importance of the measurement to astrophysics, we would urge that another independent determination of the branching ratio of ^{176}Lu be undertaken as soon as possible.

3. Discussion

Allen, Lowenthal & De Laeter (1981) concluded that the negative value derived for the mean age of nucleosynthesis for ^{176}Lu could be explained on the basis that thermal equilibrium of the ground and isomeric states occurs in stellar interiors on a timescale less than the 3.68 h half-life of ^{176m}Lu. The application of the Schramm-Wasserburg formalism to ^{176}Lu assumes that the observed *s*-process branch at ^{176}Lu is determined solely by the isomeric branching ratio B^m. Allen, Lowenthal & De Laeter (1981) discussed a number of possible mechanisms to explain why this assumption must be invalid.

Clayton (1963, personal communication) was the first to suggest that thermalization of the ^{176}Lu ground and isomeric state populations may occur in the stellar environment. The effective half-life of ^{176}Lu is obtained from the Boltzman equation and reduces to

$$t_{-} = t_{1/2}\left[\frac{2J_0+1}{2J_1+1}\right]\exp\left[\frac{E_1-E_0}{kT}\right] = 0.14 \text{ y} \tag{3}$$

for J_0 = 7, J_1 = 1, E_1 = 127 keV, $t_{1/2}$ = 3.68 h and kT=30 keV. The changed half-life results from the weak population of the isomeric state (0.3 per cent at 30 keV) in thermal equilibrium with the stellar environment.

The branching ratio for β^- decay from ^{176}Lu depends on the effective β^- half-life and the neutron flux. The observed branching ratio (f_{-}) is obtained from the *s*-process local approximation model and can be defined as

$$f_{-} = 1 - \frac{N_{176}\langle\sigma_{176}\rangle}{\langle N_s\sigma\rangle_{176}} = 0.69 \pm 0.07. \tag{4}$$

This value is less than our isomeric branching ratio B^m of 0.79 ± 0.09. Consequently, the population of the isomeric state must be reduced significantly in less than 3.68 h to reduce the isomeric decay rate. It is unlikely that this effect could be achieved directly by photo-de-excitation (ΔJ = 6), but photon inelastic scattering and Coulomb excitation processes could establish thermal equilibrium by electromagnetic linkage to higher excited states.

Shaw & Clayton (1967) examined the effect of particle-induced electromagnetic de-excitation of nuclei in stellar matter, whilst Ward (1981) found that enhanced decay rates could occur from Coulomb collisions with the ion plasma in the stellar environment. From analytic approximations the resulting de-excitation rates are strongly dependent on the mass and charge numbers of the target and projectile, stellar temperature, multipole order and type, and energy of the transition. For ^{176}Lu, Ward (1981) estimates that enhancement could occur above 4 × 10^8 K for helium burning and above 10^9 K for carbon burning. Coulomb enhancement of indirect

transitions, linked through higher-lying states, may prove to be more significant than direct transitions in determining the thermal equilibrium rate.

Watanabe, Mukoyama & Katano (1981) have examined the implications of nuclear excitation of ^{176}Lu by positron annihilation by irradiating Lu with positrons from ^{64}Cu. Characteristic 88.35 keV γ rays from ^{176m}Lu were observed, which enabled the cross-section for the annihilation-excitation process to be established at $9.0 \pm 3.2 \times 10^{-22}$ cm^2. More recently Norman *et al.* (1985) have examined the effects of photoexcitation and positron annihilation-excitation of ^{176g} Lu to ^{176m}Lu and found that these two processes alone are capable of establishing thermal equilibrium between these two states at temperatures $>3.5 \times 10^8$ K. Norman *et al.* (1985) point out that a number of other processes (such as Coulomb excitation and inelastic neutron scattering) will tend to produce equilibration at temperatures below 3.5×10^8 K.

It is therefore apparent that the final abundance of ^{176g}Lu which survives the *s*-process stellar environment will be a very sensitive function of the thermal history that it has experienced. A detailed treatment of the temperature dependence of the Lu branching ratio is given by Beer *et al.* (1981). Using theoretical estimates for the γ-decay branching ratios of a number of known energy levels these authors found evidence for the effective reduction of the ^{176}Lu half-life for thermal energies above 16keV. Consequently the ^{176}Lu chronometer can only keep time for temperatures somewhat lower than those envisaged for the *s*-process.

Allen, Lowenthal & De Laeter(1981), on the basis of competition between β^- decay and neutron capture rates, calculated that the neutron flux must be in the range 2×10^{15} to 10^{17} cm^{-2} s^{-1}. However if thermal equilibrium between the ground and isomeric state is maintained after the neutron source is exhausted, all of the ^{176}Lu will decay to ^{176}Hf in a year or so. The temperature dependence of the neutron flux and the ^{176}Lu effective half-life could then result in a 'freeze-out' of abundances on the termination of the neutron exposure. Thus the observed f - value may not result from the branching ratio B^m nor from the effects of thermal equilibrium, but from the freezing out of abundances when the *s*-process neutron exposure terminates.

4. Conclusions

Although considerable progress has been made in elucidating the various parameters involved in the ^{176}Lu chronometer since Audouze, Fowler & Schramm (1972) first proposed it as a unique *s*-process chronometer, uncertainty still exists with respect to the correct value for the branching ratio of ^{176}Lu. The value of 0.21 ± 0.05 reported in this paper is at variance with an earlier value of $0.34 + 0.04$ by Beer & Käppeler (1980), and there is therefore an urgent need for other investigators to redetermine this parameter, which is of crucial importance in deciphering the ^{176}Lu/^{176}Hf nuclear system.

The implication of the lower value for the branching ratio is that significant equilibration has occurred between the ground and isomeric states in ^{176}Lu. A survey of possible mechanisms such as particle-induced electromagnetic de-excitation, Coulomb collisions with the ion plasma, photo-excitation and positron annihilation-excitation imply that the final abundance of the ground state of ^{176}Lu which survives the *s*-process environment in stellar interiors, is a sensitive function of the thermal

history that it has experienced. Our conclusion is that although ^{176}Lu is not a reliable *s*-process cosmochronometer, it can reveal details of the dynamics of the *s*-process. However in order to delineate details of its time and temperature dependence, a more accurate measurement of the isomeric capture cross-section, and a detailed understanding of intra-nuclear excitation and decay processes are required.

Acknowledgements

This work has been supported by the Australian Research Grants Scheme and the Australian Institute of Nuclear Science and Engineering. Mrs P. R. Harris typed the manuscript with care and patience.

References

Allen, B. J., Gibbons, J. H., Macklin, R. L. 1971, *Adv. Nucl. Phys.,* **4,** 205.
Allen, B. J., Lowenthal, G. C, Boldeman, J. W., De Laeter, J. R. 1981, Proc. Fourth Int. Symp. *Neutron Capture Gamma Ray Spectroscopy and Related Topics,* Eds T. Von Egidy, F. Gonnewein & B. Maier, Inst, of Phys. Conf. Ser. No. 62, p. 573.
Allen, B. J., Lowenthal, G. C, De Laeter, J. R. 1981, *J, Phys. G*.: *Nucl. Phys.* **7,** 1271.
Anders, E., Ebihara, M. 1982, *Geochim. Cosmochim. Acta,* **46,** 2363.
Arnould, M. 1973, *Astr. Astrophys.,* **22,** 311.
Audouze, I, Fowler, W. A., Schramm, D. N. 1972, *Nature, Phys. Sci.,* **238,** 8.
Beer, H. 1983, in *Workshop über Fragen der nuklearen Astrophysik,* Mainz, October 1982.
Beer, H., Käppeler, F. 1980, *Phys. Rev.,* **C21,** 534.
Beer, H., Käppeler, F., Wisshak, K., Ward, R. A. 1981, *Astrophys. J. Suppl. Series,* **46,** 295.
Beer, H., Walter, G., Macklin, R. L., Patchett, P. J, 1984, *Phys. Rev.,* **30,** 464.
Burbidge, E. M., Burbidge, G. R., Fowler, W. A., Hoyle, F. 1957, *Rev. Mod. Phys*. **29,** 547.
Clayton, D. D., Fowler, W. A., Hull, T. E., Zimmerman, B. A. 1961, *Ann. Phys*. **12,** 331.
Käppeler, F., Beer, H., Wisshak, K., Clayton, D. D., Macklin, R. L., Ward, R. A. 1982, *Astrophys. J.* **257,** 821.
Lepine, J. R. D., Douglas, R. A., Maia, H. A. 1972, *Nucl. Phys. A,* **196,** 83.
Macklin, R. L, Drake, D. M., Malanify, J. J. 1978, LA-7470-MS.
Macklin, R. L. Gibbons, J. H. 1967, *Phys. Rev.,* **159,** 1007.
Macklin, R. L., Halperin, J., Winters, R. R. 1975, *Phys. Rev,* **C11,** 1270.
McCulloch, M. T., De Laeter, J. R., Rosman, K. J. R. 1976, *Earth Planet. Sci. Lett.,* **28,** 308.
Norman, E. B., Bertram, T., Kellogg, S. E., Gil, S., Wong, P. 1985, *Astrophys. J.,* **291,** 834.
Patchett, P. J. 1983, *Geochim. Cosmochim. Acta,* **47,** 81.
Schramm, D. N., Wasserburg, G. J. 1970, *Astrophys. J*., **162,** 57.
Shaw, P. B., Clayton, D. D. 1967, *Phys. Rev.,* **160,** 1193.
Ward, R. A. 1981, *Astr. Astrophys.* **97,** 157.
Watanabe, Y., Mukoyama, T., Katano, R. 1981, *Phys. Rev.* **C23,** 695.

J. Astrophys. Astr. (1988) **9,** 17–24

CCD Star Images: On the Determination of Moffat's PSF Shape Parameters

O. Bendinelli *Dipartimento di Astronomia, Via Zamboni 33, I-40126 Bologna, Italy*

G. Parmeggiani *Osservatorio Astronomico di Bologna, Italy*

F. Zavatti *Dipartimento di Astronomia, Via Zamboni 33, I-40126 Bologna, Italy*

Received 1987 October 28; accepted 1988 January 8

Abstract. Among the variety of empirical models of optical Point Spread Function used in the astronomical environment, only the Moffat's (1969) one is able to describe by means of two parameters (in the circular case) both the inner and the outer star image regions. In view of this very important feature, the problem of the simultaneous estimates of Moffat's PSF shape parameters, off-centring, and the background level in CCD star images has been investigated. The problem does not seem to be rigorously resolvable, but an approximate way to calculate all the parameters except off-centring is shown. It must be stressed that, the Moffat's PSF model being a softened power law belonging to the family of modified King and Hubble models, the present discussion can be of aid in many other research fields. Also, the integral equation enabling us to convolve a spherical source with Moffat's PSF is given and applied for comparison to Multi-Gaussian convolution.

Key words: point spread functions—CCD photometry

1. Introduction

It is well known that the observed intensity distribution in long-exposure star images can be described, in favourable background conditions, up to about 10 mag arcsec^{-2} below the central value by a variety of empirical smooth fitting functions. Among them, the more widely employed are the Moffat (1969) distribution, a central truncated Gaussian overlapping an exponential wing (King 1971), the Lorentzian (Franz 1973) and a sum of Gaussians (Brown 1974). The parameters of these distributions, under moderate or bad seeing conditions, are usually estimated with sufficient accuracy for most practical purposes by using standard fitting routines or graphical methods. But a serious problem arises with very good seeing conditions if the full resolution content of data is pursued. This is because neither the integration on the pixel surface nor the off-centring of the image with respect to the central pixel (*i.e.* that of local maximum intensity) can be neglected, when the seeing inner scale factor is of the order of the pixel size. In a previous paper (Bendinelli *et al.* 1987; hereafter Paper 1) all the parameters involved in the multi-Gaussian approximation of the intensity distribution in symmetrical CCD star images were simultaneously estimated. This was

done by improving the centring algorithms of Van Altena & Auer (1975) and Chiu (1977) by useful analytical properties of Gaussians and using the Newton-Gauss regularized method to secure the convergence of the iterative process leading to the estimates of parameters. The aim of this work is to look for parameters using as star image model the Moffat's (1969) distribution, which contains only 2 parameters and shows a softened decreasing power law behaviour, so that it can describe better than a sum of Gaussians the PSF wings observed by King (1971), Kormendy (1973) and Capaccioli & de Vaucouleurs (1979). A reliable method to determine these PSF wings may greatly improve the analysis of many astrophysical observations such as, for example, imaging of distant extragalactic sources, stellar photometry in crowded fields and astrometry of double stars. Also, it should be noted that the bi-dimensional extension of Moffat's distribution to represent non-circular star images contains only one extra parameter. It seems therefore more useful, for understanding the effects of non-circular PSFs on extended sources, than a sum of bi-dimensional Gaussians, in which the number of parameters at least doubles and the useful analytical properties pointed out in Paper 1 are lost.

2. Estimation of model parameters

2.1 *Correct Formulation of the Problem*

Let us assume the normalized intensity distribution $F(r)$ in star images following Moffat(1969), *i.e.,*

$$F(r) = F_0[1 + (r/\alpha)^2]^{-\beta}, \tag{1}$$

where $F_0 = (\beta - 1)(\pi\alpha^2)$. The integrated intensity in a pixel with size $2l$ centred at (x_n, y_m) is therefore given by

$$i(x_n, y_m) = i_0 \int_{x_1}^{x_2} \int_{y_1}^{y_2} [1 + (x'^2 + y'^2)/\alpha^2]^{-\beta} \mathrm{d}x' \mathrm{d}y' + f(x_n, y_m), \tag{2}$$

where α and β are the seeing-dependent parameters, $i_0 = F_0 L_T$ ($L_T = \Sigma_n \Sigma_m\, i(x_n, y_m)$ being the integrated luminosity of the star), $f(x_n, y_m)$ the background point distribution and the integration limits x_1, x_2, y_1, y_2 read as

$$x_1 = x_n - l - x_c \qquad y_1 = y_m - l - y_c$$

$$x_2 = x_n + l - x_c \qquad y_2 = y_m + l - y_c$$

depending on the displacement x_c and y_c of the star image centre from the central pixel (x_0, y_0) with local maximum intensity in the frame. The searched parameters α, β, x_c, y_c, and f cannot be estimated by a Newton-like method from Eq. (2), since the double integral there is not expressible, unless β is an integer, by a differentiable function of the parameters themselves. Nevertheless, such a function can be found considering the mixed second order moments of the pixel intensity, *i.e.*,

$$M(x_n) = |x_n - x_0| \sum_m |y_m - y_0|\, i(x_n, y_m)$$

$$M(y_m) = |y_m - y_0| \sum_n |x_n - x_0|\, i(x_n, y_m), \tag{3}$$

where the background is assumed constant on account of simplicity. This assumption can be released, if necessary, by introducing two or more background parameters, whose estimate, in any case, is less difficult than shape and centring parameters, being the starting Eq. (2) more linear in background parameters (see also Paper 1). The calculated distribution $M(x_n)$ sufficiently approximates the value of the integral

$$M(x_n)=i_0\int_{x_1}^{x_2}\int_{-\infty}^{+\infty}x'y'[1+(x'^2+y'^2)/\alpha^2]^{-\beta}\,\mathrm{d}x'\,\mathrm{d}y'+|x_n-x_0|\sum_m|y_m-y_0|f, \qquad (4)$$

in which the double integration can be easily performed, giving the equation

$$M(x_n)=i_0\alpha^4[2(\beta-1)(\beta-2)]^{-1}\{[1+(x_n-l-x_c)^2/\alpha^2]^{2-\beta}-$$
$$[1+(x_n+l-x_c)^2/\alpha^2]^{2-\beta}\}+|x_n-x_0|\sum_m|y_m-y_0|f, \qquad (5)$$

and a corresponding one holds for $M(y_m)$, containing y_m, y_c and y_0 instead of x_n, x_c and x_0. The analytical expressions of $M(x_n)$ and $M(y_m)$ enable us to estimate, in principle, the model parameters by the Newton-Gauss regularized method, because they are differentiable with respect to the searched parameters. Further, Eq. (5) can be immediately extended to a bidimensional elliptical Moffat's PSF model, if, an uncommon case, the image axes and the CCD frame axes are parallel, or if the data consist of PDS scans of a photographic plate previously oriented. In practice, unfortunately, the parameters are strongly linked in Eq. (5), violating the identifiability conditions (i.e., the derivatives of the fitting function with respect to the parameters are not linearly independent, see for more details Beck & Arnold 1977), so that parameters themselves cannot be simultaneously and uniquely estimated.

2.2 *An Approximate Solution*

Let us consider the sequence of integrated luminosities $L(x_n)$ over the squares A_n with side $2(2n-1)l$, centred on the. star image (neglecting its off-centring), i.e.,

$$L(x_n)=\int_{A_n}i(x,y)\,\mathrm{d}A+A_nf. \qquad (6)$$

It can be easily verified that the difference between $L(x_n)$ and $L(r_n)$, the integrated luminosity over a circle of the same area as the square, is some per cent at the centre and rapidly reduces outwardly, so that $L(x_n)$ can be considered as an approximate value of $L(r_n)$. But, in terms of the normalized Moffat's distribution, $L(r_n)$ reads as

$$L(r_n)=L_T[1-(1+r^2/\alpha^2)^{1-\beta}]+A_nf, \qquad (7)$$

which is an analytical expression enabling us to estimate the parameters by the Newton-Gauss regularized method. The link between α and β violates again the identifiability condition, but the convergence of the iterative process, with the present reduced number of parameters, is due to use of Penrose (1956) inversion which, as pointed out in Paper 1, works also with nearly singular matrices. The fitting procedure closely follows that extensively described in Paper 1 to derive from CCD frames the multi-Gaussian approximation of the PSF. In effect, the same code has been used, adding only few statements to extract from CCD original data the new 'input data'

(see Eq. 7) and to specify the new PSF model and its derivatives with respect to parameters. A block diagram description of the code is reported in Bendinelli, Parmeggiani & Zavatti (1984). As far as the off-centring is concerned, it can be derived, before the search of shape parameters, from the moments of the marginal pixel intensity distributions (see Chiu 1977).

3. Results and discussion

The approximate method described in the above last sub-section was tested by fitting the *V* band star images in the field of M 31 obtained by S. G. Djorgovski at the Kitt Peak 4-m telescope with a TI 800 × 800 CCD (pixel size of 0.298 arcsec). The intensity distributions in a star image obtained by the present Moffat's model and by the 3-Gaussians model of Paper 1 are shown in Fig. 1 and compared there with the brightness profile derived in a model-independent way using the QPHOT code (Djorgovski 1987, personal communication). The model parameters are reported in Table 1, and the joint residuals (calculated — model brightness) are shown in Fig. 2. It is evident from Fig. 1 that the brightness profiles computed by both models agree

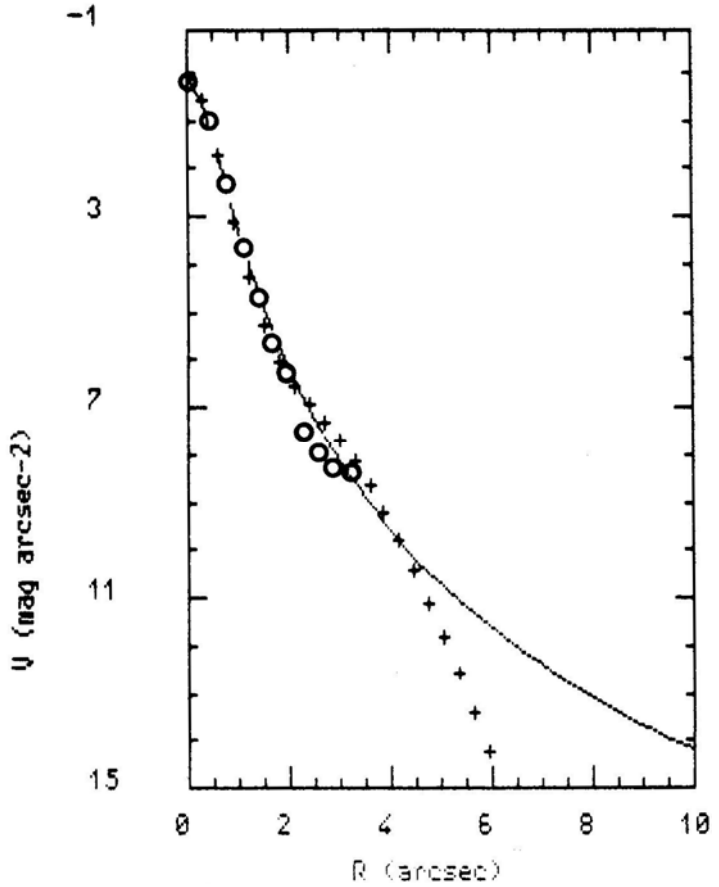

Figure 1. Comparison between the observed *V* brightness distribution in star images (circles) and the calculated ones by Moffat (dotted line) and multi-Gaussian (crosses) PSF models.

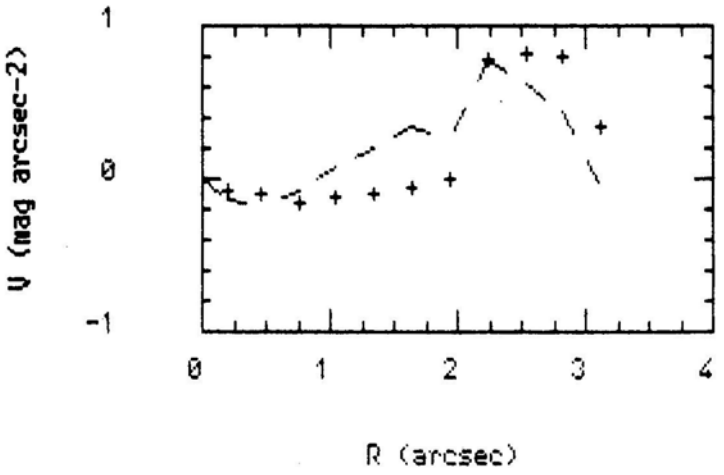

Figure 2. Residual (see text) of Moffat (dotted line) and multi-Gaussian (crosses) PSF models.

Table 1. Parameters of Moffat's and multi-Gaussian PSF models.

3-Gaussian			
	$a_1 = 0.523$	$a_2 = 0.375$	$a_3 = 0.101$
	$\sigma_1 = 0.302$	$\sigma_2 = 0.545$	$\sigma_3 = 1.483$
Moffat			
	$\alpha = 0.6135$	$\beta = 2.3124$	

Note: a_i is the partition coefficient of the ith Gaussian.

reasonably with the observed data. The magnitude of residuals is not surprising if one keeps in mind that in reality the star images overlap outer regions of M31, and not an uniform background. The models diverge out of about 4.5 arcsec (i.e. roughly speaking $3\sigma_3$ and 7α), but it should be stressed that the integrated luminosity of Moffat model from 7α to infinity (see Eq. 7) is less than one hundredth of the total, so that the true brightness distribution in extreme wings is irrelevant for any reasonable application (see, for instance, Appendix A). Further, the radial range in which the Moffat curve is overlapped by a sum of N Gaussians depends only on N, as shown for example in Bendinelli et al. (1984) and in Paper 1. In conclusion, it seems that parameters of both the multi-Gaussian and Moffat models can be calculated taking into account the finite pixel size, with practically the same accuracy. The choice of the model evidently depends on the particular research field. For instance in astrometry the multi-Gaussian is surely preferable, giving also the off-centring, while in extragalactic astronomy the other one should be used (see Schweizer 1981, and Djorgovski 1984 for the effects of PSF wings on the appearance of distant sources). Finally, one must stress the impossibility of deriving the parameters of King's and Lorentzian PSF models taking into account the pixel integration. In the first case owing to the discontinuity at the connection point between the inner Gaussian and the outer exponential, in the second since parameters are linked in a too complicated way.

Acknowledgements

We wish to thank G. G. C. Palumbo for careful reading of the manuscript, and useful comments, and S. G. Djorgovski for making available CCD frames. The financial support of the Comitato Nazionale Ricerche (Contract PSN 85-078) is acknowledged.

Appendix A

Convolution of a spherical source with Moffat's PSF

In a series of papers (see Bendinelli *et al.* 1986, and references therein) it has been shown that convolution-deconvolution of a spherical source with the PSF, approximated by a sum of weighted Gaussians, can be performed by the monodimensional integral equation

$$f(r)=\sum_{i=1}^{N}(a_i/\sigma_i^2)\exp(-r^2/2\sigma_i^2)\int_0^{\infty}\exp(-\rho^2/2\sigma_i^2)I_0(r\rho/\sigma_i^2)\phi(\rho)\,\mathrm{d}\rho \qquad \text{(A1)}$$

relating the true brightness distribution ϕ(r) and the observed one f(r). Let us assume

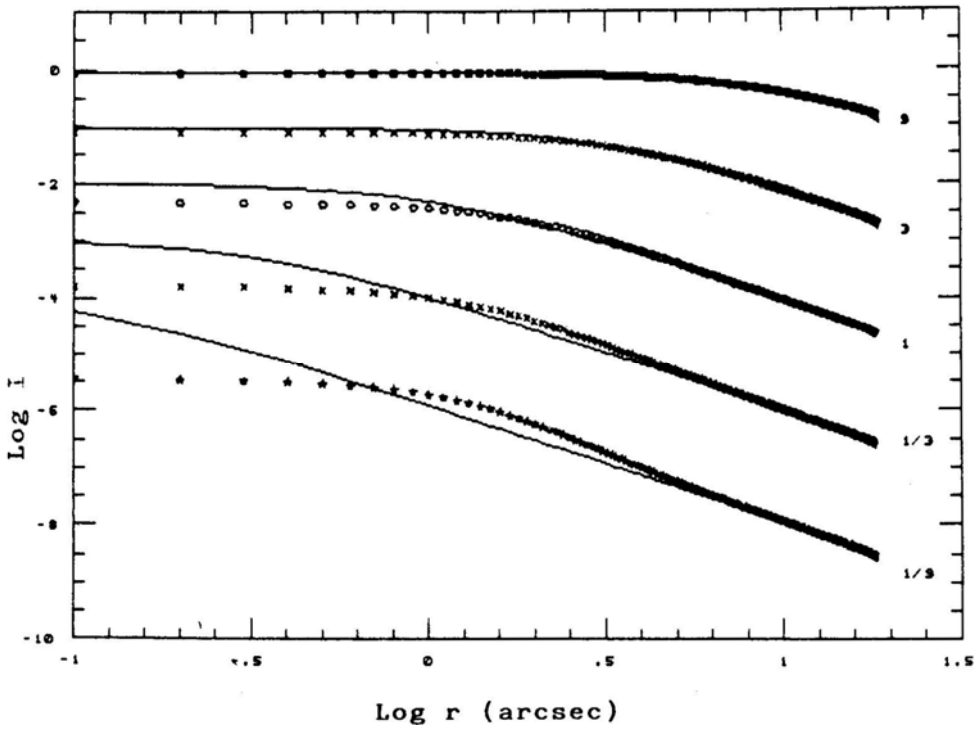

Figure A1. Set of empirical King's models with $\log(r_t/r_c)$ = 2.25 and r_c indicated at the end of each profile (continuous lines), vertically shifted, and their · convolution with Moffat's PSF of Table 1 (symbols).

Moffat's PSF approximation; then convolution is expressed by the double integral equation

$$f(r)=[2(\beta-1)/\pi\alpha^2]\int_0^{\infty}\rho F(\rho)\int_0^{\pi}[1+(\rho^2+r^2-2\rho r\cos\theta)/\alpha^2]^{-\beta}\,\mathrm{d}\rho\mathrm{d}\theta \qquad \text{(A2)}$$

which requires, to be computed or inverted up to the radial distance where the left-hand side term becomes negligible, about a factor of four in time more than Equation (Al). To prove the substantial equivalence of Equations (Al) and (A2), a set of empirical King's model have been chosen. They are characterized by the same, concentration index c = 2.25, with core radius r_c varying from 9 to 0.111 arcsec, in order to simulate the distance effect or smaller and smaller intrinsic sizes. Convolutions of models with the Moffat PSF specified in Table 1 are shown in Fig. Al, and differences between convolutions of any model with both Moffat and multi-Gaussian PSFs in Fig. A2. It seems that from these figures some main conclusions can be drawn:

1. Dealing with large sources (r_c > 1 arcsec) both PSF approximations give practically the same results.
2. For small sources (r_c < 1 arcsec) local differences of the order of 1 mag arcsec^{-2} between PSF approximations may cause about 0.1 mag arcsec^{-2} in convolved profiles, but in this case the problem is which is the better approximation.

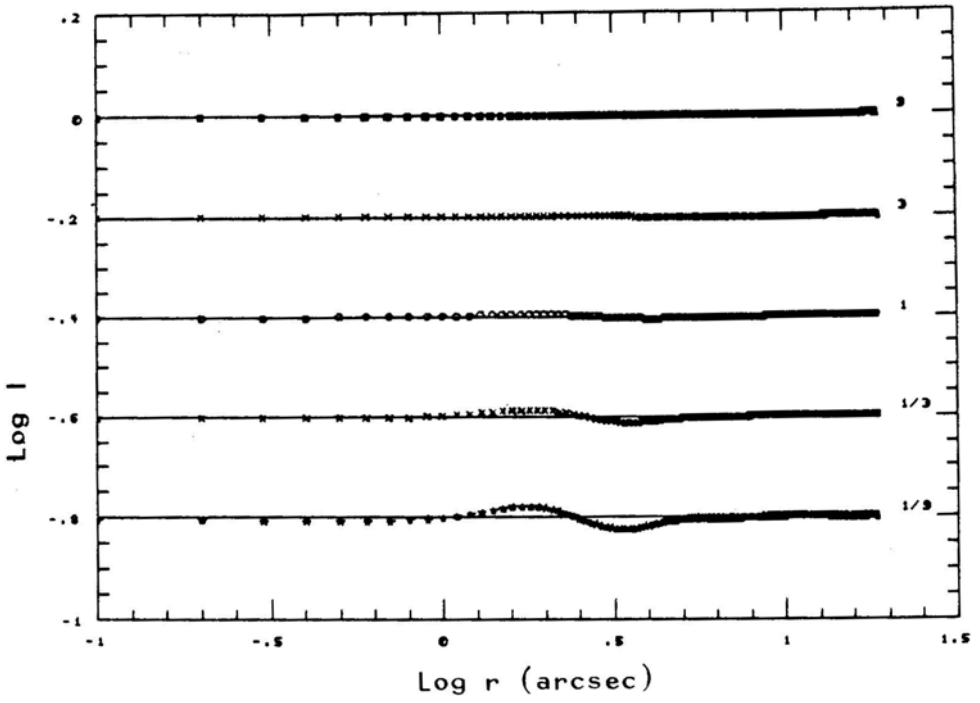

Figure A2. differences between convolutions of King's models with respectively Moffat's and multi-Gaussian PSF approximations of Table 1.

3. Convolution effects become negligible for both PSF approximations at compareable distances from the centre, roughly speaking at $3\sigma_3$ or 7α, so that we must be reasonably confident that the outer profile of distant sources is not an artefact of convolution with seeing.

References

Beck, J. V., Arnold, K. J. 1977, in *Parameters Estimation in Engineering and Science,* J. Wiley, New York.

Bendinelli, O., Parmeggiani, G., Zavatti, F. 1984, in *Astronet* 1983, Ed. G. Sedmak, SAIt Firenze, p. 347.

Bendinelli, O., Parmeggiani, G., Zavatti, F. 1986. *Astrophys. J.,* **308,** 611.

Bendinelli, O., Parmeggiani, G., Piccioni, A., Zavatti, F. 1987, *Astr. J.,* **94,** 1095 (Paper 1).

Brown, G. S. 1974, *Univ. Texas Publ. Astr. No.* 11.

Capaccioli, M., de Vaucouleurs, G. 1979, *Astrophys. J. Suppl. Ser.,* **52,** 465.

Chiu, L. T. G. 1977, *Astr. J.,* **82,** 842.

Djorgovski, S. 1984, *J. Astrophys. Astr.,* **4,** 271.

Franz, O. G. 1973, *J. R. Astr. Soc. Can.,* **67,** 81.

King, I. R. 1971, *Publ. Astr. Soc. Pac,* **83,** 199.

Kormendy, J. 1973, *Astr. J.,* **78,** 255.

Moffat, A. F. J. 1969; *Astr. Astrophys.,* **3,** 455.

Penrose, R. 1956, *Proc. Cambridge Phil. Soc,* **52,** 17.

Schweizer, F. 1981, *Astr. J.,* **86,** 662.

Van Altena, V. F., Auer, L. H. 1975, in *Image Processing Techniques in Astronomy,* D. Reidel, Dordrecht, p. 411.

J. Astrophys. Asr. (1988) **9,** 25–39

Accretion Effects on Compact Members of Binary Stars

N. Spyrou *Astronomy Department, University of Thessaloniki, 54006 Thessaloniki, Greece*

Received 1987 April 16; revised 1987 December 12; accepted 1988 January 12

Abstract. We explore the change in the period of axial rotation and in the radius of a magnetized compact star in a binary system, induced by the accretion on it of mass with angular momentum from the surface of its non-compact companion. No specific assumption is made concerning the accretion model, and the primary's interior is described by the Fermi-Dirac statistics for degenerate matter. The rate of change with time of the period and radius is expressed in terms of the compact primary's physical parameters and total absolute luminosity. The conditions are fully derived under which the above changes can be positive, negative or even vanish. In the case of the millisecond pulsars in binary X-ray sources the predicted values of the period time derivative, depending on the values of the accretion rate and. the absolute luminosity, can be positive or negative—if not vanishing—and they fall absolutely in the range 10^{-21} –10^{-17} ss^{-1}, in good agreement with current observational data. The corresponding rate of change of radius, either positive or negative, fall in the range of 10^{-3} –10^{-1} cm y^{-1}. Finally, it is proved that the well-known bursters can be explained by thermonuclear flash due to gravitational instability in the accreted matter, but their explanation as a result of direct contraction could be possible only for quite high accretion rates ($>10^{-7}$ $M_{\odot}\,y^{-1}$). This last result indicates that, in contrast to the accretion-induced change in period, which can be of either sign irrespective of the primary's age, the accretion-induced non-catastrophic contraction is impossible, while according to repent results the contraction in general is possible for young compact objects.

Key words: binary stars—collapsed stars—period and radius change—accretion

1. Introduction and Motivation

One of the most interesting areas of current research in astrophysics, relativistic or not, from either theoretical or observational point of view, is related to the compact stars in binary systems. Much effort has been devoted to the study of the astrophysical and dynamical behaviour of members of such a system and of the binary as a whole. Thus in semi-detached binaries, white dwarfs give rise to cataclysmic variables, while neutron stars give rise to binary X-ray sources, bursters and quasi-periodic X-ray sources (Lewin & van den Heuvel 1983; Shapiro & Teukolsky 1983; Lamb & Paterson 1985). The main idea underlying the above is the accretion of mass with angular

momentum on the surface of the compact primary from the photosphere of a normal, giant or supergiant companion star (Ghosh & Lamb 1977; van den Heuvel 1984; for recent results see *e.g.* Hayakawa 1985; Taylor & Stinebring 1986; van den Heuvel, van Paradijs, Taam 1986).

According to standard results, the members, whether compact or not, of a clean binary act on each other gravitationally as point masses. This means that the linear dimensions of the members are small compared to their mutual separation. So the tidal interactions between the members can be ignored as compared with their point-mass gravitational attraction, either Newtonian or relativistic. Of particular interest in this case are the clean binary pulsars, and especially the clean relativistic binary, containing the pulsar PSR 1913+16, which provides strong indication for the detection of gravitational radiation (Weisberg & Taylor 1984; Ehlers & Walker 1984; Spyrou & Papadopoulos 1985). Furthermore, we shall assume that the same dynamical description is applicable even in the case of mass and angular-momentum exchange between the members, due to either gravitational fields or stellar winds from the non-compact member. Such an assumption is justified, especially if the non-compact member is in a stage of stellar evolution, in which it does not fill its Roche lobe. In this case, we shall assume that the mass exchange between the members is through the inner Lagrangian point only, and through the subsequent formation of an accretion disc around the compact member. Under these conditions we are allowed to apply the results of Spyrou (1981a, b) for a dynamical description of the orbital motion of a realistic binary valid to the first post-Newtonian approximation of general relativity.

Due to interaction, with or without mass-exchange, the physical characteristics and parameters of the members change in time due to evolutionary reasons (in case of no mass exchange) or non-evolutionary reasons (in case of mass exchange). For this reason, recently we examined (Spyrou 1985; quoted here as paper 1) the possibility of the change of the radius of a compact star in a binary. More precisely we explored the change of the orbital period of a clean relativistic binary induced by the *evolutionary change* of the radii and axial periods of its members. By applying to the binary pulsar PSR 1913 + 16 we proved that a slow contraction of the younger companion could explain part of the possibly non-vanishing difference between the observed and the predicted values of shortening of the orbital period (see also Spyrou 1987). Finally we proved that the slowing down of axial rotation and the possible contraction, in principle, can occur in young compact stars and contraction is more likely for white dwarfs than for neutron stars, the inverse being true for the slowing down of the axial period.

In this paper we explore the changes of radius and of period of axial rotation of a compact member of a binary system, induced by the accretion on it of mass with angular momentum from the surface of its non-compact companion. This problem is of obvious interest, in view of the multiplicity of interesting phenomena occurring in such systems, especially in those involving millisecond pulsars (Alpar *et al.* 1982), which are being discovered continuously (Dewey *et al.* 1986; Segelstein *et al.* 1986), and at least seven such systems are known at present. From the problems to be examined here, although the accretion-induced change of the radius has been studied (for a neutron-star primary: Ghosh, Lamb & Pethick 1977; Ghosh & Lamb 1979; Shapiro & Teukolsky 1983), the solution has not been explicitly obtained and applied in terms of the binary's physical characteristics. On the other hand, the problem of

accretion-induced change of period cannot be considered as generally solved, because the sign of the time derivative of the period is not certain over the whole range of permitted total mass and equations of state for the interior of a neutron star or a white dwarf. The obvious difference with the results of Paper 1 is that there the change of the radius of the *young* compact star, considered as the relic of the violent event, during which the compact star was born, is a decrease, while the change of period is an increase, as due to the loss of electromagnetic radiation (or/and to starquakes, in the form of the *glitches*). Finally, these results themselves could be of some interest to the very problem of the evolutionary history of non-clean binaries with a compact star.

In Section 2 we describe the physics of the binary star and evaluate its total absolute luminosity as a result of the accretion of mass with angular momentum on the magnetized compact member. Hence the rates of change of the period and of the radius are expressed in terms of the accretion rate and the (observationally derived) total absolute luminosity. In Section 3 we apply the results to the millisecond pulsars, binary X-ray sources and bursters, and finally in Section 4 we discuss the results.

2. The physics of the binary system

We consider a binary system composed of a compact primary star (neutron star or white dwarf) and a non-compact companion (normal star, giant or supergiant). As in Paper 1, we assume for simplicity that the compact primary remains spatially homogeneous, spherically symmetric, and uniformly and rigidly rotating, magnetized collapsed star. Also its interior will be described by the Fermi-Dirac statistics of non-relativistic, degenerate matter composed of noninteracting particles (electrons or neutrons).

The binary system is at the stage of accretion of mass with angular momentum on the compact star from the surface of its companion, due mainly to the strong gravitational action of the primary on the photosphere of the companion, or to a lesser degree due to the stellar wind from the companion. Moreover, we shall assume that practically there are no mass losses (*e.g.* through the inner Lagrangian point) or angular-momentum losses, from the system. So the total angular momentum is conserved and the mass removed from the surface of the companion, most probably through an accretion disc, eventually is transfered fully to the surface of the primary. Due to this transfer of mass with angular momentum, the internal characteristics of the two members change in time, and the same is true for the total *inertial mass* (or total mass energy) of the binary. As explained in Spyrou (1981a, b), in order to examine the influence on the orbital motions of the internal characteristics of the binary members, we have to know the orbital motion to post-Newtonian accuracy. In this case the binary's total inertial mass, namely the system's effective mass,

$$M = m_{\mathrm{p}} + m_{\mathrm{c}} \tag{1}$$

in terms of its total *rest mass*

$$\bar{M} = \bar{m}_{\mathrm{p}} + \bar{m}_{\mathrm{c}} \tag{2}$$

and its total *Newtonian self-energy*

$$E^{(\mathrm{s})} = \varepsilon_{\mathrm{p}}^{(\mathrm{s})} + \varepsilon_{\mathrm{c}}^{(\mathrm{s})} \tag{3}$$

is expressed as

$$M = \bar{M} + c^{-2} E^{(\mathrm{s})} \tag{4}$$

where c is the velocity of light in vacuum, the subscripts p and c denote the primary and the companion, respectively, and the symbols $\bar{m}$ and $\varepsilon^{(s)}$ with the proper subscript stand for the rest mass and the total self-energy of the corresponding member.

As a consequence of the above definitions, the binary's absolute luminosity L is defined as

$$L \equiv -\dot{M}c^2 = -\dot{\bar{M}}c^2 - \dot{E}^{(s)} \tag{5}$$

with the dot denoting total time derivative. The luminosity L results from the changes of the rest masses and self-energies of generally both members. Furthermore, according to our basic assumption that no mass (and angular momentum) is lost from the system during the accretion, we shall have

$$\dot{M} = 0 \tag{6a}$$

or equivalently,

$$\dot{m} \equiv \dot{\bar{m}}_p = -\dot{\bar{m}}_c > 0. \tag{6b}$$

The condition (6a) does not imply that there is no transfer of mass between the two members, as was the case in Paper 1. In its form (6b) it simply implies that the rest mass removed from the companion's surface, is eventually transfered fully to the compact primary's surface. Thus the definition (5) reduces to

$$L = -\dot{E}^{(s)} \tag{7}$$

according to which the absolute luminosity of the pair is due to the change of only the self-energy of the members, resulting from the accretion of mass with angular momentum from the companion to the primary.

Moreover, in a binary like the one considered here, the change of the internal characteristics, due to the mass and angular momentum changes, is not so important for the non-relativistic companion. In fact, it is rather obvious that, unless the accretion rate is extremely heavy, the changes of the companion's radius and rest mass are negligible, and hence the same is true for the change of its various forms of energy (potential, kinetic etc.). Under such conditions, if additionally the linear dimensions of the members are considerably smaller than their mutual distance, then the mutual dynamical interaction of the members will not differ from that of two point-masses. On the other hand, the accretion-induced change of the internal characteristics of the relativistic compact primary can be important, so that structural changes of the latter become important. In view of the above we shall reasonably assume that the pair's luminosity L is practically due to the change of the self-energy of only the primary, namely

$$L \sim -\dot{\varepsilon}_p^{(s)} \equiv -\dot{\varepsilon}^{(s)}. \tag{8}$$

Furthermore, since the accreting matter has also angular momentum, quite generally the conservation of the total angular momentum requires (Shapiro & Teukolsky 1983)

$$\dot{\mathbf{S}} = \dot{\mathbf{s}} + \mathbf{N} \tag{9}$$

where $\mathbf{S}$ and $\mathbf{s}$ are the angular momenta of the primary's axial rotation and of the accreting matter, respectively, while $\mathbf{N}$ is the torque acting on the accreting matter due to *e.g.* viscous effects and the primary's magnetic field *etc.* Here we shall assume that $\mathbf{N}$ vanishes, postponing for a later study the examination of the case $\mathbf{N} \neq \mathrm{O}$ (see, however,

Ghosh & Lamb 1979 and Section 3 below). Then, Eq (9) reduces to

$$\dot{\mathbf{S}} = \dot{\mathbf{s}} \quad (\mathbf{N} = 0). \tag{10}$$

The two basic Eqs (8) and (10) relate the observationally derived (for known distance of the binary) absolute luminosity (L) with the characteristics of the accreting matter ($\bar{m}$, **s**) and the subsequently changing internal characteristics ($\varepsilon^{(s)}$, **S**).

In order to apply the above basic equations, we need a physical model for the primary's interior and of the accretion on it of mass with angular momentum. To this purpose we shall assume, as in Paper 1, that the primary is composed of a perfect fluid with a Fermi–Dirac equation of state of degenerate matter in the form of non-interacting particles (neutrons for neutron stars, and electrons for white dwarfs). The dynamical behaviour of a realistic binary composed of two such bodies has been studied in Spyrou (1981a, b and 1983). These results were then applied in Paper 1 in studying the influence on the binary's orbital period of the changing internal characteristics of the members, namely slowing down and contraction of the axial rotation. Here we shall assume moreover that the primary's perfect-fluid matter is magnetized and has infinite electrical conductivity. The far-field of such an isolated gravitating source has been studied by Spyrou (1984), where it was proved that the inertial (and gravitational) mass of this source is a generalization of the corresponding quantity of Spyrou (1981a, b), such as to include also the energy of the electromagnetic field.

All these results will finally be specialized to the case of a primary, spherical star of radius R, axially rotating in a uniform and rigid-body manner with period. P. In this case in the notation of Paper 1 (see Equation A7 in Paper 1)

$$\frac{\varepsilon^{(s)}}{\bar{m}c^2} = \frac{4\pi^2}{5c^2}\frac{R^2}{P^2} - \frac{3}{5}\frac{G\bar{m}}{c^2 R} + A\tilde{g}(x)x^{-3} + \frac{B^2R^3}{6\bar{m}c^2} \tag{11}$$

and

$$S = \frac{2\pi}{P}I, \quad I = \frac{2}{5}\bar{m}R^2, \quad xR = \beta\bar{m}^{\frac{1}{3}} \quad (\beta = \text{const.}). \tag{12}$$

Moreover the rate of change, $I\dot{\bar{m}}$, of the angular momentum of the primary and its neighbourhood up to the radial distance r, satisfies

$$\dot{s} = l\dot{\bar{m}} \tag{13}$$

where, according to Eq (14) of Spyrou (1981a), for relativistic orbits,

$$l = (Gm_p r)^{\frac{1}{2}} \tag{14}$$

is the specific angular momentum of the accreting matter (to post-Newtonian accuracy). In the case of a pulsar with a dipole magnetic field **B**, the above neighbourhood is simply its magnetosphere located at the *'Alfven radius*

$$r_A = (\mu^4/2Gm_p\dot{\bar{m}}^2)^{\frac{1}{7}}, \quad B = 2\mu/r^3 \tag{15}$$

where μ is the dipole's magnetic moment. If, moreover, the rate of change of the angular momentum of the pulsar's magnetosphere is negligible, then $I\dot{\bar{m}}$ can practically be identified with the rate of change of simply the pulsar's angular momentum, as is exactly expressed by Eqs (9) and (13).

From the above it becomes transparent that, as in Paper 1, we distinguish m from $\bar{m}$ as far as their inertial properties are concerned. Also we distinguish $\dot{m}$ from $\dot{\bar{m}}$, because

here the rate of change of the accreting matter's angular momentum is composed of a part $\dot{l}$, depending on the primary's inertial mass, and a part $\dot{\bar{m}}$, depending on the properties of the accreting matter.

Due to the accretion of matter, the primary's physical parameters $\bar{m}$, R, x, B and, hence, $\varepsilon^{(s)}$, s and $\bar{m}$ will change, and this will result in the change of L. The change of $\varepsilon^{(s)}$, for constant $\bar{m}$, has been evaluated in Paper 1, not taking into account the magnetic field. Here this result is generalized, with the aid of the conservation of magnetic flux in the form

$$BR^2 = \text{const.}$$

from which we find

$$\frac{\dot{B}}{B} = -\frac{2\dot{R}}{R}. \tag{16}$$

We stress that the above change of B is different from the decay of magnetic field due to ohmic dissipations, and results simply from the change of R due to accretion ($\dot{R} \gtrless 0$).

In view of that mentioned above the two basic Eqs (8) and (10) can be put in the form

$$\begin{aligned}
&\left\{-\frac{4\pi^2}{5}\bar{m}\frac{R^2}{P^2}+\frac{6}{5}\frac{G\bar{m}^2}{R}-\bar{m}c^2A\left[\frac{\bar{g}}{x^3}+\frac{x}{3}\frac{\mathrm{d}}{\mathrm{d}x}\left(\frac{\bar{g}}{x^3}\right)\right]\right\}\left(\frac{\dot{\bar{m}}}{\bar{m}}\right)\\
&+\left[-\frac{8\pi^2}{5}\bar{m}\frac{R^2}{P^2}-\frac{3}{5}\frac{G\bar{m}^2}{R}+\bar{m}c^2A\frac{\mathrm{d}}{\mathrm{d}x}\left(\frac{\bar{g}}{x^3}\right)+\frac{B^2R^3}{6}\right]\left(\frac{\dot{R}}{R}\right)\\
&+\frac{8\pi^2}{5}\bar{m}\frac{R^2}{P^2}\left(\frac{\dot{P}}{P}\right)=L,
\end{aligned} \tag{17}$$

and

$$\left(\frac{l}{l_{\mathrm{p}}}-1\right)\left(\frac{\dot{\bar{m}}}{\bar{m}}\right)-\frac{2\dot{R}}{R}+\frac{\dot{P}}{P}=0, \tag{18}$$

where

$$l_{\mathrm{p}}=\frac{4\pi}{5}\frac{R^2}{P} \tag{19}$$

is the specific angular momentum of axial rotation of the primary. Finally, we notice that direct consequence of Eqs (14), (15) and (19) is the useful relation

$$\frac{l}{l_{\mathrm{p}}}=\frac{[2^{-\frac{1}{2}}G^3\lambda^{-3}(\mu\bar{m})^2]^{\frac{1}{7}}}{\frac{4\pi}{5}\frac{R^2}{P}}\left(\frac{\dot{\bar{m}}}{\bar{m}}\right)^{-1/7} \tag{20}$$

where

$$\lambda=\frac{\bar{m}}{m}. \tag{21}$$

Eqs (17) and (18) constitute a system of equations for $\dot{P}$ and $\dot{R}$ in terms of L, $\dot{\bar{m}}$ and the companion's physical parameters m, R, P, x and B. Its solution can be written as

$$\frac{\dot{P}}{P}=\frac{1}{S_{\mathrm{p}}}(L-L_{\mathrm{p}}) \tag{22}$$

and

$$\frac{\dot{R}}{R}=\frac{1}{2S_{\rm P}}(L-L_{\rm R}) \tag{23}$$

where by definition

$$S_{\rm P}=\frac{4\pi^2}{5}\,\bar{m}\,\frac{R^2}{P^2}-\frac{3}{10}\frac{G\bar{m}^2}{R}+\frac{3}{10}\,\bar{m}c^2x^2+\frac{B^2R^3}{12}, \tag{24}$$

$$L_{\rm P}=\left[-\frac{4\pi^2}{5}\,\bar{m}\,\frac{R^2}{P^2}\frac{l}{l_{\rm p}}-\frac{3}{10}\frac{G\bar{m}^2}{R}\left(\frac{l}{l_{\rm p}}-1\right)\right.$$
$$\left.+\frac{3}{10}\,\bar{m}c^2x^2\left(\frac{l}{l_{\rm p}}-\frac{8}{3}\right)+\frac{B^2R^3}{12}\left(\frac{l}{l_{\rm p}}-1\right)\right]\left(\frac{\dot{\bar{m}}}{\bar{m}}\right), \tag{25}$$

and

$$L_{\rm R}=\left[-\frac{4\pi^2}{5}\,\bar{m}\,\frac{R^2}{P^2}\left(2\frac{l}{l_{\rm p}}-1\right)+\frac{6}{5}\frac{G\bar{m}^2}{R}-\frac{1}{2}\,\bar{m}c^2\chi^2\right]\left(\frac{\dot{\bar{m}}}{\bar{m}}\right). \tag{26}$$

We notice that in writing down Eqs (24)–(26) we assumed that the primary's degenerate matter is nonrelativistic, namely

$$x\ll 1 \tag{27}$$

and applied Eqs (A4)–(A6) of the Appendix of Paper 1. Finally we notice that the symbols $L_{\rm P}$ and L_R have entirely different meaning compared to Paper 1.

A rather interesting, although not transparent, feature of Eqs (22)–(26) is that *e.g.* in Eq (22), which is explicitly independent of $\dot{R}$, the right-hand side depends also on the coefficient of $\dot{R}$ in Eq (18) (which happens to be simply a constant). Consequently, it is obvious that if $\dot{R}$ was set equal to zero, the resulting value fo $\dot{P}$ would be different. Analogous arguments are valid for Eq (23).

Finally, from Eqs (22) and (23) it becomes transparent that P and R in general can either increase or decrease or even remain constant during the accretion phase. This problem for a rapidly rotating neutron-star primary is examined in the next section, while the case of a white-dwarf primary will be examined elsewhere.

3. The change of the period and radius of a neutron star

The accretion-induced values of $\dot{P}$ and $\dot{R}$ are evaluated, in terms of the physical characteristics of the primary and the accreted matter, directly and generally via Eqs (22)–(26) under the assumption of a vanishing total external torque. However, before applying these equations we recall the following general form of Eq (10) due to Ghosh, Lamb & Pethick (1977; Eq 58)

$$\frac{\dot{P}}{P}+\frac{\dot{\bar{m}}}{\bar{m}}\left(\frac{l}{l_{\rm p}}-\frac{{\rm d}\ln I}{{\rm d}\ln\bar{m}}\right)=0 \tag{28}$$

from which one deduces that the logarithmic derivative d ln I /d ln $\bar{m}$ is related to the accretion-induced change of the primary's radius. Actually, for a spherical star, Eqs

(10) and (28) [or the second of Eqs (12) upon differentiation] imply

$$\frac{2\dot{R}}{R}+\frac{\dot{\bar{m}}}{\bar{m}}\left(1-\frac{\mathrm{d}\ln I}{\mathrm{d}\ln \bar{m}}\right)=0$$

and so, for a given $\dot{\bar{m}}$, both $\dot{P}$ and $\dot{R}$ can be evaluated provided that the value of the logarithmic derivative d ln I/d ln $\bar{m}$ is known. As evaluated by Ghosh, Lamb & Pethick (1977; Fig. 5) using the equation of state of Baym, Pethick & Sutherland (1972) and Pandharipande, Pines & Smith (1976), for neutron stars of intermediate mass ($0.5 \lesssim \bar{m} \lesssim 1.2\ m_\odot$), this logarithmic derivative is positive and slightly above unity and so $\dot{R}$, of either sign, generally is expected to be small, but not necessarily vanishing. Under the same conditions (d ln I/d ln $\bar{m} \sim 1$), for fast-rotating ($4\pi^2/P^2 \lesssim Gm_p/R^3$) neutron stars, it can be verified that in Eq (28) l/l_p exceeds unity ($r_A \gg R$) for strongly magnetized stars ($B \sim 10^{12}$ G), while it is close to unity ($r_A \sim$ R) for weakly magnetized ones ($B \lesssim 10^9$ G).

In view of all the above we shall restrict the applications to the case of fast-rotating, weakly-magnetized neutron stars of intermediate mass, for which the accretion-induced $\dot{P}$ and $\dot{R}$ are expected to be small. It is obvious that for such neutron stars the effect of accretion on P and R is underestimated, but on the other hand it is obvious that such neutron stars are supposed to participate in the interesting phenomena of the X-ray binaries, bursters and quasi-periodic X-ray sources. Hence in the units

$$\hat{\bar{m}}=1m_\odot,\quad \hat{R}=10^6\ \mathrm{cm},\quad \hat{P}=10^{-3}\mathrm{s},\quad \hat{L}=10^{37}\ \mathrm{erg\,s^{-1}},$$
$$\hat{\mu}=10^{30}\mathrm{G\,cm^3},\quad \hat{\dot{\bar{m}}}=10^{17}\ \mathrm{g\,s^{-1}}$$

the physical parameters involved will be denoted by $\bar{m}_{(\odot)}$, $R_{(6)}$, $P_{(-3)}$, $\mu_{(30)}$ and $\dot{\bar{m}}_{(17)}$, respectively, and should not differ greatly from unity. For the above typical values, the last term on the right of Eq (24) is negligibly small compared to the difference of the second and third terms. Also, by comparison with a static neutron star (with $\lambda = 1.1$; see Table 1 of Paper 1) for which

$$0.519 \leqslant [\bar{m}_{(\odot)}^{1/3} R_{(6)}]_{\mathrm{static}} \leqslant 0.522, \tag{29}$$

we verify that the condition

$$\frac{G\bar{m}}{R} < c^2 x^2 \tag{30a}$$

reduces to the generally correct condition

$$R < \gamma R_{\mathrm{static}},\quad 2.368 \leqslant \gamma \leqslant 2.382 \tag{30b}$$

so that

$$S_P > 0. \tag{31}$$

It is interesting that the last result does not affect the sign of $\varepsilon^{(s)}$ or, equivalently, the possibility for the star to be considered or not under conditions of stable hydrodynamical equilibrium ($\varepsilon^{(s)} < 0$).

Similarly Eq (20) takes the form

$$\frac{l}{l_p}=79.238\,\bar{m}_{(\odot)}^{-3/7}\mu_{(30)}^{2/7}R_{(6)}^{-2}P_{(-3)}\dot{\bar{m}}_{(17)}^{-1/7}. \tag{32}$$

In view of Eqs (20) and (25) the condition

$$L_{\mathrm{P}} \gtrless 0$$

bounds the value of m and is equivalent to

$$\dot{\bar{m}} \gtrless \dot{\bar{m}}_{\mathrm{P}} \tag{33}$$

where, by definition,

$$\dot{\bar{m}}_{\mathrm{P}} = \frac{\left(\frac{G\bar{m}}{\lambda}\right)^3 \mu^2}{2^{\frac{1}{2}}\left(\frac{4\pi}{5}\frac{R^2}{P}\right)^7}\left[\frac{\frac{4\pi^2}{5}\frac{R^2}{P^2}+\frac{3}{10}\frac{G\bar{m}}{R}-\frac{3}{10}c^2x^2-\frac{B^2R^3}{12\bar{m}}}{\frac{3}{10}\frac{G\bar{m}}{R}-\frac{4}{5}c^2x^2-\frac{B^2R^3}{12\bar{m}}}\right]^7 \tag{34}$$

As a consequence of the condition (30a), the denominator in brackets in Eq (34) is negative. Furthermore, for the numerator we may have

$$A_{\mathrm{P}} \equiv \frac{4\pi^2}{5}\frac{R^2}{P^2}+\frac{3}{10}\frac{G\bar{m}}{R}-\frac{3}{10}c^2x^2-\frac{B^2R^3}{12\bar{m}} \gtrless 0, \tag{35}$$

or equivalently

$$P \lessgtr P_{\mathrm{P}}, \tag{36}$$

where

$$P_{\mathrm{P}} = \left\{\frac{4\pi^2}{5}R^2\left[-\frac{3}{10}\left(\frac{G\bar{m}}{R}-c^2x^2\right)+\frac{B^2R^3}{12\bar{m}}\right]^{-1}\right\}^{\frac{1}{2}}, \tag{37a}$$

or, equivalently,

$$P_{\mathrm{P}(-3)} = 0.400R_{(6)}^2\bar{m}_{(\odot)}^{-1/3}[1-0.808\bar{m}_{(\odot)}^{1/3}R_{(6)}]^{-\frac{1}{2}}. \tag{37b}$$

We observe that in view of the condition (29) the positivity of P^2 is always guaranteed provided that the condition (30b) is satisfied. Hence P_{P} is a real number, and all the three conditions (35) are meaningful.

In view of the above and since $m > 0$, we can distinguish the following three cases:

(i) If

$$A_{\mathrm{P}} > 0, \tag{38a}$$

then

$$\dot{\bar{m}}_{\mathrm{P}} < 0, \quad \dot{\bar{m}} > \dot{\bar{m}}_{\mathrm{P}}, \quad L_{\mathrm{P}} > 0, \tag{38b}$$

and so

$$\dot{P} \gtrless 0, \quad \text{if} \quad L \gtrless L_{\mathrm{P}}. \tag{38c}$$

(ii) If

$$A_{\mathrm{P}} = 0, \tag{39a}$$

then

$$\dot{\bar{m}}_{\mathrm{P}} = 0, \quad \dot{\bar{m}} > \dot{\bar{m}}_{\mathrm{P}}, \quad L_{\mathrm{P}} > 0, \tag{39b}$$

and so

$$\dot{P} \gtrless 0, \quad \text{if} \quad L \gtrless L_{\mathrm{P}}. \tag{39c}$$

(iii) If

$$A_{\mathrm{P}} < 0 \tag{40a}$$

then

$$\dot{\bar{m}}_{\mathrm{P}} > 0, \quad \dot{\bar{m}} \gtrless \dot{\bar{m}}_{\mathrm{P}}, \quad L_{\mathrm{P}} \gtrless 0, \tag{40b}$$

and so we distinguish three subcases

$$\begin{aligned} &\text{(a) for } L_P>0, \quad \dot{P}\gtrless 0, \quad \text{if} \quad L\gtrless L_P, \\ &\text{(b) for } L_P=0, \quad \dot{P}>0, \quad \text{because} \quad L>0, \\ &\text{(c) for } L_P<0, \quad \dot{P}>0, \quad \text{because} \quad L-L_{P>0}. \end{aligned} \tag{40c}$$

The above cases fully determine the conditions under which the accretion causes the compact primary to accelerate (P<0), slow down (P>0) or even retain constant (P=0) its period during the accretion.

During the accretion, radius and density also generally change. In view of Eqs (20) and (26) the condition

$$L_R\gtrless 0 \tag{41}$$

again bounds the value of m and is equivalent to

$$\dot{m}\gtrless\dot{m}_R \tag{42}$$

where by definition

$$\dot{m}_R=\frac{\left(\frac{G\bar{m}}{\lambda}\right)^3\mu^2}{2^{\frac{1}{2}}\left(\frac{4\pi}{5}\frac{R^2}{P}\right)^7}\left[\frac{\frac{8\pi^2}{5}\frac{R^2}{P^2}}{\frac{4\pi^2}{5}\frac{R^2}{P^2}+\frac{6}{5}\frac{G\bar{m}}{R}-\frac{1}{2}c^2x^2}\right]^7. \tag{43}$$

Noting that m_R must be finite, putting

$$A_R\equiv\frac{4\pi^2}{5}\frac{R^2}{P^2}+\frac{6}{5}\frac{G\bar{m}}{R}-\frac{1}{2}c^2x^2\gtrless 0, \tag{44}$$

and noting that $m > 0$, we can distinguish the following two cases:

(i) If

$$A_R<0, \tag{45a}$$

then

$$\dot{m}_R<0, \quad \dot{m}>\dot{m}_R, \quad L_R>0, \tag{45b}$$

and so

$$\dot{R}\gtrless 0, \quad \text{if} \quad L\gtrless L_R. \tag{45c}$$

(ii) If

$$A_R>0, \tag{46a}$$

then

$$\dot{m}_R>0, \quad \dot{m}\gtrless\dot{m}_R, \quad L_R\gtrless 0, \tag{46b}$$

and so we distinguish three subcases:

$$\begin{aligned} &\text{(a) for } L_R>0, \quad \dot{R}\gtrless 0, \quad \text{if} \quad L\gtrless L_R, \\ &\text{(b) for } L_R=0, \quad \dot{R}>0, \quad \text{because} \quad L>0, \\ &\text{(c) for } L_R<0, \quad \dot{R}>0, \quad \text{because} \quad L-L_R>0. \end{aligned} \tag{46c}$$

The above cases fully determine the conditions, under which the accretion causes the compact primary to expand ($R > 0$), contract ($R < 0$) or even retain constant ($R = 0$) its radius during the accretion.

Although today there is no general consensus on the intensity of the surface magnetic field of a pulsar in binary X-ray sources, bursters and quasi-periodic X-ray sources, we shall conform with the case of an old, weakly-magnetized, millisecond pulsar with typical parameters

$$m_{(\odot)}=1, \quad R_{(6)}=1, \quad P_{(-3)}=1.5, \quad \mu_{(30)}=5\times 10^{-3}.$$

Then from Eqs (24), (25), (32), (34) and (37b) we find

$$S_{\mathrm{P}}=1.40\times 10^{53}\,\mathrm{erg}, \quad \dot{m}_{\mathrm{P}}=4.026\times 10^{18}\,\mathrm{g\,s^{-1}}=6.389\times 10^{-8}\,M_{\odot}\,\mathrm{y^{-1}},$$
$$P_{\mathrm{P}}=0.914\times 10^{-3}\,\mathrm{s}\,(A_{\mathrm{P}}<0), \tag{47}$$

and

$$L_{\mathrm{P}}\gtrless 0, \qquad \text{if} \qquad \dot{m}_{(17)}\lesseqgtr 40.262, \tag{48}$$

whence Eq (22) takes the form

$$\dot{P}=1.064\times 10^{-19}[L_{(37)}+\dot{m}_{(17)}(0.915-1.552\dot{m}_{(17)}^{-1/7})]\,\mathrm{s\,s^{-1}}, \tag{49}$$

and yields

$$\dot{P}\gtrless 0, \qquad \text{if} \qquad L_{(37)}+\dot{m}_{(17)}(0.915-1.552\dot{m}_{(17)}^{-1/7})\gtrless 0. \tag{50}$$

So the value(47) of the accretion rate $m(\sim 6.39\times 10^{-8}\,M\ \mathrm{y^{-1}})$, which is critical of the sign of P, is very close to its generally accepts values ($\sim 10^{-9}\,M\ \mathrm{y^{-1}}$) in the binary X-ray sources, bursters and quasi-periodic X-ray sources. Some typical values of P, shown in Table 1, either positive or negative, fall in the range 10^{-21}–$10^{-17}\mathrm{SS^{-1}}$, and are in satisfactory aggreement with the measured ones (Alpar *et al.* 1982). From the conditions (48) we conclude that small accretion rates result always in a period increase, irrespective of the luminosity, while, for heavier accretion rates, both the period increase and decrease are possible depending on the luminosity.

As far as the change of the radius is concerned, from Eqs (26), (43) and (44) we find

$$A_{\mathrm{R}}<0, \quad \dot{m}_{\mathrm{R}}<0, \quad \dot{m}>\dot{m}_{\mathrm{R}}, \tag{51}$$

and

$$L_{\mathrm{R}}\gtrless 0, \qquad \text{if} \qquad \dot{m}_{(17)}\gtrless 2.456, \tag{52}$$

whence Eq (23), due to Eqs (47) takes the form

$$\dot{R}=1.119\times 10^{-3}[L_{(37)}+\dot{m}_{(17)}(1.836\dot{m}_{(17)}^{-1/7}-1.615)]\,\mathrm{cm\,y^{-1}}, \tag{53}$$

and yields

$$\dot{R}\gtrless 0, \quad \text{if} \quad L_{(37)}+\dot{m}_{(17)}(1.836\dot{m}_{(17)}^{-1/7}-1.615)\gtrless 0. \tag{54}$$

So, again, the value of the accretion rate $m(\sim 3.903\times 10^{-9}\ \mathrm{M}\ \ \mathrm{y^{-1}})$, which is critical of the sign of R, is very close to its generally accepted values ($\sim 10^{-9}\ \mathrm{M}\ \ \mathrm{y^{-12}}$) in the same sources as in the case of P. Some typical values of R, shown in Table 1, either positive or negative, fall in the range 10^{-3}–10^{-1} cm $\mathrm{y^{-1}}$ for typical absolute lumenosities 10^{37}–10^{39} $\mathrm{ergs^{-1}}$. From the conditions (52) we conclude that small accretion rates result always in the star's expansion, irrespectively of the luminosity, while for heavier accretion rates both changes are possible depending on the luminosity.

The special case of a burster ($\mathrm{L}\sim 10^{39}$ $\mathrm{ergs^{-1}}$) is attributed to instabilities in the accretion of matter or to thermonuclear flashes in the smoothly accreted matter on the

Table 1. Typical values of P and R for binary X-ray sources(**BXS**) and bursters (**BST**).

$(\bar{m}_{(\odot)} \equiv 1,\ R_{(6)} = 1,\ P_{(-3)} = 1.5,\ \mu_{(30)} = 5 \times 10^{-3},\ \dot{\bar{m}}_{P(17)} = 40.262,\ \dot{\bar{m}}_R < 0)$

$\dot{\bar{m}}_{(17)}$	$L_{(37)}$	$\dot{P}(\mathrm{s\,s^{-1}})$	$\dot{R}(\mathrm{cm\,y^{-1}})$	Object
1	1	3.870×10^{-20}	1.367×10^{-3}	BXS
1	10^2	1.060×10^{-17}	1.122×10^{-1}	BST
2.456	1	-1.122×10^{-20}	1.119×10^{-3}	BXS
2.456	10^2	1.052×10^{-17}	1.119×10^{-1}	BST
5	1	-6.288×10^{-20}	9.447×10^{-4}	BXS
5	10^2	1.047×10^{-17}	1.117×10^{-1}	BST
40	1	-2.570×10^{-21}	-2.264×10^{-2}	BXS
40	10^2	1.060×10^{-17}	8.815×10^{-2}	BST
41	1	1.160×10^{-19}	-2.341×10^{-2}	BXS
41	10^2	1.060×10^{-17}	8.739×10^{-2}	BST
100	10^2	1.182×10^{-17}	3.763×10^{-2}	BXS
150	10^2	1.313×10^{-17}	-3.098×10^{-1}	BST

neutron-star's surface. In the latter case the potential energy of the (practically static) accreted matter, in the pulsar's gravitational field, changes and the flash takes place, when the extra potential energy will exceed the kinetic energy of thermal motion of accreted matter, namely (k is the Boltzamann's .constant)

$$\left(1 - \frac{kT}{5G\bar{m}\mu_{\mathrm{m}}}\right) 2\frac{\dot{\bar{m}}}{\bar{m}} - \frac{\dot{R}}{R} = 0, \tag{55}$$

where T and μ_{m} are absolute temperature and molecular weight of the accreted matter. For hydrogen burning ($T \sim 10^7$ **K**, $\mu_{\mathrm{m}} = 1.673 \times 10^{-24}$g). Eq (55) reduces to

$$\frac{\dot{R}}{R} = 2\frac{\dot{\bar{m}}}{\bar{m}} > 0, \tag{56}$$

implying a radius increase (due to the mass, accretion) followed by the thermonuclear flash (due to the compression) Eqs (53) and (56) hold simultaneously under the condition

$$\dot{\bar{m}}_{(17)} > 2.033 \times 10^{-3} \tag{57}$$

giving the smallest permissible accretion rate for thermonuclear flashes to take place, independently of the luminosity. Moreover, for $m_{(17)}$ in the range 10-100, the luminosity is typical for bursters, $L_{(37)} \sim 10^2$. However, the upper limit of this range should not be considered as a normal feature of the binary and could possibly be met during only the final catastrophic coalescence of a pair's members. On the other hand, *e.g.*, for $m_{(17)} \sim 41$ (see also Eq 48) the increase of mass and radius are 10^{-14} M and 10^{-8} cm for type-**I** bursters (preparation time ~ 10s: Kourganoff 1980), and 10^{-11} M and 10^{-5} cm for type-**II** bursters (preparation time ~1 h). Finally from Eq (53) we verify that for $L_{(37)} \sim 10^2$, direct contraction ($R < 0$) is possible provided that $m_{(17)} > 141$, whence (see last row of Table 1) the corresponding radius change is very large: ~ —10^{-1} cm y^{-1}. In view of the above, the bursters most probably cannot be explained as a result of the pulsar's direct contraction, because both the accretion rate and the radius decrease required are very large.

4. Concluding remarks and outlook

The content of the present article constitutes an as complete and consistent as possible theoretical framework for examining the changes, structural or not, induced on a spherical compact star from the accretion of mass with angular momentum from its non-compact companion in a binary star. The present contributions can be summarized as follows:

(i) To the extent of our knowledge, the article's theoretical framework is the first one in the literature, in which the changes of the compact star's radius (apart from the period) is explicitly evaluated, presented and used.

(ii) The theoretical framework is valid irrespectively of the nature of the compact star (white dwarf or neutron star), and of the specific way of accretion.

(iii) The theoretical framework takes into account all the internal characteristics of the members, assuming the primary's interior to be a uniform degenerate Fermi gas (of electrons or protons) either relativistic or not. It is important that the assumption of relativistic or non-relativistic Fermi gas is only slightly changing the dependence of the results on x (see Eqs 29 and 30 on p. 362 of Chandrasekhar 1939).

(iv) The theoretical framework takes into account and is based on the binary's relative motion correct to post-Newtonian accuracy of general relativity, and not simply the Newtonian, Keplerian orbit. In connection with this, according to Spyrou (1981a, b), such a relativistic dynamical description of a realistic binary requires the use of the binary's total inertial mass (see Eqs 1–4 in the text). This mass generalizes the concept of the Einstein-Infeld-Hoffmann (1938) point mass in the sense that the relativistic correction is described by the mass which is equivalent to the total Newtonian self-energy $\varepsilon_{p}^{(s)}$.

(v) Furthermore, the self-energy is not the same as the one derived in Paper 1, because it contains additionally the contribution of the compact star's magnetic field to its total self energy.

(vi) The compact star's absolute luminosity is defined (see Eq 8 in the text) in terms of its total Newtonian self-energy and not simply its potential energy (namely $L \sim G\bar{m}\dot{\bar{m}}/R$) as elsewhere (see *e.g.* Shapiro & Teukolsky (1983; Eqs 15.1.5, 15.2.20); Ghosh *et al* (1977; Eq 73); Ghosh & Lamb (1979; Section IIIc).

(vii) The theoretical framework provides a full determination of the conditions under which, due to the accretion, the axial period and the radius of the compact star increase, decrease or remain constant.

(viii) In the examined cases of the millisecond pulsars participating the binary X-ray sources, the predicted values for the change of the axial period, either positive or negative, conform with current observational data. Also the predicted change of the radius, for small accretion rates is always an increase irrespectively of the luminosity, while for heavier accretion rates it is either positive or negative depending on the luminosity. In terms of such changes of the radius, the usual phenomenon of the bursters is explained as a result of an accretion-induced thermonuclear flash.

(ix) The theoretical framework applied to the case of old pulsars, naturally completes and extends the results of Paper 1 valid for young compact stars.

In spite of all the advantages above, we have to stress that our results, although conforming with observational data, are approximate. Thus, the compact star has been treated as spherical and homogeneous with its interior described by the relatively

simple Fermi–Dirac statistics. Although we did not check it, we believe that these simplifications will affect our numerical results in a non-significant way. Also, in the currently unknown 2nd Post-Newtonian-Approximation (PNA) extension of the author's dynamical description of the binary's relative orbital motion, a 1st-PNA correction to $\varepsilon_p^{(s)}$ would be necessary. But this has not been examined up to now. Moreover, we neglected the external torque acting on the accreting matter. This assumption, however, at least in the case of the X-ray binaries, cannot be considered as always correct, so that it can change the sign of $\dot{P}$ (and perhaps $\dot{R}$) or even invalidate our results. In any case our results are true for at least a weakly-magnetized neutron-star companion. Furthermore, it could present some interest to examine more closely the case, in which the mass and angular-momentum losses are non-negligible. Finally, our numerical results refer only to pulsars and it certainly will be of particular interest to examine also the case of a white-dwarf primary. Such problems are currently under investigation in the context of the more general research programme initiated by Spyrou (1985, 1987) and continued with the present article.

Acknowledgements

I thank the anonymous referee for his constructive criticism, and his useful comments and suggestions which greatly improved the final form of the article.

References

Alpar, M. A., Cheng, A. F., Ruderman, M. A., Shaham, J. 1982, *Nature,* **300,** 728.
Anzer, U., Bönner, G., Mohaghan, J. J. 1986, MPI Green Report MPA 120, Munich.
Baym, G., Pethick, C. J., Sutherland, P. 1971, *Astrophys. J.*, **170,** 299.
Dewey, R. J., Maguire, G. A., Rawley, L. A., Stokes, G. R., Taylor, J. H. 1986, *Nature,* **322**, 712.
Ehlers, J., Walker, M. 1984, in *Proc. GRG 10 Conference,* Eds B. Bertotti *et al* D. Reidel, Dordrecht, p. 125.
Einstein, A., Infeld, L, Hoffmann, E. 1938, *Ann. Math.,* **39,** 65.
Ghosh, P.,. Lamb, F. K., Pethick, C. J. 1977, *Astrophys. J.,* **217,** 578.
Ghosh, P., Lamb, F. K. 1979, *Astrophys. J.,* **234,** 296.
Hayakawa, S. 1985, *Phys. Rep.,* **121,** 317.
Kourganoff, V. 1980, *Introduction to Advanced Astrophysics,* D. Reidel, Dordrecht.
Lamb, D. D., Patterson, J. Eds1985, *Cataclysmic Variables and Low-Mass X-ray Binaries,* D. Reidel, Dordrecht.
Lewin, W. M. G., van den Heuvel, E. P. J. 1983, Eds *Accretion Driven Stellar X-ray Sources*, Cambridge Univ. Press.
Pandharipande, V. R., Pines, D., Smith, R. A. 1976, *Astrophys. J.*, **208,** 550.
Rawley, L. A., Taylor, J. H., Davis M. M. 1986, *Nature,* **319,** 386.
Segelstein, D. J., Pawley, L. A., Stinebring, D. R., Fruchter, A. S., Taylor, J. H. 1986, *Nature,* **322,** 714.
Shapiro, S. L., Teukolsky, S.A.1983, *Black Holes, White Dwarfs and Neutron Stars: The Physics of Compact Objects,* John Wiley, New York.
Spyrou, N. 1981a, *Gen. Rel. Grav.,* **13,** 473.
Spyrou, N. 1981b, *Gen. Rel. Grav.,* **13,** 487.
Spyrou, N. 1983, *Gen. Rel Grav.,* **15,** 363.
Spyrou, N. 1984, *Gen. Rel. Grav.,* **16,** 411.
Spyrou, N. 1985, *Astr. Astrophys.,* **149,** 283 (Paper 1).
Spyrou, N. 1987, *Astr. Astrophys.,* **174,** 355.

Spyrou, N., Papadopoulos, D. 1985, *Gen. Rel. Grav.,* **17,** 1059.
Taylor, J. H., Stinebring, D. R. 1986, *A. Rev. Astr. Astrophys.,* **24**, 285.
van den Heuvel, E. P. J. 1984, *J. Astrophys. Astr.,* **5**, 209.
van den Heuvel, E. P. J., van Paradijs, J., Taam, R. E. 1986, *Nature,* **322,** 153.
Weisberg, J. M., Taylor, J. H. 1984, *Phys. Rev. Lett.* **52**, 1348.

J. Astrophys. Astr. (1988) **9,** 41–47

Evidence for Moving Features in the Corona from Emission Line Profiles Observed during Eclipses

A. B. Delone, E. A. Makarova, G. V. Yakunina *Sternberg Astronomical Institute, Moscow 119899, USSR*

Received 1985, November 25; revised 1987 July 14; accepted 1988 January 13

Abstract. Using the line profiles of [Fe x] 6374 Å and [Fe XIV] 5303 Å emission lines observed during five total solar eclipses, we address the problem whether the solar corona is static or contains moving features. Many of the profiles of both emission lines have complicated shapes, which we interpret as an evidence for the existence of many, small, moving features in the corona. The line-of-sight velocities observed by other investigators (*e.g.* Desai, Chandrasekhar & Angreji 1982) also support this view. On the other hand, about 15 recent interferometric and multislit investigations of coronal emission lines have not shown evidence of moving elements. We suggest that this is due to insufficient spatial resolution.

Key words: solar corona, emission line profiles—solar corona, moving features

1. Introduction

It is generally believed that the inner solar corona is static, with no macroscopic movements larger than a few km s^{-1}. On the other hand, considerable velocities are exhibited by the chromosphere and solar wind. It is difficult to understand how the static corona exists between these two. In order to resolve this apparent contradiction, we have begun observations of coronal lines [Fe x] 6374 Å and [Fe XIV] 5303 Å simultaneously during solar eclipses. The first successful observations were carried out during the total solar eclipse of 30 May 1965 (Delone & Makarova 1969). The measurements of interferograms showed that the profiles of emission lines have complicated shapes and can be decomposed into individual gaussian components. The observations of four subsequent eclipses confirmed these results.

The interpretation of interferometric profiles poses some difficulties compared with slit spectra, as the interferometric pattern is convolved with the coronal image. Therefore, the intensity at a given point of the profile would also reflect the brightness of the monochromatic corona and the white-light corona. We show in the following that the moving features persist even after the above factors are taken into account.

2. Observational data

We rely on some of the Fabry-Perot interferometric observations of the coronal emission lines obtained during five total solar eclipses: The line [Fe x] 6374 Å was

observed on 30 May 1965 (Delone & Makarova 1969); on 7 March 1970 (Delone & Makarova 1973); on 10 July 1972 (Delone & Makarova 1972); and on 31 July 1981 (Delone, Makarova & Sykora 1983; Ushakov *et al.* 1984; Yaroslavsky *et al.* 1986). The line [Fe XIV] 5303 Å was observed on 22 September 1968 (Delone & Makarova 1975); and on 31 July 1981 (Ushakov *et al.* 1984; Yaroslavsky *et al.* 1986). At all expeditions the instrument used was the same double astrograph with two interferometric devices, so that one could obtain interferometric pictures in two lines simultaneously. The full widths at half maximum (FWHM) of interference filters were 15 or 12 Å at 5303 Å and 15 or 30 Å at 6374 Å. The interferograms were calibrated using a laboratory source (Krypton-filled discharge tube). The orange and green lines of krypton were recorded for calibration just before and immediately after the total phase. Usually the exposure times were in the range 3-30 s, but in 1965 it was 140 s as the sky was poor.

3. Results

The measurements of interferograms are described in detail elsewhere (e.g., Delone & Makarova 1969, 1975; Delone 1974). For the eclipses of 1965 and 1968 the slit of the densitometer was 12 arcsec × 3 arcsec; for the eclipses of 1970, 1972 and 1981, it was 3 arcsec × 3 arcsec (see Table 1). The instrumental profile did not spoil the spatial resolution appreciably, For example, in 5303 Å, FWHM of 0.2 Å corresponds to 5 arcsec. On the radial sections of interferometric pattern of the corona we traced the background continuum in the form of a smooth curve passing through the minima between the rings.

The positions of the maxima of the interferometric pattern for the eclipse of 1970 are shown in Fig. 1. Note the deviations of maxima from the mean ring. Similar shifts were noticed during other eclipses also, and in 1968 these were over protuberances. The magnitude of these shifts corresponds to the ascent of matter up to 60-70 ± 10 km s^{-1}. These shifts indicate the presence of line-of-sight velocities in the corona. Whereas such ring shifts are rare, most line profiles exhibit complicated non-gaussian forms, the profiles of red coronal line being more complicated than the green one. The complex structure of these profiles can be explained either by Doppler shifts and/or by brightness inhomogneities of monochromatic and white-light corona. The reality of the complicated form of the profiles was checked by comparing two independent, consecutive exposures for the eclipse of 1968; some examples are shown in Fig. 2. (The noise in this figure is not smoothed out; the signal-to-noise ratio is 7-10.)

Since the Fabry-Perot fringes are convolved with the spatial distribution of intensity, the inhomogeneities in the background continuum as well as line emission affect the profile.

We have attempted to study the effects of both these factors on the observed line profiles. The evaluation of white-light coronal inhomogeneities was made by a comparison of line profiles with the features observed in the white-light corona. The results are shown in Fig. 3.

Brightness inhomogeneities in emission lines can be seen till 0.2 of free spectral region (FSR), from the positions of line intensity maxima if the reflectivity of the interferometer plates is about 85 per cent. Line emission outside this is cut by the instrumental function. Inside 0.2 of FSR we can estimate the influence of inhomogeneities if we have a simultaneous direct photograph of the emission corona.

Table 1. Catalogue of Fabry-Perot (FP) and multislit (MS) observations of coronal emission lines.

Eclipse	Authors	Method	Spatial resolution (arcsec²)
21 September 1941	Kalinijak (1949)	FP	Unknown
30 July 1954	Jarett & Klüber (1955)	FP	Unknown
12 October 1958	Jarett & Klüber (1961)	FP	Unknown
30 May 1965	Delone & Makarova (1969)	FP	3 × 12
	Liebenberg, Bessey & Watson (1975)	FP	1380
12 November 1966	Liebenberg, Bessey & Watson (1975)	FP	Unknown
22 September 1968	Delone & Makarova (1975)	FP	3 × 12
7 March 1970	Delone & Makarova (1973)	FP	c × 3
	Hirschberg, Wouters & Hazelton (1971)	FP	Unknown
	Marshall & Henderson (1973)	FP	0.1 $R_\odot$
	Livingston, Harvey & Doe (1970)	MS	100
10 July 1972	Kim & Nikolsky (1975)	FP	190
	Delone & Makarova (1973)	FP	10
30 June 1973	Bessey & Liebenberg (1984)	FP	
16 February 1980	Chandrasekhar, Desai & Angreji (1981)	FP	80
	Desai, Chandrasekhar & Angreji (1982)	FP	80
	Livingston & Harvey (1982)	MS	70
	Singh, Bappu & Saxena (1982)	MS	220
	Singh (1984)	MS	220
	Singh (1985)	MS	220
	Bhatnagar *et al.* (1982)	MS	Unknown
31 July 1981	Ushakov *et al.* (1984)	FS	10
	Yaroslavsky *et al.* (1986)	FS	10
11 June 1983	Singh (1984)	MS	5 × 9

At the eclipse of 1981 we have photographed the corona in 5303 Å and 6374 Å lines. The variation of emission-line intensity and the corrections required by it in the observed line profile are shown in Fig. 4 in the case of two examples. Note that the correction required is rather small.

The smoothed line-profiles, corrected for the influence of background continuum and emission line variations, can be decomposed into individual gaussian components as shown in Fig. 5. The number of components appear to be different for the red and green lines at a given location, the red line exhibiting more structure. The sizes of the moving feature are in the range 10-30 arcsec, which agrees with the range 5–35 arcsec

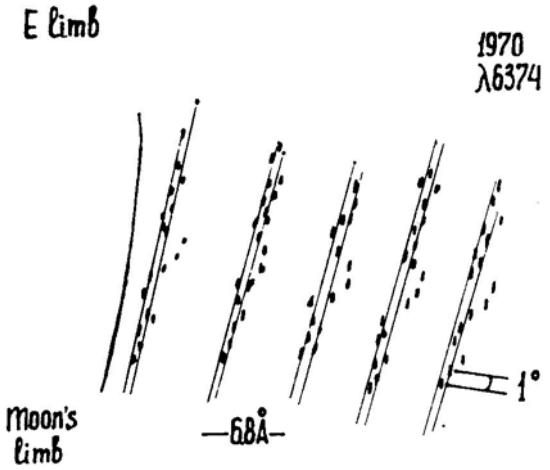

Figure 1. Positions of interference maxima showing ring shifts along a narrow coronal beam; 1970, 6374 Å.

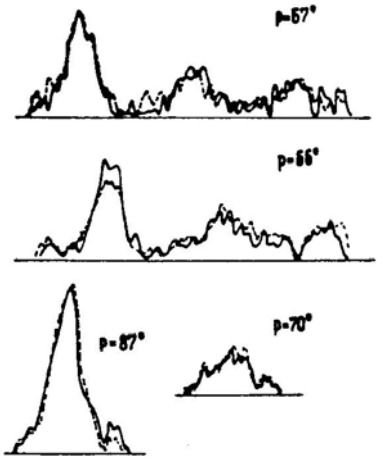

Figure 2. The profiles of the 5303 Å line in 1968:– – – t = 5^s;——1 = 3^s.

in the sizes of small-scale features measured in the emission-line corona (Picat *et al.* 1973; Fort & Picat 1975; Tsubaki 1975). The continuum variations affect the line profiles much more than the monochromatic ones. A large fraction of features persist even after these corrections are made.

4. Discussion

It is well-known that the brightness of solar corona decreases sharply with distance from solar limb. Assuming that moving features have their velocity vectors in the radial direction, the line profiles close to the solar limb would have a predominant contribution from features closer to the limb, moving perpendicular to the line of

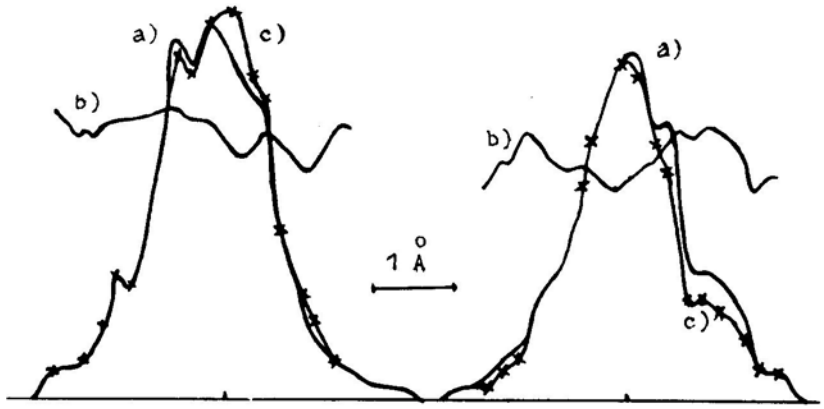

Figure 3. 5303 Å line profiles; (a) observed profiles; (b) monochromatic brightness distribution; (c) corrected profiles.

Figure 4. Examples of nongaussian profiles in 1981: (a) 5303 Å, (b) 6374 Å.

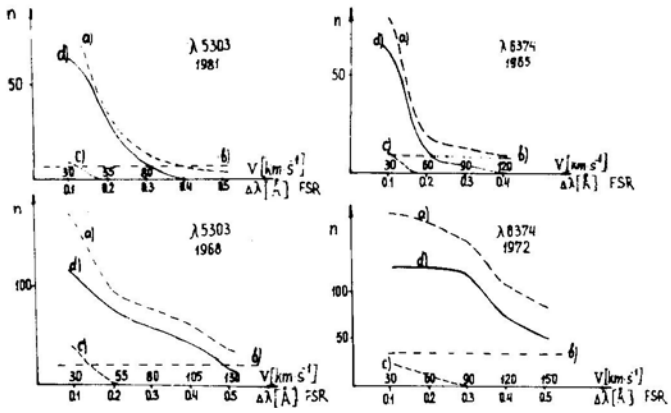

Figure 5. Velocity distribution of 5303 Å and 6374 Å features; (a) total number of moving features; (b) white light photometrically, induced features: (c) monochromatic photometrically induced features; (d) corrected velocity distribution.

sight. On the other hand, as one moves away from the solar limb, contribution from features moving at different angles would become more important. Thus we would expect the halfwidth of the profiles to increase with radial distance from the solar limb. This is clearly seen in Fig. 6 (a) providing indirect support for the existence of moving features: However, in the case of the corona of 1965 above an active region with very

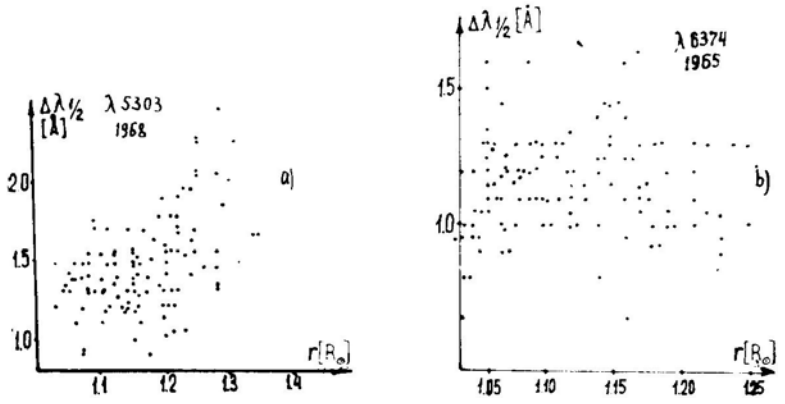

Figure 6. 5303 Å and 6374 Å halfwidth variation with distance from solar limb, (a) 1968; 5303 Å. (b) 1965; 6374 Å; the observations were near an active region.

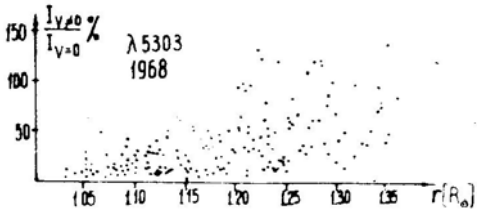

Figure 7. Dependence of the relative brightness of the moving features with distance from the solar limb; 1968; 5303 Å.

closed configuration, the halfwidth did not decline as sharply with radial distance (see Fig. 6b). A similar effect is seen in the intensities of moving features shown in Fig. 7.

Table 1 shows that most of the past results on coronal line profiles were based on rather poor spatial resolution (observational plus microdensitometric). We believe that increased spatial resolution would reveal the moving features. We quote Athay (1976); 'It is more generally believed that these phenomena [moving features in the corona] are present, as they are everywhere else in the solar atmosphere, but that we do not yet have sufficiently good observations to reveal them.'

Since the moving features add to the width of lines, one needs to exercise caution in estimating coronal temperature from the halfwidths of line profiles.

Acknowledgements

We wish to acknowledge helpful comments by the referees and Drs J. Singh and T. Chandrasekhar.

References

Athay R. G. 1976, in *The Solar Chromosphere and Corona*: *Quite Sun,* D. Reidel, Dordrecht. p. 123.

Bessey, R. J., Liebenberg, D. H. 1984, *Solar Phys.*, **94,** 239.

Bhatnagar, A., Jadhav, D. B., Jain, R. M., Shelke, R. N., Purohit, S. P. 1982, *Proc. Indian Nat.* Sci. *Acad.*, A48, Suppl. 3, 29.

Chandrasekhar, T., Desai, J. N., Angreji, P. D. 1981, *Appl. Opt.,* **20,** 2172.
Deone, A. B. 1974, *PhD Thesis,* Moscow Univ.
DeOne, A. B., Makarova, E. A. 1969, *Solar Phys.,* **9,** 116.
DeOne, A. B., Makarova, E. A. 1970, *Astron. Cirk,,* No. 572, 1.
DeOne, A. B., Makarova, E. A. 1972, *Astron. Cirk.,* No. 727, 1.
DeOne, A. B., Makarova, E. A. 1973, *Astron. Cirk.,* No. 772, 1.
DeOne, A. B., Makarova, E. A. 1975, *Solar Phys.,* **45,** 157
DeOne, A. B., Makarova, E. A., Sykora, J. 1983, *Publ. Debrezen Heliphys. Observ.,* 517.
Desai, J. N., Chandrasekhar, T., Angreji, P. D. 1982, *J. Astrophys. Astr.,* **3,** 69.
Fort, B., Picat, J. P. 1975, *Astr. Astrophys.,* **44,** 17.
Hirschberg, J. G., Wouters, A., Fried, W. I., Cooke, F. N. Jun., Duke, D., Read, M. 1970, *Nature,* **226,** 1142.
Hirschberg, J. G., Wouters, A., Hazelton, L. Jr. 1971, *Solar Phys.,* **21,** 448.
Jarrett, A. H., Klüber, H. von 1955, *Mon. Not. R. astr. Soc, US,* **115,** 343.
Jarrett, A. H. Klüber, H. von 1961, *Mon. Not. R. astr. Soc,* **122,** 223.
Kalinijak, A. A. 1949, in *Trudy expedicii nabludenij polnogo solnechnogo zatmeniy* 21 *sentijbiy* 1941 goda, Moskow, p. 352.
Kim, I. S., Nikolsky, G. M. 1975, *Solar Phys.,* **43,** 351.
Liebenberg, D. H., Bessey, R. J., Watson, B. 1975, *Solar Phys.,* **44,** 345.
Livingston, W., Harvey, J. 1982, *Proc. Indian Nat. Sci. Acad.* **A48,** Suppl. 3, 18.
Livingston, W., Harvey, J., Doe, L. A. 1970, *Solar Eclipse* 1970 *Bulletin.* F., 72.
Marshall, P., Henderson, G. 1973, *Solar Phys.,* **33,** 153.
Picat, J. P., Fort, B., Dantel, M., Leroy, J. L. 1973. *Astr. Astrophys.* **24,** 259.
Singh, J. 1984, *PhD Thesis,* Punjabi University, Patiala.
Singh, J. 1985, *Solar Phys.,* **95,** 253.
Singh, J., Bappu, M. K. V., Saxena, A. K. 1982, *J. Astrophys. Astr.,* **3,** 249.
Smartt, R. N., Zirker, J. B., Mauter, H. A. 1982, *Proc. Indian Nat. Sci. Acad.* **A48,** Suppl. 3, 102.
Tsubaki, T. 1975, *Solar Phys.,* **43,** 147.
Ushakov, A. N., Yaroslavsky, L. P., Delone, A. B., Makarova E. A., Yakunina, G. V. Charugin, V. M., Dagaev, M. M. Degulev, V. S., 1984, *Astron Cirk.,* No. 1340, 2.
Yaroslavsky, L. P., Ushakov, A. N., Delone, A. B., Makarova, E. A., Yakunina, G.V., Charugin, V. M. Dagaev, M. M., Jegulev, V. S., 1986, in *Resultaty nabludeniy solnechnogo zatmeniy* 31 *iuliy* 1981 *goda,* VAGO, Moskow, p. 54.

J. Astrophys. Astr. (1988) **9,** 49–61

Spacetime with Self-Gravitating Thick Disc

Sandip K. Chakrabarti* *Theoretical Astrophysics, California Institute of Technology, Pasadena, CA 91125, U.S.A.*

Received 1987 October 5; accepted 1988 January 28

Abstract. We compute the metric coefficients and study some properties of the spacetime comprising of a Schwarzschild hole distorted by a self gravitating thick disc.

Key words: black hole, accretion disc—self gravity

1. Introduction

Thick accretion discs are formed when the radiation emitted during accretion interacts with the accreting matter dynamically, resulting in puffing up of the disc. The description of such discs can be obtained in a number of papers (*e.g.* Abramowicz, Jaroszynski & Sikora 1978; Jaroszynski, Abramowicz & Paczyński 1980; Paczyński & Abramowicz 1982; Paczyński & Wiita 1980; Chakrabarti 1985a,b, henceforth referred to as Papers 1 & 2). In these works the disc structures are calculated assuming the self-gravity effect due to the disc is negligible. The characteristic density of the disc at which this effect becomes important is $M_{\rm hole}^3/r_{\rm c}$ ($\simeq 0.05$ g cm $^{-3}$ for a hole of mass $10^8\,M_\odot$, $r_{\rm c}$ is the radius of the centre of the disc). It is not clear at what maximum mass the disc is still stable against the local gravitational instabilities, but even when the ratio $M_{\rm disk}/M_{\rm hole} = m$ is as small as 0.01, the numerical works (*e.g.* Wilson 1981) with self-gravity effect has shown the outer edge of the disc to be sensitive to the disc mass. Some work on self-gravitating discs with pseudo-Newtonian geometry has been carried out by Abramowicz, Calvani, & Nobili (1983) and Abramowicz *et al.* (1984). In a somewhat different approach, Will (1974, 1975) has discussed the effect of a ring in Kerr geometry. His analysis was carried out by perturbation theory. However, for static, axially symmetric, spacetime the solution of the problem is exact. In this paper we determine the metric coefficients of the spacetime with a black hole surrounded by a self-gravitating disc and study some of the properties.

The approach of the present analysis will be the following: When some matter is distributed around a hole, the hole cannot be considered to be isolated. It becomes distorted, so to speak, due to the gravitating matter outside the horizon. Under the circumstances when the matter is static, and axially symmetrically distributed around a hole, it is possible to write down the metric of the region of the spacetime devoid of

* Present address: International Center for Theoretical Physics PO Box 586, Miramare, Strada Costiera 11, 34100 Trieste, Italy.

matter in terms of the so-called distorted hole metric (Mysak & Szekeres 1966; Geroch & Hartle 1982, henceforth referred as GH; Chandrasekhar 1983). Because of the complexity of the problem, we shall replace the disc by a ring of the same mass located at the centre of the disc. Since most of the mass of the disc *is* concentrated near the centre of the disc, this may not be a bad assumption. Essentially, we shall be studying the properties of the matter in the combined field of the black hole and the ring of matter instead of the field of the black hole alone.

Here we give expectations of what might happen when the self-gravity is turned on. One would naively think that the centripetal force upon an element of matter orbiting between the hole ($r = r_{\rm h}$, $r_{\rm h}$ being the horizon size) and the ring ($r = r_{\rm c}$) will be reduced because of the outward pull by the ring than otherwise. Thus the angular momentum needed by the element to stay in a Keplerian orbit would be less than what is needed if the ring were absent. Similarly, the required angular momentum will be more if the element orbits beyond the ring. This changes the nature of the pressure gradient force needed to support the disc for a given angular momentum distribution. Below we point out that one has to be somewhat careful in talking about cases with and without self-gravity side by side. This is essential because in the framework of general relativity, strictly speaking, it is meaningless to compare the two problems. For example, if one solves the problem without self-gravity turned on with a black hole mass $M_{\rm hole}$, then when the ring of 'mass' $M_{\rm ring}$ is present, what mass of the hole should be used so that the comparison is a meaningful one? What is the definition of the mass of the hole anyway? The mass arises as a constant of integration which is identified as the mass of the hole because at infinity, the potential term 'looked' like that of a Newtonian body of mass $M_{\rm hole}$. With the ring present, the potential at infinity will be that due to the sum of the hole mass and that of the disc. Thus, dealing with the properties of the hole between $r = r_{\rm h}$ and $r_{\rm ring}$ one does not know how to separate the contributions of the mass of the disc, the mass of the hole and the binding energy between the hole and the disc. This problem appears because there is no 'Newtonian limit' of the region between the horizon and the ring. A similar problem arises in the definition of angular momentum. It can easily be shown that several different definitions of angular momentum (henceforth always assumed to be the specific quantity, namely, the angular momentum per unit mass) go over to the Newtonian value when the proper limit at a large distance is taken. For example, $-u_\phi$, $-u_\phi/u_t$, $u_\phi u_t$ all go over to ΩR^2 at infinity but between the hole and the ring only $-u_\phi$ can be considered as the conserved angular momentum. The situation is further aggravated by the question: suppose we have a well-defined quantity to compare. Then, one should quite reasonably compare them at the same spacetime point and not at the same coordinate point. For example, the potential at some $r = r_0$ before self-gravity of the disc is turned on, should not be compared with that after the self-gravity at $r = r_0$ where r is, say, the spherical polar coordinate used in both spacetimes. We shall put emphasis on these points clearly whenever such confusions arise.

Other than the complexities mentioned above, the problem of finding the equi-potentials for the discs is not at all different from what is done in Papers 1 and 2 as both the cases are stationary and axisymmetric. We remind the readers what is done in these papers: When the matter distribution is assumed to be barotropic, the surfaces of constant specific angular momentum l and the surfaces of the constant angular velocity Ω coincide provided matter is predominantly rotating. The solution of the Euler equation is obtained by using an angular momentum distribution as a power

Law of von-Zeipel parameter λ given by,

$$\lambda^2 = \frac{l}{\Omega}. \tag{1}$$

The behaviour of λ(Papers 1 and 2, also Abramowicz 1982, where it is denoted by R) is similar to axial distance R in Newtonian geometry and it is always possible to define this quantity in any axisymmetric spacetime. Thus, with $l = c\lambda^n$ (c and n being a pair of constants defining the distribution) one obtains the effective potential W defined to be $dW = -\int dp/(p+\varepsilon)$, (where, ρ and ε are the isotropic pressure and the energy density respectively and the equation of state is chosen to be barotropic) as given by,

$$\frac{e^W}{u_t(1-c^2\lambda^{2n-2})^\alpha} = \text{constant}. \tag{2}$$

Here α is given by,

$$\alpha = \frac{n}{2n-2}$$

and u_t is the specific binding energy and can be calculated from the normalization condition as,

$$u_t = \left[\frac{-(g_{t\phi}^2 - g_{tt}g_{\phi\phi})}{(g_{\phi\phi} + lg_{t\phi})(1-c^2\lambda^{2n-2})}\right]^{1/2} \tag{3}$$

The quantities $g_{\mu\nu}$ are the metric coefficients for the axisymmetric spacetime considered. Therefore, the same solution as given by equation (2) is valid in the case where the disc is massive. In Papers 1 and 2, λ was calculated using the Schwarzschild metric: $\lambda = \left(-\frac{g_{\phi\phi}}{g_{tt}}\right)^{1/2}$. Here, however, Λ (defined here in capital letter so as to distinguish from that without the self-gravity of the disc) has to be calculated with the new metric components. Thus, solving the problem with self-gravity boils down to determining the new metric coefficients.

2. The metric coefficients

The calculation of the metric coefficients is done with the assumption that the ring is static and is symmetrically placed in the equatorial plane around a Schwarzschild hole. It is easy to show that the rotational energy of the matter at the centre of the disc is less than 10 per cent of the rest mass energy. The rotational effect will introduce a small $g_{t\phi}$ component of the metric which is proportional to $m = M_{\text{disk}}/M_{\text{hole}}$ and the specific angular momentum of the ring. Thus, our analysis of replacing the rotating disc by a static ring is justified for $m < 1$.

In Weyl coordinates (ρ and z) the line element of a static axisymmetric spacetime takes the form (Synge 1964),

$$ds^2 = \exp[2(\gamma-\psi)](d\rho^2 + dz^2) + \rho^2\exp(-2\psi)d\phi^2 - \exp(2\psi)dt^2 \tag{4}$$

where, ρ and z are the Weyl coordinates given by,

$$\rho = r\sin\theta\sqrt{\left(1-\frac{2}{r}\right)} \tag{5a}$$

and

$$z=(r-1)\cos\theta \tag{5b}$$

in the usual spherical coordinate system. The hole mass has been chosen to be unity as before, $\psi = \psi(\rho, z)$ and $\gamma = \gamma(\rho, z)$ are two scalar functions. In the empty spacetime, the Einstein equation $R_{\mu\nu} = 0$ takes the form,

$$\psi_{,\rho\rho}+\frac{1}{\rho}\psi_{,\rho}+\psi_{,zz}=0 \tag{6a}$$

$$\gamma_{,\rho}=\rho[(\psi_{,\rho})^2-(\psi_{,z})^2], \tag{6b}$$

and

$$\gamma_{,z}=2\rho\psi_{,\rho}\psi_{,z} \tag{6c}$$

where the comma in front of ρ and z denotes the differentiation with respect to them. Notice from equation (6a) that ψ satisfies the 'flat' metric Laplacian. In particular, this means that the sum of two solutions, namely, ψ_h (potential due to the hole alone) and ψ_r (potential due to the ring alone) is another solution. In our case, ψ_h will be given by,

$$\psi_h=\tfrac{1}{2}\log\left(1-\frac{2}{r}\right) \tag{7}$$

corresponding to the Schwarzschild metric. The potential ψ_r will be due to the ring and $\psi_t = \psi_h + \psi_r$ will be the total potential due to the hole ring system, γ is calculated by the requirement that it should vanish on the axis of symmetry and then performing the integration,

$$\gamma=\int_{ABC}\rho\left[\left[\left(\frac{\partial\psi}{\partial\rho}\right)^2-\left(\frac{\partial\psi}{\partial z}\right)^2\right]d\rho+2\frac{\partial\psi}{\partial\rho}\frac{\partial\psi}{\partial z}dz\right], \tag{8}$$

where, ABC denotes any path lying entirely in the region devoid of matter, beginning on the axis of symmetry and ending on the field point (see Fig. 1). The solution for ψ_r and γ are obtained (Weyl 1917; Bach & Weyl 1922) in terms of the complete elliptic functions and are given by,

$$\psi_r=-\frac{\frac{2}{\pi}mK(\kappa)}{[(\rho+b)^2+z^2]^{1/2}}. \tag{9a}$$

When the hole is absent, so $\psi_h = 0$ and Equations (5) become $\rho = r\sin\theta$ and $Z = r\cos\theta$, the Bach-Weyl solution for γ is

$$\gamma=\frac{m^2\kappa^4}{4\pi^2b\rho}[-K^2+4(1-\kappa^2)K\dot{K}+4\kappa^2(1-\kappa^2)\dot{K}^2]$$

$$+\frac{m^2\kappa^4}{4\pi^2b^2}[-K^2+4(1-\kappa^2)K\dot{K}-4\kappa^2(1-\kappa^2)(2-\kappa^2)\dot{K}^2], \tag{9b}$$

where, $K = dK/d\kappa^2$ and

$$\kappa\equiv\left[\frac{4b\rho}{(\rho+b)^2+z^2}\right]^{1/2}. \tag{9c}$$

The ring is placed at $\rho = b$ and m is the mass of the ring.

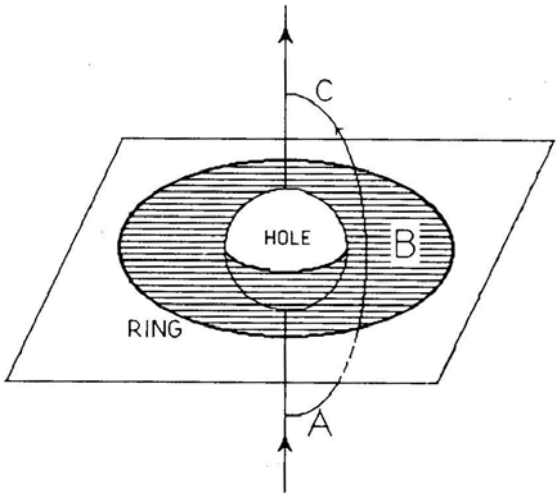

Figure 1. The geometry of hole and thick disc is modeled as a Schwarzschild hole surrounded by a ring on the equatorial plane. Integration in equation (8) is done along the curve ABC which lies entirely in the empty space between the hole and the ring intersecting the equatorial plane in the shaded region.

Although, these solutions are in closed form, and for some extreme limiting cases they can be written down in terms of elementary functions, for our purposes we would like to re-derive ψ_r by using a new 'spherical' polar coordinate system Π and Θ, such that, $z = \Pi\cos\Theta$ and $\rho = \Pi\sin\Theta$. Thus, in terms of the usual polar coordinates r and θ,

$$\Pi^2 = r^2 - 2r + \cos^2\theta \tag{10a}$$

and

$$\Theta = \tan^{-1}\frac{\rho}{z} = \frac{\sqrt{r(r-2)}\tan\theta}{(r-1)}. \tag{10b}$$

If now the ring be kept on the equatorial plane $\left(\theta = \frac{\pi}{2} = \Theta\right)$ at $r = r_c$, then in terms of the new coordinate system it is located at $\Pi_c = \sqrt{r_c(r_c - 2) = b}$. The solution of the Laplace equation for the ring of matter is given by,

$$\psi_{r<} = -m \sum_{l(\text{even})} \frac{\Pi^l}{\Pi_c^{l+1}} P_l(\cos\Theta) P_l(0) \tag{11a}$$

for $\Pi < \Pi_c$, and

$$\psi_{r>} = -m \sum_{l(\text{even})} \frac{\Pi_c^l}{\Pi^{l+1}} P_l(\cos\Theta) P_l(0) \tag{11b}$$

for $\Pi > \Pi_c$. The P_l are the Legendre polynomials of order l. Odd l polynomials give zero contribution so the sum is over even l only. Here m denotes the ratio of the disc mass in the unit of the original hole mass. Upon expansion, Equations (1 1a,b) become,

$$\psi_{r<} = -m\left[\frac{1}{\Pi_c} - \frac{\Pi^2}{4\Pi_c^3}(3D-1) + \frac{3\Pi^4}{64\Pi_c^5}(35D^2 - 30D + 3) - \ \ldots\ \right] \tag{12a}$$

and

$$\psi_{r>} = -m\left[\frac{1}{\Pi} - \frac{\Pi_c^2}{4\Pi^3}(3D-1) + \frac{3\Pi_c^4}{64\Pi^5}(35D^2-30D+3) - \cdots\right] \tag{12b}$$

Where

$$D = \cos^2\Theta = \frac{(r-1)^2\cos^2\theta}{r^2-2r+\cos^2\theta}.$$

At this point it is important to remember that Equation (6a) is linear, so that even if the series expansion for ψ_r is terminated after some finite terms, ψ_r still remains the solution of that equation. But, unless all the terms are kept in the series, ψ_r will not represent the potential due to a ring but some other matter distribution close to it. Fig. 2 shows the surface of constant ψ_r with terms up to $l = 6$. (Ignore the kinks in the contours, as they are due to the choice of a coarse grid.) Near the ring it resembles the potential due to a torus, but far away from the hole the potential is almost spherically symmetric as expected. With this potential the new metric coefficients g_{tt} and $g_{\phi\phi}$ can be calculated from,

$$g_{tt} = \left(1 - \frac{2}{r}\right)e^{2\psi_r} \tag{13a}$$

and

$$g_{\phi\phi} = -r^2\sin^2\theta e^{-2\psi_r}. \tag{13b}$$

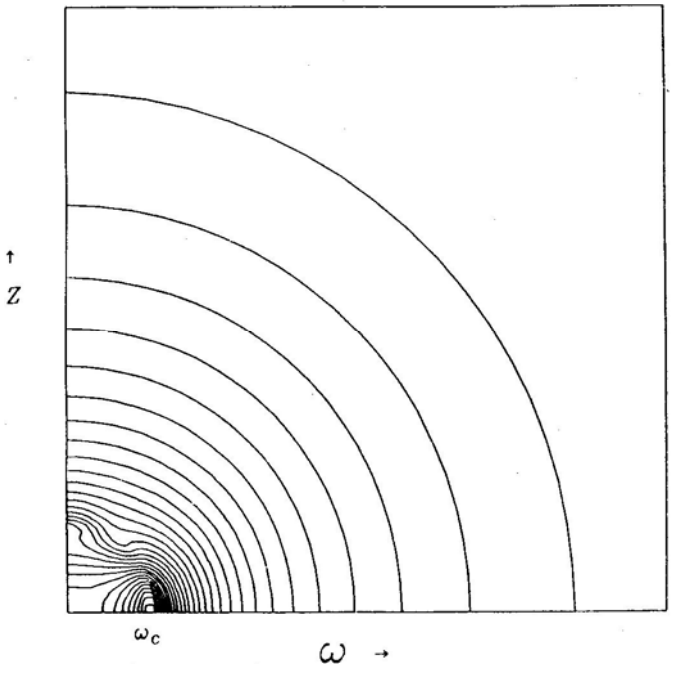

Figure 2. The equipotential surfaces due to the ring in Schwarzschild geometry with terms up to $l = 6$ (see equations 1 la and l1b). Ignore the kinks in the contours, as they are due to choice of a coarse grid. Near the ring it resembles the potential due to a torus, and far away the potential is almost spherically symmetric and is due to a total mass of $M_{\text{hole}} + M_{\text{ring}}$ as expected.

Hence the von Zeipel parameter Λ is given by,

$$\Lambda = \frac{r\sin\theta}{\sqrt{1-\frac{2}{r}}} e^{-2\psi_r} \tag{14}$$

One word of caution is in order. A natural, geometrical definition of 'radius' and a definition intimately connected with angular momentum is (radius) ≡ ϖ= (circumference)/2π.In the metric without the ring $\varpi = r\sin\theta$, while in the new metric $\varpi = \sqrt{-g_{\phi\phi}} = r\sin\theta\, e^{-\psi_\Gamma}$. Hence any property at $R = r\sin\theta$ in the old metric should be compared with that property at $Re^{-\psi_\Gamma}$ and not at R.

3. Properties of hole-ring spacetime

We now study very briefly the properties of the hole-ring spacetime. Notice first that both the $\psi_{r<}$ and $\psi_{r>}$ are regular in their respective domains. On the axis with $r<r_c$,

$$\psi_{r<}|_{\text{axis}} = -m\left[\frac{1}{\Pi_c} - \frac{\Pi^2}{2\Pi_c^3} + \frac{3\Pi^4}{8\Pi_c^5} - \ldots\right] \tag{15}$$

and on the equatorial plane,

$$\psi_{r<}|_{\text{eq}} = -m\left[\frac{1}{\Pi_c} + \frac{\Pi^2}{4\Pi_c^3} + \frac{9\Pi^4}{64\Pi_c^5} + \ldots\right] \tag{16}$$

Now the equation of the horizon is given by,

$$g_{tt} = 0 = \left(1-\frac{2}{r}\right)e^{2\psi_r}. \tag{17}$$

On the equator, the horizon is located at ,$\varpi_{EH} = 2e^{-\psi_{r<}|EH}$, with ($\Pi^2 = 0$),

$$\psi_{r<}|_{EH} = -\frac{m}{\Pi_c},$$

whereas on the axis, the horizon is at $\varpi_{AH} = 2e^{-\psi_{r<}|AH}$, with ($\Pi^2 = 1$),

$$\psi_{r<}|_{AH} = -m\left(\frac{1}{\Pi_c} - \frac{1}{4\Pi_c^3} + \frac{9}{64\Pi_c^5} - \ldots\right).$$

Clearly, as a result of the ring, the horizon is of oblate shape and bulged in the equatorial plane.

The Keplerian angular momentum can be derived from the geodesic equation,

$$\frac{d^2x^\mu}{d\tau^2} + \Gamma^\mu_{\alpha\beta}u^\alpha u^\beta = 0. \tag{18}$$

Here $\Gamma^\mu_{\alpha\beta}$ is the Christoffel symbol and τ is the proper time measured along the geodesic. The first term vanishes since $u^\phi = d\phi/d\tau$ and $u^t = dt/d\tau$, which arc the only nonvanishing components of the velocity vector, are along Killing directions. Expanding the second term in terms of the components we obtain.

$$\Gamma^\mu_{\alpha\beta}u^\alpha u^\beta = (\Gamma_{rtt}dt^2 + 2\Gamma_{rt\phi}dtd\phi + \Gamma_{r\phi\phi}d\phi^2)d\tau^{-2} = 0. \tag{19}$$

Substituting the Christoffel symbol we find the Keplerian frequency Ω_k to be,

$$\Omega_k \equiv \frac{d\phi}{dt} = \sqrt{-\frac{g_{tt,r}}{g_{\phi\phi,r}}} = \Omega_0 e^{2\psi_r}, \tag{20}$$

where,

$$\Omega_0 = \left[\frac{1 + r(r-2)\dfrac{\partial \psi_r}{\partial r}}{r^3 - r^4 \dfrac{\partial \psi_r}{\partial r}}\right]^{1/2}$$

Hence the Keplerian specific angular momentum is given by,

$$l_k = \Omega_0 e^{-2\psi_r} \frac{r^2}{1 - \dfrac{2}{r}}. \tag{21}$$

The distribution is clearly discontinuous at $\Pi = \Pi_c$ because of the discontinuity of $\partial\psi_r / \partial_r$.

The above equations have been written down in spherical polar coordinates. They become much simpler and more transparent if the following tetrads arc chosen instead, namely,

$$\lambda_t^{(t)} = \sqrt{\left(1 - \frac{2}{r}\right)} \exp(\psi), \tag{22a}$$

$$\lambda_\phi^{(\phi)} = (r \sin\theta)\exp(-\psi), \tag{22b}$$

$$\lambda_\rho^{(\rho)} = \exp(\gamma - \psi), \tag{22c}$$

$$\lambda_z^{(z)} = \exp(\gamma - \psi). \tag{22d}$$

It is useful to write down the equations in the form in which a comparison can be made with the result calculated without self-gravity (WSG) terms. First we note that (with self-gravity included) the use of a new radial distance $\omega = re^{-\psi_r}$ and the use of the unit of $M' \rightarrow M_{\text{hole}} e^{-\psi_r}$, simplify the equations very much. (This 'reduced' mass of the hole goes over to $Me^{-\psi_{r(\text{horizon})}}$ as prescribed by Geroch & Hartle 1982.) In this unit, we derive,

$$\Lambda(\omega) = \frac{\omega \sin\theta}{\sqrt{1 - \dfrac{2}{\omega}}}, \tag{23a}$$

$$\Omega_k(\omega) = \left[1 + \omega(\omega - 1)\frac{\partial \psi_r}{\partial \omega}\right]^{1/2} \frac{1}{\omega^{3/2}}, \tag{23 }$$

$$l_k(\omega) = \Omega_k \Lambda^2 = \left[1 + \omega(\omega - 1)\frac{\partial \psi_r}{\partial \omega}\right]^{1/2} \frac{\omega^{3/2}}{(\omega - 2)}. \tag{23c}$$

(The Equations 23b–c are defined in the plane of the ring.) The plot of Keplerian specific angular momentum versus ω is shown in Fig. 3(a–c) for various values of *m*, the ratio of the disc mass to the hole mass. Angular momentum has been measured in the unit of M' since the hole size is changed. The dotted line corresponds to the

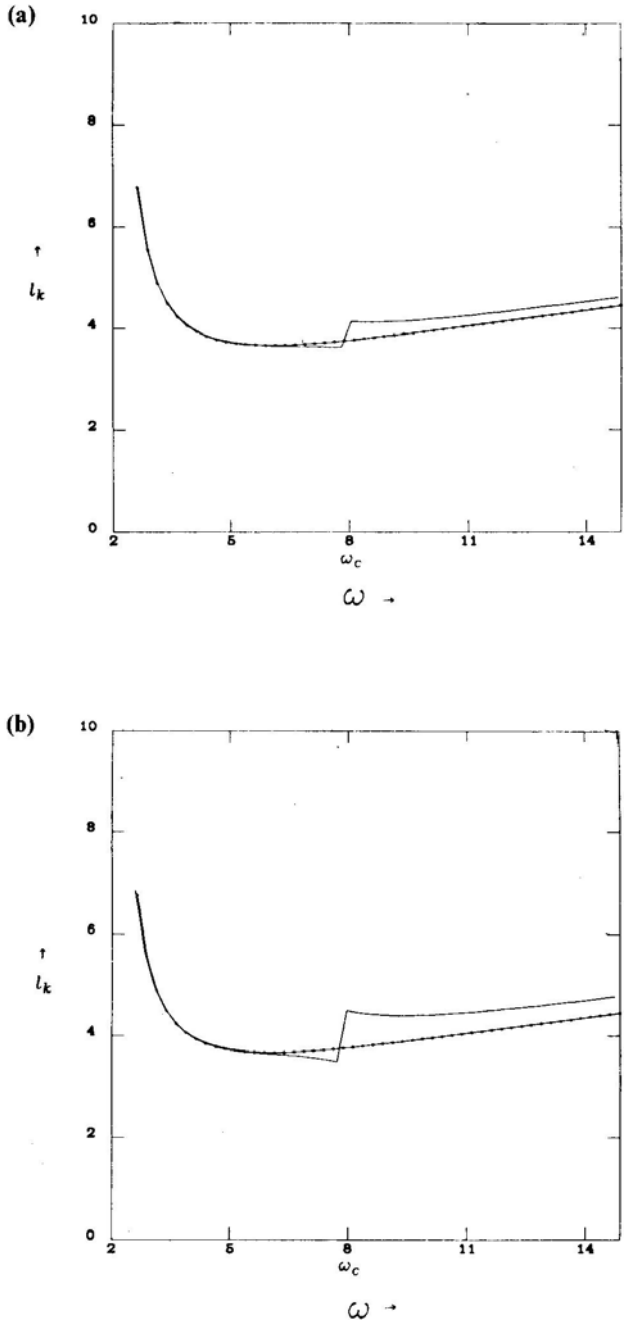

Figure 3. The Keplerian angular momentum distribution is compared without (dotted curve, plotted against $\omega = R$) and with (undotted curve, plotted against $\omega = Re^{-\psi_r}$) the self-gravity effect for various values of $m = M_{\text{hole}}/M_{\text{ring}}$. The dotted curve is given by Equation (23c); the undotted curve is the same equation with $\psi_r = 0$. In (a), $m = 0.05$, in (b) $m = 0.1$, and in (c) $m = 0.2$. Because of the ring, angular momentum needed to stay in a circular orbit is less or greater than what is necessary when the ring is absent, depending upon whether the particle is between the hole and the ring or between the ring and infinity.

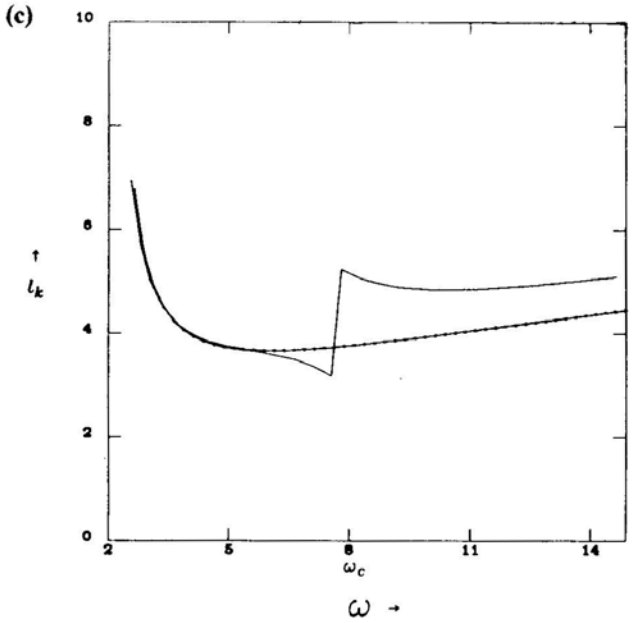

Figure 3. Continued

Keplerian angular momentum in WSG case. The unit of both ω and l_k is such that M' = 1. Very near the hole, angular momentum remains almost the same but near the ring $l_k(\omega)$ decreases for $r<r_c$. Away from the ring it increases in the same way as we discussed earlier. Notice the discontinuity of the angular momentum at the ring. For a real disc with nonsingular matter distribution, the angular momentum increases smoothly from the lower value to the higher value passing through the original Keplerian curve at r_c.

4. Discs and inner jets in the hole-ring spacetime

In Papers 1 and 2, we have shown the surfaces of constant potentials for the discs and the inner jets. By using the von-Zeipel parameter Λ and the new metric coefficients as discussed above the effective potential W and the enthalpy density h of Papers 1 and 2 can be calculated in the case where the self-gravity is important. They are given by,

$$e^{(W-\psi_r)} = C_1\sqrt{(1-2/\omega)}(1-c_\phi^2\Lambda^{2n-2})^{\frac{1}{2n-2}} \tag{24a}$$

and

$$he^{\psi_r} = \frac{C_2}{\sqrt{(1-2/\omega)}(1-c_\phi^2\Lambda^{2n-2})^{\frac{1}{2n-2}}}, \tag{24b}$$

where C_1 and C_2 are the constants to be evaluated by using proper boundary conditions. The presence of ψ_r in both the equations and ω and Λ instead of r and λ respectively, make all the difference between the two cases. One has to remember that both ω and Λ were measured in the units of the variable 'hole mass' $M' = M_{\rm hole}e^{-\psi_r}$. This makes the comparison at the same spacetime point meaningful. The decrement of

the potential makes the disc more strongly bound. In fact, it has been recently shown (Goodman & Narayan 1988) that moderate self-gravity *damps* out the non-axisymmetric instabilities of the disc.

One can calculate the variation of the total energy content of the disc when some small amount of matter (few baryons) is transferred from the ring to the hole. The potential of the ring at the horizon is obtained by puting $z = \pm M_{\rm hole}$ (Notice that in Weyl coordinate the black hole is represented as a line mass of length $2M_{\rm hole}$ placed along the axis.),

$$\psi_{\rm h} = \frac{m}{(1+b^2)^2}. \tag{25}$$

Now, if n baryons of total rest mass ε accretes axisymmetrically to the hole, the variation of the total energy content of the ring is calculated from the first law of thermodynamics (see for example, GH),

$$\delta Q = \delta M_{\rm hole} - \frac{\kappa \delta A}{8\pi}. \tag{26}$$

As seen from infinity, $\delta M_{\rm hole} = 0$. The change in area δA is given by,

$$\delta A = 2\varepsilon A\left[1 + \frac{1}{(1+b^2)^{1/2}} + \frac{m}{(1+b^2)^{3/2}}\right]. \tag{27}$$

The surface gravity κ is calculated from $\kappa = e^{2\psi\tau}/4$. The change in the energy content δQ is therefore,

$$\delta Q = -\varepsilon\left[1 + \frac{1}{(1+b^2)^{1/2}} + \frac{m}{(1+b^2)^{3/2}}\right]. \tag{28}$$

The first term is just the change in the baryon number in the ring. The second term is due to the reduction of the potential energy of the ring when the baryons separated. The third term is also the loss of the potential energy due to the baryon loss as the distance between the ring and the hole increases by a small distance. Since there was no rotation of the hole or the ring, no other energy terms appear in the expression for δQ .

If the self-gravity of the surrounding matter were important, any small perturbation (caused by passing compact object in highly eccentric orbit, say) on the black hole would cause the black hole to oscillate up and down. Classically, the frequency of vertical oscillation is given by,

$$\nu = (m/b^3)^{1/2}. \tag{29}$$

The estimate of the luminosity of the gravity wave generated is calculated from (see, for example, Misner, Thorne & Wheeler 1973),

$$L_{\rm GW} = \frac{1}{5}\frac{G}{c^5}\langle \dddot{I} \rangle^2 \tag{30}$$

which, in our present case is given by,

$$L_{\rm GW} \approx \frac{G}{c^5}(M_{\rm hole}\, a^2)^2 v^6 \ {\rm erg\,s^{-1}}. \tag{31}$$

This is usually insignificant unless the ring is also of comparable mass and both the ring and hole take part in large amplitude oscillation. Assume a hole of mass 10 $M_{\odot}$.

being surrounded by a ring of radius $b = 10$ and of equal mass. The classical angular frequency of the oscillation is $\nu = 600$ Hz and the timescale of oscillation is $\sim 10^{-2}$ s, whereas, the light crossing time in the hole is $t_h = 10^{-4}$ s. Hence the estimation made by classical approach may be in the right range. This system, being very compact, will have strong radiation reaction. The timescale in which such oscillation damps out will be on the order $\tau_r = \dfrac{c^5 4\pi^2}{\nu^2 G E_k}$, where $E_k = \dfrac{1}{2} M_{\text{hole}} a^2 \nu^2$ is the kinetic energy of the hole. This is about 5000 seconds for the parameters considered! For the observational purposes, one will like to calculate the perturbation to the flat metric at earth by this oscillation. The estimation is made by expanding g_{tt} in series so that the effective 'Newtonian' potential Φ, at a large distance r becomes:

$$\Phi = -\frac{G(M_{\text{hole}} + m)}{r} - \frac{Gmb^2}{4r^3}(3\cos^2\Theta - 1)(3\sin^2\alpha - 1) - \ldots \tag{32}$$

where, $\alpha = \alpha_0 \cos(\nu t)$ is the instantaneous angular amplitude of the oscillation ($\alpha_0 = a/b$). The quadrupole moment is obtained from the second term of the expansion and metric perturbation h becomes,

$$h = \frac{2\ddot{I}}{r} = \frac{3\alpha_0^2 \nu^2 Gmb^2}{c^4 r} \tag{33}$$

For the parameters mentioned above and with $\alpha_0 = 0.1$, and the source located at the centre of our own galaxy, we obtain $h = 2.5 \times 10^{-17}$ which is comparable to other suggested sources and should be detectable. Realistically, however, the mass of the stable disc may be much smaller compared to the mass of the hole which reduces the effect very much.

The self-gravity may have other important effects. For example, the lowering of Keplerian distribution of the angular momentum near the centre of the disc implies that the binding energy release will also be higher. This will cause the temperature to be higher. Since matter is more tightly bound near the centre, the residence time may be higher unless some instability shows up. Both of these effects will enhance the rate of thermonuclear reactions at the centre of the disc (Chakrabarti 1986, Chakrabarti, Jin, & Arnett 1987, Chakrabarti 1988). Fig. 1 of Chakrabarti (1988) shows how the temperature at the centre of the disc goes up in the self-gravity regime. The increase in temperature may even produce neutron tori postulated recently by Hogan & Applegate (1987). Clearly, many questions remain unanswered. We hope to be able to explore them in future.

The author thanks Dr. Kip Thorne for helpful suggestions and acknowledges NSF grant AST 85-14911 and a Tolman fellowship.

References

Abramowicz, M. A. 1982, *Astrophys. J.*, **254,** 784.
Abramowicz, M. A., Calvani, M., Nobili, L. 1983, *Nature,* **302,** 597.
Abramowicz, M. A., Curir, A., Schwarzenberg-Czerny, A., Wilson, R. E. 1984 *Mon. Not. R. Astr. Soc.,* **208,** 279.
Abramowicz, M. A., Jaroszynski, M., Sikora, M. 1978, *Astr. Astrophys.,* **63,** 221.
Bach, R., Weyl, H. 1922, *Math.* Z., **13,** 134.

Chakrabarti, S. K. 1985a, *Astrophys. J.,* **288,** 1. (Paper 1).
Chakrabarti, S. K. 1985b, *Astrophys. J.,* **288,** 7 (Paper 2).
Chakrabarti, S. K. 1986, *Accretion Processes in Astrophysics,* Eds J. Audouze & J. T. T. Vanh.
Chakrabarti, S. K. 1988, *Astrophys. J*., **324,** 391.
Chakrabarti, S. K., Jin, L., Arnett, W. D. 1987, *Astrophys. J.*, **313,** 674.
Chandrasekhar, S. 1983, *Mathematical Theory of Blackholes*, Chapter 11, Oxford Univ. Press.
Geroch, R. P., Hartle, J. 1982, *J. Math. Phys.,* **23,** 376 (GH).
Goodman, J., Narayan, R. 1988, *Mon. Not. R. astr. Soc.,* (in press).
Hogan, C. J., Applegate, 1987 preprint.
Jaroszynski, M., Abramowicz, M. A., Paczyński, B. 1980, *Acta astr.* **30,** 1.
Kozlowski, M., Jaroszynski, M., Abramowicz, M. A. 1978, *Astr. Astrophys,* **63,** 209.
Misner, C, Thorne, K. S., Wheeler, J. A. 1973, *Gravitation,* Freeman, San Francisco.
Mysak, L., Szekeres, G. 1966, *Can. J. Phys.,* **44,** 617.
Paczynski, B., 1980, *Acta astr.* **30,** 1.
Paczynski, B., Abramowicz, M. A. 1982, *Astrophys. J*., **253,** 897.
Paczynski, B., Wiita, P. 1980, *Astr. Astrophys.,* **88,** 23.
Synge, J. L. 1964, *General Relativity,* North Holland, Amsterdam.
Weyl, H. 1917, *Ann. Phys.,* **54,** 117.
Will, C. F. 1974, *Astrophys. J*., **191,** 521.
Will, C. F. 1975, *Astrophys. J*., **196,** 41.
Wilson, R. E. 1981, *Astrophys. J.,* **251,** 246.

J. Astrophys. Astr. (1988) **9,** 63–65

Occultations by Possible Material in Saturn's Outer Magnetosphere

R. Vasundhara *Indian Institute of Astrophysics, Bangalore 560034*

Received 1988 January 27; accepted 1988 March 4

Abstract. Results of a search for occultations of stars in the SAO catalogue by Saturn's outer magnetosphere during 1988 are presented.

Key words: occultations—Saturn—magnetosphere

Anomalous dips in low energy plasma ion density in regions of Saturn's magnetosphere around 14 and 19 Saturn radii (R) were measured by Voyager 1,2 and Pioneer 11 spacecrafts. Lazarus, Hasegawa & Bagenal (1983) suggested that these density dips may be arising due to absorption by long-lived particulate or gaseous material in the equatorial plane of the planet. Baron & Elliot (1983), from their CCD imaging of the region of magnetosphere between 10—35R, set an upper limit of + 22 mag arcsec^{-2} for material distributed over a region larger than the 3 arcsec seeing disc in the I band. However such an imaging needs to be repeated at the time of ring plane crossings and with proper masks to ensure that the diffraction effects do not corrupt the frame.

Following predictions by Mink (1983), occultations of the star SAO 158913 (1984 March 24-26 and SAO 158763 (1984 May 12-13) were observed from Vainu Bappu Observatory at Kavalur and Uttar Pradesh State Observatory at Naini Tal. The 1984 March observations indicate radially symmetric distributions of absorbing matter probably in the form of a ring at 12.5R, although there was no evidence of any material at 14R. (Vasundhara *et al.* 1984; Bhattacharyya & Vasundhara 1985; Vasundhara & Bhattacharyya 1987). The May 1984 occultations were observable from India when Saturn's magnetosphere at 19R occulted the star. A comparative study of the observations from the two stations in India indicate fragmented or clumpy matter in this region, rather than a continuous ring system (Mahra *et al.* 1985, Vasundhara, Bhattacharyya & Rozario 1986).

Cheng, Lanzerotti & Maclennan (1985) raised serious doubts on the existence of any absorbing matter in Saturn's magnetosphere, their main argument being lack of substantial evidence from Voyager 2 LECP data in the energy range 30–1,000 keV. It is interesting to note that even for the E ring, whose existence is now well established, there exist discrepancies in the spacecraft measurements (Burns, Showalter & Morfill 1984 and references therein).

Further occultation observations will help in understanding this part of Saturn's magnetosphere. Therefore search was carried out in the SAO catalogue for occultations of stars by Saturn's magnetosphere occurring during 1988. In the search program, instantaneous apparent position of the star, angle of inclination of the ring plane to the line of sight, and position angle of the projection of the north pole of the planet on the sky plane were used. The planet coordinates were obtained from the Astronomical Almanac 1988 (DE 200). The apparent position of the stars were

Table 1. Predicted occultations by Saturn's magnetosphere during 1988.

Date (UT) 1988	mag	SAO no.	sp. type	Position (1950.0) R.A. Dec.	Geocentric impact parameter (arcsec) Sky plane velocity ($km\,s^{-1}$)	Event*		UT	Position angle N–E	Distance from Saturn (arcsec)
1. Feb. 17–18		186141		$17^h\ 59^m\ 17^s.445$	18	19*R*	Imm	22:59	96°	150
	9.0		M0	$-22°\ 19'\ 49.91$	+25.09	12.5*R*	Imm	03:27	100	98
						12.5*R*	Em	18:24	257	83
						19*R*	Em	22:56	262	136
2. May 10–11		186344		18 05 40.073	33	19*R*	Imm	00:21	256	140
	9.3		B5	−22 16 52.39	−12.74	12.5*R*	Imm	10:25	244	76
						12.5*R*	Em	10:42	108	103
						19*R*	Em	20:23	101	168
3. May 12–14		186335		18 05 08.281	33	19*R*	Imm	16:02	256	141
	8.5		B5	−22 16 55.19	−13.63	12.5*R*	Imm	01:20	244	77
						12.5*R*	Em	00:23	108	104
						19*R*	Em	09:23	100	169
4. Nov. 10–11		186063		17 56 46.029	49	19*R*	Imm	01:31	61	98
	9.1		K5	−22 37 50.18	+31.88	19*R*	Em	14:57	295	123
5. Nov. 10–11		186064		17 56 48.979	38	19*R*	Imm	01:19	107	136
	8.9		A0	−22 39 18.30	+31.89	12.5*R*	Imm	06:10	124	70
						12.5*R*	Em	12:44	226	53
						19*R*	Em	17:34	252	115

* R = 60 300 km; Imm: immersion; Em: emersion.

computed from SAO 1950.0 positions using the software package developed by A. V. Raveendran (1984, personal communication). The program uses the rigorous method for precession till the beginning of the year and computes the Besselian day numbers to correct for the precession for the fraction of the year, nutation and aberration. As the origin of the DE 200 reference frame is the mean equator and dynamical equinox of J2000.0, the apparent stellar positions were corrected for the zero point shift of

$$\Delta\alpha = 0^s.035 + 0^s.085(T - 19.50)$$

where T is counted in centuries (Fricke 1982).

Table 1 gives the UT date, the star's SAO catalogue number, its visual magnitude, spectral type and its 1950.0 position with proper motion up to the time of event added. The geocentric impact parameter is the closest approach of the planet to the star, measured in arcsec as would be seen from the centre of earth. In all the cases this distance is more than 18 arcsec, therefore the disc and the visible rings will not be occulting the star. Star 5 will only be occulted by the 19R region. The sky plane velocity is positive when the planet is in prograde motion and it is negative when it is in retrograde motion. For each star, the predicted universal time, position angle and distance of the star from the planet's centre in the sky plane at the time of the event are given for occultations at 12.5R and 19R. The May events occurring near planet's opposition have good observing conditions whereas February and November events are observable only along a narrow longitude belt and that too at large zenith distances.

A two-star multichannel photometer would be an ideal instrument to observe these events. Multicolour extinction measurements would directly lead to an estimation of the average size of the grains. Continuous monitoring of the star centred around the time of prediction is essential. In case of a single-channel photometer, simultaneous monitoring of a nearby star from an adjacent telescope (Mahra *et al.* 1985) would help in estimating sky transparency changes.

The author wishes to thank Prof. J. C. Bhattacharyya for his guidance and encouragement in carrying out the project, B. G. Marsden and D. J. Mink for helpful comments.

References

Baron, R. L., Elliot, J. L.1983, *Astr. J.,* **88,** 562.

Bhattacharyya, J. C., Vasundhara, R.1985, *Current Sci.,* **54,** 601.

Burns, J. A., Showalter, M. R., Morfill, G. E. 1984, in *Planetary Rings*, Ed. R. Greenberg & A. Brahic, Univ. Arizona Press, p. 200.

Cheng, A. F., Lanzerotti, L. J., Maclennan, C. G. 1985 *Nature,* **317,** 508.

Fricke, W.1982, *Astr. Astrophys.,* **107,** L13.

Lazarus, A. J., Hasegawa, T., Bagenal, F. (1983) *Nature* **302,** 230.

Mahra, H. S., Pandey, A. K., Vijay Mohan, Sanwal, B. B. 1985, *Nature* **313,** 38.

Mink, D.J.1983, *Astr.* J., **88,** 559.

Vasundhara, R., Bhattacharyya, J.C.1987 *Gerlands Beitr. Geophysik. Leipzig.* **96,** 52.

Vasundhara, R., Bhattacharyya, J. C, Rozario, M.1986, *Bull. Astr. Soc. India,* **14,** 232.

Vasundhara, R., Santhanam, P., Pande, A. K., Vijay Mohan, Mahra, H. S. 1984, *Nature,* **312,** 621.

J. Astrophys. Astr. (1988) **9,** 67–74

On the Scalar-Tensor Theory of Lau and Prokhovnik

S. D. Maharaj *Department of Mathematics and Applied Mathematics, University of Natal, King George V Avenue, Durban 4001, South Africa*

A. Beesham *Department of Mathematics and Applied Mathematics, University of Durban-Westville, Private Bag X54001, Durban 4000 South Africa*

Received 1987 August 19; accepted 1988 January 25

Abstract. Recently Lau & Prokhovnik (1986) have formulated a new scalar-tensor theory of gravitation which reconciles Dirac's large numbers hypothesis with Einstein's theory of general relativity. The present work points out an error in the time-dependent cosmological term and the scalar potential given by Lau and Prokhovnik. The correct forms for these quantities are derived. Further, a vacuum Robertson–Walker solution to the generalized field equations is obtained, under an anasatz that we propose, which illustrates that the theory is, in some sense, incomplete.

Key words: other theories of gravitation—Cosmology

1. Introduction

A conceptually simple way to extend Einstein's theory of general relativity is to suppose that the gravitational term G is time dependent. In the past there have been several attempts at constructing consistent theories with variable G (Dirac 1938; Brans & Dicke 1961; Hoyle & Narlikar 1964; Canuto *et al.* 1977). Possibly the most simple of the suggested theories is the theory based on the large numbers hypothesis (LNH) of Dirac. The LNH is essentially a statement of the simplicity of the mathematical relation between some very large numbers that occur in nature.

The theory based on the Dirac LNH is not compatible with a constant cosmological term λ (Lau 1985), and requires the use of 'two metrics' (Dirac 1975, 1979). To overcome these problems Lau (1985) proposed that, in addition to a time varying G, the cosmological term λ be nonzero and time dependent. With this conjecture the Dirac LNH and general relativity (with $G = G(t)$ and $\lambda = \lambda(t)$) are reconciled. Furthermore Lau's theory reduces to Einstein's theory of general relativity in a limiting case and yields a viable dust cosmological model. Motivated by the success of this approach Lau & Prokhovnik (1986) generalized Lau's theory by formulating a new scalar-tensor theory in terms of an action principle. A time dependent scalar potential $\psi=\psi(t)$ is introduced such that $\lambda = \lambda(\psi)$ and $G = G(\psi)$ are coupled.

In this paper we point out an error in the paper by Lau and Prokhovnik (LP). A differential equation is incorrectly given so that the resulting solutions for the cosmological term and the scalar potential have to be modified. In this paper we present the corrected solutions. Further we obtain a vacuum solution to the generalized field equations of LP for the flat Robertson–Walker Spacetimes. This is in

contrast to the earlier theory of Lau (1985) in which vacuum solutions turn out to be identical to the corresponding general relativistic solutions with constant λ (Beesham 1987). Vacuum solutions are significant because in our present interpretation the vacuum itself has a dynamical effect, *i.e.* the vacuum has an energy and matter content.

We emphasize that we consider the LP theory to be a viable generalization of Einstein's general relativity. However our vacuum solution illustrates that the theory is incomplete in the sense that there are more variables than there are equations. We are therefore forced to assume an ansatz to solve the field equations. In the conclusion we indicate how the LP theory can be supplemented and made complete by an additional condition utilizing the technique of Beesham (1986).

A further motivation for the study of theories which incorporate variable cosmological terms is the following. Nowadays, the parameter Λ is believed to correspond to the vacuum energy density of the quantum field (Zeldovich 1968), and it is thought that Λ was large during the early stages of the evolution of the universe, having strongly influenced its dynamics (Kasper 1985; Villi 1985; DerSarkissian 1985). The mass of the Higgs boson is thought to be related to Λ and G(Dreitlein 1974). Many workers have suggested the possibility of Λ being a variable quantity (*e.g.* Bergmann 1968; Wagoner 1970), with Linde (1974) having proposed that Λ is a function of temperature and relating it to the process of broken symmetry. Further interest in Λ arises within the context of quantum gravity, supergravity theories, Kaluza-Klein theories, the inflationary universe scenario, particle physics and grand unified theories (see Singh & Singh 1983; Lorenz-Petzold 1984; Banerjee & Banerjee 1985). There has been renewed interest in cosmological models with variable Λ, and the problems of singularity, horizon, flatness and monopole can be solved in some such models (*e.g.* Ozer & Taha 1986, 1987). The problem of fine tuning can also be explained naturally in certain variable Λ theories (*e.g.* Canuto *et al.* 1977). We remark in this connection that inflation, which also purports to solve some of the problems of the standard model is beset with many difficulties (Rothman & Ellis 1985; Olivo-Melchiorri & Melchiorri 1985).

In this paper we adopt the convention that the signature of the metric tensor is –2 and the speed of light is taken to be unity. For notational convenience dots will denote differentiation with respect to time, commas denote partial derivatives and semicolons denote covariant derivatives.

2. Field equations

Lau & Prokhovnik (1986) obtained the generalized field equations

$$R_{ij} - \tfrac{1}{2} R g_{ij} + \Lambda g_{ij} = -8\pi G T_{ij} - \psi_{,i}\psi_{,j} \tag{1}$$

using a variational principle formulation. R_{ij} *is* the Ricci tensor, $R = R_i^i$ is the Ricci scalar, T_{ij} is the energy-momentum tensor and g_{ij} is the metric tensor. Λ becomes the new cosmological term and is related to λ by

$$\Lambda = \lambda(t) - \tfrac{1}{2} g^{00} \dot{\psi}^2.$$

In general Λ is also dependent on the spatial coordinates because of the term containing g^{00}. But for spatially homogeneous spacetimes g^{00} can be taken to be unity,

in which case $\Lambda = \Lambda(t)$. The scalar potential ψ is strictly time dependent and couples Λ and G:

$$\psi = \psi(t),\ \Lambda = \Lambda(\psi),\ G = G(\psi).$$

Coupled to Equation (1) is the field equation for ψ,

$$\dot{\psi}\,\Box\psi + \dot{\Lambda} + \tfrac{1}{2}\dot{g}^{00}\dot{\psi}^2 + g^{00}\dot{\psi}\ddot{\psi} + 8\pi\dot{G}L_{\mathrm{m}} = 0, \tag{2}$$

where L_m is the matter Lagrangian density including all non-gravitational fields and

$$\Box\psi = g^{ij}\psi_{;i;j}.$$

All of the field Equations (1) and (2) are not independent because of the Bianchi identities. On taking the divergence of Equation (1) we obtain

$$g^{j}_{i}\Lambda_{,j} = -8\pi\dot{G}\,T_{io} - (\psi_{,i}\psi^{,j})_{;j}, \tag{3}$$

thereby relating Λ and G.

In the special case of vacuum ($L_{\mathrm{m}} = T_{ij} = 0$) we can immediately predict the behaviour of the gravitational term G. For vacuum we observe that G is absent from the field Equations (1) and (2). Hence G can be arbitrarily chosen.

3. Dirac LNH

The spatially homogeneous and isotropic Robertson-Walker specetimes with flat spatial sections are characterized by the metric

$$\mathrm{d}s^2 = \mathrm{d}t^2 - l^2(t)(\mathrm{d}x^2 + \mathrm{d}y^2 + \mathrm{d}z^2). \tag{4}$$

The energy-momentum tensor

$$T^{ij} = \rho u^i u^j$$

represents a pressure-free ('dust') perfect fluid where u^i is the comoving fluid four-velocity and ρ is the energy density of the fluid. For compatibility with the Dirac LNH we must have (Dirac 1938, 1979; Lau 1985)

$$l^2(t) = \beta t^{2/3}, \tag{5}$$

$$G(t) = \beta_1 \frac{1}{t}, \tag{6}$$

$$(L_{\mathrm{m}} =)\rho(t) = \beta_2 \frac{1}{t}, \tag{7}$$

where β, β_1, β_2 are constants.

Using the metric (4) it is easy to show that the field Equation (2) reduces to (see Appendix)

$$2\dot{\psi}\ddot{\psi} + \dot{\Lambda} + 3\frac{\dot{l}}{l}\dot{\psi}^2 + 8\pi\dot{G}\rho = 0. \tag{8}$$

The term $3\dot{l}\dot{\psi}^2/l$ in equation (8) is missing from the corresponding equation obtained by LP (p. 344). Consequently the forms for ψ and Λ will be modified on incorporation

of the missing term. Substituting Equations (5)–(7) in Equation (8) we obtain

$$(\dot{\psi}^2)^{\cdot} + \dot{\Lambda} + \frac{1}{t}\dot{\psi}^2 = 8\pi\beta_1\beta_2\frac{1}{t^3}. \tag{9}$$

The (0, 0) component of Equation (1) is given by

$$3\frac{\dot{l}^2}{l^2} - \Lambda = \dot{\psi}^2 + 8\pi G\rho. \tag{10}$$

Substituting Equations (5)–(7) in Equation (10) we obtain

$$\frac{1}{3t^2} - \Lambda - \dot{\psi}^2 = 8\pi\beta_1\beta_2\frac{1}{t^2}. \tag{11}$$

On differentiating Equation (11) with respect to time we have

$$-\frac{2}{3t^3} - \dot{\Lambda} - (\dot{\psi}^2)^{\cdot} = -16\pi\beta_1\beta_2\frac{1}{t^3}. \tag{12}$$

Adding Equations (9) and (12) we obtain

$$\dot{\psi}^2 = (\tfrac{2}{3} - 8\pi\beta_1\beta_2)\frac{1}{t^2}. \tag{13}$$

Equation (13) has the general solution

$$\psi = (\tfrac{2}{3} - 8\pi\beta_1\beta_2)^{1/2}\ln t + A, \tag{14}$$

where A is constant. Substituting Equation (13) in Equation (11) yields

$$\Lambda = -\frac{1}{3t^2}. \tag{15}$$

Note that the corresponding expression for Λ found by LP contains an additional term, $-\dot{\psi}^2$. Thus we have obtained expressions for ψ and Λ, namely Equations (14) and (15), thereby correcting the solutions found by Lau and Prokhovnik. Since $\Lambda \sim t^{-2}$ the qualitative features of the solution obtained by LP remain unchanged. In particular the magnitude of Λ will decrease as the age of the universe increases.

4. Vacuum solutions

The existence of vacuum solutions to the field Equations (1) and (2) is of particular interest. With $T_{ij} = 0$ the field equation (1) can be written as

$$R_{ij} - \frac{1}{2}Rg_{ij} = -(\Lambda g_{ij} + \psi_{,i}\psi_{,j}). \tag{16}$$

The term $-(\Lambda g_{ij} + \psi_{,i}\psi_{,j})$ may be interpreted as the energy-momentum tensor of the vacuum in the presence of the gravitational field. This interpretation is possible because of the theory of modern quantum electrodynamics. An empty space is not considered as an inert region anymore, instead it continually gives rise to quantum fluctuations. Thus the vacuum itself has energy and momentum.

The theory Equations (16) for the metric (4) yield

$$3\frac{\dot{l}^2}{l^2}-\Lambda=\dot{\psi}^2, \tag{17}$$

$$2\frac{\ddot{l}}{l}+\frac{\dot{l}^2}{l^2}-\Lambda=0, \tag{18}$$

and Equation (8) becomes

$$2\dot{\psi}\ddot{\psi}+\dot{\Lambda}+3\frac{\dot{l}}{l}\dot{\psi}^2=0. \tag{19}$$

The divergence relation (3) also gives the result (19). The Equations (17)–(19) are a system of three equations for the three unknowns l, Λ and ψ. Therefore it seems possible to specify the general solution of this system. However this is not the case since Equations (17)–(19) are not independent. A linear combination of Equations (17) and (18) gives

$$2\frac{\ddot{l}}{l}-2\frac{\dot{l}^2}{l^2}=-\dot{\psi}^2. \tag{20}$$

On differentiating Equation (17) with respect to time we have

$$\dot{\Lambda}+2\dot{\psi}\ddot{\psi}=6\frac{\dot{l}}{l}\left(\frac{\ddot{l}}{l}-\frac{\dot{l}^2}{l^2}\right). \tag{21}$$

Substituting Equation (20) into Equation (21) we obtain exactly Equation (19), thereby demonstrating that only two of the Equations (17)–(19) are independent. This means that we have to specify one of l, Λ or ψ. Then Equations (17)–(19) will yield the remaining two variables.

In Section 3 we specified the scale factor $l(t)$ and obtained Λ and ψ. In this section we specify a form for ψ and attempt to obtain l and Λ. The simplest form of ψ would be linear. However, this is not a physical choice because then Λ grows larger as the age of the universe increases.

Guided by the form specified for ψ for compatibility with the Dirac LNH (*cf.* Equation 14) we choose

$$\psi=A\ln t+B, \tag{22}$$

where A and B are constants. Using Equation (22) we can write Equation (20) as

$$2\frac{\dot{l}}{l}=A^2\left(\frac{1}{t}\right)^{\cdot},$$

which has the general solution

$$2\frac{\dot{l}}{l}=A^2\frac{1}{t}+C \tag{23}$$

where C is a constant. Equation (23) can also be integrated and we obtain the solution

$$l^2(i)=\exp(A^2\ln t+Ct+D), \tag{24}$$

where D is a constant. Finally substituting Equation (24) in Equation (18) we get

$$\Lambda = -A^2\frac{1}{t^2}+\frac{3}{4}\left(A^2\frac{1}{t}+C\right)^2. \tag{25}$$

Equations (22), (24) and (25) constitute a vacuum solution to the generalized field equations of LP.

5. Conclusion

LP have presented a very interesting scalar-tensor theory which generalizes the earlier theory proposed by Lau (1985). However, our vacuum solution illustrates a somewhat unpleasant feature of the theory, *viz.,* that, in a certain sense, it is incomplete. There are more unknowns than equations and thus, to obtain specific solutions, one has to assume some ansatz. The situation here is very similar to that in the scale-covariant theory of Canuto *et al.* (1977). LP give no indication of how to overcome the difficulty present in their theory. This feature of their theory contrasts sharply with general relativity, which, in the above sense, is complete.

We indicate how it may be possible to achieve completeness by applying the ideas of Beesham (1986). For definiteness, we consider the Robertson-Walker models with energy density ρ and pressure p. From the field Equations (1), the Robertson-Walker metric (4) and the perfect fluid form of the energy-momentum tensor, we derive the following equation

$$\dot{\rho}+\rho\frac{\dot{G}}{G}+3(\rho+p)\frac{\dot{l}}{l}+\frac{1}{8\pi G}\dot{\Lambda}+\frac{1}{8\pi G}\left[(\dot{\psi}^2)^{\cdot}+3\frac{\dot{l}}{l}\dot{\psi}^2\right]=0.$$

This reduces to the usual equation of conservation of mass-energy

$$\dot{\rho}+3(\rho+p)\frac{\dot{l}}{l}=0,$$

if we take

$$\rho\dot{G}=-\dot{\Lambda}/8\pi-\frac{1}{8\pi}\left[(\dot{\psi}^2)^{\cdot}+3\frac{\dot{l}}{l}\dot{\psi}^2\right].$$

With this ansatz, the condition $G \sim 1/t$ (Dirac 1938), and an equation of state relating ρ to p, the solution to the field equations is fully determined.

Appendix

In this appendix we obtain the field Equation (8), governing the behaviour of ψ, and explicitly identify the missing term in the corresponding equation given by LP. The field equation for ψ is just Equation (2):

$$\dot{\psi}\,\Box\,\psi+\dot{\Lambda}+\tfrac{1}{2}\dot{g}^{00}\dot{\psi}^2+g^{00}\dot{\psi}\ddot{\psi}+8\pi\dot{G}L_{\mathrm{m}}=0 \tag{A1}$$

where $\psi = \psi(t)$. The matter Langrangian density L_m is equal to the energy density ρ since we are considering a 'dust' distribution of matter and g^{00} is unity by the metric

(4). Hence Equation (Al) reduces to

$$\dot{\psi}\,\Box\psi + \dot{\Lambda} + \dot{\psi}\ddot{\psi} + 8\pi\rho\dot{G} = 0. \tag{A2}$$

We now evaluate the quantity $*\psi$:

$$\begin{aligned}\Box\psi &= \psi_{;i;j}g^{ij}\\ &= (\psi_{,i})_{;j}g^{ij}\\ &= (\psi_{,i,j} - \psi_{,k}\Gamma^{k}_{ij})g^{ij},\end{aligned} \tag{A3}$$

where Γ^{k}_{ij} are the connection coefficients. (Note that $\psi_{;i} = \psi_{,i}$ because ψ is a scalar). Since $\psi = \psi(t)$ equation (A3) becomes

$$\begin{aligned}\Box\psi &= \ddot{\psi} - \dot{\psi}\,\Gamma^{0}_{ij}g^{ij}\\ &= \ddot{\psi} - \tfrac{1}{2}g^{ok}(g_{jk,i} + g_{ki,j} - g_{ij,k})g^{ij}\\ &= \ddot{\psi} + \tfrac{1}{2}\dot{\psi}\,g_{ij,o}\,g^{ij}\\ &= \ddot{\psi} + 3\frac{\dot{l}}{l}\dot{\psi}\end{aligned} \tag{A4}$$

The appearance of the term $3(\dot{l}/l)\psi$ is directly related to the nonvanishing of the connection coefficients Γ^{0}_{ij}. The term involving Γ^{0}_{ij} arises because covariant differentiation is not commutative. Substituting Equation (A4) in (A2) we obtain

$$2\dot{\psi}\ddot{\psi} + \dot{\Lambda} + 3\frac{\dot{l}}{l}\dot{\psi}^{2} + 8\pi\dot{G}\rho = 0 \tag{A5}$$

and we have derived Equation (8). The term $3(\dot{l}/l)\dot{\psi}$ in Equation (A5) has been omitted from the corresponding field equation in the paper by LP.

Acknowledgements

The authors are grateful to the referees for useful suggestions which led to an improvement in the manuscript.

References

Banerjee, A., Banerjee, N. 1985, *Astrophys. Sp. Sci.,* **114**, 165.
Beesham, A. 1986, *Int. J. Theor. Phys.,* **25**, 1295.
Beesham, A. 1987, *Austr. J. Phys.,* **40**, 23.
Bergmann, P. G, 1968, *Int. J. Theor. Phys.,* **1**, 25.
Brans, C., Dicke, R. H. 1961, *Phys. Rev.,* **124**, 925.
Canuto, V., Adams P. J., Hsieh, S. H., Tsiang, E. 1977, *Phys. Rev.,* **D 16**, 1643.
DerSarkissian, M. 1985, *Nuovo Cim.,* **88B**, 29.
Dirac, P. A. M. 1938, *Proc. R. Soc. London,* **A 165**, 199.
Dirac, P. A. M. 1975, *The General Theory of Relativity,* Wiley, New York
Dirac, P. A. M. 1979, *Proc. R. Soc. London,* **A 365**, 19.
Dreitlein, J. 1974, *Phys. Rev. Lett.,* **33**, 1243
Hoyle, F., Narlikar, J. V. 1964, *Proc. R. Soc. London,* **A282**, 191.
Kasper, V. 1985, *Gen. Relativ. Gravitation,* **17**, 725.

Lau, Y. K. 1985, *Austr. J. Phys.,* **38**, 547.
Lau, Y. K., Prokhovnik, S. J. 1986, *Austr. J. Phys.,* **39**, 339.
Linde, A. D. 1974, *JETP Lett.,* **19**, 183.
Lorenz-Petzold, D. 1984, *Astrophys. Sp. Sci.,* **100**, 461.
Olivo-Melchiorri, B., Melchiorri, F. 1985, *Riv. del Nuovo Cim.,* **8**, 1.
Ozer, M., Taha, M. O. 1986, *Phys. Lett.* B, **171**, 363.
Ozer, M., Taha, M. O. 1987, *Nucl. Phys.,* **B287**, 776.
Rothman, T., Ellis, G. F. R. 1985, *Metqflation,* Univ. Cape Town preprint 85/18.
Singh, T., Singh, Tarkeshwar, 1983 *Astrophys. Sp. Sci.,* **97**, 127.
Villi, C. 1985, *Nuovo Cim.,* **85A**, 175.
Wagoner, R. V. 1970, *Phys. Rev.,* **Dl** , 3209.
Zel'dovich, Ya. B. 1968, *Sov. Phys.,* USPEKHI, **11**, 381.

J. Astrophys. Astr, (1988) **9,** 75–78

Spectroscopic Binaries near the North Galactic Pole Paper 14: HD 118234

R. F. Griffin *The Observatories, Madingley Road, Cambridge, England CB3 0HA*

Received 1988 January 20; accepted 1988 February 25

Abstract. Photoelectric radial-velocity measurements show that the Seventh-magnitude star HD 118234 is a spectroscopic binary in a very eccentric 59-day orbit.

Key words: radial velocities—spectroscopic binaries—stars, individual

HD 118234 is a seventh-magnitude object near the south-following boundary of the area covered by the Cambridge radial-velocity survey of the North Galactic Pole field ($b > 75°$). It is on the extreme eastern edge of Coma Berenices, near the fifth-magnitude star 1 Bootis and about 10° preceding Arcturus. Photoelectric magnitude measure ments of it have been published by Haggkvist & Oja (1973), who found V=7.57, (B–V)=1.08, (U–B)=0.93. Unpublished photometry in the Copenhagen system (Hansen & Kjaergaard 1971), carried out at Palomar Observatory by Dr G. A. Radford and the author in 1976 and reduced by Dr L. Hansen, indicates that the object is a giant; furthermore, it shows signs of being photometrically composite, having a value of res (k) of $0^m.12$, very similar to that given (for example) by 73 Leo, which is supposed (Griffin 1966) to consist of a K giant plus a main sequence star with a type of about F1. No modern spectral classification is known to exist for HD 118234; the HD classify-cation is K0, and a type of K0 or Kl III would suit the photometry quite well.

The first radial-velocity observation of HD 118234 was made in 1971, but it was not until 1980 that the second one was made and the spectroscopic-binary nature of the object was discovered. Since then it has been observed systematically, and the 61 measurements listed in Table 1 have been accumulated. They yield the orbit plotted in Fig. 1 and having the following elements:

$P = 59.054 \pm 0.004$ days
$\gamma = -19.24 \pm 0.08$ km s^{-1}
$K = 9.66 \pm 0.15$ km s^{-1}
$e = 0.589 \pm 0.010$
$\omega = 271.7 \pm 1.8$ degrees

$(T)_{83}$ = MJD 45851.74 ± 0.13
$a_1 \sin i = 6.34 \pm 0.12$ Gm
$f(m) = 0.00292 \pm 0.00016\, M_\odot$

Rms residual = 0.6 km s^{-1}

The period of 59 days is quite short for a giant star. Giants with periods so short tend to show photometric variability of the RS CVn variety, in which the variations arise from non-uniform surface brightness coupled with stellar rotation. However, the widths of the dips on radial-velocity traces do not suggest that HD 118234 has an unusually rapid rotation.

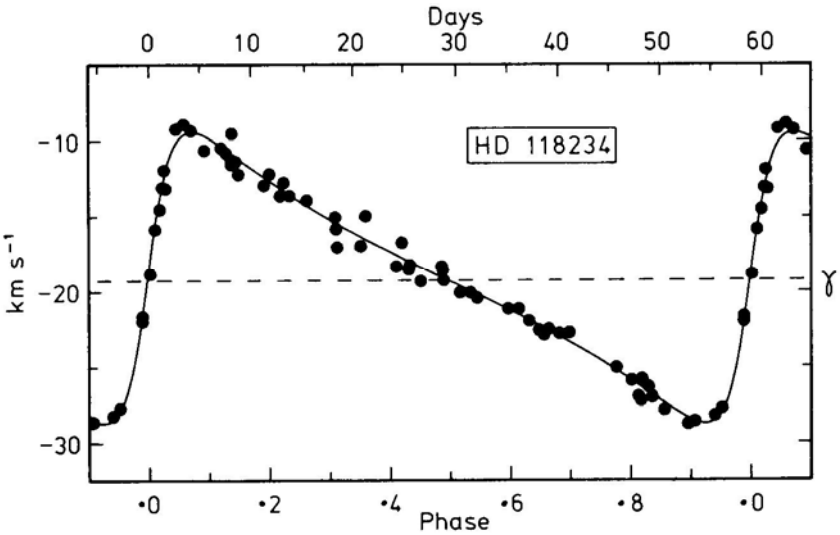

Figure 1. The computed radial-velocity curve of HD 118234, with the measured radial velocities plotted.

Table 1. Photoelectric radial-velocity measurements of HD 118234.

Date	MJD	Velocity km s^{-1}	Phase	$(O-C)$ km s^{-1}
1971 Feb 16.22	40998.22	−26.9	0.812	−0.7
1980 May 17.00	44376.00	−15.8	58.010	+0.1
1981 May 5.03	44729.03	−21.6	63.988	+0.5
1982 Jan 21.21	44990.21	−18.3	68.411	−0.7
Mar 4.13	45032.13	−10.5	69.121	−0.1
Apr 15.02	074.02	−26.3	.830	+0.4
May 23.96	112.96	−19.2	70.490	0.0
1983 Feb 3.57*	45368.57	−27.2	74.818	−0.9
4.57*	369.57	−27.0	.835	−0.2
15.36*	380.36	−14.5	75.018	−0.5
18.47*	383.47	−9.3	.070	+0.1
23.12	388.12	−12.2	.149	−1.0
28.13	393.13	−13.6	.234	0.0
Mar 7.11	400.11	−16.9	.352	−0.5
11.14	404.14	−16.7	.420	+1.1
15.12	408.12	−18.5	.488	+0.6
Apr 16.03	440.03	−13.1	76.028	−1.1
22.01	446.01	−10.8	.129	−0.2
May 9.97	463.97	−18.2	.434	−0.1
15.96	469.96	−20.1	.535	−0.1
June 6.94	491.94	−28.6	.907	0.0
8.92	493.92	−28.2	.941	+0.3
15.92	500.92	−8.9	77.059	+0.6
30.92	515.92	−17.0	.313	−1.5

Table 1. Continued

Date			MJD	Velocity km s^{-1}	Phase	$(O-C)$ km s^{-1}
1984	Jan	2.26	45701.26	−19.3	80.452	−0.9
	Feb	9.13	739.13	−10.6	81.093	−0.9
	Apr	2.06	792.06	−21.9	.989	−0.1
		14.04	804.04	−12.9	82.192	−0.4
		15.96	805.96	−12.7	.225	+0.7
		21.04	811.04	−15.0	.311	+0.5
		23.98	813.98	−14.9	.361	+1.7
	May	8.98	828.98	−21.1	.615	+0.5
		11.00	831.00	−22.6	.649	−0.3
		11.93	831.93	−22.5	.665	+0.1
		12.99	832.99	−22.8	.683	+0.2
		13.94	833.94	−22.7	.699	+0.7
	June	8.92	859.92	−9.5	83.139	+1.4
1985	Jan	1.20	46066.20	−21.9	86.632	+0.1
		12.26	077.26	−25.8	.819	+0.6
		23.08	088.08	−18.8	87.002	−0.6
		24.22	089.22	−13.0	.021	+0.3
	Feb	17.49*	113.49	−18.5	.432	−0.5
		24.15	120.15	−20.4	.545	−0.2
	June	1.94	217.94	−12.1	89.201	+0.6
1986	Jan	25.21	46455.21	−13.6	93.219	−0.4
	Feb	27.16	488.16	−25.0	.777	+0.3
	Mar	6.13	495.13	−28.7	.895	−0.3
	Apr	10.09†	530.09	−18.3	94.487	+0.8
	May	13.04	563.04	−9.2	95.045	+1.0
		18.93	568.93	−11.3	.145	−0.2
		25.92	575.92	−13.9	.263	+0.5
	Aug	24.83†	666.83	−25.9	96.803	0.0
	Dec	12.28	776.28	−22.9	98.656	−0.4
1987	Feb	1.16	46827.16	−20.1	99.518	−0.4
		21.18	847.18	−27.8	.857	−0.4
	Mar	3.12†	857.12	−11.9	100.025	+0.7
		20.07	874.07	−15.7	.312	−0.2
	May	7.94	922.94	−11.5	101.139	−0.6
	June	3.97	949.97	−21.1	.597	+0.2
		24.92	970.92	−27.7	.952	+0.2
	July	5.91	981.91	−11.2	102.138	−0.3

* Observed with the Dominion Astrophysical Observatory 48-inch telescope (Fletcher *et al.* 1982).

† Observed with the Geneva Observatory's 'Coravel' at Haute Provence (Baranne, Mayor & Poncet 1979)

Acknowledgements

I am pleased to acknowledge the guest-investigator privileges granted to me at the Dominion Astrophysical Observatory and on the Geneva Observatory's 'Coravel' radial-velocity spectrometer and 1-m telescope at Haute Provence. This is the first

paper in this series to include observations made with 'Coravel', which will probably feature in most, if not all, succeeding papers.

References

Baranne, A., Mayor, M., Poncet, J. L. 1979, *Vistas Astr.,* **23**, 279.
Fletcher, J. M., Harris, H. C., McClure, R. D., Scarfe, C. D. 1982, *Publ. astr. Soc. Pacific,* **94**,1017.
Griffin, R. F. 1966, *Observatory,* **86**, 145.
Haggkvist, L., Oja, T. 1973, *Astr. Astrophys. Suppl.,* **12**, 381.
Hansen, L., Kjaergaard, P. 1971, *Astr. Astrophys.,* **15**, 123.

J. Astrophys. Astr. (1988) **9,** 79–91

Global Properties of Star Formation in Spiral Galaxies

T. N. Rengarajan & K. V. K. Iyengar *Tata Institute of Fundamental Research, Homi Bhabha Road, Bombay 400005*

Received 1987 August 5; accepted 1988 February 26

Abstract. Samples of spiral galaxies from two catalogues of 21 cm line observations and a catalogue of near-infrared observations of nearby galaxies have been used in conjunction with Infrared Astronomical Satellite data to study correlations involving M_G, the dynamic mass of the galaxies, the luminosities in the *H* band (1.6 μm), the blue band and the far infrared bands and the mass of atomic hydrogen, it is found that both the blue and the far-IR luminosities which are indicators of star formation averaged over ~3 × 10^9 and ~10^7 years respectively, have a linear dependence on M_G. On the other hand, the *H* luminosity which is a measure of star formation averaged over the lifetime of galaxies, has a steeper power law dependence on M_G. The correlations observed do not have significant dependence on the morophological type of the galaxies There is a poor correlation between the far-infrared luminosity and the mass of atomic hydrogen. The mass of atomic hydrogen has a dependence of the form M_G. Because of the decrease in the mean mass for later morphological types and due to differences in power law dependences of luminosities in different bands on M_G, the mean value of luminosity-to-mass ratio is a constant for blue and far-IR bands, decreases for the *H* band and the gas-to-mass ratio increases as morphological type increases.

Key words: galaxies, star formation–galaxies, infrared radiation–galaxies, neutral hydrogen

1. Introduction

A study of large scale properties of star formation in spiral galaxies is of great interest to understand the process of star formation (SF), its history over the galactic lifetime and possible factors governing the morphological appearance of galaxies. In recent times, there have been several studies in this regard making use of relationships between luminosites in various bands and also their relationships to the gas content of galaxies (Gallagher, Hunter & Tutukov 1984; Iyengar, Rengarajan & Verma 1985; Rengarajan & Verma 1986; Young *et al.* 1986; Young 1986; Young 1987; Sandage 1986; Persson & Helou 1987; Thronson & Telesco 1986; Jackson *et al.* 1987). Luminosities in different bands are indicators of star-formation rate averaged over different periods. In the study of Gallagher, Hunter & Tutukov (1984), Hα luminosity was used as a probe for the current star formation rate (SFR) averaged over ~ 10^7 years, the blue band luminosity as SFR over ~3 × 10^9 yr and the mass of the galaxy itself as a probe of SFR over the life of the galaxy. With the advent of Infrared Astronomical Satellite (IRAS), it has been possible to use the far-infrared (far-IR)

observations of a large sample of galaxies for a study of the present day SF. Further, it has been shown that there is an intimate connection between the amount of molecular hydrogen and the far-IR activity of galaxies (Rengarajan & Verma 1986; Young 1986; Young 1987). For a few galaxies, it has also been shown that the radial distribution of L_{IR}, the far-IR luminosity, L_B, the blue luminosity, and M_{H_2}, the mass of molecular hydrogen gas as revealed through ^{12}CO observations, are very similar while the radial distribution of $M_{H\,I}$, the atomic hydrogen mass is quite different (Scoville & Young 1983; Tacconi & Young 1986; Kenney & Young 1986). Since $M_{H\,I}$ is expected to be the reservoir of gas for eventual conversion to H_2 and hence to star formation, it is of interest to study the relationship between the H I gas content and other indicators of SF. Since the mass of a galaxy is an important parameter governing the history of star formation (Sandage 1986), one would like to study SF as a function of the mass of the galaxy.

In the present study, we make use of samples of spiral galaxies that have been observed in the 21 cm line of atomic hydrogen and for which a measure of the dynamic mass of the galaxy is available from the measurement of the 21 cm line width. We also make use of a sample of nearby galaxies with measurements of H (1.6 μm) magnitude along with 21 cm observations. H magnitude essentially samples old late-type giants (Aaronson, Huchra & Mould 1979; Rieke & Lebofsky 1979) and thus provides a measure of SFR over the life of the galaxy. We then study the correlations involving luminosities in various bands, M_G, the dynamic mass of the galaxy, and $M_{H\,I}$.

2. Data

A measure of the dynamic mass of the galaxy is provided by W_{20}, the width of the 21 cm line at 20 per cent of the peak. Tully & Fisher (1977) first discovered the relationship between W_{20} and the absolute blue magnitude of galaxies. Following this, they have published a catalogue of 21 cm observations of a large sample of spiral galaxies (Fisher & Tully 1981; hereafter FT). In this catalogue they have also listed besides the intrinsic properties of galaxies, derived and corrected quantities like the absolute blue magnitudes and dynamic mass of the galaxy. We use this catalogue as our primary source of information of M_G and L_B . In order to be able to assess selection effects, sample composition, etc. on the parameters studied, we also make use of another catalogue of 21 cm observations viz., the high signal-to-noise ratio observations of Lewis, Helou & Salpeter (1985; hereafter LHS) of galaxies lying in the plane of the local supercluster. Finally, for a sample of H magnitude observations we use the catalogue of nearby galaxies (with inclination >45°) published by Aaronson *et al.* (1982; hereafter AHM) which is the basis for the infrared counterpart of Tully-Fisher relation and use the derived and corrected quantities as given by them. Most of the galaxies in this sample are also found in the FT sample and H I information for them is also taken mostly from FT.

We searched for IRAS counterparts for all the galaxies having H I width information in the Catalogued Galaxies in the IRAS Survey (1985). We selected only those galaxies for which definite flux densities were available for both the 60 and 100 μm bands. The listed values of FIR (W m^{-2}) were taken as measures of the broad band 40–120 μm far-IR flux. The statistics of IRAS detections for the three catalogues are given in Table 1.

The diameters, morphological types, distances and other properties of galaxies were

Table 1. Fraction of IRAS detections at both 60 and 100 μm.

	Fraction of detections	
Sample	dia. $\leqslant$ 5 arcmin	dia. $\leqslant$ 20 arcmin
FT	151/354	399/694
LHS	130/239	133/243
AHM	170/216	213/305

taken from the respective catalogues. All distances were, however, normalized to a Hubble constant H_0 = 100 km s^{-1} Mpc^{-1}. Distances in AHM are given relative to Virgo cluster. These were converted to absolute distances by assuming a distance of 10.7 Mpc to the Virgo cluster. The observed and derived quantities of interest to this study are listed below.

B_0: the corrected apparent blue magnitude of the galaxy.

H: the corrected *H* band (1.6 μm) apparent magnitude referred to an isophote of log A/D_i,= –0.5.

H I: 21 cm flux density integral (Jy km s^{-1}).

W_{20}: the corrected width of the 21 cm line at 20 per cent of the peak.

FIR: 40–120 μm flux (W m $^{-2}$) listed in the IRAS Catalogue.

M_G: = $\kappa\theta D\ W_{20}$, dynamic mass of the galaxy within diameter θ (optical diameter) where D is the distance to the galaxy and κ is a constant. This assumes that the velocity-maximum is within the optical diameter which is likely to be realized in most of the galaxies (FT).

B_0(abs), L_B: the absolute blue magnitude and luminosity derived using the listed distances.

H_0(abs), L_H: the absolute *H* magnitude and the *H* band luminosity.

L_{IR}: the 40–120 μm luminosity.

$M_{H\,I}$: the mass of atomic hydrogen.

It may be noted that diameters and distances given in the catalogues are derived from different sources. We do not therefore attempt to compare absolute values of parameters, but will only be concerned with relative changes.

3. Analysis

3.1 *Correlations Involving Luminosities*

(i) L_B versus M_G

In Fig. 1 we show a plot of B_0(abs) against log ($M_G/M_\odot$) for all galaxies in the FT sample. The various symbols represent galaxies of different morphological types. It is seen that there is a good correlation between the two plotted quantities. The line in Fig. 1 is obtained from a least squares fit to the data points; the parameters of the fit are

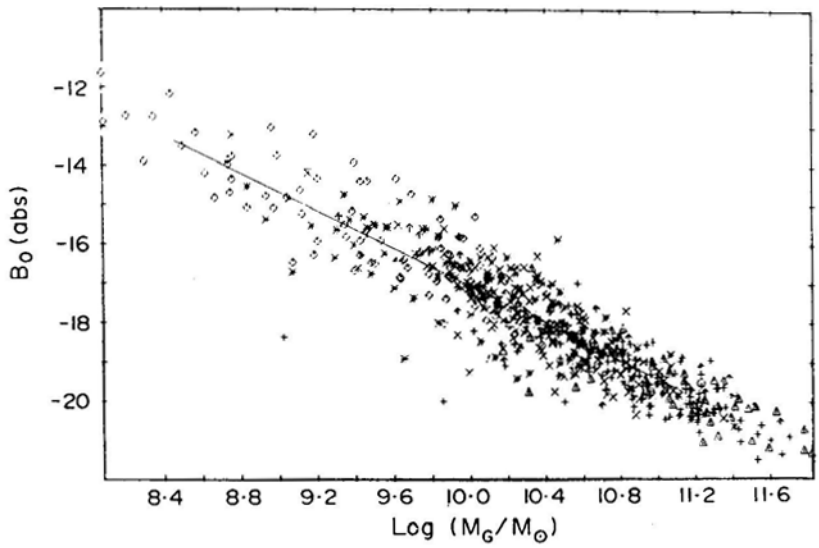

Figure 1. B_0(abs), the absolute blue magnitude of galaxies in the FT sample plotted against $\log(M_G/M_\odot)$ where M_G is the dynamic mass of the galaxy. The symbols identifying the morphological types are: ⬡ types 0, 1; Δ types 2, 3; + types 4, 5; × types 6, 7; ∗ types 8, 9; ◇ types 10, 11; ⧋ ambiguous subclasses. The solid line drawn is the least-squares best fit line

listed in Table 2. The significance of the correlation as shown by the correlation coefficient r^2 is quite high. The plot is nothing but the original Tully-Fisher relation, but with M_G as the variable. The best fit line is represented by

$$L_B \propto M_G^{\alpha_B}$$

where $\alpha_B = 0.95$. The rms scatter in log L_B with respect to the fitted line is 0.27. Though M_G is not the total mass of the galaxy, under the assumption that it represents a constant fraction of the total mass, the correlation implies that the mass-to-luminosity ratio is a constant. If we divide the sample as a function of morphological type, it is found that there is small increase in α_B, its value changing from 0.84 for types 1–3 to 0.95 for types 7–10.

(ii) L_H versus M_G

Fig. 2 shows a plot of H_0(abs) against log $(M_G/M_\odot)$. Again this is the infrared counterpart of Tully-Fisher relation, but plotted with M_G as the variable. It is seen that

$$L_H \propto M_G^{\alpha_H}$$

where $\alpha_H = 1.34$. Aaronson, Huchra & Mould (1979) found that $L_H \propto W_{20}$ and argued that this implies that $L_H \propto M_G$. The deviation of α_H from unity is most probably due to correlations between diameter and W_{20} (Shostak 1978). As in the case of α_B, there is a small increase in the value of α_H as one proceeds from earlier morphological types to later ones.

Table 2. Luminosity correlations in spiral galaxies: Fits for log $Y = A + \alpha \log X$.

X mag	Y W m^{-2}	Sample	Size limit	No.	α	r^2	$(\delta \log Y)_{rms}$
M_G	L_B	FT	20	618	0.95 ± 0.03	0.92	0.26
M_G	L_H	AHM	20	305	1.34 ± 0.04	0.95	0.20
W_{20}	L_{IR}	AHM	20	213	3.27 ± 0.19	0.65	0.36
M_G	L_{IR}	AHM	20	213	0.98 ± 0.05	0.78	0.35
M_G	L_{IR}	LHS	20	133	0.76 ± 0.07	0.68	0.45
M_G	L_{IR}	FT	20	399	0.92 ± 0.04	0.75	0.40
M_G	L_{IR}	AHM	5	170	1.05 ± 0.06	0.80	0.33
M_G	L_{IR}	FT	5	151	0.85 ± 0.06	0.74	0.37
M_G	L_{IR}[(b)]	FT	20	399	0.91 ± 0.04	0.77	0.38
M_G	M_d	FT	20	399	1.12 ± 0.04	0.84	0.35
H[(a)]	FIR	AHM	20	213	-0.29 ± 0.02	-0.79	0.28

[(a)] Magnitude used in place of log X.
[(b)] For 82 galaxies L_{1R} is from the IRAS Small Scale Structures Catalogue.

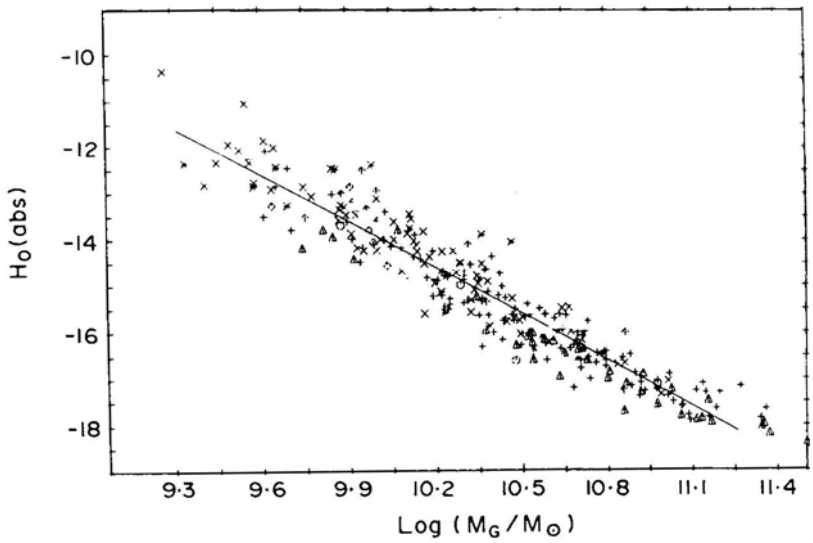

Figure 2. H_0(abs), the absolute H magnitude plotted against log $(M_G/M_\odot)$ for galaxies in the AHM sample. Symbols are as in Fig.1.

(iii) L_{IR} versus M_G

First we look for correlations between L_{IR} and W_{20}, the result of which is shown in Table 2 for the AHM sample. The power-law index for the relation $L_{IR} \propto W_{20}^{\alpha}$ is almost the same as that for the blue band (Tully & Fisher 1977), but significantly less than that for the H band (Aaronson, Huchra & Mould 1979). We now use M_G instead of W_{20} as a variable, and list the results in Table 2. Since the IRAS beams are about 5 arcmin, the flux densities as given in the Point Source Catalogue (PSC) are likely to be underestimated for galaxies of larger diameters. In order to see the effect of this, we

studied the correlations for galaxies with $\theta < 5$ arcmin and also for $\theta < 20$ arcmin. It is seen from Table 2 that the correlations for both the groups as well as for the three samples are all very similar. Eightytwo galaxies in the FT sample also appear in the IRAS Small Scale Structures Catalogue (1986). For these galaxies, we determined the quantity FIR using the flux densities listed in this catalogue. We studied the L_{IR}–M_G correlation using these values along with the FIR values from the PSC for the rest of the galaxies and the results are also shown in Table 2. Once again, the correlation is almost the same as for the data based entirely on the PSC data.

In Fig. 3, we show the plot of log ($L_{IR}/L_\odot$) computed using the PSC data against log($M_G/M_\odot$) for all galaxies ($\theta < 20$ arcmin) in the largest FT sample. The mean value of α_{IR} is 0.9 which is about the same as α_B, but significantly less than α_H. As for the other bands, for the far-IR band also, α_{IR} increases slightly for later morphological types.

If we group the galaxies as function of T_c, the colour temperature obtained from the ratio of 60 and 100 μm flux densities we find that the correlations are tighter. In fact, instead of L_{IR}, we can use M_d, the amount of warm dust responsible for the far-IR emission given by

$$M_d \propto L_{IR}/(\int B(\nu, T_c)\, \varepsilon(\nu)\, d\nu$$

where $\varepsilon(\nu)$ is the emissivity of dust ($\propto \lambda^{-1}$) and $B(\nu, T_c)$ is the Planck function and the integration is performed from 40 to 120 μm. Since the total luminosity is $\propto T^5$ for $\varepsilon \propto \lambda^{-1}$, we can also write

$$M_d \propto L_{IR}\, R(T_c)/T_c^5$$

where $R(T_c)$ is the factor by which the 40–120 μm luminosity is to be multiplied to get the total luminosity and is listed as a function of T_c in the Catalogued Galaxies in the IRAS Survey (1985). For all the three samples, the correlations between M_d and M_G

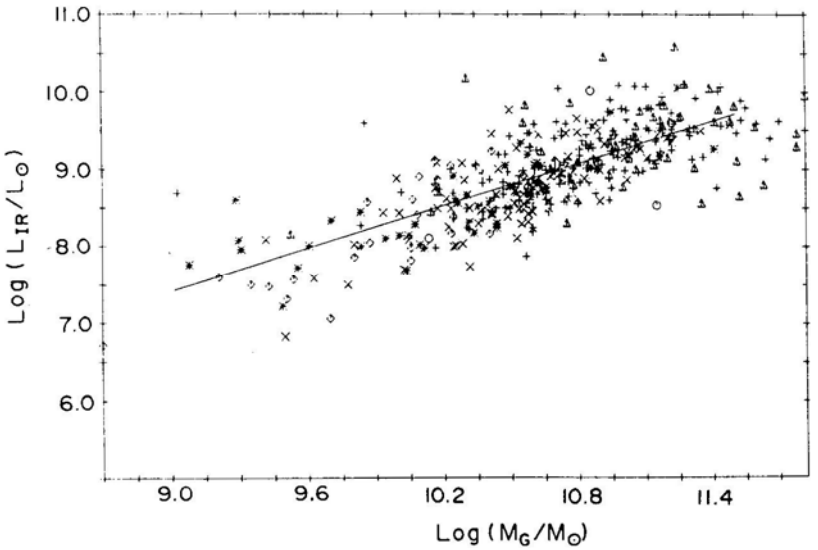

Figure 3. Log($L_{IR}/L_\odot$) plotted against log ($M_G/M_\odot$) for the FT sample. L_{IR} is the 40–120 μm luminosity. Symbols are as in Fig. 1.

are tighter than those between L_{IR} and M_G. The slope of the fit is also ~20 per cent higher. Fig. 4 shows a plot of log M_d against log($M_G/M_\odot$).

(iv) L_H versus L_{IR}

In Fig. 5, we show a plot of observed quantities, *viz., H* magnitude against log FIR. The relationship between the two can be represented by $L_{IR} \propto L_H^{0.73}$. This correlation is due to correlation of L_H and L_{IR} individually with M_G.

3.2 *Correleations Involving* $M_{H\,I}$

It is known that the average mass of the galaxy decreases and the fractional mass of atomic hydrogen increases as one goes from early morphological types to later types (Shostak 1978). In Fig. 6, we show a plot of log ($M_{H\,I}/M_\odot$) against log($M_G/M_\odot$) for the FT sample having the largest number of galaxies. As shown in Table 3, the relationship is of the form

$$M_{H\,I} \propto M_G^{\alpha_{H\,I}}$$

where $\alpha_{H\,I}$ =0.78. The correlation coefficient is 0.84 and the rms scatter in log $M_{H\,I}$ is 0.3, *i.e.,* a factor of only 2 in mass. The value of $\alpha_{H\,I}$ is found to be essentially the same for different morphological types. It is clear that since $\alpha_{H\,I} < 1$, the mean value of M_{HI}/M_G will increase as the mean value of M_G decreases for later morphological types.

Next, we look for correlations in the observed quantities, *viz.,* between H I and FIR. As seen in Table 3, the correlations are poor for both FT and LHS samples. If we plot the derived quantities, *viz.,* log ($L_{IR}/L_\odot$) against log ($M_{H\,I}/M_\odot$) instead of the observed

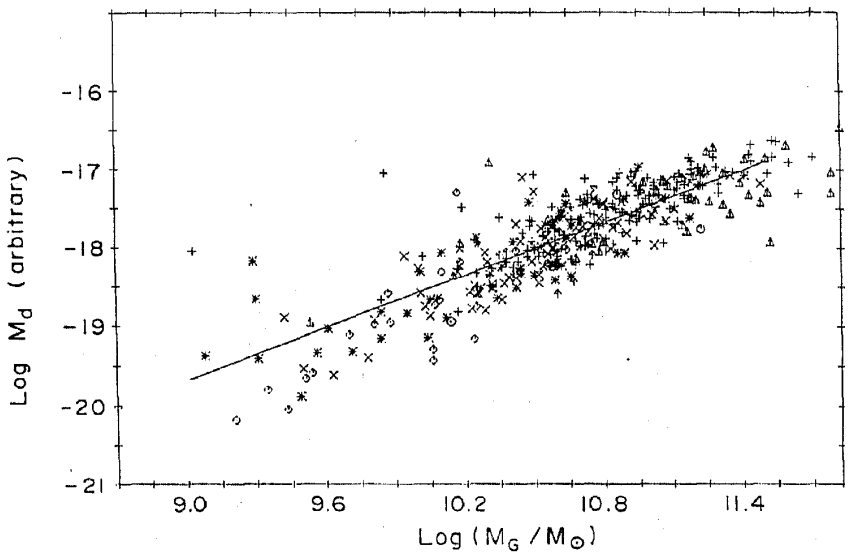

Figure 4. Plot of log M_d against log ($M_G/M_\odot$) for the FT sample. M_d is the mass of warm dust radiating in the 40–120 μm band. Symbols are as in Fig. 1.

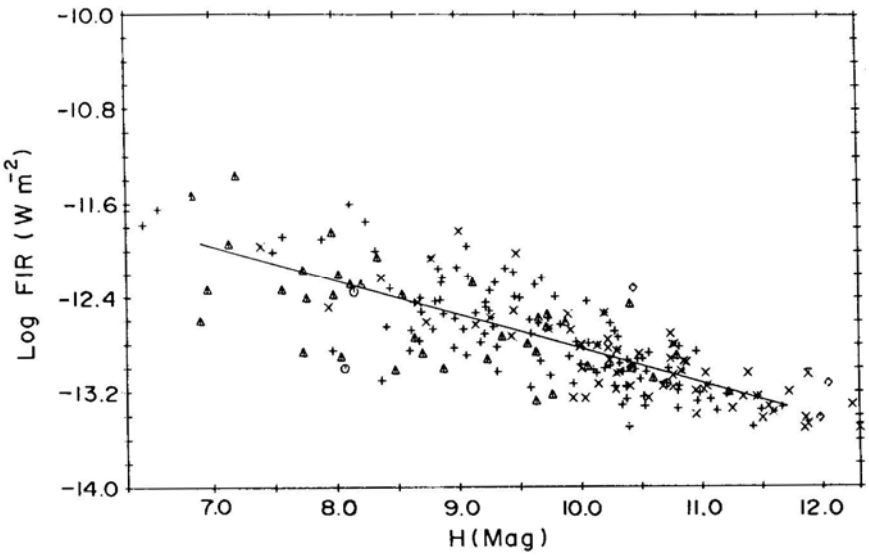

Figure 5. Log (FIR) plotted against apparent H magnitude where FIR is the 40–120 μm flux in units of W m^{-2}. Symbols are as in Fig. 1.

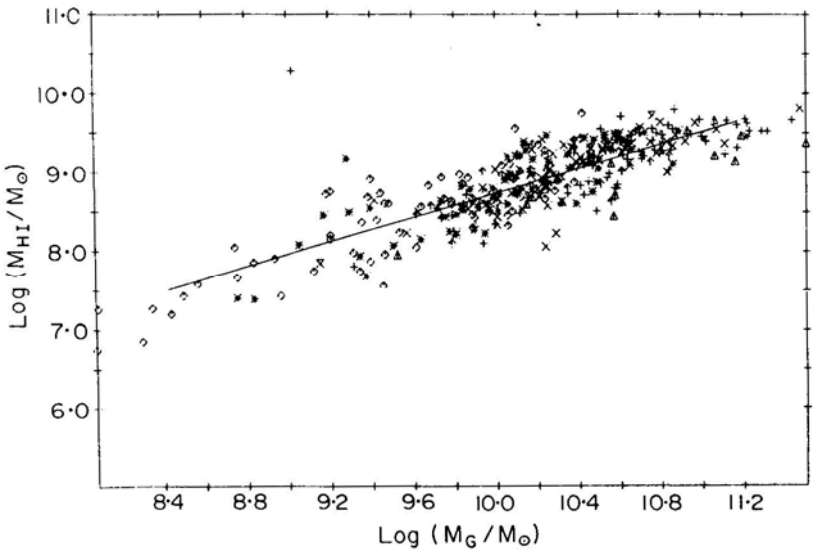

Figure 6. Plot of log $M_{\rm H\,I}/M_\odot$) against log($M_{\rm G}/M_\odot$) for the FT sample. $M_{\rm H\,I}$ is the mass of atomic hydrogen in the galaxy. Symbols are as in Fig. 1.

quantities, it is seen from Table 3 that the significance of correlation increases and the slope is ~0.9. Figs 7 and 8 show the FIR versus H I and $L_{\rm IR}$ versus $M_{\rm H\,I}$ plots respectively, for the FT sample. The increased significance in the plot for derived quantities is most probably due to the increased range in derived quantities resulting from the multiplicative factor of D^2 for both the quantities. The correlation between

Table 3. Correlations involving atomic hydrogen: Fits for log $Y=A + \alpha \log X$

X	Y	Sample	α	r^2	$(\delta \log Y)_{rms}$
FIR ($W\ m^{-2}$)	H I ($Jy\ km\ s^{-1}$)	FT	0.54 ± 0.06	0.43	0.44
"	"	LHS	0.15 ± 0.1	0.12	0.33
$M_{H\,I}$	L_{IR}	FT	0.89 ± 0.06	0.65	0.46
$M_{H\,I}$	L_{IR}	LHS	0.89 ± 0.06	0.78	0.39
M_G	$M_{H\,I}$	FT	0.78 ± 0.03	0.84	0.30
$M_{H\,I}$	L_H	AHM	1.13 ± 0.07	0.72	0.44

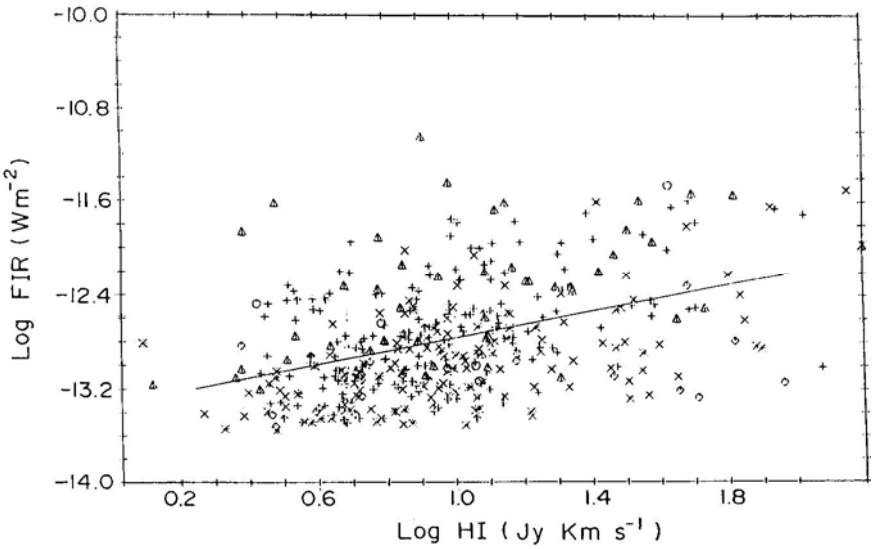

Figure 7. Plot of log FIR ($W\ m^{-2}$) against log H I ($Jy\ km\ s^{-1}$) for the FT sample.

$M_{H\ I}$ and L_{IR} is hence to be treated with caution. It may be noted that because of correlation of $M_{H\,I}$ and L_{IR} individually with M_G, we do expect to see some correlation between $M_{H\,I}$ and L_{IR}. Similarly, we also see a correlation between L_H and $M_{H\,I}$. In summary, we can state that the correlation of atomic hydrogen mass with L_{IR} is not as good as that seen for M_{H_2}, the mass of molecular hydrogen gas (Rengarajan & Verma 1986).

4. Discussion

The integrated luminosity in a given band is the result of contributions from stars of different masses. In general one can write

$$L = \int \xi(M) L(M)\ T(M)\ f(M)\, \mathrm{d}M$$

where $\xi(M)$, the IMF is the number of stars per unit mass interval at mass M born per unit time, $L(M)$ is the total luminosity of a star of mass M, $f(M)$ is the fraction of the

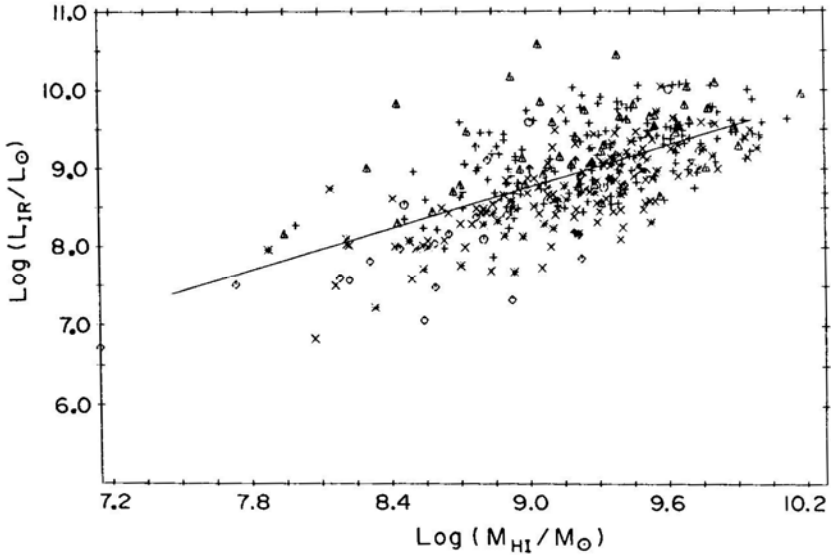

Figure 8. Plot of log ($L_{IR}/L_{\odot}$) against log ($M_{HI}/M_{\odot}$) for the FT sample.

total luminosity that is radiated in the given band and $T(M)$ is the lifetime of the star or that of the galaxy whichever is lower. For the far-IR band, if we assume a dust re-radiation mechanism, $f(M)$ represents the fraction of bolometric luminosity that is absorbed and reradiated by the dust. For more massive stars ($>30M_{\odot}$) having lifetime of $<10^7$ yr, the dust column density surrounding them could be large enough for $f(M)$ to be ~ 1 resulting in most of the stellar luminosity being radiated in the far-IR. As mass decreases, the star lives longer, the dust environment depletes, and $f(M)$ will decrease. Since the parent molecular clouds have probably lifetime of ~ 10^8 yr (Solomon & Sanders, 1980), $f(M)$ becomes $\leqslant 1$ by this time. With an IMF similar to that in the solar neighbourhood (Scalo 1986) one then finds that the period over which contribution to L_{IR} is effective is $\sim 10^7$ yr.

Some authors (Cox, Krugel & Mezger 1986; Persson & Helou 1987) have proposed that the far-infrared emission of galaxies consists of two components: a warm one associated with OB stars and a cooler one from dust in the interstellar medium with a significant contribution from nonionising stars with the two components having approximately the same luminosity. For the average temperatures quoted for these two components, we estimate for an $1/\lambda$ emissivity dependence, the contribution of the cold component to the 40–120 μm luminosity to be ~30 per cent. Since about 70 per cent of the 40–120 μm luminosity is from the warm dust component associated with OB stars it is reasonable to take it as a measure of recent star-formation activity Thronson & Telesco (1986) are also of this view. Even if the average dust optical depth is such that only a fraction of the OB star luminosity is reradiated in the warm dust environment, 40–120 μm luminosity can still be Used as a measure of the OB star luminosity as long as the contribution to this band from the cooler component is small.

For the blue luminosity an analysis similar to the above indicates that the effective period of contribution is $\sim 3 \times 10^9$ yr.

To convert the observed luminosities to SFR, *viz.,* the average rate of production of stellar mass per unit time, we need a knowledge of $\xi(M)\ f\ (M)$. Because of the uncertainties in these we do not attempt to get absolute rates.

The linear relationship observed between L_B and $L_{\rm IR}$ has been interpreted to imply that both L_B and $L_{\rm IR}$ originate from newly formed massive stars (Rickard & Harvey 1984). However, it has been argued that the presence of correlation between $T_{\rm c}$, the dust temperature derived from the ratio of 60 and 100 μm IRAS flux densities and $L_{\rm IR}$, and the absence of such a correlation between $T_{\rm c}$ and L_B imply different sources for the two luminosities (Iyengar, Rengarajan & Verma 1985; Rieke & Labofsky 1986; Soifer *et al.* 1987). The correlation between L_B and $L_{\rm IR}$ ($L_{H\alpha}$) is then a result of connection through the mass function. Our analysis shows that the primary correlation is between the luminosity and $M_{\rm G}$. The correlations between luminosities are a result of individual correlations with mass. Since both α_B and $\alpha_{\rm IR}$ are about the same, we get a linear dependence between L_B and $L_{\rm IR}$ leading to the conclusion that the current SFR and SFR over 10^9 yr is the same.

The situation is different with H band luminosity which measures SFR over the life of the galaxy. The steeper dependence of L_H on $M_{\rm G}$ implies that more massive galaxies have had more star formation in the past than the less massive galaxies. Since the luminosities in different bands are sensitive to different ranges of steller masses, the increased H luminosity can arise either due to a change in the SFR itself or due to changes in the IMF. The changes in power law indices also lead to changes in the mean values of L/M for different bands as a function of morphological type. We have shown in Table 4 the logarithmic mean values of $M_{\rm G}$, L_H/M_G, L_B/M_G, L_{lR}/M_G and $M_{\rm H\,I}/M_G$ for three groups of morphological types. It is seen that while the luminosity-to-mass ratio is a constant for B and far-IR, it decreases for H and the fractional gas mass increases as morphological type increases and the mean galaxy mass decreases. The anti-correlation between the mean values of L_H/M_G and $M_{\rm H\,I}/M_{\rm G}$ simply reflects the fact that more star formation means a larger use of available gas.

It is clear that mass of the galaxy plays an important role in the process of star-formation. However, it is also seen that the mass dependence of various luminosities does not change much with morphological type. Further, the change in mean mass as morphological type increases is small compared to the range in the masses of the galaxies. Thus, galaxies of same mass can be of different morphological types. The morphological appearance is probably determined by the very early history of star-formation during the stage in which the collapse to a disc took place.

Table 4. Mean values *versus* morphology (arbitrary units).

	Type					
	1, 2, 3		4, 5, 6		7, 8, 9, 10	
	mean	rms	mean	rms	mean	rms
$\mathrm{Log}(M_G/M_\odot)$	10.98	0.47	10.71	0.42	10.01	0.59
$\log(L_B/M_G)$	−3.22	0.23	−3.14	0.25	−3.04	0.44
$\log(L_H/M_G)$	−4.1	0.15	−4.28	0.21	−4.54	0.20
$\log(L_{\rm IR}/M_G)$	−1.56	0.35	−1.47	0.32	−1.57	0.31
$\log(M_{\rm H\,I}/M_G)$	−0.88	0.27	−0.63	0.25	−0.45	0.20

5. Conclusions

We have made use of data on spiral galaxies from three catalogues of 21 cm observations and studied the correlations between dynamic mass of the galaxy and luminosities in various bands.

(1) We find the following correlations:

$$L_H \propto M_G^{1.3},$$
$$L_B \propto M_G,$$
$$L_{IR} \propto M_G,$$
$$M_{H\,I} \propto M_G^{0.78}.$$

It is seen that while the blue and infrared luminosities are, within errors, linearly dependent on the mass of the galaxy, the H luminosity is a steeper function of M_G.

(2) Correlations are also observed between L_B and L_{IR}, L_{IR} and L_H etc. which reflect individual correlations with M_G

(3) The mass of atomic hydrogen is poorly correlated with L_{IR}.

(4) More massive galaxies have had larger SFR in the past as compared to the present $\sim 10^9$ years. This leads to the anti-correlation between mean L_H per unit galaxy mass and mean gas mass (H I) per unit galaxy mass as the morphological type increases (mean galaxy mass decreases).

References

Aaronson, M., Huchra, J., Mould, J. 1979, *Astrophys. J.,* **229,** 1.

Aaronson, M., Huchra, J., Mould, J. R., Tully, R. B., Fisher, J. R., Van Woerden, H., Goss, W. M., Chamaraux, P., Mebold, U., Siegman, B., Berrimann, G., Persson, S. E. 1982, *Astrophys. J. Suppl. Ser.,* **50,** 241 (*AHM*).

Catalogued Galaxies and Quasars observed in the IRAS Survey, 1985, prepared by C. J. Lonsdale, G. Helou, J. C. Good, W. Rice, Jet Propulsion Laboratory.

Cox, P., Krugel, E., Mezger, P. G. 1986, *Astr. Astrophys.,* **155,** 380.

Fisher, J. R., Tully, R. B. 1981, *Astrophys. J. Suppl. Ser.,* **47,** 139 (*FT*).

Gallagher, J. S., Hunter, D. A., Tutukov, A. V. 1984, *Astrophys. J.,* **284,** 544.

IRAS Small Scale Structures Catalogue, 1986,, prepared by G. Helou & D. Walker, US Government Printing Office, Washington D.C.

Iyengar, K. V. K., Rengarajan, T. N., Verma, R. P. 1985, *Astr. Astrophys.,* **148,** 43.

Jackson, J. M., Barret, A. H., Armstrong, J. T., Ho, P. T. P. 1987, *Astr. J.,* **93,** 531.

Kenney, J. F., Young, J. S. 1986, in *Proc. Caltech Symp. Star Formation in Galaxies,* Ed. C. J. Lonsdale Persson, NASA Conference Publication 2466, p. 287.

Lewis, B. M., Helou, G., Salpeter, E. E. 1985, *Astrophys. J. Suppl. Ser.,* **59,** 161 (LHS)

Persson, C. J., Helou, G. 1987, *Astrophys. J.,* **314,** 513.

Rengarajan, T. N., Verma, R. P. 1986, *Astr. Astrophys.,* **165,** 300.

Rickard, L. J., Harvey, P. M. 1984, *Astr. J.,* **89**, 1520.

Rieke, G. H., Lebofsky, M. J, 1979, *A. Rev. Astr. Astrophys.,* **17,** 477.

Rieke, G. H., Lebofsky, M. J. 1986, *Astrophys. J.,* **304,** 326

Sandage, A. 1986, *Astr. Astrophys.,* **161,** 89

Scalo, J. M. 1986, *Fund. Cosmic Phys.,* **11,** 1

Scoville, N., Young, J. S. 1983, *Astrophys. J.,* **265,** 148.

Shostak, G. S. 1978, *Astr. Astrophys.,* **68,** 321.

Solomon, P. M., Sanders, D. B. 1980, *Giant Molecular Clouds in the Galaxy,* Eds P. M. Solomon & M. G. Edmunds, Pergamon Press, Oxford, p. 41.
Soifer, B. T., Sanders, D. B., Madore, B. F., Neugebauer, G., Danielson, G. E., Elias, J. H., Lonsdale, C. J., Rice, W. L. 1987, *Astrophys. J.,* **320,** 238.
Tacconi, L. J., Young, J. S. 1986, *Astrophys. J.,* **308,** 600.
Thronson, H. A., Telesco, C. M. 1986, *Astrophys. J.,* **311**, 98.
Tully, R. B., Fisher, J. R. 1977, *Astr. Astrophys.,* **54,** 661.
Young, J. S. 1986, in *Proc. Caltech Symp. Star Formation in Galaxies,* Ed. C. J. Lonsdale Persson, NASA Conference Publication 2466**,** p. 197.
Young, J. S., 1987, in *IAU Symp. 115*: *Star Forming Regions,* Eds M. Piembert & J. Jugaku, D. Reidel, Dordrecht, p. 557.
Young, J. S., Schloerb, F. P., Kenney, J. D., Lord, S. D. 1986, *Astrophys. J.,* **304,** 443.

J. Astrophys. Astr. (1988) **9,** 93–106

Spectroscopic Observations of SN1987a in the LMC

J. B. Hearnshaw, V. J. McIntyre & A. C. Gilmore *Mt John University Observatory and Department of Physics, University of Canterbury, Private Bag Christchurch, New Zealand*

Received 1987 December 16; accepted 1988 March 4

Abstract. This paper describes the results of optical spectroscopy of SN1987a carried out at Mt John University Observatory on a regular basis since 1987 February 25. Typical spectra are presented in an evolutionary sequence, and velocities of Balmer and selected metallic lines are measured in either emission or absorption. The velocities are interpreted together with the results of photoelectric photometry. The Barnes-Evans relationship has been applied to the photometry to give an angular diameter of the photosphere. The expansion velocity of the photosphere is initially about 3700 km s^{-1} which is similar to the asymptotic value from weaker absorption lines such as the MgIb line. After 40 days the photosphere appears to expand more slowly and it reaches a maximum size of about 145 A.U. after about 100 days before receding inwards. The photometry and spectroscopy together result in a distance modulus of 18.3 ± 0.2.

Key Words: Supernovae—SN1987a—optical spectra

1. Introduction

We have obtained optical spectra of SN1987a on a regular basis since 1987 February 25. The purposes of this paper are: (i) to display a selection of typical spectra in an evolutionary sequence, (ii) to show that the velocities of absorption and emission features are consistent with the predictions of a simple model, and (iii) to derive the radius of the photosphere from published photoelectric photometry and to show that its initial velocity is in agreement with the spectroscopic data on Doppler shifts.

2. Observations and reductions

2.1 *Spectroscopic Data*

We have obtained medium resolution red photographic spectra of SN1987a on 86 nights between 1987 February 25 and October 31 inclusive, and blue spectra on 87 nights in the same interval. Most of the spectra were obtained on the 0.61 m Boller and Chivens telescope at Mt. John University Observatory. A few were obtained on the 0.61 m Optical Craftsmen telescope, and those taken since August 24 have been on the 1 m McLellan telescope. The emulsion used was mainly Kodak IIIaF for red plates

and IIaO for blue plates. These were sometimes hypersensitised for several hours in H_2. The dispersions were 9.0 nm mm^{-1} (second order red), and 6.0 nm mm^{-1} (third order blue), and the resolutions were respectively 0.16 and 0.11 nm corresponding to about 83 km s^{-1} (red) and 70 km s^{-1} (blue).

The plates were digitised on the Joyce-Loebl model 3CS microdensitometer at the Physics Department, University of Canterbury, and the spectra were subsequently analysed and displayed using the ATLAS spectroscopic reduction program on the University's Burroughs 6900 computer. This program fits a third order least squares curve through the positions of selected comparison lines from a He-Ar lamp, allowing wavelengths of a given pixel to be determined to aprecision of about 2Å, which is much less than the intrinsic line widths in the supernova spectrum.

2.2 *Photometric Data*

The photoelectric photometry used for this analysis was the Johnson-Cousins *UBVRI* photometry of Menzies *et al.* (1987) and Catchpole *et al.* (1987) from SAAO. An extinction correction of $A_V = 0.60$ (West *et al.* 1987) and $R = A_V/E(B - V) = 3.2$ were applied to the photometry. The reddening in $(V - R)_c$ was in the range 0.11 ± 0.01, the actual value depending on colour index according to the methods recommended by Taylor (1986). The Cousins $(V - R)_0$ colour index was transformed to the Johnson $(V - R)_0$ index using the calibrations of Taylor (1986), assuming these results to be valid for SN 1987a. Both the Cousins and Johnson photometry is affected by the lines, especially the Hα line in the *R* band. The strong absorption components of the P Cygni profiles partially compensate for the emission. The effect of this contamination is discussed further in Section 7. The results in Section 5 are fairly insensitive to the adopted extinction and reddening.

3. Spectroscopic results

Typical blue and red spectra are displayed in Figs 1 and 2. These are density plots. No correction for instrumental response has been made. Some line identifications are included, mainly from the work of Ashoka *et al.* (1987). The spectrum is classified as a Type II supernova; Hα is always a strong P Cygni profile. However the *H*β and higher Balmer lines faded during March to be weak or, in the case of Hβ, absent by March 27. They were clearly visible again by mid-May and strengthened rapidly during the first week of June. Hβ became completely dark in its centre by June 6.

Numerous changes in the spectrum occurred in the regions of Hα and Hβ during March. In particular we note the emission bump at 647 nm on the short wavelength side of the Hα emission, which was visible March 18.33 to about April 17 with a maximum strength on March 22 (Hearnshaw & Haar 1987; Hanuschik & Dachs 1987), and also the double-peaked Hα emisson which we observed March 19.37 to April 19.34 with a maximum strength of the second component (668 nm; He I?) around March 25 (Hearnshaw & Haar 1987).

The virtual disappearance of Hβ at the end of March may have been partly due to blending by other features (see March 27.42 spectrum in Fig. 1); however the simultaneous weakening of Hγ and Hδ absorptions suggests that blending was not the sole cause.

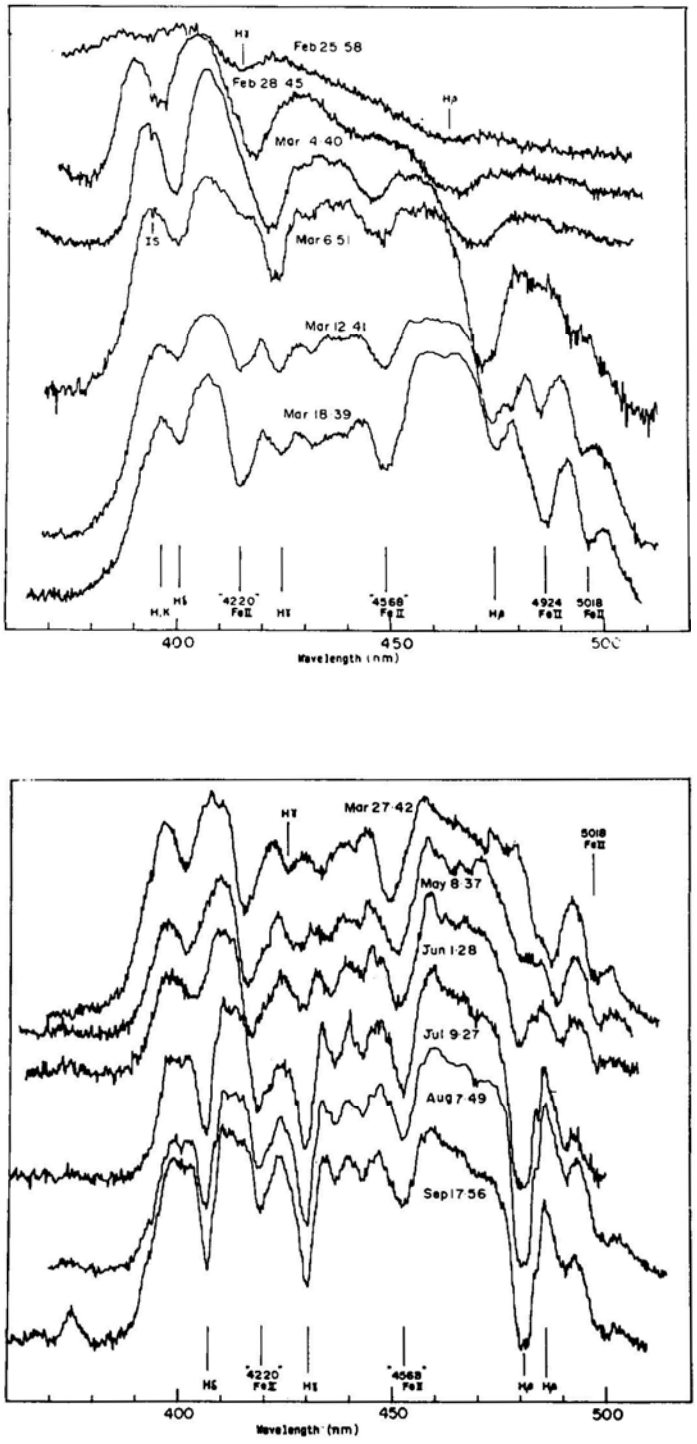

Figure 1. SN 1987a: Density tracings of blue spectrograms between 1987 February 25 and September 17.

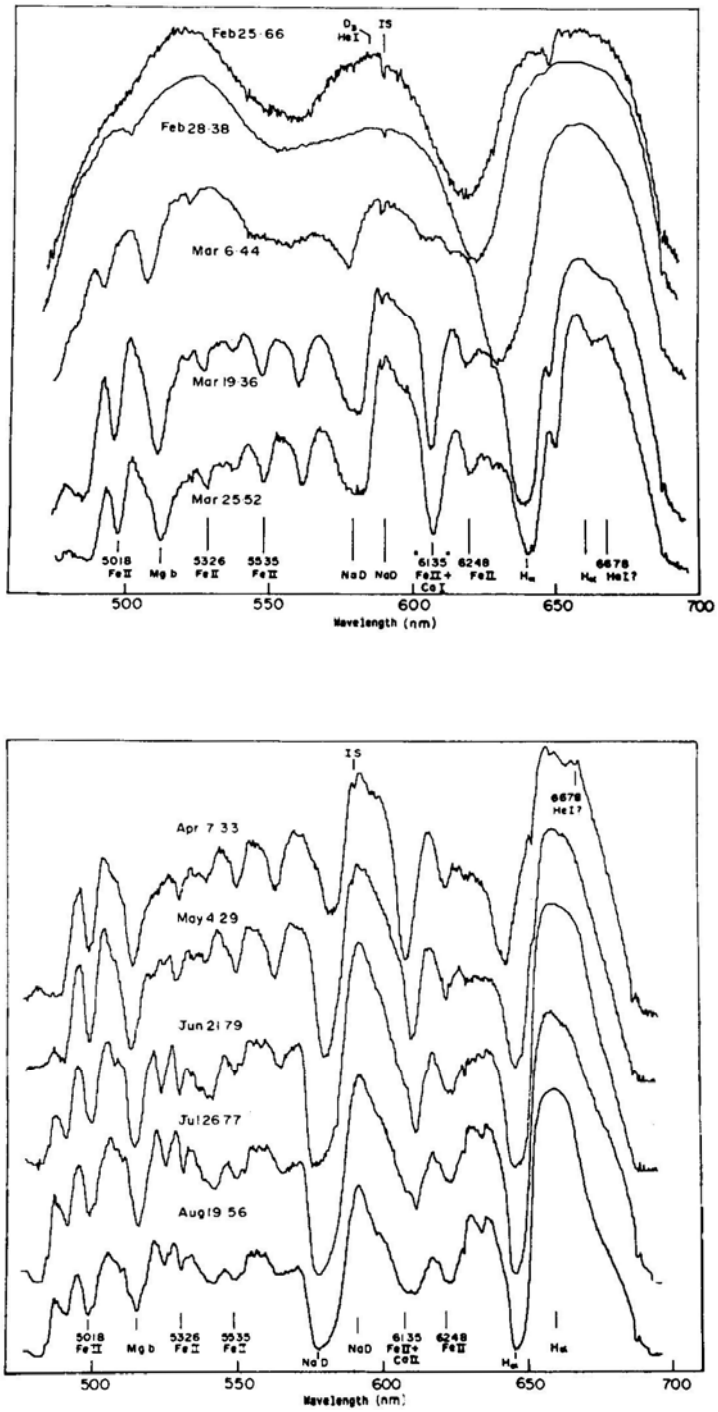

Figure 2. SN 1987a: Density tracings of red spectrograms between 1987 February 25 and August 19.

The emission in the near-UV was initially strong but declined rapidly. The spectrum was completely dark below 380 nm from about March 6. However, two weak emission features at 367 and 375 nm first seen on August 7.49 increased slowly in strength during September (Hearnshaw & McIntyre 1987). One of these lines (probably that at 375 nm) may be nebular [O II] 373 nm which appeared and strengthened at about the same time as [O I] 630 and 636 nm appeared (Anupama *et al.* 1988).

According to Branch (1987), strong Ti II 376 nm should have been visible from March for envelope temperatures below 7000K. Our spectra show no sign of this line at least during the first five months.

4. Radial velocities

The optical spectra consist of broad P Cygni profiles with emission components relatively close to their rest wavelengths and blue-shifted absorption components. These latter in general declined rapidly to smaller velocities of expansion during the first approximately 80 days but changed only slightly in velocity thereafter until the present (late October). We have concentrated on the measurement of the velocities of a few representative absorption and emission features which appeared well-defined in most of our spectra and were readily identifiable. The emission lines measured were: Hα and Na D, while the absorption lines measured were Hα, β, γ and δ, Na D, Mg b and Fe II 501.8 and '456.5', the latter being a blend of five Fe II lines (452.26, 454.95, 455.59, 458.38 and 462.93 nm).

Figs 3 to 7 show the velocity curves from the measured features in the LMC rest frame (using v(LMC) = +270 km s^{-1}).The data refer to the deepest mimima of the respective absorptions, as estimated from the plotted spectra. Weighted mean rest wavelengths of blended features were calculated from Kurucz & Peytremann (1975) *gf* values for obtaining velocities, namely 517.82 nm for the Mg b triplet, 589.195 nm for Na D and 456.53 nm for the Fe II blend in the blue. The velocities plotted are apparent expansion velocities relative to the supernova centre of mass, i.e. (270 km s^{-1}–$v_{\rm rad}$), where $v_{\rm rad}$ is the radial velocity as measured from the earth. These values are also tabulated in Tables 1 and 2.

The best defined velocity curve is that for Hα absorption. The extrapolated blueshift at time t = 0 (corresponding to the neutrino pulse at 1987 February 23.32 UT) was v_0 = – (20.15 ± 0.5) Mm s^{-1} with an initial apparent deceleration of (690 ± 70) km s^{-1} d^{-1}.

One striking feature of both the Hα and Na D emission lines investigated is that they have redshifts of about 1.0 Mm s^{-1} (as seen in the LMC red frame). These are plotted as negative expansion velocities in Figs 3 and 5. These redshifts are considerably smaller than the full widths of the emissions at zero intensity, which were around 12 Mm s^{-1} for both lines in most of the time interval under study (t>80d), except the early stages when they were broader. Since infalling matter is not a plausible scenario, we interpret the redshifts as evidence for nonspherical asymmetry of the expansion, with more material being ejected on the far side of the expanding envelope than towards the observer on the near side. The asymmetry of some of the emission lines (including Hα and Na D) may also be partly due to the asymmetry of the expansion, and the strongly wavelength-dependent polarization found by Cropper & Bailey (1987) and by Schwarz & Mundt (1987) also suggests that the ejecta lacked spherical symmetry (see Jeffery 1987 for discussion of polarimetry).

Table 1. Velocities measured from red plates (All velocities are in km s^{-1}, measured in the rest frame of SN).

Days since 1987 February 23.32	Hα (Emn)	Hα (Absn)	Na I D (Emn)	Na I D (Absn)	Mg I b (Absn)	Fe 501.8 (Absn)
2.341	−287	18156	1999	16154	...	...
5.055	1725	...	1082	18038	...	...
5.177	536	16338	...	...	10499	...
9.106	307	13701	879	7141	7482	7518
11.116	−973	12874	751	6021	6456	6111
13.171	−332	11542	60	5563	5922	6071
17.036	−743	10011	−1140	5007	5148	...
19.093	−1247	9379	−1121	5016	4638	...
23.008	−972	8533	−1082	4711	4450	...
24.044	−1064	8172	−940	4646	4140	...
25.013	−1201	8441	−148	4941	3830	3552
26.034	...	8195	...	...	...	...
27.018	−1567	8041	−1603	3949	4000	3139
29.049	−1064	8004	−1377	4642	3830	...
30.197	−195	7831	−635	4717	3360	...
32.128	...	7704	...	...	...	...
32.136	−1430	7513	−1334	4298	3543	...
38.047	−1338	7112	−1753	3769	3150	...
39.058	−744	7112	−1467	4157	3150	...
41.061	−607	7875	−1265	3708	3320	...
42.042	−698	7090	−1867	3928	3210	2607
43.014	−561	6873	−914	4017	3110	2675
46.068	−698	6917	−1226	3532	2930	2465
46.984	−561	6433	−635	4389	2780	2420
48.057	−652	6526	−1463	4201	3170	2289
51.043	−561	6589	...	...	...	...
52.158	...	6327	−1442	4130	...	2830
53.086	−150	6213	−680	4780	3210	2693
54.033	−607	6312	−881	3785	2970	2250
55.024	−927	6136	−1561	4130	3039	2482
67.142	−927	5427	−718	4388	3024	2342
68.009	−790	5591	−1028	4405	2880	2332
70.110	−836	5363	−707	4671	3120	2454
71.083	−1201	5363	−1169	4581	2710	...
73.193	−881	5299	−939	4377	2710	2340
74.020	−1247	5235	−1000	4575	2780	...
75.010	−1110	5363	−1292	4675	2750	...
75.972	−1201	5299	−1158	4743	2650	...
76.991	−1658	5671	−1252	4682	2740	...
77.988	−1110	5171	−852	4489	2940	2200
79.118	−652	5171	−1030	4525	3115	2183
79.968	−744	5038	−1050	4687	3185	2368
79.976	...	5299	...	...	...	...
88.966	−515	5171	−872	4789	2886	2224
95.008	−790	5038	−1231	5044	2656	2233
97.048	−1247	...	−1119	4828	2725	1994
97.056	−790	5130	−1150	5244	3158	2394
97.995	−881	5102	−1282	5123	2941	2362
99.111	−927	...	−1142	4998	2688	2130
102.037	−927	4974	−1249	5136	2813	2104
103.043	−1201	5038	−887	5123	2503	2058

Table 1. Continued.

Days since 1987 February 23.32	Hα (Emn)	Hα (Absn)	Na I D (Emn)	Na I D (Absn)	Mg I b (Absn)	Fe 501.8 (Absn)
106.357	−58	5102	−1031	5835	2484	2066
107.163	−1384	4974	−1151	5639	2767	2068
108.107	−698	5235	−1208	5354	2351	2071
109.063	...	5235	...	...	...	...
111.014	−835	4910	−1317	5367	2346	1989
114.008	−835	5038	−877	5860	2241	2044
117.410	−927	5103	−927	6187	...	...
118.470	−972	4910	−1465	5980	2299	2022
119.447	−927	4910	−1171	5883	2250	2136
130.218	−515	5102	−732	6076	2177	2618
132.031	−515	5038	−1173	5986	2060	2344
133.063	−835	5038	−934	5800	1964	1877
136.097	−790	4975	−1272	5720	1714	2250
152.143	−561	4910	−948	5749	2236	2238
153.452	−378	4924	−1151	5950	2015	2082
155.078	−790	4924	−1062	6091	1919	2146
156.165	−927	5062	−1280	6007	1916	2215
156.208	...	4970	...	...	...	...
167.417	−1429	5094	−990	6019	2096	2545
168.294	−652	4975	−1283	5817	1885	2390
171.386	−1155	...	−1312	5946	1967	2540
171.413	−1475	4911	−1304	5868	1804	2478
175.194	−1475	4911	−947	6145	2079	2297
176.295	−1292	4911	−1144	5891	1852	2378
177.243	−1064	4924	−1249	5930	1874	2282
189.069	−1155	5058	−1135	5787	1636	2195
198.320	−1247	5052	−1047	5647	1685	2202
217.252	−1292	4713	−1135	5390	2648	2320

Table 2. Velocities measured from blue plates (All velocities are in km s^{-1}, measured in the rest frame of SN).

Days since 1987 February 23.32	Hβ (Absn)	Hγ (Absn)	Hδ (Absn)	Fe 456.5 (Absn)
2.256	13369	13241	...	...
5.132	13151	11466	10859	...
9.078	9979	8857	8168	7337
11.185	8784	7927	7833	6511
13.149	7945	7409	8096	6070
17.085	7709	7324	7711	5595
19.037	7565	7213	7915	5344
23.067	7292	6977	7340	5425
25.033	7083	6336	7171	5277
26.013	7058	6470	6935	4896
29.018	6600	6088	6820	5009
30.338	6104	6005	6925	4895
32.112	5738	6043	6610	4820
38.092	5723	5768	6817	4794

Table 2. Continued.

Days since 1987 February 23.32	Hβ (Absn)	Hγ (Absn)	Hδ (Absn)	Fe 456.5 (Absn)
42.018	5671	5654	6670	4718
46.031	5633	5750	6791	4717
47.024	...	5488	6926	4648
53.122	...	5535	6815	4576
68.030	...	5072	6456	4025
70.020	3897	3889	6521	4264
74.054	3490	4547	6485	4070
75.034	3584	3803	6100	3957
77.010	3976	4747	6471	3986
79.041	2793	4552	6429	3855
80.004	3703	4117	6047	3838
80.070	2959	4501	6165	3690
88.927	3902	4009	6178	3543
97.963	3968	3819	5284	3386
102.038	3964	3799	5218	3212
106.247	4088	3868	4507	3556
108.020	4036	3615	4217	2877
111.047	4050	3577	3937	3153
113.968	3953	3525	3638	2959
117.453	3853	3404	3632	2985
119.474	3923	3573	3593	3132
132.074	3827	3495	3321	2937
133.039	3673	3279	3535	2948
135.954	3787	3489	3291	2811
146.444	3794	3406	3283	2770
153.405	3777	3205	3209	2810
155.020	3729	3288	3189	2870
156.003	3746	3234	3049	2805
157.151	3824	3258	3054	2833
165.170	3658	3187	3268	2680
171.372	3667	3178	3085	2611
177.362	3586	3090	3038	2660
189.118	3557	3017	2782	2561
196.156	3436	2743	2784	2595
206.237	3592	2969	2661	2728
215.347	3744	3174	2958	2937

One feature of the D line emission velocity is that the redshift of 1.0 Mm s^{-1} (in LMC frame) was only observed for t >20d. It fell linearly from 2.4 Mm s^{-1} in the interval $0 < t < 20$d. Part of this early velocity change may be due to the feature being composed mainly of He I(D_3) 587.6 nm in the early stages, which would be seen to have an apparent 900 km s^{-1} blueshift if it were assumed to be Na I($D_{1,2}$) 589.2 nm as in this analysis.

The absorption velocities show a correlation with line strength and hence optical depth. The strongest features such as Hα have the largest velocities and highest optical depths. Higher Balmer lines form deeper in the envelope at lower velocities. This is shown clearly in Fig. 4 where the absorption velocity of Hα at t = 200d is about 5500 km s^{-1}; of Hβ 3100 km s^{-1}; and of Hγ and Hδ 1800 km s^{-1}. The same

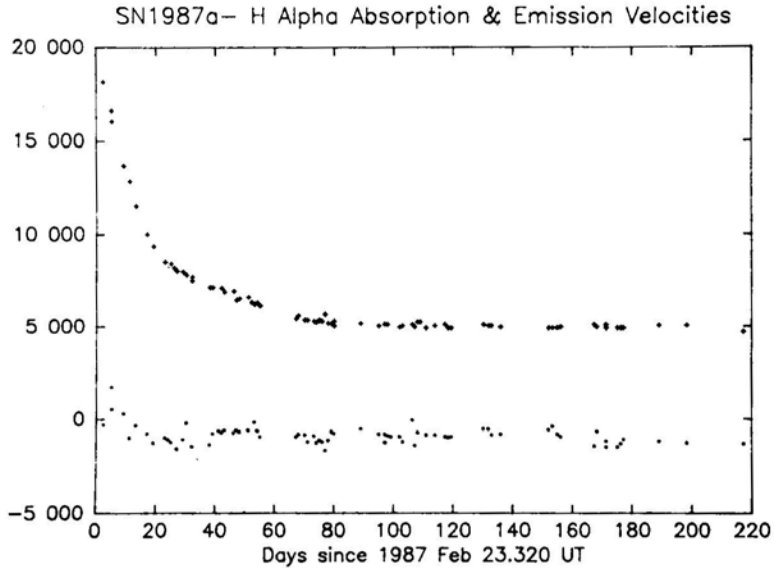

Figure 3. SN 1987a: Absorption and emission velocities of Hα line.

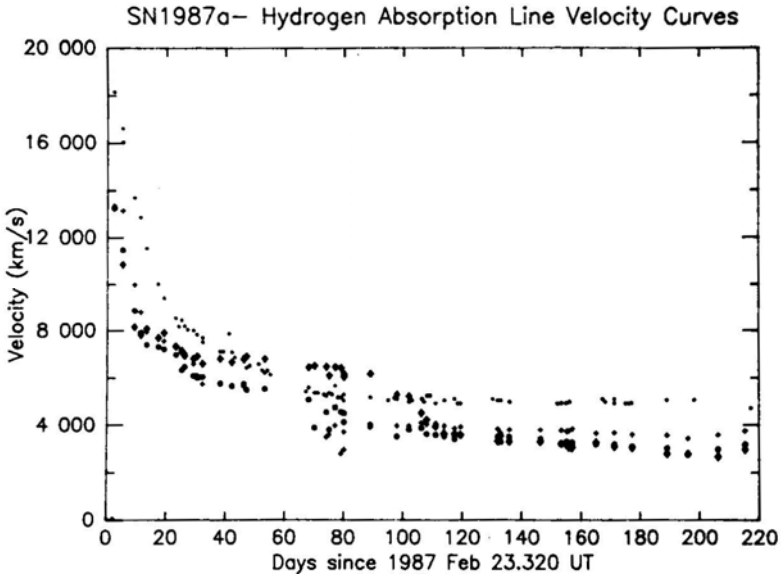

Figure 4. SN 1987a: Absorption and emission velocities of Hα (dots), Hβ (crosses), Hγ (circles) and Hδ (diamonds) lines.

phenomenon is observed for the two Fe II absorption features studied (Fig. 7) which approached different asymptotic velocities of 2800 km s^{-1} (456.5 nm) and 2300 km s^{-1} (501.8 nm).

The lower velocities of weaker lines are expected from the Type II supernova model of Kirshner & Kwan (1974) in which the lines form by scattering in a homologously

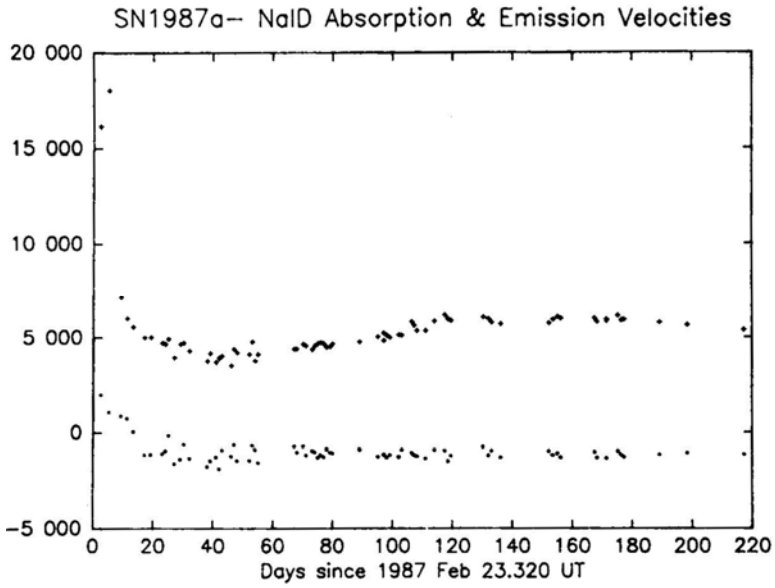

Figure 5. SN 1987a: Absorption and emission velocities of Na I D line.

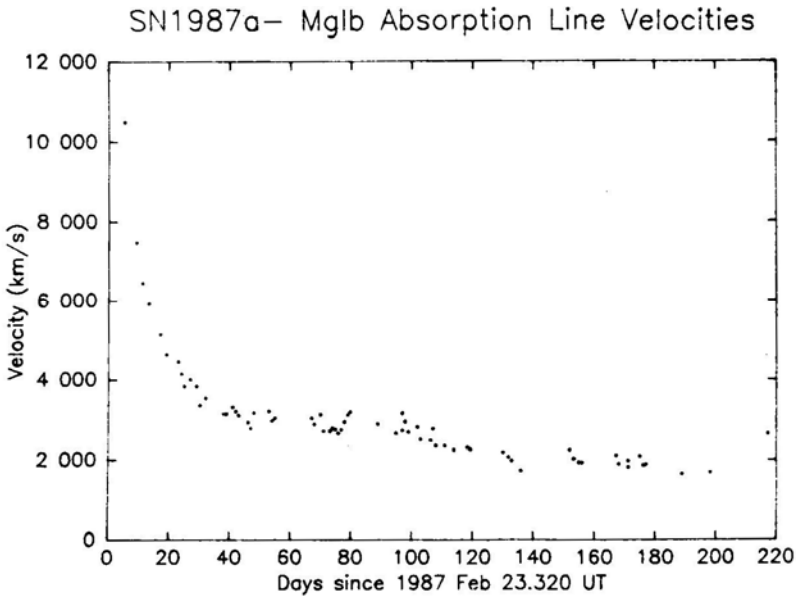

Figure 6. SN 1987a: Absorption velocities of Mg I b line.

expanding envelope above the photosphere. The expansion velocity $v \propto r$, where $r = R/R_{\max}$ and $R_{\max}$ is the maximum size of the outer edge of the envelope ($R_{\max} \sim v_0 t$). Since the density in the envelope is expected to increase very rapidly with decreasing r ($p \propto r^{-7}$) for this model, it follows that optically thin lines should form close to the photosphere, whereas optically thick lines are observed to have the larger velocities of the material at a higher level.

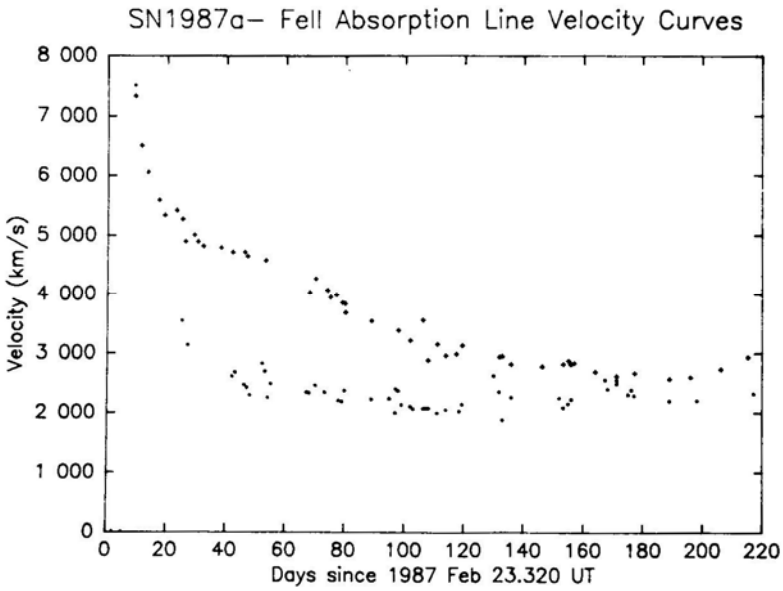

Figure 7. SN1987a: Absorption velocities of Fe II '456.5' (crosses) and 501.8 (dots) lines.

Our results for Balmer and metallic line absorption velocities appear to be in good agreement with data reported by other workers for the earlier stages of the expansion, including Blanco *et al.* (1987), Ashoka *et al.* (1987), and Danziger *et al.* (1987).

5. Angular radius of photosphere

The Barnes–Evans relationship (Barnes & Evans 1976; Barnes *et al.* 1976) was used to determine the angular size of the photosphere of SN1987a. The analysis followed that used by Ashoka *et al.* (1987). We used here the following equation for the visual surface brightness parameter F_V

$$F_V = 3.977 - 0.429(V-R)_{0J}$$

as determined by Barnes and Evans (1976). This gives

$$\log \phi = 0.4874 - 0.2V_0 + 0.858(V-R)_{0J}$$

where ϕ is the angular diameter of the photosphere in milli-arcsec. The radius of the photosphere is then

$$R_{phot} = 52.5(\phi/2)\text{A.U.}$$

where a distance modulus of 18.6 corresponding to D = 52.5 kpc has been adopted (Feast 1984).

The results are shown in Fig. 8 and are derived from the SAAO photometry of Menzies *et al.* (1987) and Catchpole *et al.* (1987) (see Section 2.2). The photospheric radius of a blue B3 I supergiant, such as Sk– 69°202, before the explosion is about 0.2 A.U. Presumably the outer layers of the star are suddenly restructured on shock-wave breakout, and the first photometric radius at t = 1.5d gives R = 20 A.U. Then

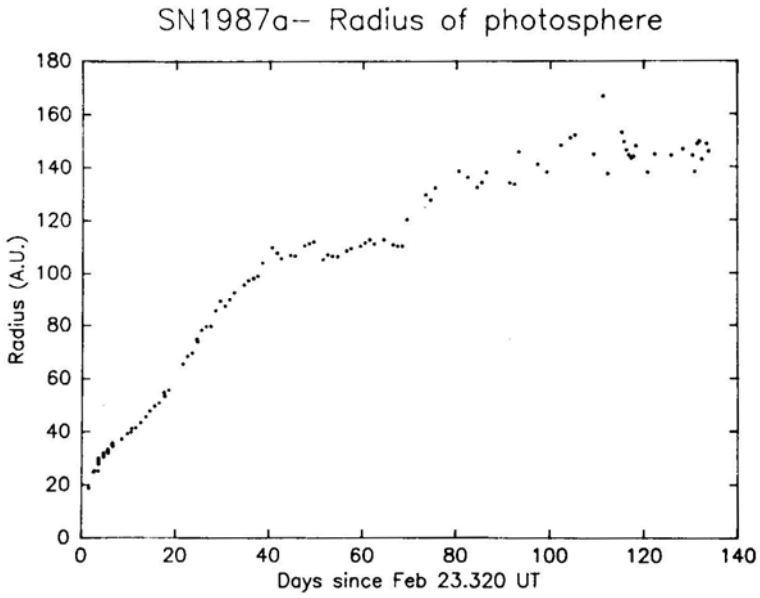

Figure 8. SN 1987a: Radius of the photosphere as deduced from *VR* Photometry.

there is a nearly linear increase until t = 38d of slope 3.7 ± 0.1 Mm s^{-1} . This velocity decreases to 300 ± 200 km s^{-1} in the interval 38d < t < 70d. For t >70d the results show a large scatter presumably due to the low altitude of SN 1987a from SAAO during June and July. However, by $t \simeq$ 100d the slope is zero, indicating a maximum photospheric radius of about 145 A.U. These computations were repeated with A_V = 0.4 instead of 0.6, and the changes in the results were negligible.

In terms of angular measure, our results indicate a maximum angular radius (ϕ/2) of about 2.8 milli arcsec at $t \simeq$ l00d. These results are in quite good agreement with those of Catchpole *et al.* (1987) who found (ϕ_{max}/2) of about 3.4 milli arcsec also at about $t \simeq$ l00d. In their case the angular radius came from fitting a black-body curve using *UBVRIJHKL* photometry to derive a blackbody colour temperature and hence the surface flux and angular radius. In our case the surface flux used to derive the angular radius comes from the assumption that SN 1987a obeys the empirical relation between surface flux and $(V-R)_0$ calibrated for normal stars such as Cepheids.

6. Interpretation of velocities

In free expansion the total size of the ejecta must be at least $R_{max} \sim v_0 t$, where $v_0 \simeq$ 20.15 Mms^{-1} = 11.6 A.U d^{-1} . Hα absorption occurs in a thick shell far above the photosphere. The shell's position moves inwards relative to the expanding material, and its actual radius is therefore less than $\int v(H\alpha)dt$.

The absorption from weaker metallic lines is not so optically thick and occurs deeper and closer to the photosphere. It seems plausible that the photosphere was stationary in mass coordinates for t<38d but started to move inwards relative to the expanding material after that time. The weaker metallic lines such as Mg b and Fe II

501.8 nm had initial velocities of nearly 8 Mm s^{-1} when they first appeared at t~9d. They were therefore expanding at over twice the photospheric velocity of 3.7 Mm s^{-1} in a shell of correspondingly greater radius than $R_{\text{phot.}}$ However, the velocities from these lines decline to about 2 to 3 Mm s^{-1} by t~40d, which means they are forming very close to the photosphere at that time. The optical depth between the photosphere and the outer extremity of the ejecta in the line centres must have declined considerably in this early period. The fact that the weaker absorption velocities decline to about equal the initial photospheric velocity is at least consistent with this model.

As the photosphere appears to expand less rapidly after t = 38d, it moves inwards into more slowly expanding material. If the absorption shells also shrink inwards so as to stay close to the photosphere, then the absorption velocities would also show a decline. The fall of the Mg I b velocity from 2.9 to 2.0 Mm s^{-1} between t = 100 and 140d may be evidence for a further decrease in the size of the Mg I b shell due to the shrinkage of the photosphere.

7. Distance to SN 1987a

The rate of increase of the angular size of the supernova photosphere derived photometrically can be compared with the velocities of the absorption shell in the envelope derived spectroscopically. The comparison will lead to a distance for the supernova provided both photosphere and absorption shell have the same velocity which we assume to be the case for t<38d. This is essentially Baade's (1926) distance method as applied by Kirshner & Kwan (1974) to the Supernovae SN19691 and 1970g and recently by Branch (1987) to SN1987a based on an angular radius derived from black-body fits to the photometry.

Our initial observed rate of increase of the angular radius was

$$\frac{1\,\mathrm{d}\phi}{2\,\mathrm{d}t} = (4.1 \pm 0.1) \times 10^{-2} \text{ milli-arcsec d}^{-1}$$

which corresponds to 3700 km s^{-1} at 52.5 kpc (distance modulus = 18.6). Our smallest absorption velocity was the asymptotic value for Fe II 501.8 nm of 2300 km s^{-1} However, this is the mean value of the line of sight component of the expansion over a hemispherical shell close to the photosphere. The actual values will be zero near the photospheric limb and only equal to R_{phot} in the disc centre. The mean value depends on limb darkening and is well known to be 17/24 of R_{phot} when the limb darkening coefficient is 0.6, the value usually adopted for pulsating variables such as Cepheids. In this case the true expansion rate of the Fe II 501.8 nm shell is 3250 km s^{-1}. This is compatible with the photometric rate of increase of angular radius if d = (45.8 ± 5) kpc or distance modulus = 18.3±0.2. The error bars refer to random (1σ) errors only.

The effect of the Hα line on the photometry is one source of systematic error. If this causes a 5 per cent brightening of the R magnitude, then the effect of this is that the angular sizes from the Barnes–Evans relationship are about 10 per cent too large and the distance is 10 per cent too small. Thus a corrected distance modulus of 18.5 would allow for 5 per cent contamination in R due to Hα Given the theoretical and observational uncertainties, this is considered to be in very satisfactory agreement with the accepted values of distance modulus 18.5 to 18.6. It is also close to a distance of 55 ± 5 kpc obtained by Branch (1987) by a similar method.

References

Anupama, G. C., Prabhu, T. P., Ghosh, K. K., Ashoka, B. N., Giridhar, S., Kameswara Rao, N. 1988, in *Proc. Fourth IAU Asian-Pacific Regional Meeting,* Beijing (preprint).
Ashoka, B. N., Anupama, G. C., Prabhu, T. P., Giridhar, S., Ghosh, K. K., Jain, S. K., Pati, A. K., Kameswara Rao, N. 1987, *J. Astrophys. Astron.,* **8,** 195.
Baade, W. 1926, *Astr. Nachr.* **288,** 359.
Barnes, T. G., Evans, D. S. 1976, *Mon. Not. R. astr. Soc.,* **174,** 489.
Barnes, T. G., Evans, D. S., Parsons, S. B. 1976, *Mon. Not. R. astr. Soc.,* **174,** 503.
Blanco, V. M. *et al.* 1987, *Astrophys. J.,* **320,** 589.
Branch, D. 1987, *Astrophys. J.,* **320,** L23.
Catchpole, R. M. *et al.* 1987, *Monthly Not. R. astr. Soc.,* **229,** 15p.
Cropper, M., Bailey, J. A. 1987, *IAU Circ. No.* 4319.
Danziger, I. J., Fosbury, R. A. E., Alloin, D., Cristiani, S., Dachs, J., Gouiffes, C., Jarvis, B., Sahu, K. C. 1987, *Astr. Astrophys.,* **177,** L13.
Feast, M. W. 1984, in *IAU Symp. 108; Structure and Evolution of the Magellanic Clouds,* Eds Sidney van den Bergh & K. E. De Boer, D. Reidel, Dordrecht, p. 157.
Hanuschik, R. W., Dachs, J. 1987, *Astr. Astrophys.* **182,** L29.
Hearnshaw, J. B., Haar, J. 1987, *IAU Circ. No.* 4352 and 4355.
Hearnshaw, J. B., McIntyre, V. J. 1987, *IAU Circ. No.* 4456.
Jeffery, D. J. 1987, *Nature,* **329,** 419.
Kirshner, R. P., Kwan, J. 1974, *Astrophys. J.,* **193**, 27.
Kurucz, R. L., Peytremann, E. 1975, Smithsonian Astrophys. Obs. Special Report 362.
Menzies, J. W. *et al.* 1987, *Mon. Not. R. astr. Soc.,* **227,** 39p.
Schwarz, H. E., Mundt, R. 1987, *Astr. Astrophys.,* **177,** L4.
Taylor, B. J. 1986, *Astrophys. J. Suppl. Ser.,* **60,** 577.
West, R. M., Lauberts, A., Jorgensen, H. E., Schuster, H.-E. 1987, *Astr. Astrophys.,* **177,** L1.

J. Astrophys. Astr. (1988) **9,** 107–116

Effects of Rotation On The Colours and Line Indices of Stars 1. The Alpha Persei Cluster

R. Rajamohan & Annamma Mathew *Indian Institute of Astrophysics, Bangalore 560034*

Received 1987 November 23; accepted 1988 March 25

Abstract. Analysis of the available observational data for the α-Persei cluster members shows that rotation effects on the intermediate-band indices c_1 and $(u - b)$ are considerable. In c_1, rotation produces a reddening of 0.040 magnitudes per 100 km s^{-1} In $(u - b)$ the effect for B stars is found to be 0.06 magnitudes per 100 km s^{-1} of V sin i.

The binaries and peculiar stars are found to behave differently in the colour excess (due to rotation) versus V sin i diagrams. These empirical effects can be utilised to recalibrate these colour indices and also to separate members that are either chemically peculiar or in binary systems.

Key words: stars, rotation—stars, colours—star clusters, individual

1. Introduction.

The effects of rotation on colours and line indices of stars is a subject of some controversy though not actually appreciated as such. Empirical calibrations of *uvby* and Hβ system in terms of intrinsic colour and absolute magnitudes have been carried out (Crawford 1978) on the assumption that differences in rotational velocities of stars does not substantially affect their colours. Theoretical work by Collins & Sonneborn (1977) and Collins & Smith (1985) seems to indicate that such effects are appreciable only for stars that rotate close to their break-up speeds. Warren (1976) discussed the proposed effects of rotation in some detail for B stars in the Orion region and showed that no systematic effects are present for Vsin i less than 250 km s^{-1}. Similar conclusions were reached by Petrie (1965) based on Hγ equivalent-width data. Dickens, Kraft & Krzeminski (1968) found no large systematic effects in $(U - B)$ colours at a fixed $(B - V)$ for stars in Praescepe. Crawford & Barnes (1974) found that no rotation effect can be discerned in the data for B stars in α-Persei cluster, whereas the data for A stars indicated that the c_1 index may be affected by as much as 0.035 magnitudes per 100 km s^{-1} of V sin i.

On the other hand, Kraft & Wrubel (1965) found that the ultraviolet excess is related to V sin i in the Hyades. Rajamohan (1978) showed that the c_1 index in α-Persei and the Scorpio-Centaurus association is correlated with V sin i. The work by Maeder & Peytremann (1970, 1972) seems to indicate that predicted theoretical effects are still smaller than the observed effects. However due to other parameters that affect the observed colours, no consistent picture has emerged. A systematic study of this effect would be needed for not only calibrating the indices, but also for comparison with

existing theories that could then be used for differentiating between uniform solid-body rotation and differential rotation.

We have decided to reinvestigate this problem systematically and determine empirically whether the colours and line indices of stars are affected by rotation at all values of $V \sin i$. Cluster members provide the best homogeneous data since the members can be assumed to be coeval. We begin with the α-Persei cluster since it has a low binary frequency (Kraft 1967; Heard & Petrie 1967). We plan to analyse each cluster separately and later take the effects of rotation into account in recalibrating the line indices as a function of absolute magnitude and spectral type. Comparison with theory will become feasible and easy once the analysis is extended to all clusters.

2. The data and analysis

The basic observational data for u,v,b,y and Hβ are taken from Crawford & Barnes (1974). The $V \sin i$ data are taken from Kraft (1967). The identification numbers for the stars are from Heckmann, Dieckvoss & Kox (1956). Only early-type stars (earlier than F5) are considered here. There are totally 34 stars of type B and 28 of type A and early F (Tables IV, V, VI of Crawford & Barnes 1974).

Before the data for these objects can be analysed for rotation effects, the following factors that affect their colours have to be taken into account.

1. Binary nature: This makes the star generally lie above the main sequence defined by non-rotating single stars. This factor, first suggested by Atkinson (1937) for identifying binaries from colour-magnitude diagrams depends on the mass ratio and evolutionary status of the components. Binaries in general rotate synchronously and hence have lower rotational velocities than single stars of the same spectral type. This effect leads to the inverse correlation between mean rotational velocities and binary frequency of clusters found by Abt & Hunter (1962).

2. The chemically peculiar stars are likely to have their colours affected by line-blanketing. These are in general slow rotators and some of them are magnetic and spectrum variables. The binary frequency amongst magnetic stars is very low, whereas almost all Am stars are likely to be in binary systems (Abt 1965)

3. Evolutionary effects: If the sample does not conform to a homogeneous coeval group, then evolutionary effects (even within the main-sequence lifetime) have to be taken into account as this would introduce a spread in the observed colour–magnitude diagrams. The advantage of analysing cluster data is that this effect would be a minimum, though in some clusters and associations it is known that not all members are coeval.

4. Differential reddening across the cluster: Since rotation effect is also to redden the stars, it is not clear whether the stars must be dereddened for this effect before analysing the data. The two effects being similar, we have decided to analyse the observed data as though the interstellar reddening is uniform across the cluster.

5. Large systematic errors in photometry: Eventhough there is no evidence that such systematic observational errors exist, it is worth noticing that Trimble & Ostriker (1978, 1981) found that some unknown effect exists which complicates the analysis of cluster data for discriminating between double and rotating stars. We plan to overcome this problem by analysing each cluster independently.

In order to minimize the first two effects, we decided to eliminate stars which are already known to be binary, variable or chemically peculiar. This we assume leaves a sample of single main-sequence normal stars at the same stage of evolution and only differing in their rotational velocities. Any reddening effect found then can be confidently attributed to the effect of rotation alone.

3. The effect of rotation on colours

3.1 *The Effect on* c_1: *B-Stars*

Tables 1 and 2 list the relevant data for the B and A stars. Because of the various factors listed in the previous section, which affect the colour indices, we cannot hope to derive

Table 1. Rotation effect on c_1 and $(u-b)$ for B stars.

Star No.	BD	β	c_1	$u-b$	$V \sin i$	Δc_1	$\Delta(u-b)$	Remarks
167	48°862	2.887	0.945	1.367	20	−0.051	−0.080	
212	49 876	2.807	0.865	1.169	280	0.052	0.063	
285	47 792	2.848	0.999	1.557	35	0.074	0.242	Ap
333	50 731	2.794	0.762	1.054	230	−0.014	0.006	
383	49 899	2.683	0.356	0.514	145	−0.026	−0.015	
401	49 902	2.668	0.393	0.549	320	0.076	0.094	
423	48 886	2.856	0.990	1.358	280	0.056	0.040	
557	48 899	2.688	0.407	0.563	250	0.059	0.028	SB ?
575	51 728	2.886	0.965	1.377	85	−0.030	−0.066	
581	48 903	2.813	0.821	1.099	200	−0.008	−0.033	
601		2.597	0.356	0.802		0.323	0.673	non-member
625	47 817	2.875	0.940	1.368	25	−0.014	−0.071	velocity var.
675	48 913	2.726	0.462	0.616	70	−0.089	−0.120	
692	47 821	2.856	0.947	1.275	340	0.032	−0.084	SB ?
729	47 826	2.868	0.962	1.374	225	0.002	0.006	
735	47 828	2.766	0.795	1.039	375	0.105	0.117	
774	48 920	2.702	0.407	0.543	65	−0.041	−0.116	velocity var.
775	47 831	2.804	0.786	1.100	200	−0.018	0.007	
780	49 938	2.888	1.005	1.513	230	0.007	0.062	
810	49 944	2.688	0.495	0.687	385	0.147	0.096	SB ?
817	48 927	2.866	0.998	1.438	270	0.043	0.078	
831	47 835	2.828	0.831	1.125	135	−0.037	−0.073	
835	49 945	2.678	0.373	0.497	190	0.012	−0.007	
861	46 760	2.735	0.579	0.975	150	0.006	0.158	non-member
868	48 933	2.858	0.930	1.344	180	−0.008	0.018	
875	47 840	2.858	1.008	1.418	250	0.070	0.092	
904	47 844	2.745	0.683	0.889	380	0.074	0.220	shell star
955	47 846	2.743	0.718	0.964	215	0.116	0.120	velocity var.
965	48 943	2.747	0.662	0.892	225	0.036	0.058	
985	47 847	2.695	0.369	0.511	50	−0.062	−0.076	
1082	48 949	2.829	0.847	1.167	205	−0.024	−0.035	
1153	46 773	2.766	0.648	0.888	25	−0.042	−0.034	
1164	47 857	2.491	0.379	0.503	385	−0.243	0.055	non-member
1259	47 865	2.850	0.873	1.189	45	−0.048	−0.103	

Table 2. Rotation effect on c_1 for A stars.

Star No.	BD	β	c_1	$V \sin i$	Δc_1	$\Delta\beta$	Remarks
151	47°780	2.765	0.763	140	0	0	
220	48 865	2.792	0.805	85	−0.010	0.005	
228		2.759	0.727		−0.024	0.012	
314	50 728	2.736	0.754	110	−0.045	−0.033	SB ?
386	49 900	2.901	1.013	260	0.025	−0.020	
481	47 808	2.763	0.772	180	0.013	−0.007	
501	48 894	2.770	0.741	75	−0.032	0.016	
522	51 723	2.868	0.936	200	−0.111	−0.004	velocity variable
595		2.790	0.978		0.067	−0.105	non-member
606	48 905	2.775	0.765	50	−0.018	0.009	A 8 m ?
609	49 918	2.755	0.789	175	0.046	−0.023	
612	48 906	2.911	0.987	85	−0.014	−0.010	
635	49 921	2.758	0.721	20	−0.028	−0.014	
639	48 907	2.896	1.007	210	0.026	−0.020	
651	48 909	2.862	0.993	250	0.061	−0.043	
658	47 819	2.850	0.888	85	−0.130	0.005	non-member
694	47 822	2.902	0.956	75	−0.033	0.024	
721	47 825	2.730	0.686		−0.005	0.002	
756	47 830	2.908	1.002	145	0.005	−0.004	
802	48 924	2.893	0.976	200	−0.001	0.001	
885	48 934	2.856	0.867	80	−0.164	0.023	velocity variable
906	47 842	2.872	0.939	150	−0.008	0.006	
921	49 953	2.880	0.970	200	0.011	−0.008	
931	49 954	2.894	0.960	90	−0.018	0.013	
958	49 858	2.739	0.741	155	0.031	−0.015	
970	48 944	2.886	0.938	120	−0.029	0.020	
1050	49 967	2.834	0.893	60	−0.098	−0.014	SB ?
1218	46 780	2.729	0.733	120	−0.051	−0.028	SB ?

meaningful results by defining a standard main sequence, or a zero age main sequence (ZAMS) or zero rotation main sequence (ZAZRMS) (see also Trimble & Ostriker 1978,1981). We have therefore decided to use the data for each cluster to define its own relationship between different indices. Fig. 1 is a plot of β versus c_1 for all members listed in Tables 1 and 2. A second-order polynomial was fitted to the data and for each star, a calculated c_1 value was derived using the polynomial coefficients for its observed β. We define Δc_1 as the observed minus computed value of c_1 for its observed value of β. We have plotted Δc_1 versus $V \sin i$ using different symbols for B and A stars. It was found that strong rotation effects are present independently for B and A stars and that a single polynomial fit is not appropriate for B and A stars taken together.

Fig. 2 shows the result for the B stars analysed independently, omitting the probable binaries and peculiar stars. The c_1 indices were represented by an equation of the type.

$$c_1 = f + g\beta + h\beta^2$$

The $(O - C)$ values in c_1 for each star derived using the above coefficients are given in Columns 6 and 7 of Table 1. These $(O - C)$ values in c_1 are denoted by Δc_1. A linear fit

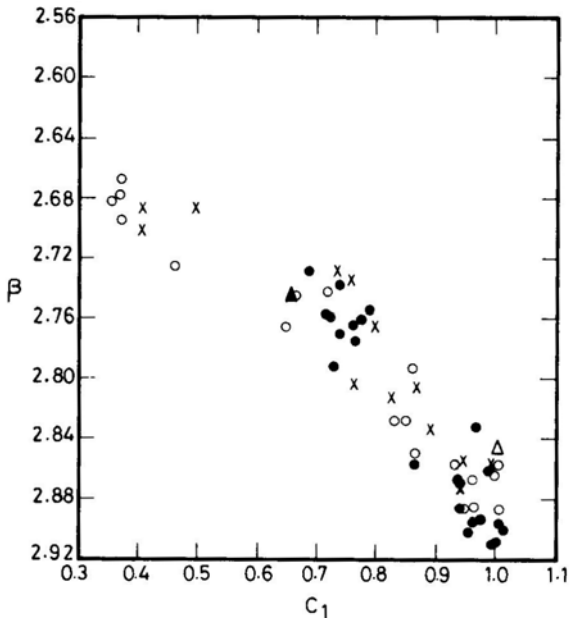

Figure. 1 The β, c_1 plot for B stars (open circles) and A stars (filled circles) in the α-Persei cluster. Stars with variable radial velocities, and suspected binaries are plotted as crosses. A peculiar star is plotted as an open triangle, and a shell star by a filled triangle.

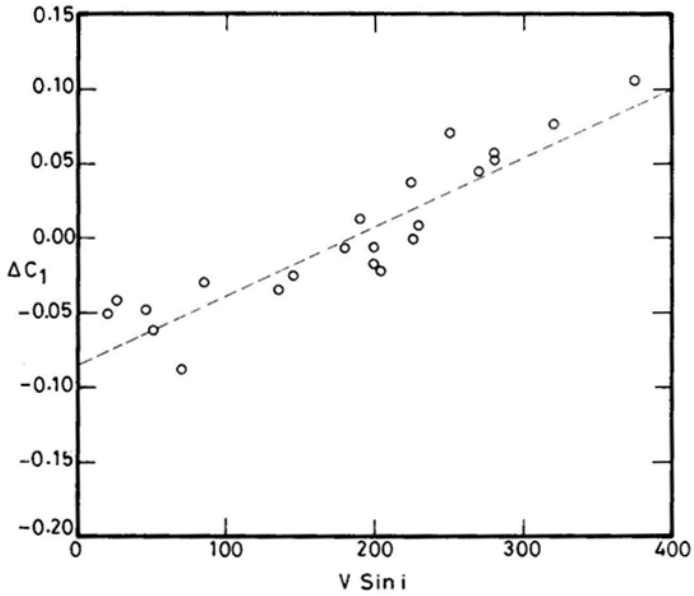

Figure 2. The deviation in c_1 is plotted against V sin i for B stars.

to the data points in Fig. 3 gives

$$\Delta c_1 = 0.454(\pm 0.032) \times 10^{-3} V \sin i - 0.084(\pm 0.006).$$

3.2 *The Effect on c_1 : A Stars*

A similar analysis was done for the A stars in Table 2. The deviations are given in Column 6 of Table 2 and are plotted against V sin i in Fig. 3. A linear fit to the data points given for the A stars.

$$\Delta c_1 = 0.326(\pm 0.038) \times 10^{-3} V \sin i - 0.044(\pm 0.006).$$

The effect of rotation on c_1 for the B and A stars taken together (Fig. 4) is of the order of 0.040 magnitudes per 100 km s^{-1} of V sin i.

3.3 *The Effect on* (u b)

The β, (u – b) relation was also represented by a second-order polynomial for the B stars.

The deviations in (u – b) are given in Column 8 of Table 1. These are plotted against V sin i in Fig. 5. It is obvious that the effect of rotation on the (u – b) colour at a given β is considerable. A linear fit to the data points in Fig. 5 gives

$$\Delta(u-b) = 0.618(\pm 0.046) \times 10^{-3} V \sin i - 0.114(\pm 0.009).$$

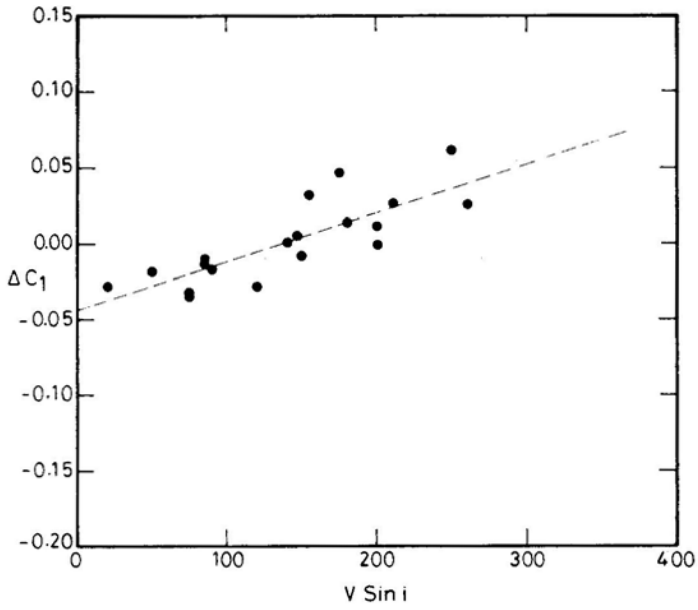

Figure 3. The deviation in c_1 is plotted against V sin i for A stars.

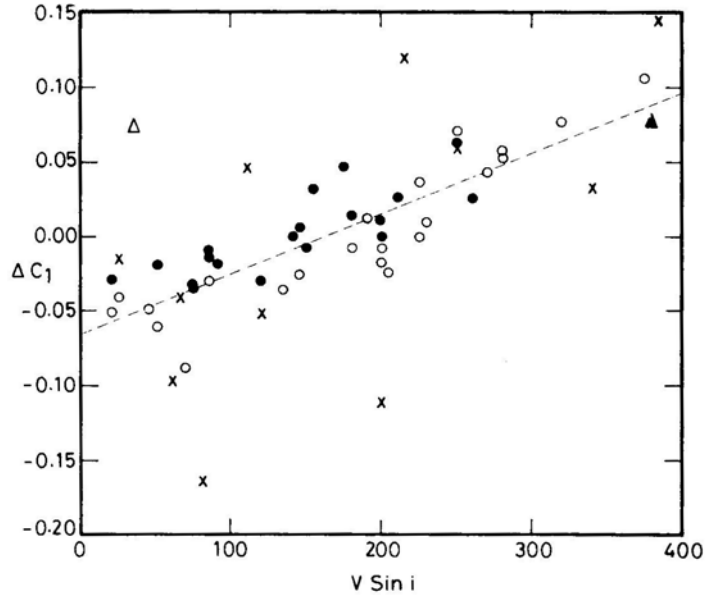

Figure 4. The deviation in c_1 for all stars. Symbols are the same as in Fig. 1

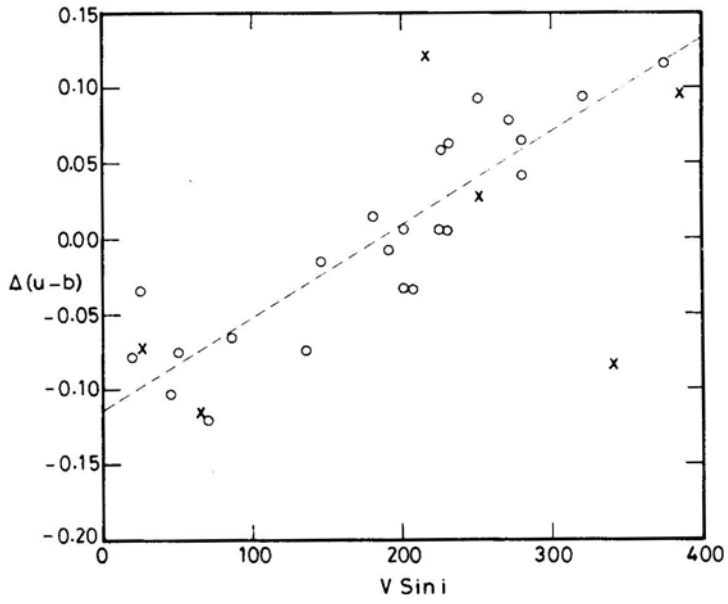

Figure 5. The deviation in $(u - b)$ is plotted against $V \sin i$ for B stars.

3.4 *The Effect on* $(b - y)$, m_1

No striking correlation is found with excess in $(b - y)$ or m_1, when these quantities are interrelated with β, c_1 or $(u - b)$ except in the case of c_1 versus $(b - y)$ relation for A stars. This effect is shown in Fig. 6. The procedure adopted is probably not best-suited

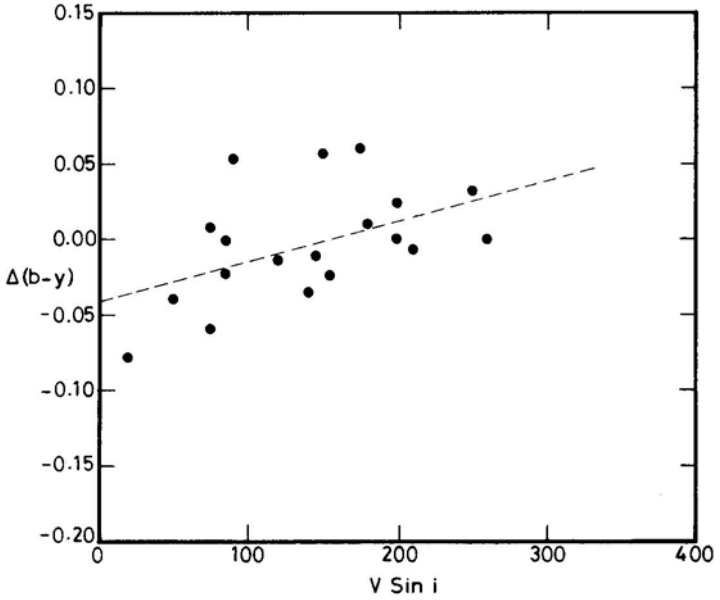

Figure 6. The deviation in $(b - y)$ is plotted against V sin i for A stars.

to find the effects of rotation on these colour indices. We defer the conclusions regarding the indices to a later paper.

4. Discussion

The effect of rotation on the observed intermediate-band indices c_1 and $(u - b)$ seems to be considerable. The complicating factors that introduce scatter in the colour–colour and colour–magnitude diagrams are the incidence of peculiar and binary stars, evolutionary effects, and reddening. If these are taken into account by eliminating peculiar and binary stars and confining ourselves to the analysis of main sequence normal single stars in a cluster, the rotation effect comes out strikingly for c_1 and $(u - b)$. Hence in the calibration of these indices with spectral type and absolute magnitude or the β index, we must make allowance for rotation effects; this has not been done in earlier work (*e.g.* Crawford 1978).

Trimble & Ostriker (1978, 1981) tried to derive the binary frequency in clusters by analysing the displacement of stars in the colour-magnitude diagrams and taking into account the expected effects of rotation. The effort was not fully successful since they found that different clusters do not define a unique zero rotation main sequence According to them, an unknown parameter influenced the observed colours up to a 0.05-magnitude level. We avoid this problem by analysing clusters individually, eventhough this leaves us with a smaller sample of stars for analysis.

In Δc_1 and $\Delta(u - b)$ versus V sin i diagrams the binaries seem to be displaced to a position below the mean relationship while the peculiar stars seem to lie considerably above this relationship. The region above this mean relationship can also be occupied

by stars whose indices are affected by incipient emission in β. These objects, in general, would occur at high values of V sin i excepting those that are seen pole on. However, emission occurs in general in very early B stars and hence it should be possible, in principle by the position of the objects in Δc_1, $\Delta(u - b)$ versus V sin i diagrams, to identify these three different kinds of objects.

The tight relationship found for Δc_1 and $\Delta(u - b)$ with V *sin* i leads to some interesting questions. Collins & Sonneborn (1977) found that the relationship between rotational velocity and the rotational displacement of an object from the main sequence is almost independant of sin i. Low values of V sin i could be a combination of high V and very low sin i or a low value of V itself. In that case we must expect a large spread in the observed values of Δc_1 at low values of V sin i. The spread would be expected to be low at large values of V sin i, since the spread in V itself would be expected to be small at high values of V sin i. Two possibilities exist. For a random distribution in V and i, the expected number of stars at low values of V sin i would be small. However we find in Fig. 3 and 4 the distribution of stars for different values of V sin i is more or less uniform. The other possibility is that the effect of differing inclination is much larger than that predicted by theory. In that case, these results seem to support the arguments by Rajamohan (1978) that the normal single stars of a given mass arrive on the main sequence with a small spread in their angular momentum. We will address this question in greater detail after the analysis of data on other clusters is completed.

We have completely left out the late-type stars from our analysis. The colours of these stars, with outer convection zones, are likely to be affected not only by rotation but also by chromospheric phenomenon and star spots. Chromospheric activity enhanced by duplicity (Young & Koniges 1977) would further complicate the analysis of their data. They belong to a separate class of interesting objects and the role of rotation in these objects is a totally different problem. Also some young Pleiades K dwarfs have been found to have very high values of V sin i (Stanffer & Hartmann 1987). We plan to analyse only the data for early-type stars in different clusters where the rotation effects on colours and line indices seem much less complicated than in their late-type counterparts.

5. Conclusion

For the α-Persei cluster members the effect of rotation is found to be + 0.04 magnitudes per 100 km s^{-1} in c_1 and + 0.06 magnitudes per 100 km s^{-1} of V sin i in $(u - b)$.

Binaries, peculiar stars and emission-line objects seem to occupy different regions in the Δc_1, $\Delta(u - b)$ versus V sin i diagrams. This fact can be used as a criterion for selecting the most probable peculiar and binary stars in distant young clusters.

These effects were fairly easy to determine in α-Persei since the cluster has a low frequency of spectroscopic binaries and has been fairly extensively studied both photometrically and spectroscopically. In fact, no confirmed short period binaries exists in the α-Persei cluster.

We plan the comparison of empirically-determined rotation effects on colours with available model calculations after analysing the data for other clusters for which extensive observational material exists.

Acknowledgements

The data analysis in this paper was carried out with the TDC-316 computer of the Indian Institute of Astrophysics, we are thankful to Mr. A. V. Raveendran for lending his computer programmes.

References

Abt, H. A. 1965, *Astrophys. J. SuppL.*, **11,** 429.
Abt, H. A., Hunter, J. H. Jr. 1962, *Astrophys. J.*, **136,** 381.
Atkinson, R. d'E 1937, *Observatory*, **60,** 299
Collins, G. W., Smith, R. C. 1985, *Mon.Not.R.Astr.Soc,* **213**, 519.
Collins; G. W., Sonneborn, G. H. 1977, *Astrophys. J. SuppL.*, **34,** 41.
Crawford, D. L. 1978, *Astr. J.,* **83,** 48.
Crawford, D. L., Barnes, J. V. 1974**,** *Astr. J.*, **79,** 687.
Dickens, R. J., Kraft, R. P., Krzeminski, W. 1968, *Astr. J.,* **73,** 6.
Heckmann, O., Dieckvoss, W., Kox, H. 1956, *Astr. Nachr.,* **283,** 109.
Kraft, R. P. 1967, *Astrophys. J.*, 1**48,** 129.
Kraft. R. P., Wrubel, M. 1965, *Astrophys. J.,* **142,** 703.
Maeder, A., Peytremann, E. 1970, *Astr. Astrophys.* **7,** 120.
Maeder, A., Peytremann, E. 1972. *Astr. Astrophys.,* **21,** 279.
Petrie, R. M. 1965, *Publ. Dominion Astrophys. Obs.,* **12,** 317.
Heard, J. F., Petrie, R. M. 1967, *IAU Symp. No*: 30: *Determination of Radial Velocities and their Applications,* Eds A. H. Batten & J. F. Heard, D. Reidel, Dordrecht, p. 179.
Rajamohan, R., 1978, *Mon. Not. R. Astr. Soc,* **184,** 743
Stauffer, J. R., Hartman, L. W. 1987, *Astrophys. J.*, **318,** 337
Trimble, V. L.; Ostriker, J. P. 1978, *Astr. Asjrophys.,* **63,** 433.
Trimble, V. L., Ostriker, J. P. 1981, *Astr. Astrophys*., **97,** 403.
Warren, W. H. 1976 *Mon. Not. R. Astr. Soc,* **174,** 111.
Young, A., Koniges, A. 1977 *Astrophys. J.*, **211,** 836.

J. Astrophys. Astr. (1988) **9,** 117–124

Kinematical Distances to Open Star Clusters

Ram Sagar & Harish C. Bhatt *Indian Institute of Astrophysics Bangalore 560034*

Received 1988 February 3; accepted 1988 April 12

Abstract. Kinematical distances are estimated for six open star clusters. They agree fairly well with the photometric distances. The kinematical distances cannot, at present, be estimated better than the photometric distances. When more accurate proper motion measurements become available the kinematical distances will improve considerably and may then be used to calibrate the cosmic distance scale.

Key words: open clusters—distances—kinematics

1. Introduction

An accurate estimate of distances to open star clusters is required for many astrophysical investigations. One application is in tracing the spiral arms of the Galaxy because these clusters can be detected to large distances. It is therefore of interest to evaluate their distances by as many different independent methods as possible. The distances to open clusters have generally been estimated by using methods based upon main sequence fitting. Other, less accurate, methods are: the use of variables, stellar evolutionary gaps in the photometric sequences of open clusters, *etc.* In these methods, one must consider reddening/extinction and metallicity corrections, as well as the photometric calibration (Lyngpå 1980).

The current best photometric distances of open clusters are correct to within 20–30 per cent. Even so, it would clearly be useful to check them with a totally independent technique when possible, as has been done here. We discuss a method of open cluster distance estimation that is based on the observable kinematical parameters, namely, proper motions and radial velocities of open cluster members. The method is, therefore, independent of interstellar extinction and metallicity corrections as well as of photometric calibration but requires precise measurements of the above-mentioned kinematical parameters which are now becoming available. This technique has been used successfully for the distance estimates of globular clusters (Cudworth & Peterson 1987 and references therein). The method discussed here can, in principle, also be used for calibrating the cosmic distance scale.

2. The Method

If the distribution of the stellar velocities in a cluster could be assumed to be isotropic, the resulting velocity dispersions along three orthogonal axes would be identical. Representing the proper motions along two orthogonal axes (x, y) in the plane of the

sky by μ_x and μ_y and the radial velocity along the line of sight, *i.e.* perpendicular to the plane of the sky, by v, one could write

$$\sigma_v = D\,\sigma_{\mu x} = D\,\sigma_{\mu y}, \tag{1}$$

where D is the distance to the cluster, and σ_v, $\sigma_{\mu\chi}$ and $\sigma_{\mu\gamma}$ are the intrinsic dispersions in v, μ_x and μ_y respectively. The distance D to the cluster can thus be written as

$$D = \sigma_v/\sigma_\mu$$

where $\sigma_\mu = \sigma_{\mu x} = \sigma_{\mu\gamma}$. Expressing the measured quantities in units commonly used, one can write

$$D = 2.1 \times 10^{-2}\ \sigma_v/\sigma_\mu, \tag{2}$$

where D is in kpc, σ_v in km s^{-1} and σ_μ in arcsec/century.

Before applying the method outlined above, it is essential to discuss the question of velocity isotropy in open star clusters. Theoretical predictions about this are subject to a number of uncertainities. As a consequence of dynamical evolution, it is expected that the velocity dispersion would vary inversely as the square root of the stellar mass. But open star clusters are not isolated systems and the effects of encounters with interstellar clouds, tidal forces, mass loss from the massive stars, and vestiges of its initial formation conditions, *etc.,* could also be present in the velocity distributions within these objects. In the interior of an open star cluster, relaxation time is short enough to establish isotropy. Galactic tidal forces randomize the velocity directions of outer low-mass stars ejected in eccentric orbits from the cluster centre due to dynamical evolution and consequently, yield a flattened global velocity-mass relation (*cf.* Prata 1971; Mathieu 1983). Under these circumstances, the mass dependence of the velocity dispersion expected from the dynamical evolution of an open star cluster may not be observed. Analyses of the proper motion data by McNamara & Sanders (1977) for M 11; by McNamara & Sekiguchi (1986) for M 35; and by Sagar & Bhatt (1988) for NGC 2287, 2516, 1C 2391, NGC 2669, 3532, 4103, 4755 and 5662 open star clusters have shown that $\sigma_{\mu x} \simeq \sigma_{\mu v}$ supporting the basic assumption of the present method. Therefore, the assumption of isotropic stellar velocity dispersions in open star clusters could be justified in general.

3. Distance estimates

Six open clusters for which measurements of both proper motion components and accurate radial velocities of member stars are available are the subject of the present analysis. Ideally, all cluster members should have proper motion and radial velocity measurements together with estimates of the associated errors so that their intrinsic dispersions can be derived. This is because both the intrinsic dispersion and the dispersion due to errors contribute to the observed dispersion (McNamara & Sekiguchi 1986). The distance to the cluster can then be evaluated by using Equation (2). In practice, however, the number of members with proper motion measurements is often considerably larger than of those with radial velocity determinations. Therefore, usually the intrinsic dispersion in radial velocity is determined from available data, which in turn is used with the intrinsic proper motion dispersion estimated from the larger proper motion sample to derive the distance.

3.1 *Estimation of Intrinsic Dispersion*

The procedure given by Jones (1970) is used to estimate here the intrinsic dispersions in proper motion components and radial velocities. The observed proper motion dispersion in one coordinate can be written as

$$\sigma_0^2 = \frac{1}{n-1}\sum_{i=1}^{n}\mu_i^2$$

where μ_i represents the proper motion of star i relative to the mean cluster motion and n is the sample size. Assuming that the proper motion and error distributions are gaussian, one has for the true dispersion σ_κ as

$$\sigma_I^2 = \sigma_0^2 - \frac{1}{n}\sum_{i=1}^{n}\xi_i^2 \tag{3}$$

where ξ_i is the mean error of the proper motion of the ith star. The error in σ_κ is

$$\Delta\sigma_I = \left\{\frac{1}{4\sigma_I^2}[\varepsilon^2(\sigma_0^2)+\varepsilon^2(\sigma_m^2)]\right\}^{1/2}, \tag{4}$$

with

$$\varepsilon(\sigma_0^2) = \sigma_0^2\left(\frac{2}{n}\right)^{1/2},$$

and

$$\varepsilon(\sigma_m^2) = \frac{\sqrt{2}}{n}\left(\sum_{i=1}^{n}\xi_i^4/n_i\right)^{1/2},$$

where n_i is the number of plate pairs on which star i appears.

3.2 *Intrinsic Dispersion in Radial Velocities*

The precise radial velocities (error $\leqslant$1 km s $^{-1}$) of members in NGC 2682 and 6705 are given by Mathieu *et al.* (1986) and in NGC 2420 by Liu & Janes (1987). Stars showing no sign of radial velocity variation as well as having proper motion, radial velocity, and *UBV* photometric data compatible for cluster membership are used to estimate the intrinsic dispersion in radial velocities. Gieseking (1981) for NGC 3532 and Mathieu (1986) for NGC 1976 and 2264 have given the values of σ_v. The number of stars (n) used for this purpose and the values of σ_v are listed in Table 1.

3.3 *Dispersion in Proper Motions*

As the clusters under study do not all have the same quality of proper motion data, the error treatments for the estimation of their intrinsic dispersion σ_μ differ. For NGC 3532 and 6705, proper motion components with errors are available, and hence σ_μ is estimated using stars with proper motion membership probability greater than or equal to 70 per cent and having *UBV* data compatible with cluster membership. The assumption of $\sigma_{\mu\chi} \simeq \sigma_{\mu\gamma}$, is satisfied and their weighted average is considered as σ_μ. For NGC 1976, we adopt σ_μ from McNamara (1976) while for NGC 2682 from McNamara

Table 1. Intrinsic dispersion in proper motions and radial velocities for six open clusters.

		Intrinsic dispersion in					
		Proper motions			Radial velocities		
Cluster name	IAU Designation	σ_μ (arcsec/ century)	n	Source	σ_v (km s^{-1})	n	Source
NGC 6705 (M 11)	C 1848–063	0.019 ± 0.003	562	Mathieu (1984, personal communication)	1.4 ± 0.2	25	Mathieu *et al.* (1986)
NGC 3532	C 1104–584	0.08 ± 0.01	410	King (1978)	1.5 ± 0.3	84	Gieseking (1981)
NGC 1976 (Trapezium)	C 0532–054	0.10 ± 0.02	76	McNamara (1976)	2.0	—	Mathieu (1986)
NGC 2682 (M 67)	C 0847 + 120	0.024 ± 017	148	McNamara & Sanders(1978)	0.82 ± 0.07	85	Mathieu *et al.* (1986)
NGC 2264	C 0638 + 099	0.099 ± 0.087	48	Vasilevskis, Sanders & Blaz (1965); Zhao *et al.* (1985)	2.5	—	Mathieu (1986)
NGC 2420	C 0735 + 216	0.013 ± 0.069	22	Altena & Jones (1970)	1.4 ± 0.4	6	Liu & Janes (1987)

& Sanders (1978), where it has been assumed that both proper motion components have the same observed dispersion which has been estimated using the maximum likelihood method of membership estimation (Sanders 1971). The σ_μ for NGC 2264 and 2420 are estimated using the technique given by McNamara & Sanders (1977). For these two clusters, mean errors in both proper motion components are given for groups of stars and the members of the groups with better estimates are used in the analysis. Observed proper motion dispersion estimated using maximum likelihood method is taken from Zhao *et al.* (1985) for NGC 2264 and from Altena & Jones (1970) for NGC 2420. The intrinsic dispersion in proper motion σ_μ and the number of stars (n) used are listed in Table 1.

3.4 *Derived Kinematical Distances and Associated Errors*

Having evaluated the intrinsic dispersions in the radial velocities σ_v and in proper motions $\sigma_{\mu,}$ use is made of Equation (2) to derive the kinematical distances. The uncertainty in these estimates can be evaluated as:

$$\left(\frac{\Delta D}{D}\right)^2 = \left(\frac{\Delta\sigma_\mu}{\sigma_\mu}\right)^2 + \left(\frac{\Delta\sigma_v}{\sigma_v}\right)^2 \tag{5}$$

where ΔD, $\Delta\sigma_\mu$ and $\Delta\sigma_v$ are the errors in distance D, proper motion dispersion σ_μ and radial velocity dispersion σ_v respectively. The derived kinematical distances and their uncertainities are given in Table 2. The percentage of error contributed to the kinematical distances due to uncertainities in the dispersions of proper motions and radial velocities are also listed in the table. It should be noted that presently the errors due to uncertainities in the proper motion dispersions are generally larger than those in the radial velocity dispersions.

In the present work, the proper motion data used to derive σ_μ have relatively larger range in stellar mass compared to the data used for the estimation of velocity dispersion. This will not introduce any systematic error in the derived kinematical distances, if there is no dependence of velocity dispersion on stellar mass as pointed out in Section 2. To verify this statement, we estimated σ_μ using the stars in NGC 6705 having radial velocity measurements. All stars are giants and their V magnitude varies from 11.0 to 12.0. Consequently, their mass range is quite narrow. The value of σ_μ comes out to be 0.016 ± 0.005, which is almost equal to the value derived using relatively wider mass range corresponding to V = 11.0–16.0 (see Table 1).

However, in the cases where the velocity distribution is not isotropic and dispersion in velocity depends upon stellar mass, the precise radial velocity and proper motion data for the same narrow stellar mass range should be used to derive the kinematical distances. Otherwise, a systematic error will be introduced by the present method. Also the method is applicable only if the cluster is non-rotating. When rotation is present, or even suspected, it is probably best to use stars located in the central region of the cluster because the effect of rotation is almost negligible there (Prata 1971).

3.5 *Comparison with Photometric Distances*

The photometric distances of the open star clusters under discussion are given in Table 2. Their errors listed in the table are mainly due to the inaccuracies in fitting the

Table 2. Kinematical and photometric distances for the open clusters studied here. For NGC 2240, though the mean value of kinematical distance agrees with the photometric one, the formal error in it is very large.

Cluster	Kinematical distances (pc)	Percentage error due to uncertainties in the dispersion of		Photometric distances		
		Proper motions	Radial velocities	Value (pc)	Percentage error	Source
NGC 6705	1550 ± 470	16	14	1900 ± 270	14	Solomon & McNamara (1980)
NGC 3532	400 ± 130	12	20	490 ± 160	33	Fernandez & Salgado (1980)
NGC 1976*	420 ± 90	20	—	472 ± 45	10	Walker (1969)
NGC 2682	720 ± 570	71	9	830 ± 100	12	Nissen, Twarog & Crawford (1987)
NGC 2264*	530 ± 470	88	—	790 ± 75	10	Sagar & Joshi (1983)
NGC 2240	2260:	:	29	1910 ± 190	10	McClure, Forrester & Gibson (1974)

* The error in kinematical distance is only due to the uncertainity in proper motion dispersion.

Hyades sequence to the colour–magnitude diagram of the clusters. Other important sources of error are: ~ 4 per cent due to the uncertainity in the Hyades distance modulus (Hanson 1980), ~2 per cent due to errors in photoelectric quality photometry; ~ 5–10 per cent because of using an average value of $R = (A_v/E(B— V)) = 3.1$; and ~ 5–20 per cent due to not accounting for the variation in metallicity of the open clusters relative to Hyades metallicity (Lyngå 1980; Nissen 1980). Therefore, photometric distances of open star clusters cannot at present be estimated better than ~ 20 per cent for nearby clusters and ~ 30 per cent for distant open clusters by fitting the Hyades sequence to the colour–magnitude diagram of the clusters.

A comparison of the kinematical distances with the photometric distances shows a good agreement between them (see Table 2). It would seem from Table 2 that generally the kinematical distances are smaller than the photometric ones but the errors are still quite large. The reality of this can be checked only when more accurate dispersions in proper motions and radial velocities become available in future.

It is unlikely that the current methods will improve the accuracy of photometric distances significantly. On the other hand, it is expected that the accuracy of kinematical distances will improve considerably when more accurate proper motion measurements from the HIPPARCOS space mission or from the Hubble Space Telescope or from ground-based observations become available in future. The error $\Delta\sigma_\upsilon$ and $\Delta\sigma_\mu$ are function of σ_I, ξ_i, n and n_i (see Equation 4). Radial velocities of accuracies better than presently available (error < 1 kms^{-1}) are unlikely to be attainable in the immediate future. However, a larger sample size will improve the accuracy of σ_v; but accuracies better than ~ 10 per cent in σ_υ may not be achieved in the near future (*cf.* Latham 1987). In the case of proper motion, Hubble Space Telescope and HIPPARCOS space mission are expected to improve the measuring accuracy at least by a factor of ~ 10^2–10^3, which can result in an accuracy of few percent in σ_μ. For example, in the case of NGC 3532 the proper motion data with mean error of 0.13 arcsec/century (King 1978) yields an accuracy of ~ 12 per cent in σ_μ (see Table 2). If only measuring errors are improved by a factor of 10 and other parameters are kept constant, an accuracy of ~ 5 per cent will be achieved in σ_μ. In future, therefore, kinematical distances may be estimated with accuracies better than the photometric distances. As the distances based on the present method are independent of any Standard candles, they can be used to calibrate the cosmic distance scale in future.

4. Conclusions

Kinematical distances for six open clusters have been estimated which are in good agreement with the photometric distances. At present the kinematical distances cannot generally be estimated with accuracies better than the photometric distances. It is expected that kinematical distances will improve considerably in future when more accurate proper motion measurements become available. As the method for estimating distances used here is free of the effects of interstellar extinction and other calibrations, it has potential application in the calibration of the cosmic distance scale.

Acknowledgements

We thank Dr. R. D. Mathieu for sending the unpublished errors in the proper motion data of NGC 6705 and Dr. K. A. Janes for the radial velocity measurements in NGC

2420. Useful comments by Dr. K. M. Cudworth and an anonymous referee are gratefully acknowledged.

References

Altena Van, W. F., Jones, B. F. 1970, *Astr. Astrophys.,* **8,** 112.
Cudworth, K., Peterson, R. 1987, in *IAU Symp.* 126: *Globular Cluster Systems in Galaxies,* Eds J. Grindlay & A. G. D. Philip, D. Reidel, Dordrecht (in press).
Fernandez, J. A., Salgado, C. W. 1980, *Astr, Astrophys., Suppl.,* **39,** 11.
Gieseking, F. J. 1981, *Astr. Astrophys.,* **99,** 155.
Hanson, R. B. 1980, in *IAU Symp.* 85: *Star Clusters,* Ed. J. E. Hesser, D. Riedel, Dordrecht, p. 71
Jones, B. F. 1970, *Astr. J*, **75,** 563.
King, D. S. 1978, *J. Proc. R. Soc. New South Wales,* **111,** 1.
Latham, D. W. 1987, *Vistas Astr.,* **30,** 77.
Liu, T., Janes, K. A. 1987, *Publ. astr. Soc. Pacific,* **99,** 1076.
Lynga, G. 1980, in *IAU Symp.* 85: *Star Clusters,* Ed. J. E. Hesser, D. Reidel, Dordrecht, p. 13
Mathieu, R. D. 1983. *Ph D Thesis,* Univ. California, Berkeley.
Mathieu, R. D. 1984, *Astrophys. J*., **284,** 643.
Mathieu, R. D. 1986, *Highlights of Astronomy,* **7**, 481.
Mathieu, R. D., Latham, D.W., Griffin, R. F., Gunn, J. E. 1986, *Astr. J.,* **92,** 1100.
McClure, R. D., Forrester, W. T. & Gibson, J. 1974, *Astrophys. J.,* **189,** 409.
McNamara, B. J., 1976, *Astr. J.* **81,** 375.
McNamara, B. J., Sanders, W. L. 1977, *Astr. Astrophys.,* **54,** 569.
McNamara, B. J., Sanders, W. L. 1978, *Astr. Astrophys.,* **62**, 259.
McNamara, B. J., Sekiguchi, K. 1986, *Astrophys. J.,* **310,** 613.
Nissen, P. E. 1980, in *IAU Symp.* 85: *Star Clusters,* Ed. J. E. Hesser, D. Reidel, Dordrecht, p.51.
Nissen, P. E., Twarog, B. A., Crawford, D. L. 1987, *Astr. J.,* **93,** 634.
Prata, S. 1971, *Astr. J.,* **76,** 1017.
Sagar, R., Bhatt, H. C. 1988, *Mon. Not. R. astr. Soc.* (Submitted).
Sagar, R., Joshi, U. C. 1983, *Mon. Not. R. astr. Soc,* **205,** 747.
Sanders, W. L. 1971, *Astr. Astrophys.,* **14,** 226.
Solomon, S. J., McNamara, B. J. 1980, *Astr. J.,* **85,** 432.
Vasilevskis, S., Sanders, W. L., Balz, A. G. Jr. 1965, *Astr. J.,* **70,** 797.
Walker, M. F. 1969, *Astrophys. J.*, **155,** 447.
Zhao, J., Tian, K., Jing, J., Yin, M. 1985, *Special Issue for Tables of Membership for* 42 *open clusters.* Shanghai Observatory, Akademia Sinica, Shanghai.

Corrigenda

'Evidence for Moving Features in the Corona from emission Line Profiles observed during Eclipses' by A. B. Delone, E. A. Makarova & G. V. Yakunina was published in *Journal of Astrophysics and Astronomy*, Volume 9, Number 4, December 1987.

p. 43: In Table 1, the spatial resolution on 7 March 1970 (Delone & Makarova 1973) should be 3×3 arcsec^2 instead c × 3.

p. 44: In the caption to Fig. 2 the dashed and continuous lines should be interchanged.

p. 44: '(see fig.3)' should be added at the end of the last line of Section 3.

p. 45: The figures should be renumbered as: **Figure 4** instead of **Figure 3; Figure 5** instead of **Figure 4; Figure 3** instead of **Figure 5.**

J. Astrophys. Astr. (1988) **9,** 127–136

Spectroscopic Binaries near the North Galactic Pole
Paper 15: HD 106947

R. F. Griffin *The Observatories, Madingley Road, Cambridge, England CB3 0HA*

Received 1988 May 2; accepted 1988 May 13

Abstract. Photoelectric radial-velocity measurements show that HD 106947 is a double-lined spectroscopic binary. The components have spectral types of about F6 V and G5 V and are in a 59-day orbit of moderate eccentricity. The system is a member of the Coma Cluster.

Key words: radial velocities—spectroscopic binaries—stars, individual—star clusters—Coma Cluster

1. Introduction

HD 106947 is an inconspicuous object about a degree and a half south-preceding the apparent centre of the Coma star cluster. Its magnitude and colours have been given by Eggen (1964) as $V = 8.80$, $(B - V) = 0.52$, $(U - B) = 0.08$, and its spectrum has been classified as type F7 V (Heard 1956).

2. Radial velocities

Radial velocities have been obtained for HD 106947 in the course of three quite different projects. The first measurements were made by Trumpler (1938) in the course of his classic investigation of the Coma Cluster. He took four spectrograms with small prism spectrographs attached to the 36-inch refractor of the Lick Observatory, at reciprocal dispersions of about 77 Å mm^{-1} at Hγ. The resulting velocities showed a range of 30 km s^{-1}, about seven times the supposed standard deviation of an individual observation; Trumpler added the note "probably variable" to the mean velocity of – 12 km s^{-1}. His assessment of the situation now appears to have been highly conservative, since his four velocities fit remarkably well to the orbit that is derived below.

Heard (1956) was the next observer to determine the radial velocity of HD 106947, which was one of more than a thousand stars in the +25° to +30° declination zone which occupied much of the attention of the David Dunlap Observatory staff for several years around 1950. The observations were made at the 74-inch reflector with a prism spectrograph whose reciprocal dispersion was 66 Å mm^{-1} at Hγ. Unlike Trumpler, Heard did not find any evidence of velocity variation, and he did not see fit to publish his radial-velocity measurements individually; he quoted a "probable error" of 1.0 km s^{-1} for the mean of four measurements, implying that the r.m.s deviation of each of the four from their mean was 2.6 km s^{-1}—less, in fact, than the average

observing errors for his programme. The mean velocity itself, however, was + 5.0 km s^{-1}, very different from that found by Trumpler.

Unfortunately the present author failed to alert himself to the observational history of the star and to the above-mentioned evidence of the likelihood that it is a spectroscopic binary; in the course of his survey of radial velocities in the North Galactic Pole field he treated HD 106947 as if nothing were already known about it. The object (being actually much earlier in spectral type than the G5 given in the *Henry Draper Catalogue* (Cannon & Pickering 1920), whence it was selected for the Galactic Pole programme) gives quite shallow dips on radial-velocity traces; the discordance of 3.5 km s^{-1} between the first two photoelectric measurements was regarded as only barely more than might arise through observational error, and it was not until a third observation was made, in 1985, that the star was recognized as a spectroscopic binary. An intensive observing campaign in the spring of 1986 then established that the period is a little short of 59 days, and allowed it to be extrapolated back all the way to Trumpler's measurements made 50 years earlier without any ambiguity in cycle count.

Although no secondary dip was apparent on Cambridge traces, a suspicion arose that the dips were somewhat less shallow when the velocity was close to the γ-velocity. By good fortune a Palomar radial-velocity observing run in late 1986 fell near to a nodal passage and permitted a couple of excellent traces—one of which is reproduced as Fig. 1—to be obtained to show the double-lined nature of the object. Two measures of the secondary were subsequently obtained with 'Coravel' and two very marginal ones were even managed at Cambridge. Although all six observations of the secondary are grouped within a small range of phase near a node, they serve quite well to give the amplitude of the secondary variation—which is as much as could be expected of them whatever their distribution in phase.

Altogether there are 42 photoelectric measurements of the primary star, and they are set out in Table 1 along with Trumpler's (1938) four photographic measures. Heard's (1956) observations cannot appear in Table 1 since their dates and individual results are not available. The six secondary velocities are listed in Table 2.

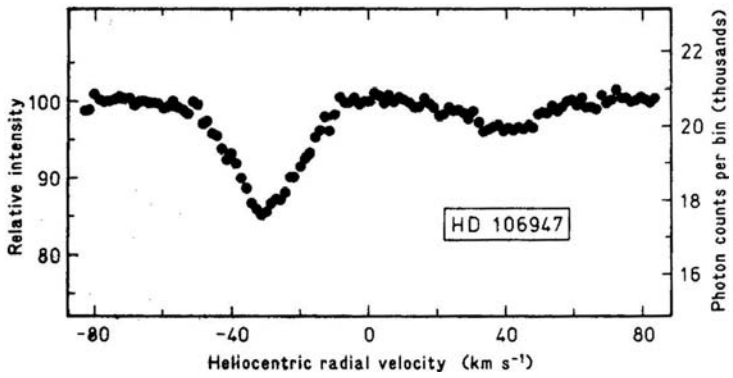

Figure 1. Palomar radial-velocity trace of HD 106947, obtained on 1986 November 24 and illustrating the double-lined nature of the object. The points represent the photon counts in a set of independent 'bins' corresponding to a uniformly spaced set of longitudinal displacements of a specially constructed mask upon which the stellar spectrum is focussed. A more comprehensive description of the equipment and procedure is given by Griffin & Gunn (1974) and updated by Griffin *et al*. (1988).

3. The orbit solution

A certain amount of pruning and weighting seemed desirable in order to achieve the optimal solution for the orbit. In the first place, those velocities in Table 1 that are near to the γ-velocity must have been 'dragged' somewhat towards that value through blending with the secondary. That effect is actually visible in the graph showing the orbit (Fig. 2). Although, owing to the disparity in dip depths, the effect is fairly small, the blended observations have been rejected from the orbit solution. Trial solutions showed that rejection of measurements for which the computed velocity separation of the components was less than 25 km s^{-1} improved the standard deviations of most of the orbital elements, notwithstanding that it meant the loss of 17 of the 42 photoelectric observations. The residuals of the rejected measures show a systematic displacement towards the γ-velocity of 1.0 km s^{-1}—a quantity larger than the r m.s random deviations of the remaining observations.

The remaining Palomar, Coravel and Victoria measures of the primary were attributed weight 4 (Cambridge =1), while the corresponding measures of the

Table 1. Radial-velocity measurements of the primary component of HD 106947, made at Cambridge except where otherwise noted.

Date	MJD	Velocity km s^{-1}	Phase	$(O-C)$ km s^{-1}
1929 May 6.27†	25737.27	−24.5	315.078	−0.1
June 18.22*†	780.22	+5.4	.809	+3.4
1937 May 9.37†	28662.37	−11.9	266.888	−0.4
1938 Feb 27.38†	28956.38	−12.4	261.894	+0.4
1980 Jan 13.15*	44251.15	+9.2	0.340	−1.0
1982 Mar 8.00	45036.00	+12.7	13.705	+0.7
1985 Feb 24.02*	46120.02	−7.1	32.164	+2.2
1986 Jan 26.11	46456.11	−12.1:	37.887	−0.7
Apr 4.89	524.89	−27.3	39.058	0.0
11.04*‡	531.04	−6.3	.163	+3.1
25.94	545.94	+14.6	.417	+0.5
May 5.93	555.93	+15.8	.587	−0.4
7.89	557.89	+15.9	.620	+0.4
13.90	563.90	+12.6	.723	+1.8
15.90*	565.90	+8.1	.757	+0.1
16.89*	566.89	+7.7	.773	+1.4
18.91*	568.91	+2.2	.808	+0.1
25.88	575.88	−19.0	.927	+0.6
27.89	577.89	−26.4	.961	−0.3
30.90	580.90	−31.3	40.012	−0.7
June 3.91	584.91	−24.8	.080	−0.8
10.93*	591.93	−1.6	.200	+2.2
11.90*	592.90	0.0	.216	+1.6
14.95*	595.95	+2.4	.268	−2.0
Nov 24.54§	758.54	−29.3	43.037	+0.3
26.54§	760.54	−25.5	.071	0.0
Dec 7.21*	771.21	+1.6	.253	−1.2

Table 1. Continued

Date		MJD	Velocity km s^{-1}	Phase	$(O-C)$ km s^{-1}
1987 Jan	6.13*	46801.13	+7.2	43.762	−0.2
Feb	1.09*	827.09	−3.5	44.204	−0.3
	21.06	847.06	+17.3	.544	+0.8
	28.15‡	854.15	+13.9	.665	−0.1
Mar	1.92‡	855.92	+11.2	.695	−1.3
	4.15*‡	858.15	+9.2	.733	−0.8
	19.99	873.99	−31.5	45.003	−1.1
	25.96	879.96	−18.3	.105	+1.4
	29.98*	883.98	−8.4	.173	−0.6
Apr	27.89	912.89	+15.1	.665	+1.1
May	7.95*	922.95	0.0	.837	+2.1
	8.92*	923.92	−3.2	.853	+1.7
	24.91	939.91	−15.5	46.125	+0.5
Dec	22.20	47151.20	+12.0	49.723	+1.3
1988 Jan	23.46*¶	47183.46	+3.0	50.273	−1.8
	30.53¶	190.53	+12.8	.393	−0.3
Feb	1.40¶	192.40	+14.5	.425	+0.1
Mar	11.02‡	231.02	−23.5	51.083	+0.1
	11.97‡	231.97	−21.0	.099	−0.2

* Observation zero-weighted in orbital solution (see text).
† Observed photographically at Lick by Trumpler (1938).
‡ Observed with 'Coravel' at Haute-Provence (Baranne, Mayor & Poncet 1979).
§ Observed, in collaboration with Dr J. E. Gunn, with the 200-inch telescope (Griffin & Gunn 1974).
¶ Observed with the Dominion Astrophysical Observatory 48-inch telescope (Fletcher *et al*. 1982).

Table 2. Radial-velocity measurements of the secondary component of HD 106947.

Date		MJD	Velocity km s^{-1}	Phase	$(O-C)$ km s^{-1}
1986 Nov	24.54§	46758.54	+38.8	43.037	−1.1
	26.54§	760.54	+34.8	.071	+0.5
1987 Mar	19.99*	46873.99	+40.8	45.003	−0.2
	25.96*	879.96	+31.1	.105	+4.5
1988 Mar	11.02‡	47231.02	+31.6	51.083	−0.2
	11.97‡	231.97	+29.2	.099	+1.2

§ Observed, in collaboration with Dr J. E. Gunn, with the 200-inch telescope (Griffin and Gunn 1974).
* Cambridge observation, zero-weighted in orbital solution.
‡ Observed with 'Coravel' at Haute-Provence (Baranne *et al*. 1979).

secondary were given unit weight. In that way the apparent weighted variances of the several types of measurements were more or less equalized. The two Cambridge attempts to measure the secondary—one of which gave a very bad residual—were set to weight zero, *i.e.* they were rejected. The weighting of Trumpler's four observations,

which are important because they greatly refine the period through extending the time base, poses something of a difficulty. According to Trumpler's own assessment they have a standard deviation of 4.5km s^{-1}, which would entitle them to a weight of about 0.05. However, after one of the observations is rejected because it was made too close to the γ-velocity, the remaining three all have residuals less than 0.5 km s^{-1}, which would entitle them to a very high weighting which is surely unrealistic. The rejected datum, on the other hand, has a relatively large residual which is in the wrong sense to be explained by dragging. Since Trumpler's estimate of his errors is based upon a much larger sample of observations than the four we are discussing here, and also because too generous a weighting would result in too optimistic an accuracy for the period, a weight of 0.1 has been adopted for the Lick observations by way of a compromise.

The finally derived orbit, illustrated in Fig. 2, has the following elements:

$P = 58.7253 \pm 0.0018$ days
$\gamma = -0.04 \pm 0.21$ km s^{-1}
$K_1 = 23.54 \pm 0.21$ km s^{-1}
$K_2 = 31.8 \pm 0.7$ km s^{-1}
$q = 1.35 \pm 0.03$ $(= m_1/m_2)$
$e = 0.302 \pm 0.012$
$\omega = 171.1 \pm 2.0$ degrees

$(T)_{43} =$ MJD 46756.4 ± 0.3
$a_1 \sin i = 18.1 \pm 0.2$ Gm
$a_2 \sin i = 24.5 \pm 0.6$ Gm
$f(m_1) = 0.069 \pm 0.002\ M_\odot$
$f(m_2) = 0.170 \pm 0.012\ M_\odot$
$m_1 \sin^3 i = 0.515 \pm 0.023\ M_\odot$
$m_2 \sin^3 i = 0.381 \pm 0.015 M_\odot$

R.m.s. residual (unit weight) = 0.9 kms^{-1}

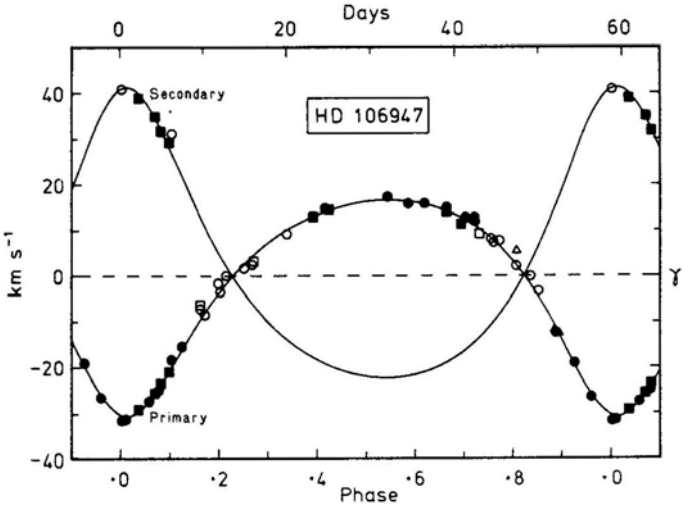

Figure 2. The computed radial-velocity curve for HD 106947, with the measured radial velocities plotted. Palomar, 'Coravel' and Victoria observations, all of which were accorded weight 4 in the orbital solution, appear as filled squares, Cambridge observations (weight 1) are represented by filled circles, while Trumpler's photographic measurements (weight 0.1) are shown by triangles. Corresponding open symbols indicate observations which were not used in the solution.

4. A model of the system

We have four data upon which to base a model of the HD 106947 system. They are:

(*a*) the mass ratio, q, of 1.35 ± 0.03;

(*b*) the ratio of dip areas on Palomar radial-velocity traces, the equivalent width of the secondary dip being 0.26 times that of the primary;

(*c*) the combined photometric colours, $(B - V) = 0^{m}.52$ and $(U - B) = 0^{m}.08$; and

(*d*) the combined spectral type, F7 V.

It is convenient to proceed by looking for a combination of spectral types that possess approximately the correct disparities given by (*a*) and (*b*), the primary being slightly earlier and secondary considerably later than the type corresponding to (*c*) and (*d*). In the present case all of the data are nicely satisfied by the model set out in Table 3, in which the types of the components are adopted as F6 V and G5 V and the colours and masses are derived from Allen (1973; by interpolation in the case of the F6 component).

The observed colours are well reproduced by the combination of types as it stands, and they could in fact be mimicked exactly if we allowed ourselves to advance the types of both components by a fraction of a subtype. The mass ratio found from the orbit is reproduced to well within its own uncertainty. In the wavelength region corresponding to the *B* photometric band, which is approximately the region used for spectral classification and also by the radial-velocity spectrometer, the disparity in luminosity between the components amounts to $1^{m}.95$ or a factor of 6.0. With such a weighting, a mean spectral type of F7 V is very close to expectation. The relationship between radial-velocity dip areas and $(B - V)$ colours for Hyades stars indicates equivalent widths of 3.5 and 5.5 km s^{-1} for single stars having colours of $0^{m}.45$ and $0^{m}.70$ respectively. When superimposed with weights of 6:1, such components would give dips of areas 3.0 and 0.78 km s^{-1} respectively in the combined trace, *i.e.* a ratio of 1:0.26, just what is observed. The model may therefore be accepted with confidence as being a good approximation to the truth.

Comparison of the masses demanded by the model with those given by the orbital solution shows that the inclination of the orbit is about 48°. There is evidence (Batten & Wallerstein 1973; Griffin 1978, 1980; Griffin & Gunn 1978; Griffin, Mayor & Gunn 1982; Griffin *et al*. 1985) that the masses given in Allen (1973) for late-type dwarf

Table 3. Model for HD 106947.

	Spectral Type	Absolute Mag. V m	B m	U m	Colour Index $(B-V)$ m	$(U-B)$ m	Mass $M_{\odot}$	Mass Ratio q
Model	F6 V	3.6	4.05	4.08	0.45	0.03	1.25	1.34
	G5 V	5.1	5.80	5.99	0.70	0.19	0.93	
	F6 V+G5 V	3.36	3.85	3.92	0.49	0.07	2.18	
HD 106947 (observed)					0.52	0.08	>0.90	1.35

stars need some upward revision; if such revision is applicable to HD 106947 the inclination is reduced to approximately 46°.

5. HD 106947 and the Coma Cluster

Both the Coma Cluster itself and the membership therein of HD 106947 have had a somewhat chequered history in the literature of astronomy. Although the cluster is obvious to the naked eye as a grouping of fifth- and sixth-magnitude stars in an otherwise sparsely populated part of the sky near the Galactic Pole, until the twentieth century there was much hesitation in accepting it as a real star cluster. For example, it does not feature at all in the *NGC* (Dreyer 1888), although Coma is a constellation that is notorious for the large number of (far less conspicuous) *NGC* objects that it contains. In 1897 Pickering noted that "The stars in the constellation Coma Berenices are so widely scattered that they can scarcely be regarded as forming a cluster". However, subsequently he (Pickering 1918) appears to have realized the Coma Cluster to be indeed a real physical entity. It seems first to appear in a catalogue of clusters in the work of Melotte (1915), in which it is listed as no. 111; the designation Mel 111 is still widely used for the Coma cluster, *e.g.* in the great *Catalogue of Star Clusters and Associations* by Alter *et al*. (1970), and by Hoffleit (1982) in the notes to 23 of the stars in the current edition of the *Bright Star Catalogue*.

In the early part of this century there were published several catalogues of stars in the area of the Coma Cluster, giving proper motions and/or photometry. HD 106947 features, for example, in the catalogues of Malmquist (1926) (as 25° 70), Ölander (1927) (as no. 34), Heckmann (1929) (as no. 56) and Meyermann (1930) (as no. 97). However, the proper motions of the cluster stars are much too small to provide a reliable criterion of membership; it was not until the comprehensive study by Trumpler (1938), who determined radial velocities as well as proper motions, magnitudes and spectral types, that a reasonably reliable separation was made between cluster members and field stars. Trumpler identified 37 stars brighter than m_{pg} = 10.5 as members, and proceeded to derive from them the fundamental characteristics of the cluster itself. He found it to have a limiting angular radius of 4°, centred on $12^{h}\ 18^{m}.0$, + 26° 30′ (1900); proper-motion $\mu_\alpha \cos\delta = -0''.013$, $\mu_\delta = 0''.017$ per annum; radial velocity – 0.4 km s^{-1}; distance modulus $(m - M) = 4^{m}.43$. All of these data have stood up very well to the test of time during the interval of exactly half a century since they were published. It is, therefore, a little embarrassing that we now wish to reverse Trumpler's verdict as to the membership of the very star (his no. 48) with which this paper is concerned.

An unusual feature of Trumpler's discussion was that he did not consider a star's qualifications for cluster membership all at once but *seriatim*. If a star failed his first test—the test of proper motions—he rejected it forthwith and ignored its other qualifications. That was what happened to HD 106947: with annual proper-motion components of 0″.033, 0″.023, it fell (just) into his category of stars that were "eliminated as nonmembers with practical certainty", and its other properties were not reviewed at all. Trumpler (1938) himself was not inclined to brook much tampering with his own membership assignments: "We conclude from this discussion that our selection of 37 cluster members brighter than photographic magnitude 10.5 within a circular area of 7° diameter is practically complete and cannot be uncertain by more

than one or two stars". Even such an august authority as The Editors of *The Observatory* (1940) commented that "future research is not likely to add more than a few, if any, additional members brighter than $10^m.5$ to Trumpler's list." However, Eggen (1964) nevertheless had the temerity to consider HD 106947 to be a member, even though he did not possess a reliable radial velocity for it, and it now seems worth while to review its candidature in the light of all the data available.

In the first place, the position of HD 106947 in the sky at $12^h\ 12^m.7$, + 25° 37′ (1900) puts it only about 1°.5 from the cluster centre—less than half the angular radius of the cluster. Secondly, its annual proper motion is given in the SAO catalogue (Smithsonian 1966) as –0″.015, –0″.017, almost identical with the cluster motion as adopted by Trumpler. Certainly there are considerable discrepancies between the proper motions given by different sources for the same star—for instance, the *AGK*3 (Heckmann & Dieckvoss 1975) gives the motion in right ascension as –0″.043, even more discordant from the cluster motion than Trumpler's value; but that surely serves to tell us more about the reliability of proper motions than about the rejectability of HD 106947. As long as the spread between the different authorities is not such as to exclude the cluster motion as a possible true value, we cannot safely reject membership on proper-motion grounds. Then, the γ-velocity found in the present paper differs from the adopted radial velocity of the Coma Cluster by + 0.4 km s^{-1}; or, if the usual offset of 0.8 km s^{-1} between the photoelectric and Lick velocities (Griffin & Herbig 1981) is applied, the discrepancy between HD 106947 and the cluster becomes – 0.4 km s^{-1}. Either way, the agreement is as good as could be desired. Finally, a comparison of the absolute magnitude of HD 106947 as modelled in Table 3 with the measured magnitude of $V = 8.80$ indicates a distance modulus of $4^m.44$—just one hundredth of a magnitude greater than the modulus of the cluster as given by Trumpler and largely confirmed by his successors (*e.g.* Eggen 1950; Johnson 1957; Becker 1958; Crawford 1963; Mendoza 1963).

Thus HD 106947 conforms so exactly with the properties of the Coma Cluster that its membership can scarcely be doubted any longer. It is unfortunate that it was not recognized as a member earlier, since many investigations of the Coma Cluster would then have included it (examples are the photometric papers of Eggen (1950, 1955), Bahner & Miczaika (1952) and Mendoza (1963), and the spectroscopic work of Kraft (1965), who would surely have drawn attention to its duplicity).

The list of stars whose candidature for membership in the Coma Cluster was reviewed by Trumpler (1938) includes 212 objects and was intended to be complete to photographic magnitude 10.5 within the area that he surveyed, which had a diameter of 7°. About 130 of the stars are bright enough to be listed also in the *Henry Draper Catalogue* (Cannon & Pickering 1920), and about 60 of those 130 *HD* stars are of spectral type G5 or later. (The reason that these numbers are given only approximately is not any difficulty of enumeration but of definition: is a double star that is listed with two numbers by Trumpler but only one number in the *HD* one *HD* star or two?) Since the area surveyed by Trumpler lies wholly within the North Galactic Pole field as defined for the purposes of the Cambridge radial-velocity survey ($b > 75°$), all of the ~60 late-type *HD* stars have been observed from Cambridge. One of them, HD 107742, has already featured in this series of papers (Griffin 1983). However, very few of the candidates that are truly members of the Coma Cluster are among the 60 stars, for the simple reason that cluster stars as late as type G5 (the earliest *HD* type for inclusion

in the Galactic Pole project) are in general too faint to have been listed in the *Henry Draper Catalogue*; it was only because of its misclassification as a G5 star that HD 106947, which is really F7 V, got onto the programme. Oddly enough, HD 106947 appears on the very first list of Coma stars (Pickering 1897) as having spectral type F; but we must be grateful to Miss Cannon for her slight lapse, without which *this* paper would never have been written!

Acknowledgements

It is a pleasure to acknowledge the guest-investigator privileges accorded me by the Palomar, Geneva and Dominion Astrophysical observatories, and the assistance of Dr R. E. M. Griffin in the observations made there.

References

Allen, C. W. 1973, *Astrophysical Quantities*, Athlone, London, pp. 206, 209.
Alter, G., Ruprecht, J., Vanysek, V. 1970, *Catalogue of Star Clusters and Associations*, Akadémiai Kiadó, Budapest.
Bahner, K., Miczaika, G. R. 1952, *Z. Astrophys*., **31,** 236.
Baranne, A., Mayor, M., Poncet, J. L. 1979, *Vistas Astr*., **23,** 279.
Batten, A. H., Wallerstein, G. 1973, *Publ. Dom. astrophys. Obs., Victoria*, **14,** 175.
Becker, W. 1958, *Z. Astrophys*., **45,** 269.
Cannon, A. J., Pickering, E. C. 1920, *Ann. Harv. Coll. Obs*., **95.**
Crawford, D. L. 1963, *Publ. astr. Soc. Pacific*, **75,** 410.
Dreyer, J. L. E. 1888, *Mem. Roy. astr. Soc*., **49,** 1.
Eggen, O. J. 1950, *Astrophys. J*., **111,** 414.
Eggen, O. J. 1955, *Astr. J*., **60,** 407.
Eggen, O. J. 1964, *Astr. J*., **69,** 570.
Fletcher, J. M., Harris, H. C., McClure, R. D., Scarfe, C. D. 1982, *Publ. astr. Soc. Pacific*, **94,** 1017.
Griffin, R. F. 1978, *Observatory*, **98,** 257.
Griffin, R. F. 1980, *Observatory*, **100,** 113.
Griffin, R. F. 1983, *J. Astrophys. Astr*., **4,** 19.
Griffin, R. F., Gunn, J. E. 1974, *Astrophys. J*., **191,** 545.
Griffin, R. F., Gunn, J. E. 1978, *Astr. J*., **83,** 1114.
Griffin, R. F., Gunn, J. E., Zimmerman, B. A., Griffin, R. E. M. 1985, *Astr. J*., **90,** 609.
Griffin, R. F., Gunn, J. E., Zimmerman, B. A., Griffin, R. E. M. 1988, *Astr. J*., in press.
Griffin, R. F., Herbig, G. H. 1981, *Mon. Not. R. astr. Soc*., **196,** 33.
Griffin, R. F., Mayor, M., Gunn, J. E. 1982, *Astr. Astrophys*., **106,** 221.
Heard, J. F. 1956, *Publ. David Dunlap Obs*., **2,** 105.
Heckmann, O., 1929, *Veröff. Univ.-Stern. Göttingen*, **1,** 141.
Heckmann, O., Dieckvoss, W. 1975, *AGK3*, Hamburger Sternwarte, Hamburg-Bergedorf, **5,** 196.
Hoffleit, D. 1982, *Bright Star Catalogue*, Yale Univ. Obs., New Haven.
Johnson, H. L. 1957, *Astrophys. J*., **126,** 121.
Kraft, R. P. 1965, *Astrophys. J*., **142,** 681.
Malmquist, K. G. 1926, *Medd. Lunds astr. Obs*., Ser. II, no. 37.
Melotte, P. J. 1915, *Mem. Roy. astr. Soc*., **60,** 175.
Mendoza V, E. E. 1963, *Bol. Obs. Ton. y Tac*., **3,** 137.
Meyermann, B. 1930, *Veröff. Univ.-Stern. Göttingen*, **1,** 313.
Ölander, V. 1927, *Soc. Sci. Fennica Comm. Phys.-Math*., **4,** no. 11.
Pickering, E. C. 1897, *Ann. Harv. Coll. Obs*., **26,** part II. (See p. 273.)

Pickering, E. C. 1918, *Harv. Coll. Obs. Circ.*, no. 206.
Smithsonian Astrophysical Observatory Star Catalog, 1966, Smithsonian Inst., Washington, D.C., part 2.
The Editors of *The Observatory*, 1940, *Observatory*, **63,** 26.
Trumpler, R. J. 1983, *Lick Obs. Bull.*, **18,** 167.

J. Astrophys. Astr. (1988) **9,** 137–154

Sunspot Proper Motions in Active Region NOAA 2372 and its Flare Activity during SMY Period of 1980 April 4–13

Ashok Ambastha & Arvind Bhatnagar *Udaipur Solar Observatory, 11 Vidya Marg, Udaipur 313001*

Received 1988 March 7; accepted 1988 May 21

Abstract. Solar Active Region NOAA 2372 was observed extensively by the Solar Maximum Mission (SMM) satellite and several ground-based observatories during 1980 April 4–13 in the Solar Maximum Year. After its birth around April 4, it underwent a rapid growth and produced a reported 84 flares in the course of its disc passage. In this paper, we have studied photospheric and chromospheric observations of this active region together with Marshall Space Flight Center magnetograms and X-ray data from HXIS aboard the SMM satellite. In particular, we discuss the relationship of the flare-productivity with sunspot proper motions and emergence of new regions of magnetic flux in the active region from its birth to its disappearance at the W-limb.

Key Words: sunspot proper motion—magnetic energy buildup—flare productivity

1. Introduction

It is well known that a variety of factors may lead to the energy build-up in an active region, *e.g*., magnetic complexities, particularly a δ-configuration in the region (Zirin 1970), flux emergence (Vorpahl 1973, Tur & Priest 1976), and motion at the photospheric level resulting in shearing and/or stretching of the magnetic field structures (Sakurai 1976, Zirin & Lazareff 1975). A part of this stored or free energy may be subsequently liberated in the form of flares when triggered by an instability in the region. In a detailed study of the 1972 August flares, Zirin & Tanaka (1973) inferred the presence of highly sheared transverse magnetic fields from the twisted appearance of penumbral filaments and thus explained the occurrence of major flares in the active region McMath 11976. Sunspot motion and its relation with flares has also been studied in a series of papers by Kalman (1984), Gesztelyi (1984) and Dezso *et al*. (1984). From these papers it appears that sunspot proper motions have a close relationship with flare productivity of an active region.

We undertake here a study of sunspot proper motions in the active region NOAA 2372 observed extensively from the Udaipur Solar Observatory during its disc transit in the SMY period of April 4–13, 1980. The objective is to investigate as to how these motions are related to its flare productivity. This region was conspicuous by its exceptionally high activity. NOAA 2372 first appeared as an H-alpha plage (Hale Plage Region No. 16747) on April 4 in the NE-quadrant of the solar disc near an old

region, Hale No. 16752 (Fig. 1). It exhibited a remarkably rapid growth in the magnetic field intensity and complexity after its birth on April 4 and developed into a $\beta\gamma$ spot-group with a δ-configuration within 24 hours from its birth. Embedded within the main leader 'P' and trailer 'Q', an intermediate inverted bipolar group 'R-S' was also observed, thus, constituting a N-S-N-S configuration (Fig. 2).

NOAA 2372 produced its first reported large flare (M5/1B) on April 5/1554 UT. Altogether, it produced 84 flares of varying magnitudes in H-alpha and X-rays (Solar and Geophysical Data, pt.l, Nos.429 & 430). Earlier, Krall *et al*. (1982) have studied evolution of vector magnetic fields in this region over a three-day period (April 5–7). They reported a shear in the horizontal velocity field and that the flare activity occurred along the magnetic neutral line, particularly during April 5–6. Machado *et al*. (1983) have discussed spatial and temporal characteristics and locations of soft X-ray flares occurring in this region during April 6–13. They attribute the occurrence of a number of flares in the region to the presence of the intermediate bipolar region near which large magnetic shear was observed during the period of April 5–7.

In the present paper, we measured proper motions of the main leader 'P', trailer 'Q' and the sunspots 'R'-'S', forming the intermediate bipole, and ask how they relate to the flare-productivity of NOAA 2372 during its entire disc passage. We shall note that although the net energy release, in the form of H-alpha flares, peaked around April 7, the frequency of occurrence of reported flares peaked around April 10 by which time photospheric motions associated with the sunspots, as well as magnetic shear, had reduced considerably. The flares of this phase of the development of NOAA 2372, and their relationship with various parameters of the active region have not been well studied. Thus, in order to understand the overall flare activity of the region during its various phases of development, we have examined suspot motions during the entire period of transit of the region, *i.e*., April 4–13, together with the emergence of new flux regions. We also make rough estimation of the magnetic energy build-up by the sunspot proper motions and compare it with the energy release observed in the region.

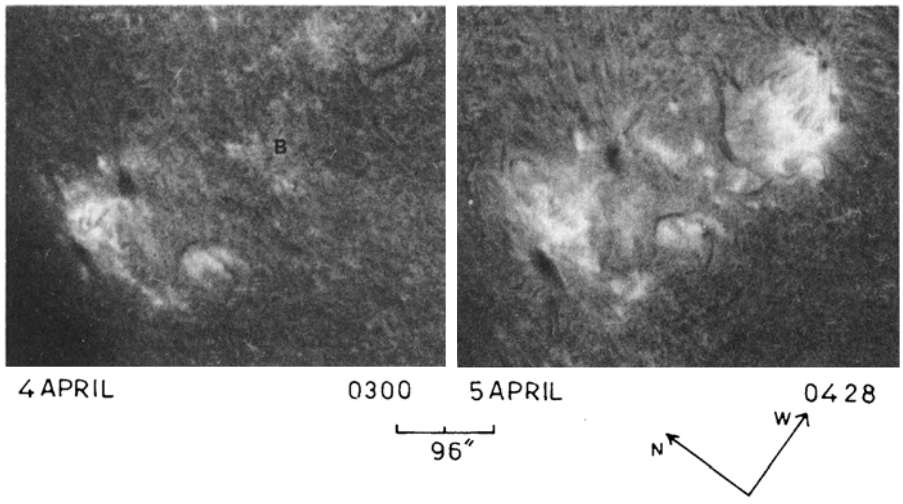

Figure 1. H-alpha Filtergrams indicating the birth of the Active Region NOAA 2372 (Hale No. 16747) at the location marked 'B' to the west of the existing Hale No. 16752.

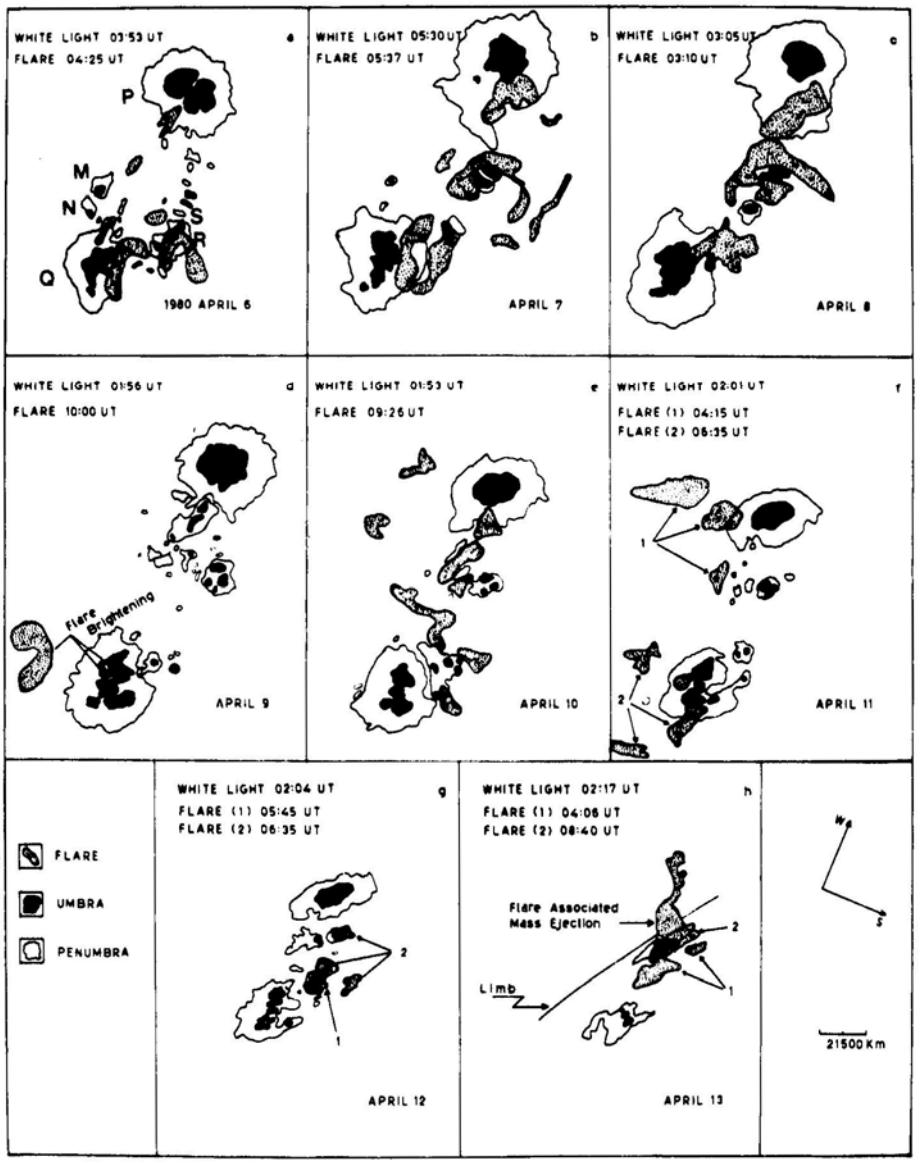

Figure 2. White light drawings of the main sunspots of NOAA 2372 during 1980 April 6–13. Locations of major flares, at their maximum phases, are given as dotted ribbons.

Flare activity in a sunspot group is known to depend on the stage of development of the sunspots; generally, maximum flare activity is observed when sunspot-area of the group reaches a maximum (Waldmeier 1955, Enger *et al.* 1966). Hence, we examine here the growth and decay of sunspot-areas, to see its relation with the flare productivity of the region. Chromospheric and photospheric observations of NOAA 2372, along with the reported X-ray data from HXIS aboard SMM satellite (Machado *et al*. 1983) and MSFC magnetograms (Sawyer 1982), will also be discussed.

2. Observational data and measurements

Here we shall describe the observational data of NOAA 2372, during its disc passage from 1980 April 4–13. Daily full-disc photoheliograms were obtained from the Indian Institute of Astrophysics, Kodaikanal for the periods of April 5–6, April 9–13 and from the Heliophysical Observatory, Debrechen for April 4, and April 7–8. The H-alpha observations were taken from the Udaipur Solar Observatory using a 150-mm aperture diffraction limited singlet *f*/13 objective, in conjunction with a narrow passband (0.5 Å), H-alpha Halle filter. A relay lens of focal length of 180 mm yielded a solar image of 44 mm diameter. Filtergrams were taken on 35 mm format by a time lapse camera at 10–15 seconds interval with SO-115 Eastman Kodak film (now Kodak Technical Pan 2415).

Sunspot positions and the calculations of heliographic coordinates (*L*,*B*) from white-light photoheliograms were digitized with a digitizer interfaced with an IBM PC/AT microcomputer, using a computer program developed by one of the authors (Ambastha 1987). This digitizer has a resolution of 0.0125 mm at an accuracy of 0.0125 mm. We selected only those sunspots for measurement which could be identified and followed with reasonably good confidence over at least a couple of days. The heliographic coordinates determined for the centres of some major sunspots of NOAA 2372 are plotted in the Carrington Map (Fig. 3) where proper motions of sunspots are clearly seen. In the cases where umbrae consisted of a number of fragments, we measured the average positions of all the umbrae in the sunspot.

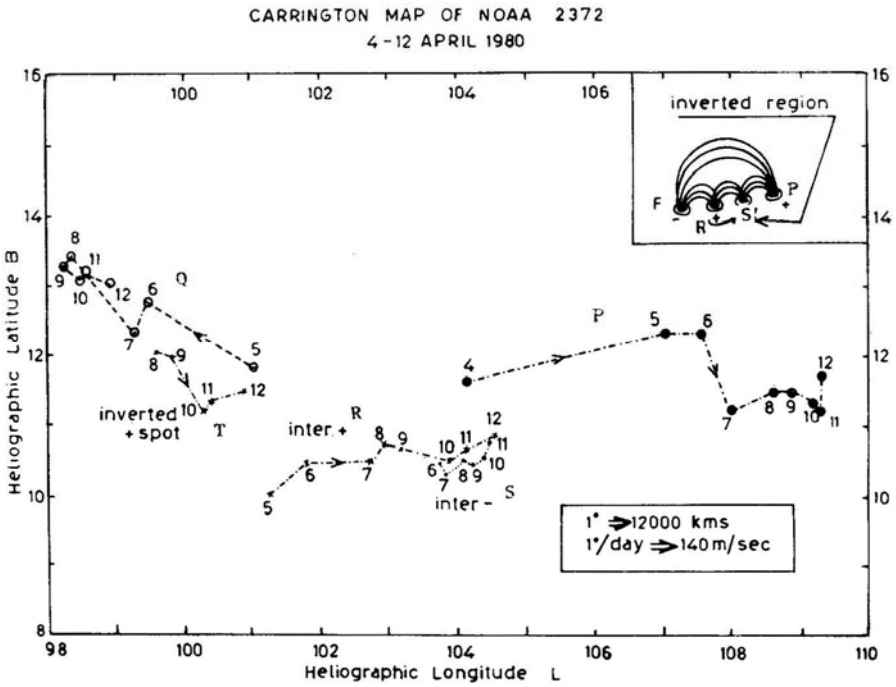

Figure 3. Daily heliographic positions of the main sunspots of NOAA 2372. Arrows indicate directions of their motion.

To obtain good accuracy of sunspot-area measurements we enlarged the photoheliograms to image-size of 180 cm diameter. Both the umbral and penumbral areas of major sunspots were measured. We used the following expression (Enger *et al*. 1966) to correct the measured areas for the effect of foreshortening:

$$\text{C.A.} = \text{A.A.}/[0.2\,\hat{r} + (1 - \hat{r}^2)^{1/2}] \tag{2.1}$$

where, C.A. and A.A. are the corrected and apparent areas, respectively, of a sunspot. Also, $\hat{r} = r/R$ where r is the radial distance of the centre of the sunspot from the disc centre and R is the radius of the photoheliogram. The growth and decay of the main leader P and trailer Q of NOAA 2372 are plotted in Fig. 4 for the period April 5–12.

The flare-activity of NOAA 2372 is illustrated in Fig. 5. It gives the following details:

a) Number of reported H-alpha flares per day (Solar and Geophys. Data Nos. 429 & 430, 1980). In the histogram, we have included flares of all important classes.

b) Daily flare indices (solid line) and the H-alpha flare energy release (dashed line). Heights of the vertical bars and their positions along the abscissa denote the energy release in units of 10^{30} erg (scale at right-hand side ordinate) and the time of occurrence of the flare, respectively. We have presented in this plot flares of energy $\gtrsim 10^{30}$ erg only, whereas the histogram in (a) include all reported flares. Here we have used empirically estimated H-alpha energies associated with flares under the assumption that flare energy is approximately proportional to the duration of flare (Obashev 1968) such that

$$E_{H\alpha} = 2.5\alpha UT \times 10^{23} \text{ erg}, \tag{2.2}$$

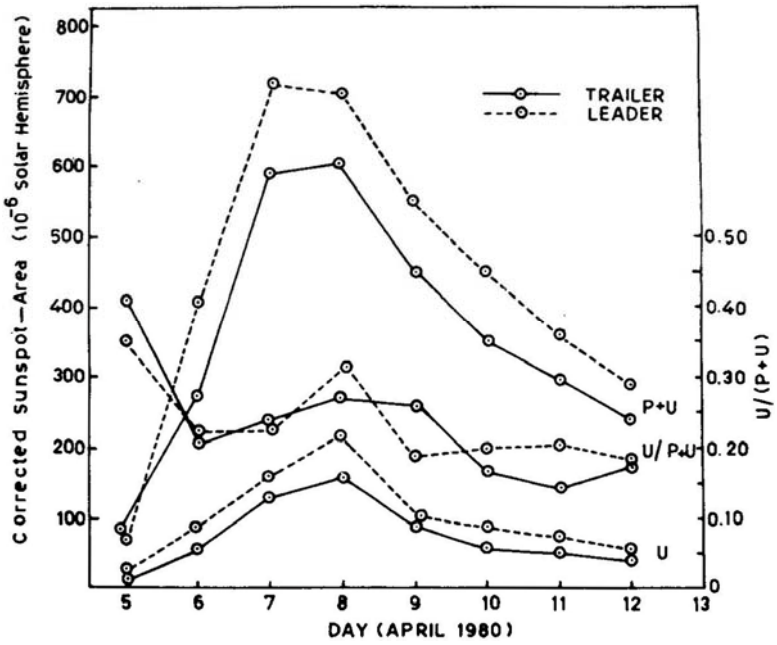

Figure 4. Development of the umbral (U) and the total (P + U) sunspot areas for the main sunspots of NOAA 2372. Ratio of the umbral to the total sunspot area, U/(P+U), is also plotted with its scale marked at the right.

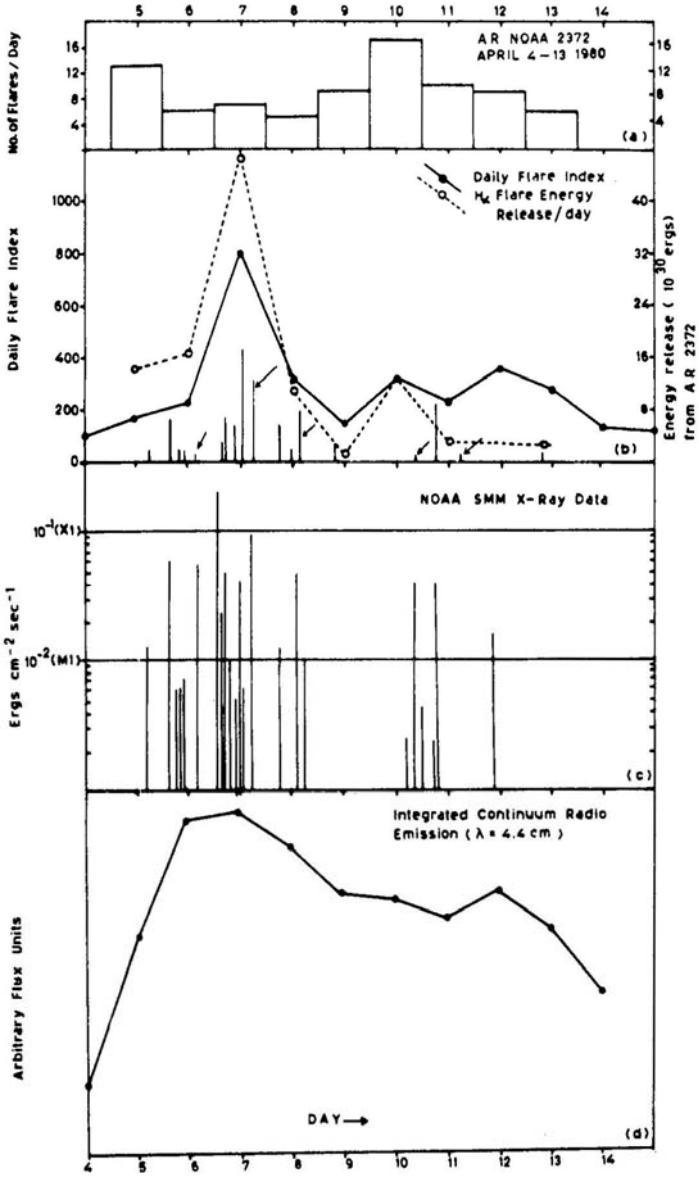

Figure 5. A composite diagram of (a) the frequency of flares per day, (b) the H-alpha energy release per day and total Daily Flare Index. Vertical bars indicate times of occurrence of some flares and the associated energy release, (c) the X-ray flares (from Krall *et al*. 1982) and (d) the integrated continuum radio emission at λ 4.4 cm (Solnechnye Dannye 1980).

where U is the energy per unit volume per unit time radiated from the region of the flare, T the duration of the flare and α the transformation coefficient such that $0.75 < \alpha < 1$. If we take the average energy $U = 0.02$ erg cm^{-3} s^{-1} and $\alpha = 0.8$ then the above relation transforms to

$$E_{H\alpha} = 4 \times 10^{21}\, T^{2.5} \text{ erg}, \tag{2.3}$$

where T is expressed in seconds.

The trends of the Daily Total Flare Index (which includes all active regions on the visible solar disc) and the H-alpha flare energy release from NOAA 2372 calculated using Equation (2.3) correspond well during April 5–11. This indicates that this active region alone dominated the flare activity of the solar disc during this period.

c) NOAA SMM X-ray data (adopted from Krall *et al*. 1982). One notices, by comparing Figs 5 b-c, that not all X-ray flares correspond well with the H-alpha flares.

d) The integrated continuum radio emission in λ 4.4 cm (Solnechnye Dannye 1980). This agrees well with the H-alpha flare index and X-ray data.

3. Development of sunspots in NOAA 2372

In Fig. 4 is given the daily development of the sunspot areas, *i.e*., the umbral (U) and the total (umbral and penumbral) area (P + U), as well as, their ratio, U/(P + U), of the main leader or preceding spot (dashed lines) and the trailer or following spot (solid lines). The areas are expressed in the units of millionths of solar disc. The plot shows that the sunspot areas increased rapidly during April 5–7, reaching their maximum growth around April 7/8. Thereafter they decreased with a slower rate. Similarly, the ratio of umbral area to the total sunspot area peaked on April 8. Of course, this ratio was even larger on April 5 around the time of birth of the sunspots, however, almost no penumbra had developed at that time. It is known that generally flare-activity in a

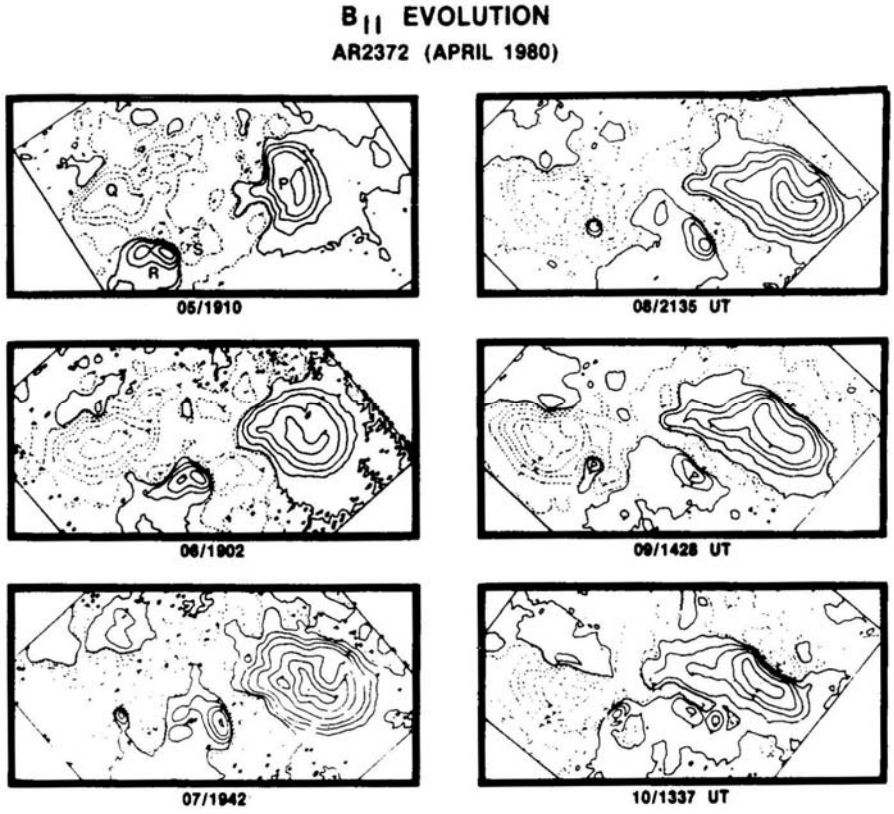

Figure 6. The evolution of *B* in NOAA 2372 (from Sawyer 1982).

sunspot-group depends on the stage of the development of the group; it is maximum when the area of the group is maximum; thereafter, its activity declines (Waldmeier 1955, Enger *et al*. 1966). Flare activity also depends on the magnetic classification of the group—increasing from simple unipolar α type through the bipolar β, $\beta\gamma$ type, and to magnetically complex γ type (Kunzel 1960; Zirin 1970). The number of flares observed per day, in this case, however, was maximum around April 10, *i.e*., much beyond April 7/8, the phase of the maximum sunspot-areas. From Fig. 5 a–c, we note that although the number of flares observed on April 10 was larger, the net energy release in H-alpha, as well as, in soft X-rays was considerably higher on April 7.

NOAA 2372 was indeed a complex $\beta\gamma$ bipolar group with an embedded intermediate bipole. A number of sunspots were observed growing and/or decaying rapidly within the group (Fig. 2). For instance, south polarity sunspots M & N were quite prominent as on April 6, but later they decayed in sizes (and fluxes) and vanished completely by April 8. This is also reflected from the magnetograms of the region (Fig. 6). A similar overnight disappearance of magnetic flux (around 4×10^{20} Maxwells) was reported by Rabin, Moore & Hagyard (1984) in an area of 30 arcsec^2 having low shear and low activity in the same active region to the north-east of the leader. The cause of this disappearance, according to Rabin *et al*., was submergence of the magnetic flux below the photospheric level.

Since sunspots are centres of maximum magnetic fields, their motion, and variations in their areas also represent the changes in overlying magnetic structures and flux. The release of energy in the form of flares, which may lead to a decrease in net magnetic flux, may, perhaps, also result in a detectable decrease in sunspot areas (Rust 1972, Harvey & Recely 1984).

4. Evolution of longitudinal magnetic field

The longitudinal magnetic field variations in NOAA 2372 are illustrated in the sequence of MSFC magnetograms adopted here from Sawyer (1982) (Fig. 6). The magnetic configuration of N–S–N–S constituted by the main sunspot P, Q and the inverted intermediate bipole R, S is clearly displayed in these magnetograms.

The positive magnetic flux of R was observed as pushing into the negative flux region, Q (the trailer) as seen on April 6/1902 UT. This intrusion into Q developed further on April 7 and a part of the positive flux of R detached from the parent region. This positive flux, trapped in the negative polarity region, thus constituted another inverted polarity region. Later as the group developed, it diffused gradually and reconnected back with R as on April 10/1337 UT. During this period, the intermediate bipolar region appeared to have moved as a whole toward P. But a clearer picture of the motion of the associated sunspots may be inferred from the Carrington Map (Fig. 3). New opposite polarity fluxes also emerged to the north-west of both P and Q. The entire region simplified considerably by the time the group reached near the W-limb as the intermediate bipole gradually decayed or merged with the main sunspots.

5. Sunspot proper motions

Sunspot groups forming an active region usually occupy roughly an oval shape area whose major axis is slightly inclined to the parallels of the latitude such that the

preceding sunspot lies at a lower latitude than the following sunspot. For this reason, even in the absence of individual sunspot motions, differential solar rotation will cause divergence in longitude between sunspots (Bray & Loughhead 1964). If one adopts the following for the rate of rotation of sunspots with area greater than 15 millionths-of-hemisphere (*cf*. Howard & Gilman 1984):

$$\omega = [14.282 - 2.636 \sin^2 B] \text{ deg day}^{-1}, \quad (5.1)$$

where B is the latitude of a sunspot, one obtains a divergence of 0.016 deg day^{-1} in longitude for sunspots located at $B = 10°$ and 11°, respectively. However, sunspots are found to possess even larger proper motions over the general rotational motion given by Equation (5.1).

Figure 3 shows daily proper motions of the leading and trailing sunspots of the main bipole, marked as P and Q in Fig. 2, sunspots R and S of the inverted bipole as well as an inverted north polarity sunspot T near Q. Except on April 5, the leader was located at a lower latitude compared to the trailer. During April 5–8, both p- and f-spots moved rapidly to the west and to the east, respectively, from their initial positions and covered large distances on the photosphere. Thus, the separation between them increased from around 6° to 10.5°. After April 8 their proper motions decreased. Due to foreshortening, the position-measurement of the sunspots near the limb may have larger errors on April 12–13, hence the displacements around this period should be considered with care. In fact, this is the reason we have not plotted the sunspot positions on April 13.

As inferred by comparing white light drawings in Fig. 2 with Mt Wilson Observatory magnetic field data, we note that in the intermediate bipole the polarity of the preceding sunspot S was negative (or south) and positive (or north) than that of the following sunspot R. Embedded in an inverted configuration within the main sunspot group, there is implied a high degree of magnetic shear around the location of R–S from the time of its appearance in the active region. It is observed that these sunspots, forming an inverted bipole, moved in a manner such as to relax the high magnetic shear of the loop joining them. Thus, the positive polarity sunspot R moved rapidly to the west while the negative polarity sunspot S remained nearly anchored in the photosphere and moved very little. By April 10, the positive flux of the inverted bipole started merging with the flux of the main leader sunspot P (*cf*. Fig. 6). It is interesting to note here that Krall *et al*. (1982) observed in their paper that the inverted bipole R–S moved as a whole toward the leader. They reported a build-up of magnetic energy (and shear) as the reason for flares of this active region during the period of April 5–7. While we find that although the positive spot R moved rapidly in the direction of the main trailer P, the sunspot P also moved westward and the negative spot S moved very little. We shall see in Section 6 that the relative motion between the sunspot pair R–S of the inverted bipole gave rise to a negative magnetic energy build-up and that the net positive build-up of magnetic energy in the active region was contributed mainly by the proper motion of main sunspots P –Q.

6. Magnetic energy build-up due to sunspot proper-motion

Estimates of the total magnetic energy build-up within a force-free magnetic configureation due to horizontal sunspot motion could be obtained from the general magnetic

energy integral following the method given by Tanaka & Nakagawa (1973). The rate of magnetic energy variation, ΔM, is given by

$$\Delta M = [\, B_0^2 L_x L_y (u \sin\gamma - v \cos\gamma)]/[15\pi^2 (1 + L_x^2/L_y^2)^{1/2}], \tag{6.1}$$

where L_x, L_y, u, v are characteristic lengths and velocities, respectively, along x- and y-axes of a Cartesian coordinate system as defined in Tanaka & Nakagawa (1973). B_0 is the peak magnetic field associated with a sunspot and γ gives a measure of shear in the region. A positive u will increase ΔM by stretching, whereas, a negative v will do so by shearing the magnetic loop structures joining the sunspots. As discussed in Section 5, all the main sunspots of NOAA 2372 displayed motions along both the heliographic axes, *i.e.*, L and B. These motions can easily be resolved in the components along the line joining the sunspot-pairs and perpendicular to this line. Evidently both stretching and shearing of field-lines will contribute to ΔM and the assumption of unidirectional sunspot-motion (along only x-axis) as made by Krall *et al*. (1982) may lead to incorrect estimates.

We determine daily average sunspot-velocities, w_L and w_B, along L and B axes (in Fig. 3) from the daily displacements of various sunspots. For example, consider the magnetic loop joining the sunspot pair Q–R shown in Fig. 6. Its x-axis is defined by the line joining the centres of Q and R and the origin of the coordinate system is chosen at the intersection of the x-axis with the neutral line: perpendicular to the x-axis at the origin is defined as y-axis. We shall use the magnetograms in Fig. 6 for defining them. Angle γ is defined as the angle between the tangent to the neutral line and the y-axis at the origin. Angle $(\pi/2 - \gamma)$ represents the degree of shear in the transverse magnetic field, as in the potential configuration with the minimum energy M_p, $\gamma = \pi/2$. Any departure from the potential configuration implies a higher energy state, M. Thus, the stored energy available in the system is given by $M' = M - M_p$.

As the active region evolves, the x–y coordinate system as defined earlier may undergo both translational, as well as rotational motion with respect to the heliographic coordinate system. This change needs to be taken into account. We obtain the (x, y) components of velocity, *i.e.*, u', v' from (L, B) velocity-components, *i.e.*, w_L and w_B using

$$u' = w_L \cos\theta + w_B \sin\theta, \tag{6.2a}$$

$$v' = -w_L \sin\theta + w_B \cos\theta, \tag{6.2b}$$

where θ is the angle between the B- and the y-axes. These transformed velocities are measured with respect to the origin for a particular sunspot. The relative velocity of the spot Q with respect to the spot R may be obtained from

$$u = u'_Q - u'_R, \tag{6.3a}$$

$$v = v'_Q - v'_R. \tag{6.3b}$$

The characteristic lengths L_x and L_y in Equation (6.1) are taken as the separation between Q–R along the x-axis, and the penumbral diameter of spot Q along the y-axis, respectively, and B_0 is the peak magnetic field of Q (obtained from Mt Wilson magnetic field drawings). Having obtained all the required quantities, the magnetic energy build-up due to the motion of sunspot Q relative to the sunspot R can be obtained using Equation (6.1).

In deriving Equation (6.1) from the equation of magnetic induction, a condition of

no leakage or divergence of magnetic flux, *i.e.*, $\nabla \cdot \mathbf{B} = 0$, has been assumed. In order to satisfy this condition, it is essential to consider an area of the active region within which the magnetic field lines are contained entirely. However, it may be difficult to fulfil this condition strictly because NOAA 2372 may have been interconnected to the neighbouring, old, active region, Hale No. 16752. Here we have ignored any contribution arising from this divergence for calculating the magnetic energy build up.

In NOAA 2372, four distinct magnetic loop systems joining the main sunspots and the intermediate bipolar sunspots have been inferred on the basis of the SMM HXIS X-ray data (Machado *et al*. 1983). A three dimensional perspective of these loops, as obtained from potential field calculations using MSFC vector magnetograms, has been given by Cheng *et al*. (1982). Due to the motion of sunspots, which represent foot-points of these loops, each of the loops joining them will experience stretching and/or shearing. In order to estimate the net magnetic energy build-up in the active region, contributions arising from the relative motion between each sunspot-pair should be calculated. Of course, there may be a number of smaller sunspots, pores, *etc*., present in the active region which may also contribute to the total magnetic energy build-up. But as our interest here is to make a rough estimate only, we have chosen not to take these features into account. In any case, the four main sunspot-pairs discussed above should make major contribution to energy estimates.

The various parameters, *e.g*., L_x, L_y, B_0, γ, u and v and the daily variation of magnetic energy, ΔM, are listed in Table 2 for the period April 5–11. We find that relative motions of sunspot-pairs Q–R (*i.e*., main trailer and the positive sunspot of the inverted bipole) and R–S (*i.e*., sunspots of the inverted bipole) resulted in negative energy build-up during almost entire period of April 5–11. This does not agree with Krall *et al*. (1982) who reported a build-up of magnetic energy by the motion of the intermediate bipole towards the leader. Interestingly, we note here that Machado *et al*. (1983) reported soft X-ray emission over this region during the initial phase of flares of April 5–8. We find here that the sunspots R–S moved to reduce the inverted nature of the intermediate bipole. Thus we suggest that the relative proper motion between this sunspot-pair led to relax the magnetic loop structure joining them from a state of

Table 1. List of important flares observed from USO.

Date 1980	H-alpha flare			Location	H-alpha area (10^{-6}solar disc)/Imp.	X-ray class
	start	max. phase	end			
April 6	0405	0423	0439	N10E17	385/1N	M5
April 7	0511	0518	0524	N10E04	80/−F	—
	0529	0544	0714	N10E03	720/2B	M8
April 8	0304	0310	0430	N11W12	580/2B	M4
April 9	0958	1003	1007	N16W23	40/−F	—
April 10	0833	0835	0851	N12W45	150/1N	—
	0914	0920	0953	N12W43	281/1B	M4
April 11	0412	0417	0440	N15W60	250/1N	—
April 12	0540E	0540	0550	N13W66	90/1N	—
	0634	0637	0640	N12W64	120/1B	—
April 13	0353	0408	0439	N12W79	140/1N	—
	0828	0840	0858	N13W80	63/1B	—

Table 2. The daily magnetic energy buildup due to sunspot proper motion.

1980 April	L_x 10^9 cm	L_y 10^9 cm	B_0 Gauss	γ Deg	u 10^4 cm/s	v 10^4 cm/s	$\Delta M \times 10^{32}$ erg per day
			1. Main leader (P)–trailer (Q) sunspot pair				
5/6	8.5	1.6	2300	23	2.74	−1.41	1.83
6/7	10.0	2.8	2100	0	0.77	−1.04	2.01
7/8	11.3	2.9	2200	71	2.14	0.91	3.95
8/9	12.6	3.3	2100	50	0.56	0.12	0.95
9/10	12.8	3.4	1900	52	0.00	0.13	−0.19
10/11	12.8	3.2	1800	30	0.13	−0.42	0.80
			2. Main leader (P)–S polarity intermediate bipolar spot (S)				
6/7	5.0	0.6	2100	5	−0.15	−1.41	0.13
7/8	5.05	1.5	2300	27	−0.05	−0.12	0.06
8/9	5.73	2.5	2000	5	0.92	0.10	−0.03
9/10	5.82	2.0	1800	39	0.06	−0.43	0.27
10/11	5.74	1.5	1600	46	−0.22	−0.61	0.09
			3. Main trailer (Q)–polarity intermediate bipolar spot (R)				
5/6	3.10	1.9	2300	41	2.26	1.88	0.07
6/7	4.31	3.4	2100	27	1.26	1.21	−1.18
7/8	5.47	3.6	2200	10	1.71	0.89	−0.77
8/9	6.47	3.8	2100	19	0.52	0.21	−0.09
9/10	6.85	4.0	1900	10	0.50	0.19	−0.29
10/11	7.18	3.8	1800	37	0.42	0.17	0.28
			4. N–S intermediate bipolar sunspots (R & S)				
6/7	1.89	0.6	2100	44	−1.08	0.54	−0.10
7/8	1.60	1.5	2300	36	0.50	0.14	0.09
8/9	1.51	2.4	2000	20	−0.86	0.16	−0.32
9/10	0.90	2.0	1800	12	0.16	0.83	−0.24
10/11	0.48	1.5	1600	26	−0.06	0.27	−0.28

higher magnetic energy toward the minimum energy state (or the potential field configuration). The consequent release of the excess energy perhaps resulted in the origin of the flares over the site of the intermediate bipole during this period, as observed by Machado *et al.* (1983). Further, we find that the net magnetic energy build-up of the order of 10^{32} erg day^{-1} needed to account for the observed flares was stored in the active region by the relative motion between the main sunspots P and Q. A comparatively smaller build-up of the order of 10^{31} erg day $^{-1}$ was contributed from the motion between sunspots P–S.

We estimate here that the energy release from the observed flares in H-alpha is around 2–5 × 10^{31} erg day $^{-1}$ (*cf.* Fig. 5) and a similar amount of energy is estimated to be released in the form of X-ray flare emission (Krall *et al.* 1982). From this, it appears that only a part of the estimated magnetic energy stored in the active region was released in the form of flares. However, it is not surprising as a hundred percent efficiency in the energy conversion process is not expected. Also one should note that the above estimates provide a rough upper limit. This is found sufficient to accommodate any additional dissipation of energy.

7. Some major H-alpha flares in NOAA 2372

As mentioned earlier, H-alpha plage associated with NOAA 2372 appeared on the NE-quadrant of the solar disc on April 4, to the west of an old active region—Hale No. 16752 (Fig. 1). However, the corresponding calcium plage was already evident on April 1 (Sol. Geophys. Data No. 429). The active region developed rapidly in sunspot area, magnetic field intensity and complexity and gave rise to a large number of flares. Some important flares of NOAA 2372 observed by USO, are listed in Table 1, and Fig. 2 shows locations of various flares with respect to the sunspots in the active region. The spatial and temporal development of some major H-alpha flares are shown in the sequences of H-alpha filtergrams in Fig. 7. In the following, we shall describe some of the morphological details of these events.

(1) *April 6/0405 flare*: A 2N flare occurred between the sunspots Q and R. H-alpha filtergram taken on April 5 showed distinct arcades joining the trailer, Q, and the

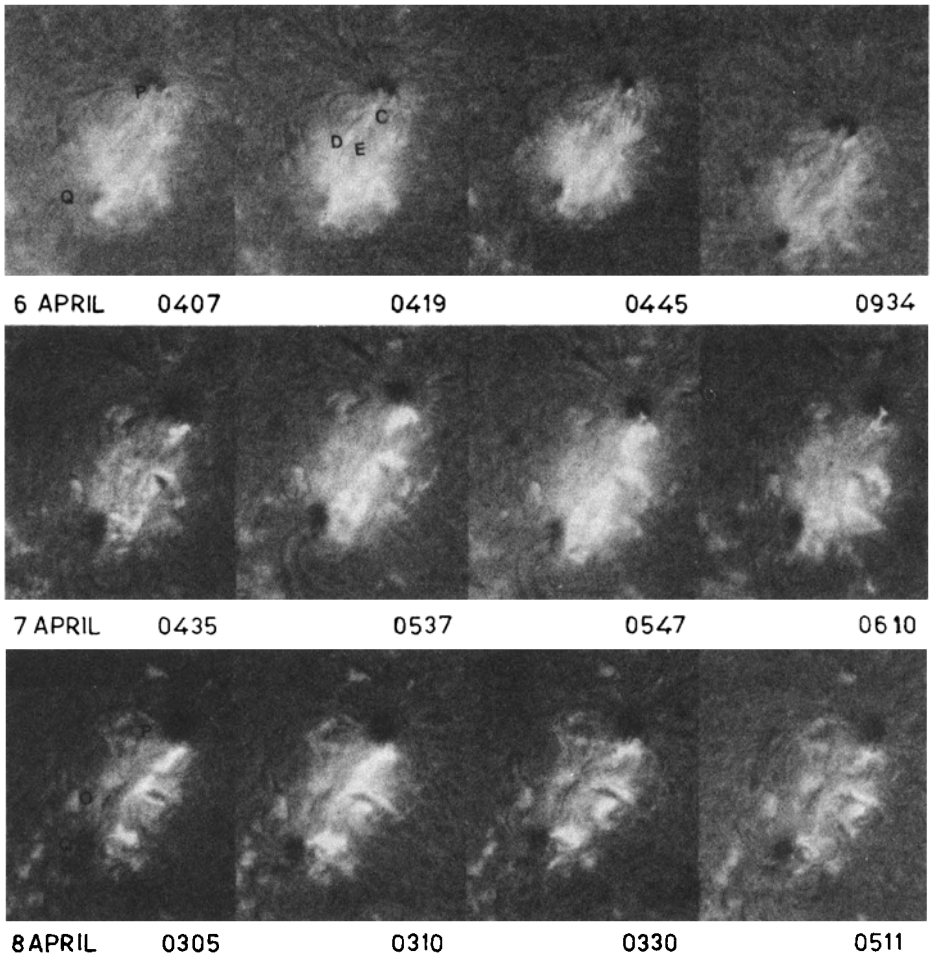

Figure 7. Sequences of H-alpha filtergrams, during April 6–12, displaying the temporal and spatial development of some important flares observed from USO.

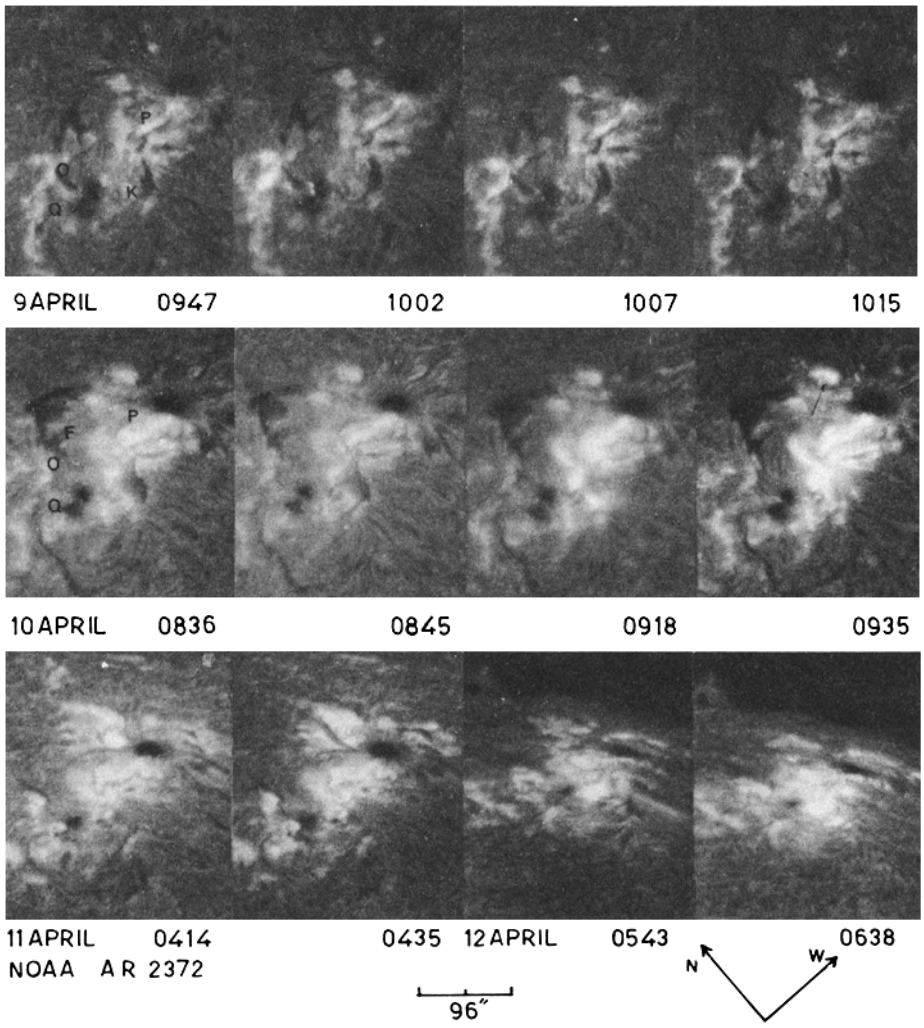

Figure 7. Continued.

intermediate bipolar region (Fig. 1). Active filament marked E disappeared and reappeared later as seen on the frames of 0445 UT and 0934 UT.

(2) *April 7/0511 & 0529 flares*: The two leading sunspot-umbrae comprising the leader P merged to form a single umbra. Two flares occurred in quick succession; the first being a 1f flare which ended at 0522 UT. Then a 2B flare ensued at 0524 UT at the same location reaching its maximum phase at 0547 UT. More flare-brightenings were repeatedly seen up to 0714 UT. Large flare-ribbons formed within the penumbrae of P and Q, as well as around the inverted bipole R–S. HXIS X-ray observations reported by Machado *et al*. (1983) showed two soft X-ray emission features over the inverted bipole around 0537 UT. They also reported a large feature in soft X-ray overlying the entire active region complex.

(3) *April 8/0304 flare*: Machado *et al*. (1983) reported initial soft X-ray brightening around 0302 UT which corresponds well with the observed H-alpha flare. A large soft

X-ray feature was again observed over the sunspots P–Q. Locations of H-alpha footpoints conform well with the magnetic configuration suggested by Machado *et al*. These footpoints may be interpreted as due to thick target bremsstrahlung by accelerated particles guided along the four magnetic loop structures joining the sunspot-pairs, P–S, S–R, R–Q, and P–Q. This flare was morphologically homologous to its predecessors on April 7. Also the flares extended across the entire length of the active region. During the period 0511–1100 UT, a number of minor flares were also observed. Dark filament-arcades joining the sunspots P–O and O–Q were seen in the region.

The MSFC magnetograms of April 5–7 show that magnetic field structures were highly sheared in the neighbourhood of the inverted bipole and also between this region and the trailer (Krall *et al*. 1982). This is also the period when the major sunspots showed large proper motions (Fig. 3). The sunspots P and Q moved towards west and east respectively increasing the separation between them. This implies a stretching of the magnetic field lines joining them. On the other hand, sunspots in the intermediate bipole moved to reduce its inverted nature. We note again that Machado *et al*. (1983) reported soft X-ray emission over this region in the initial phases of flares of April 5–8. Thus we infer that the relaxation of magnetic configuration joining sunspots R–S from a higher energy state to the lower may be the reason for flare-productivity during this period.

(4) *April 9/0958 flare*: This flare was altogether different in nature as compared to the flares of April 7–8 and belonged to a separate class of *umbral* flares, examples of which were reported earlier by Kubota *et al*. (1974), Tang (1978) and Vazquez & Harrera (1979). Tang (1978) suggested that such flares occur in p-spot of old regions with no or only fragmentary f-spots. However in this case the umbral brightenings appear in the well-developed f-spot, alongwith a simultaneous flare-ribbon near a dark arcade filament joining the f-spot with the region ‘O’. Energetically, this Sf flare was not significant and no corresponding X-ray emission was available.

(5) *April 10/0833 & 0914 flares*: The dark arcade filament F joining P – O condensed further, while the filament segment Q – O disappeared. Two large flares occurred in quick succession between the length of the active region. The flare-ribbons of 0833 UT formed near the leader P and the intermediate bipole only. A dark filament ‘K’ as seen on April 9/0947 frame, showed some activity during April 9–10 and erupted into a class 1B flare on April 10 (*cf*. 0836–0935 UT sequence in Fig. 7). The flare-ribbons in this instance formed around the detached penumbra near the main trailer Q (or f-spot), which contained an inverted polarity sunspot. An H-alpha flare marked on the 0918 UT frame was seen to the north of the leader, where the opposite polarity flux appeared to be emerging from the MSFC magnetogram.

(6) *April 11/0412 & 0635 flares*: Two main flares were observed at USO in the active region. However, their structures were quite different as compared with the earlier flares. The first flare, accompanied with a dark surge as seen on 0435 UT frame, seems to be related to the newly emerging negative polarity on the north side of the leader. The second flare occurred due to positive magnetic flux emergence on the north side of the trailer (*cf* Figs 2f and 6). Proper motions of the main sunspots had considerably decreased by this time. Thus it is suggested that most of the flares of this period occurred due to emergence of new magnetic flux in the active region.

(7) *April 12/0540 & 0634 flares*: These flares were located around the intermediate bipole (see Figs 2g and 7). From the SMM data, Sawyer (1982) reported observation of

a coronal mass ejection following a flare from the location of the emerging flux regions.

(8) *April 13/0353 & 0828 flares*: The first flare occurred between the leader and the intermediate bipole which had by this time nearly merged with the leader. A mass ejection accompanied the second flare as seen in Fig. 2h.

From the above discussion on the flares and their morphology, it is clear that most flares observed during April 9–13 differed in character as compared to those occurring in the initial phase of April 6–8. (No mention has been made about flares of April 5 as USO did not observe this region on that day.) We note that the flares of the initial phase were relatively more energetic. They stretched over the entire length of the active region with four major flare-ribbons occurring near the main sunspots and the intermediate bipole. Proper motions of major sunspots decreased by the end of this phase, however, and the magnetic flux and its gradient to the north of both the leader and the trailer spots increased (*cf*. Fig. 6). Around April 9 a prominent north-polarity sunspot was seen located at the SW-fringe of the penumbra of the trailer Q. On the next day, a part of the penumbra containing this inverted sunspot alongwith some south-polarity sunspots became detached from the main trailer. As inferred from Fig. 5a, the histogram showing the daily number of flares peaked on April 10. This is, perhaps, a reflection of the activity taking place in the region due to the variety of changes discussed above.

8. Conclusions

We have studied the development and the flare-activity of NOAA 2372 during its disc passage from April 4–13, 1980. On the basis of sunspot proper motion, H-alpha and X-ray flare emission data, and magnetograms, we have obtained the following results:

(1) Almost all major sunspots in the active region displayed large proper motions during April 5–8. The inverted bipole R–S embedded within the main sunspots P–Q implied a large magnetic shear around its location. Significantly, proper motions of the sunspots forming the inverted bipole tend to reduce the inverted nature of the bipole. On the other hand, the separation between main leader and trailer increased continuously from 6° to 10° within a week and considerably stretched the magnetic structure joining them. All the sunspots moved along both the heliographic axes.

(2) The relative motion between the sunspots of the inverted bipole R–S and that of the main trailer Q and north polarity sunspot R of the inverted bipole gave rise to a negative build-up of magnetic energy. This implies that excess energy stored in the inverted bipole reduced as the sunspots constituting the inverted bipole moved so as to reduce its inverted nature. This perhaps led to the origin of flares over this location as observed by Machado *et al*. (1983).

(3) Proper motions of main sunspots P and Q gave rise to a positive build-up of magnetic energy, *i.e*., increase in the stored energy of around 10^{32} erg day^{-1}. A smaller contribution came from the motion between P and S. The net daily magnetic energy build-up, estimated from the observed proper motions of all these sunspot pairs appears to be sufficient to account for the net energy release from the active region in the form of flares.

(4) Energetically and spatially extensive flares occurred during the initial phase, *i.e*., April 5–8, when proper motions of main sunspots were large.

(5) Proper motions of the main sunspots reduced considerably at the end of the initial phase of development of the active region. Subsequently, smaller flares occurred in the active region. It is suggested that these flares resulted due to newly emerging magnetic flux regions as well as the overall process of relaxation and simplification of the magnetic structure of the active region. Added to these, a prominent inverted polarity magnetic flux developed near the trailer Q, where some filament activation was also observed. In fact, daily occurrence of flares peaked around April 10, but as these flares were small, the net energy release was not as significant as during April 7.

In conclusion, it is suggested that sunspot proper motions led to large magnetic energy build-up in the active region NOAA 2372 during its initial development. The intermediate inverted bipole moved in a manner so as to reduce the magnetic shear in its immediate surroundings and perhaps triggered energetically extensive flares. On the other hand, when the sunspot motions reduced in the later phase of its development, fireworks of minor flares occurred as a combined result of new emerging flux and inverted polarities.

Acknowledgements

The authors wish to express their thanks to Drs K. R. Sivaraman, B. Kalman, and S. I. Gopasyuk for providing photoheliograms for this study. One of the authors (A.A.) would like to acknowledge many useful discussions with Drs J. Smith Jr., M. J. Hagyard, R. Moore, P. Venkatakrishnan during his stay at Marshall Space Flight Center, Huntsville, and with Sara F. Martin at Caltech, Pasadena.

References

Ambastha, A. 1987, USO Tech. Rep. No. TN-001-87.

Bray, R. J., Loughhead, R. E.1964, *Sunspots*, Dover Publications Inc., NewYork, p.230.

Cheng, C. -C., Bruner, E. C., Tandberg-Hanssen, E., Woodgate, B. E., Shine, R. A., Kenney, P. J., Henze, W., Poletto, G. 1982, *Astrophys. J*., **253,** 353.

Dezso, L., Csepura, G., Gerlei, O., Kovacs, A., Negi, I 1984, Preprint No. 2, Heliophys. Obs. Hungarian Acad. Sci., Debrechen.

Enger, I., Podsiadlo, R. T., Jensen, D. C., Ward, F. 1966, AFCRL-66-293, Air Force Surveys Geophys. No. 178.

Gesztelyi, L. 1984, Preprint No. 1, Heliophys, Obs., Hungarian Acad. Sci., Debrechen.

Harvey K. L., Recely, F.1984, *Solar Phys*., **91,** 127.

Howard, R., Gilman, P. A. 1984, *Kodaikanal Obs. Bull*., **4,** 1.

Kalman, B. 1984, Preprint No. 3, Heliophys. Obs., Hungarian Acad. Sci., Debrechen.

Krall, K. R., Smith J. B. Jr., Hagyard, M. J., West, E. A., Cummings, N. P. 1982, *Solar Phys*., **79,** 59.

Kubota, J., Tamenaga, T., Kawaguchi, I, Kitai, R. 1974, *Solar Phys*., **38,** 389.

Kunzel, H.1960, *Astr. Nach*., **285,** 271.

Machado, M. E., Somov, B. V., Rovira, M. G., De Jager, G 1983, *Solar Phys*., **85,** 157.

Obashev, S. O. 1968, *Solar Activity Articles* 3.

Rabin, D., Moore, R., Hagyard, M. J. 1984, *Astrophys. J*., **287,** 404.

Rust, D., 1972, *Solar Phys*., **25,** 141.

Sakurai, K. 1976, *Solar Phys*., **47,** 261.

Sawyer, C. 1982, *Adv. Space Res*., **2(11),** 265.

Solar and Geophys. Data (Pt. 1) 1980, Nos. 429 & 430.

Solnechnye Dannye No. 4 1980, Academia Nauk, USSR.
Tanaka, K., Nakagawa, Y. 1973, *Solar Phys*., **33,** 187.
Tang, F. 1978, *Solar Phys*., **60,** 119.
Tur, T. J., Priest, E. R. 1976, *Solar Phys*., **48,** 89.
Vazquez, M., Harrera, F. 1979, *Solar Phys*., **64,** 329.
Vorpahl, J. A. 1973, *Solar Phys*., **28,** 115.
Waldmeier, M. 1955, *Ergebnisse und Problem der Sonnenforschung*, 2 Edn., Leipzing Geest Portig.
Zirin, H. 1970, *Solar Phys*., **14,** 328.
Zirin, H. Lazareff, B. 1975, *Solar Phys*., **41,** 425.
Zirin, H. Tanaka, K. 1973, *Solar Phys*., **32,** 173.

J. Astrophys. Astr. (1988) **9,** 155–160

Search for 12.6 Millisecond Periodicity in TeV Gamma Rays from Cygnus X-3

P. N. Bhat, P. V. Ramana Murthy & P. R. Vishwanath
Tata Institute of Fundamental Research, Homi Bhabha Road, Colaba, Bombay 400005

Received 1987 September 29; revised 1988 May 30; accepted 1988 June 4

Abstract. Cygnus X-3, an X-ray binary with an orbital period 4.8 hr was seen to be emitting γ-rays with the same period at TeV energies by several groups. In addition the Durham group (Chadwick *et al*. 1985) published their observations on the existence of a pulsar in the Cyg X-3 system, emitting TeV γ-rays with a periodicity of approximately 12.6 ms. We observed this object during 1986 October–November and did not detect any pulsed emission of TeV γ-rays in the range of periods from 12.5850 to 12.5967 ms.

Key words: γ-ray astronomy—X-ray binaries—TeV γ-rays—Cygnus X-3

1. Introduction

The celestial object Cygnus X-3, an X-ray binary (Parsignault *et al*. 1972) with an orbital period $\simeq$ 4.8 hr, was observed to emit also in the infrared (Becklin *et al*. 1973), at TeV and PeV γ-ray energies (see for example, Weekes 1984) with the same periodicity as in the X-ray region. At energies of a few hundred MeV, the SAS-2 satellite group reported (Lamb *et al*. 1977) seeing the emission at the same periodicity while a later satellite experiment, COS-B, with a much larger data base did not find (Hermsen *et al*. 1987) any evidence. The observed luminosities of the object at TeV and PeV energies are 8×10^{35} and 6×10^{36} ergs^{-1} respectively (Weekes 1984), with the latter figure obtained by taking the effect of interstellar absorption (Gould 1983; Cawley & Weekes 1984) by the microwave background radiation into account. It was long suspected that one of the components of the binary system must be a pulsar which would accelerate charged particles that eventually produce TeV and PeV γ-rays at the observed luminosities. Searches (see for example, Damashek *et al*. 1978 and Stokes *et al*. 1985) in the radio wavelength region did not, however, detect any pulsar in the direction of Cyg X-3 in the period range $0.004 \leqslant P \leqslant 3.9$ s. While these negative results could be explained away in terms of the searches not being sensitive to objects having large dispersion measure and the flux values being lower than the detection threshold, the question of the existence of the pulsar persisted.

Chadwick *et al* (1985) operating an atmospheric Cerenkov telescope in Utah (USA) reported seeing pulsed emission of TeV γ-rays with a periodicity of 12.5908 ± 0.0003 ms. Since there was nothing known about the pulsar period prior to their analysis, Chadwick *et al.* had to carry out a parametric search for periodicity in the enormous range 10 ms to 50 s which necessarily involved a very large number of trial

periods. For the signal to stand out clearly over trivial chance occurrence probability in the vast number of trials, the signal had to be of sufficient strength and size. On 1983 September 12, the gross counting rate in their detector had gone up sufficiently higher than the average rate which allowed the authors to carry out their parametric search. The authors observed pulsations at the period of 12.5908 ms during two of the 8 observations made during 1983. In each instance, the pulsed emission was seen to occur over a time interval of 7 minutes at an orbital phase $\phi_{48\,h} = 0.625$. Indeed the pulsations were found to occur even over time intervals as short as 1 minute which allowed the authors to establish a correlation between signal strength and counting rate over independent 1 minute intervals. The combined probability that the result was due to chance fluctuations in the cosmic ray shower background (taking all degrees of freedom into account) was given as 3×10^{-7} by the authors. A subsequent search of the data taken earlier during 1982 by the same group also showed evidence (see Fig. 2 of Chadwick *et al*. 1985) for a 12.6 ms pulsar at $\phi_{48\,h} = 0.59$. At a recent workshop on very-high-energy γ-ray astronomy, the same Durham group (Chadwick *et al*. 1987) claimed seeing the pulsar on 1985 October 12 at a period of 12.5928 ms at an orbital phase of $\phi_{48\,h} = 0.55 \pm 0.10$ (Ramana Murthy 1987). Though the Mt Haleakala collaboration (Resvanis *et al*. 1987) presented at the workshop evidence confirming millisecond periodicity over time intervals of the order of 100 s at $\phi_{48\,h} = 0.74$, this report is not confirmed in later and fuller reanalyses described in their paper. In addition, the Mt Hopkins collaboration (Fegan *et al*. 1987) reported at the same meeting that the results of their period search failed to substantiate the result of Chadwick *et al*. (1985). In view of the obvious importance of the topic and the conflicting results, it appeared important to independently check if there is a pulsar in the Cyg X-3 system emitting TeV γ-rays with a 12.6 ms periodicity.

2. Observations and analysis

We observed Cyg X-3 recently at TeV energies using the atmospheric Čerenkov technique at Pachmarhi (longitude: 78°.26 E, latitude: 22°.28N and altitude 1075 m above sea level), India. Details of the technique and apparatus are already published (Ramana Murthy 1980; Vishwanath 1982). We used 3° diameter masks in front of the photomultipliers at the focal plane of the reflectors. Cyg X-3 was tracked for 1 to 2 hours during 7 different runs taken in as many nights during the period 1986 October 27–November 3, for a total of approximately 10 hours. The 4.8 hr phase during our observations was in the range 0.3 to 0.7, with the phase region $0.45 < \phi_{48\,h} < 0.7$ accounting for 60 per cent of the observation. This range in $\phi_{48\,h}$ matches well with the full range of values reported in the past detections as mentioned in the Introduction. The time of occurrence of each event, derived from an accurate ($\pm$ 30 μs with respect to UTC) clock was recorded to an accuracy of $\pm$ 0.05 ms. The observed event times were converted to those at the solar system barycentre.

From the publication of Chadwick *et al*. (1985), the pulsations seem to occur over time spans of as short as 1 minute. We therefore divided all our data into segments of 1 minute duration and performed Rayleigh test (Mardia 1972; Protheroe 1985) on each data segment. We tried 40 periods in the range $12.585 \leqslant P \leqslant 12.5967$ ms with an incremental step of $\Delta P = 3 \times 10^{-7}$ s. Admittedly such a fine step leads to an over-

sampling by a factor of 9. However, such an oversampling does not mask the signal at all, but lets one detect the growth and decay of the signal with the test period. This search range in period encompasses all the published or reported periods so far. We assumed $\dot{P} = 0$. This assumption is well justified in view of the data set in each trial being limited to 1 minute duration; only P in excess of 5×10^{-9} (or 0.15 s yr^{-1}) would have changed the period by more than the step size used in the search, during one minute.

Assuming an arbitrary epoch t_0, the phase of an event occurring at time t is calculated as

$$\phi = \phi_0 + \frac{t - t_0}{P_j}. \tag{1}$$

We make $\phi_0 = 0$, as this does not affect the result. We then compute for each minute and each assumed period P_j the Rayleigh power, Q, as given by

$$Q = \frac{1}{N}\left[\left\{\sum_{i=1}^{N} \cos(2\pi\phi_i)\right\}^2 + \left\{\sum_{i=1}^{N} \sin(2\pi\phi_i)\right\}^2\right]. \tag{2}$$

Here N is total number of events in a given minute.

We have also computed for each minute and for each period (in the same range as used in the Rayleigh test) the traditional phasograms by the epoch-folding method.

Our estimated detection threshold for γ-ray showers is 1.4 TeV. We note that, once the approximate value of the period is known, there is no longer any need to insist on a significant increase in the gross event rate unlike in the situation faced by Chadwick *et al.* (1985) in their discovery paper when nothing was known about the period. In our analysis, we test the possibility that the period can be anywhere in the range 12.585–12.597 ms and may not lie exactly on the straight line in Fig. 7 of Chadwick *et al.* (1987). Likewise, though Chadwick *et al.* (1985) observed the light curve to be broad, we have analysed our data for this possibility (Rayleigh test method) as well as for a possible narrower light curve (epoch folding method). In effect, we did not restrict ourselves to the procedure followed by Chadwick *et al.* (1985) in their discovery paper.

3. Results

At the outset, we want to state that, since our exposure is confined to the 4.8 hr phase region $0.30 \leqslant P \leqslant 0.70$ (and that too unevenly in this range), we will not be able to say anything about the 4.8 hr periodic emission of TeV γ-rays by Cyg X-3. Nor can we say anything about the unpulsed emission of TeV γ-rays as we did not make any drift scans of this region and cosmic-ray induced showers dominate the observed events. We therefore confine our attention to the 12.6 ms periodic emission.

The differential distribution of the Rayleigh power, Q, as computed by us on the basis of our data is shown in Fig. 1. It consists of 23120 entries which is a product of the number of periods (= 40) searched and the number of minutes (= 578) of observation. The quantity $2Q$ for a purely randomly occurring sequence of events with no periodic signal present (null hypothesis) is expected (Protheroe 1985) to be distributed as χ^2 for

2 degrees of freedom, *i.e.*,

$$F(Q)\,dQ = M\,e^{-Q}\,dQ, \tag{3}$$

where M is the total number of entries (23120) and Q is already defined by the Equation (2). The expectation for the null hypothesis is shown by the straight line in Fig. 1. There is a very good agreement between the computed Rayleigh power distribution and the one expected on the basis of null hypothesis.

Leahy, Eisner & Weisskopf (1983) have pointed out that the epoch-folding method of analysis, *i.e.*, constructing a phase histogram on the basis of event times *modulo* the period of pulsations is more sensitive than the Rayleigh test if the pulsar light curve were to consist of a narrow pulse. To investigate this possibility, we subjected our data to the epoch-folding analysis by doing a periodicity scan in the range $12.585 \leqslant P \leqslant 12.5967$ ms incrementing the period by $\Delta P = 3\times10^{-7}$ s. These search parameters a re identical to those used in the Rayleigh test. While calculating the phase of any event, we assumed the same arbitrary epoch $t_0 = .48600.0$ s UTC on 1986 October 27 (see Equation 1) for the entire data and made $P = 0$. Phasograms with 20 phase bins for each minute's data (total: 578 minutes) for 40 periods were computed and whenever any phasogram showed 4σ or greater excess or deficiency in any of its bins in comparison with the average, the full phasogram, the period and the time were printed out.

The calculations showed a total of 81 cases of phasograms (out of 23120) where a bin showed an excess of $> 4\sigma$ over the average while the expectation on purely random poisson fluctuations basis is 84 cases (=prob. ($>4\sigma$) × no. of minutes × no. of trial

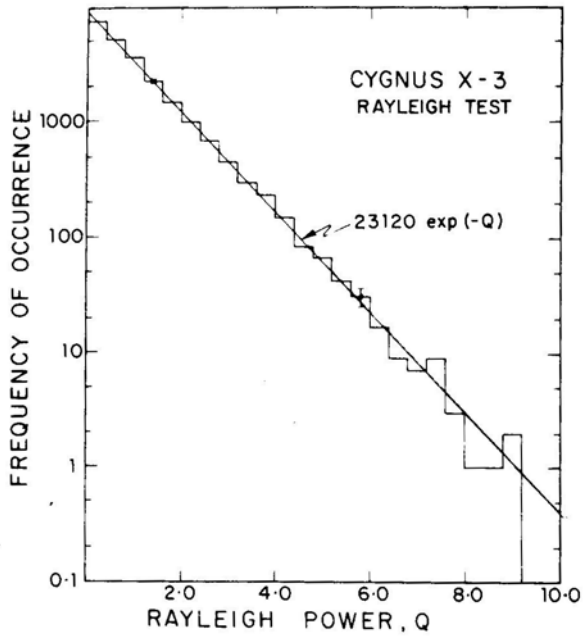

Figure 1. Rayleigh power distribution resulting from search for a periodicity in the range $12.585 \leqslant P \leqslant 12.5967$ ms (40 periods) for 578 minutes' data is shown in the histogram. The straight line is the expectation for the same distribution for null (no signal) hypothesis.

periods × no. of bins). We also note that the excesses are distributed all over the period range that was tried rather than being confined to one particular period as one would expect for a genuine periodicity.

4. Conclusions

We observed Cyg X-3 for approximately 10 hours during the time 1986 October 27–November 3 to see if the object emits TeV γ-rays in a pulsed mode with a periodicity of 12.6 ms. We found no evidence for such an emission either by the Rayleigh test (case of broad light curve) or by the epoch-folding method (case of light curve with a narrow emission peak). The 95 per cent confidence level upper limits obtained by these two methods are 2.4×10^{-9} and 5.8×10^{-10} cm^{-2} s^{-1} respectively for pulsed ($12.585 \leqslant P \leqslant 12.5967$ ms) emission of γ-rays over time intervals of the order of 1 minute by Cyg X-3. Expressed as a fraction of cosmic ray shower rate (with a 3° diameter viewing aperture), showers due to pulsed γ-rays were less than 12 per cent in any minute during the entire observation.

Our conclusion that there was no pulsed emission during the period 1986 October 27–November 3 does not necessarily conflict with the claim of Chadwick *et al*. (1985) on two counts: (i) the epoch of our observation is different from theirs, and (ii) the duty cycle for 12.6 ms pulsed emission seems to be quite low, *e.g*., the object pulsed only for 7 minutes during 6 hours of observation by Chadwick *et al*. (1985) and it is just possible that the object failed to pulse during our observations. It appears, therefore, important to continue observations on this object to confirm independently the 12.6 ms pulsed emission in TeV γ-rays first claimed by the Durham group (Chadwick *et al*. 1985).

Acknowledgements

We are indebted to Hon. Shri Motilal Vora, the then Chief Minister, Madhya Pradesh for making two buildings and a site available to us for our observations; to Prof. B. V. Sreekantan, the then Director of our institute, for his help in acquiring the site; and to Prof. T. S. Murthy and Messrs N. R. Krishnan, Vinay Shankar and Samar Singh for their help in our obtaining facilities at Pachmarhi. We thank Mr A. R. Apte for setting up the array and for help with observations, and Messrs G. P. Sathyanarayana, S. N. Kanal, A. I. D'Souza for help with observations, and Mr. A. V. John and Mrs. C. V. Raisinghani for help with data reduction.

References

Becklin, E. E., Neugebauer, G., Hawkins, F. J., Mason, K. O., Sanford, P. W., Matthews, K., Wynn-Williams, C. G. 1973, *Nature*, **245,** 302.

Cawley, M. F., Weekes, T. C.1984, *Astr. Astrophys*., **133,** 80.

Chadwick, P. M., Dipper, N. A., Dowthwaite, J. C., Gibson, A. I., Harrison, A. B., Kirkman, I. W., Lotts, A. P., Macrae, J. H., McComb, T. J. L., Orford, K. J., Turver, K. E., Walmsley, M. 1985, *Nature*, **318,** 642.

Chadwick, P. M., Dipper, N. A., Dowthwaite, J. C., McComb, T. J. L., Orford, K. J., Turver, K. E. 1987, *Very High Energy Gamma Ray Astronomy*, Ed. K. E. Turver, D. Reidel, Dordrecht, p.115.

Damashek, M. *et al*. 1978, *Astrophys. J. Lett*., **225,** L31.

Fegan, D. J., Cawley, M. F., Gibbs, K., Gorham, P. W., Lamb, R. C , Porter, N. A., Reynolds, P. T., Stenger, V. J., Weekes, T. C. 1987, *Very High Energy Gamma Ray Astronomy*, Ed. K. E. Turver, D. Reidel, Dordrecht, p. 111.

Gould, R. J. 1983, *Astrophys. J*., **271,** L23.

Hermsen, W. *et al*. 1987, *Astr*. *Astrophys*., **175,** 141.

Lamb, R. C., Fichtel, C. E., Hartmar, R. C., Kniffen, D. A., Thompson, D. J. 1977, *Astrophys. J. Lett*., **212,** L63.

Leahy, D. A., Elsner, R. F., Weisskopf, M. C. 1983, *Astrophys. J*., **272,** 256.

Mardia, K. V. 1972, *Statistics of Directional Data*, Academic press, New York.

Parsignault, D. R., Gursky, H., Kellog, E. M., Matilsky, T., Murray, S., Schreier, E., Tannenbaum, H., Giacconi, R., Brinkman, A. C. 1972, *Nature Phys. Sci*., **239,** 123.

Protheroe, R. J. 1985, *Proc. Workshop on Techniques in Ultra High Energy Gamma Ray Astronomy*, p. 91.

Ramana Murthy, P. V. 1980, *Non-solar Gamma Rays* (COSPAR) Eds. R. Cowsik & R. D. Wills, Pergamon press, New York, p. 71.

Ramana Murthy, P. V. 1987, *Very High Energy Gamma Ray Astronomy*, Ed. K. E. Turver, D. Reidel, Dordrecht, p. 39.

Resvanis, L. R. 1987, *Very High Energy Gamma Ray Astronomy*, Ed. K. E. Turver, D. Reidel, Dordrecht, p. 105.

Stokes, G. H., Taylor, J. H, Weisberg, J. M, Dewey, R. J. 1985, *Nature*, **317,** 787.

Vishwanath, P. R. 1982, *Proc. International Workshop on very high energy gamma ray astronomy*, Eds. P. V. Ramana Murthy & T. C. Weekes, p. 21.

Weekes, T. C. 1984, *Preprint*, no. 2312.

J. Astrophys. Astr. (1988) **9,** 161–172

Study of the Wolf-Rayet Members of the Cluster NGC 6231

B. S. Shylaja *Indian Institute of Astrophysics, Bangalore 560034*

Received 1987 November 17; revised 1988 June 3; accepted 1988 June 21

Abstract. Two Wolf-Rayet members of the cluster NGC 6231 are studied spectrophotometrically. HD 151932, a suspected variable, shows variations in the emission line flux as well as continuum magnitude measurements. An attempt is made to understand this variation as due to the asymmetric atmospheric structure. The other, HD 152270, a (WC7 + O) binary, shows variation of emission line flux for C III and C IV lines only. This variation is studied as a possible phenomenon of atmospheric eclipses.

Key words: stars, emission-line—stars, Wolf-Rayet—open clusters, NGC 6231.

1. Introduction

The open cluster NGC 6231 is considered to belong to the Sco OB1 Association. Many detailed investigations like the determination of the H-R diagram, the distance modulus and the reddening have been carried out extensively (Struve 1944; Schild, Hiltner & Sanduleak 1969, 1971; Graham 1965; Crawford *et al*. 1971; Garrison & Schild 1979; Lundstrom & Stenholm 1980). There are two Wolf-Rayet (WR) stars in this cluster: HD 152270 (WC 7 + O) which is in the central region of the cluster, and HD 151932 (WN 7), which is situated 22 arcmin west of the centre. The membership of these two to the cluster has been discussed in detail (Seggewiss 1974 a, b; Seggewiss & Moffat 1979; Lundstrom & Stenholm 1980).

HD 152270 (MR 65, WR 79) is one of the six binaries with a WC component (Moffat *et al*. 1986) and was established as a spectroscopic binary with O-type companion by Struve (1944). Radial velocity curves were studied by Seggewiss (1974b), who improved the period to 8.893 days. Proper motion measures (Braes 1967) and radial velocity (RV) measures of the interstellar lines (Seggewiss 1974b) have confirmed the membership to the cluster. Line profiles have the absorptions due to the companion, as well as the violet-shifted absorptions moving with the WC component (Seggewiss 1974b). The profile of the C III line at λ 5696 has been particularly studied in great detail (Schumann & Seggewiss 1975; Schmidt & Seggewiss 1976; Neutsch, Schmidt & Seggewiss 1981; Neutsch & Seggewiss 1985), and a cone model explanation has been offered for the double-peaked profile. Polarimetric observations (Luna 1982) have been used for deriving the angle of inclination of the orbit to be 35° ± 8°. Recent observations by St Louis *et al*. (1987) have improved this value to 45° ±5°.

HD 151932 (MR 64, WR 78) was classified as WN 7A by Hiltner & Schild (1966) because of the narrow emission lines, Its membership in the cluster itself has been debated about not only because of its location 22 arcmin west of the centre, but also

because of the large reddening it displays. Based on the interstellar line velocities and interstellar diffuse-band equivalent widths, Seggewiss & Moffat (1979) have included it in the cluster. Recent photometric investigations of the cluster (Heske & Wendker 1985) puts it as a post-main-sequence member.

Schild, Hiltner & Sanduleak (1969) studied the radial velocity measures of Struve (1944) and suspected that there is an unseen companion with an orbital period of about 3.3 d. Bappu (1973) attributed the excess reddening to a late-type companion. Seggewiss (1974a) studied the RV curves and found that the 3.3 d periodicity was spurious because even the interstellar lines showed the same period. Hill, Kilkenny & Van Breda (1974) also did not find any orbital motion. A further detailed investigation by Seggewiss & Moffat (1979) showed that the excess reddening can be explained by normal interstellar reddening and an unseen companion need not be invoked. Recently the variability of the Si IV line also has been reported (Vreux *et al*. 1987).

These two objects are important for the following reasons:

1. Although HD 152270 is not an eclipsing binary, based on the previous studies of CQ Cep and HD 50896 (Shylaja 1986a, b) we may expect to see atmospheric eclipses, which by virtue of the relatively low angle of inclination, may be partial.

2. In the case of HD 151932 any similar effect of flux variation may throw some light on the possibility of a companion.

2. Observations

Spectrophotometric observations were carried out at the Cassegrain focus of the 102 cm reflector at the Vainu Bappu Observatory with the automated spectrum scanner (Bappu 1977). The wavelength range was 4000–6000Å in the first order (later this was extended to 8500 Å for measuring the continuum distribution only). The Standards from the list of Hayes (1970), Breger (1976) and Kuan & Kuhi (1976) were used for estimating the instrumental corrections. Sample scans are shown in Fig. 1.

The monochromatic magnitudes at 5560 Å (mainly continuum) derived from the energy distributions are tabulated in Table 1.

3. Results

3.1 *HD 152270*

The phases have been calculated from an initial epoch of JD 2441796.233 and a period of 8.8908 d, following St Louis *et al*. (1987). Although the photometric results at 5560 Å show a small dip near phase 0.1 (Fig. 2) there is too much scatter to be attributed to an eclipse effect.

Spectrophotometric results were used to derive the line flux of the broad features like (C III/C IV + He II) near λ4650, C IV λ5470, (C IV λ5808 +He I λ5876) and also C III/C IV λ5696; all these measurements are listed in Table 2 and indicated in Fig. 2.

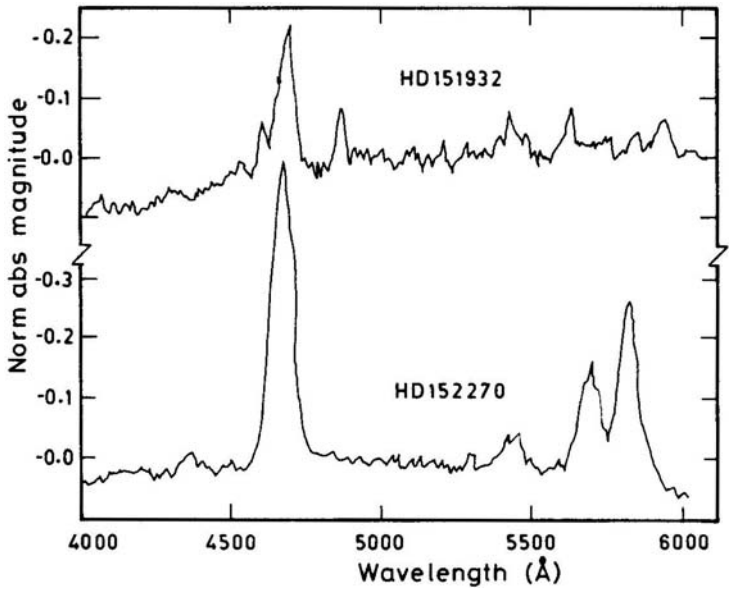

Figure 1. Sample scans of HD 152270 and HD 151932 uncorrected for reddening. The ordinate is magnitude normalized at 5000 Å.

3.2 *HD 151932*

The photometric data of HD 151932 were searched for any possible periodicities by the method of least squares (Raveendran, Mohin & Mekkadan 1982) between 1 and 10d. This showed that there is an indication of a period of about 6 d, but the amplitude of variation is very small, 0.05 mag (Fig. 3). However, such a period determination is not completely free of alias effects and further continuous monitoring only can establish this. The light curve of Seggewiss & Moffat (1979) also shows similar scatter. The scanner observations were used for estimating the flux values of N IV λ4058, N V λ4603, C IV λ5808, He II λ4860, 5410, 4686, He I λ5876 and the blend of λ4540.The line of N III could not be resolved to measure the flux accurately. All the measured fluxes are listed in Table 3 and variations may be seen in Fig. 4.

3.3 *Interstellar Reddening*

For a study of the colour excesses of the various members of the cluster, previous investigators have pointed out that the interstellar reddening across the face of the cluster is not very smooth and therefore a single value of $E(B-V)$ is not applicable for all the members of the cluster (Schild, Neugebauer & Westphal 1971; Garrison & Schild 1979). This aspect is made clear in Fig. 5 which shows the observed (normalized at 5000 Å) energy distributions of a few cluster members. Therefore, it was necessary to derive the colour excesses separately for the two WR stars (Shylaja & Bappu 1983).

The excess red light, which was attributed to a possible late-type companion by Bappu (1973) was explained as a consequence of interstellar reddening (Seggewiss &

Table 1. Monochromatic magnitudes of HD 151932 and HD 152270, at $\lambda 5560$.

JD 2440000+	Magnitudes HD 151932	Phase	Magnitudes HD 152270	Phase	JD 2440000+	Magnitudes HD 151932	Phase	Magnitudes HD 152270	Phase
4711.331	0.731	0.481	—	—	4740.317	0.710	0.317	—	—
4711.396	0.739	0.492	—	—	4740.300	—	—	0.819	0.136
4711.475	0.718	0.505	—	—	4740.330	—	—	0.823	0.140
4711.383	—	—	0.815	0.884	4740.356	—	—	0.814	0.143
4711.454	—	—	0.820	0.892	5065.426	—	—	0.831	0.705
4711.480	—	—	0.829	0.895	5065.436	0.714	0.499	—	—
4712.325	0.714	0.647	—	—	5068.443	0.702	0.000	—	—
4712.349	0.727	0.651	—	—	5068.454	0.711	0.002	—	—
4712.475	0.722	0.672	—	—	5068.466	0.705	0.004	—	—
4712.350	—	—	0.822	0.993	5068.434	—	—	0.826	0.044
4712.425	—	—	0.829	0.001	5068.461	—	—	0.815	0.047
4712.461	—	—	0.826	0.005	5068.476	—	—	0.822	0.048
4713.335	0.708	0.815	—	—	5069.446	—	—	0.821	0.157
4713.366	0.717	0.821	—	—	5069.466	—	—	0.819	0.160
4713.373	—	—	0.827	0.108	5069.450	0.719	0.168	—	—
4713.443	—	—	0.816	0.116	5069.475	0.708	0.172	—	—
4739.386	0.705	0.157	—	—	5070.426	—	—	0.824	0.268
4739.446	0.716	0.167	—	—	5070.450	—	—	0.817	0.270
4739.459	0.725	0.169	—	—	5070.474	—	—	0.822	0.273
4739.393	—	—	0.822	0.034	5070.434	0.735	0.332	—	—
4739.419	—	—	0.815	0.037	5070.456	0.729	0.336	—	—
4739.468	—	—	0.812	0.043	5070.478	0.732	0.339	—	—
4740.308	0.718	0.310	—	—	5071.348	0.724	0.484	—	—
4740.313	0.728	0.313	—	—	5071.359	—	—	0.821	0.373

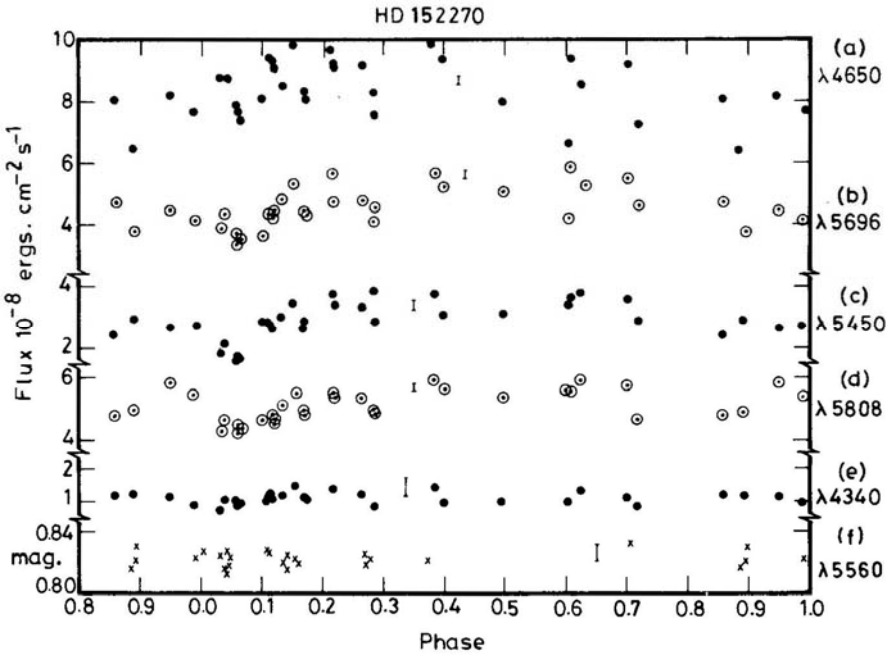

Figure 2. Flux variations of HD 152270: (a) λλ4650 + 4686, (b) λ5696, (c) λλ5410+ 5470, (d) λ5808, (e) λ4340, and (f) λ5560 magnitude.

Moffat 1979). In Fig. 5 it may be noticed that HD 151932 and HD 152003, which are located 20 arcmin away from the nucleus of the cluster, have similar energy distributions and somewhat different from the other members of the cluster. Therefore, it may be inferred that there is some source of excess reddening in this region. The recent photometric investigation by Heske & Wendker (1984, 1985) also shows that the reddening is not uniform in this region.

3.4 *The Possibility of a Companion to HD 151932*

The evolutionary calculations of de Loore (1980) for the WR phase in a binary show that a late-type companion is not possible. Therefore, in the light of the explanation of anomalous reddening near HD 151932, the possibility of another type of companion may be sought.

The detailed spectroscopic investigation by Seggewiss (1974a) has clearly shown that there is no apparent RV variation. Based on the 6d period derived from the photometry, an attempt was made to fold the absorption line RV measures of Seggewiss & Moffat (1979), which did not yield any meaningful RV curve for any line. The other emission lines show smooth RV variation and therefore it is unlikely that any compact companion, if present, can be detected by such velocity curves.

The existence of a compact companion would imply a very high mass ratio of $q = m_{WR}/m_c > 10$, assuming the WN 7 to be $\sim 2\ M_\odot$ and the compact star to be about $2\ M_\odot$. However, in the case of CQ Cep, another binary with WN 7, the mass derived

Table 2. Flux ($\times 10^{-11}$ erg cm^{-2} s^{-1}) of emission lines of HD 152270.

JD 240000+	Phase	Blend λ4340	C IV λ5808	Blend λ5450	Blend λ4650	C III λ5696
4663.468	0.495	93.0	530.0	305.0	795.0	506.0
4664.442	0.604	95.0	558.0	330.0	655.0	418.0
4665.458	0.718	82.0	460.0	286.0	722.0	457.0
4684.467	0.857	119.0	475.0	238.0	797.0	465.0
4711.429	0.889	106.0	492.0	285.0	642.0	371.0
4712.332	0.991	89.0	544.0	272.0	758.0	408.0
4713.336	0.104	97.0	461.0	280.0	801.0	362.0
4714.344	0.217	135.0	550.0	372.0	983.0	565.0
4739.397	0.035	65.0	422.0	182.0	835.0	382.0
4740.281	0.134	115.0	506.0	297.0	852.0	483.0
4780.208	0.625	130.0	590.0	375.0	849.0	520.0
5065.392	0.701	110.0	570.0	352.0	907.0	545.0
5068.421	0.042	98.0	462.0	210.0	875.0	430.0
5069.417	0.154	146.0	545.0	342.0	982.0	535.0
5070.399	0.265	115.0	536.0	315.0	915.0	470.0
5071.478	0.386	140.0	587.0	368.0	995.0	561.0
5405.461	0.951	109.0	585.0	262.0	815.0	440.0
5406.441	0.061	95.0	412.0	150.0	785.0	370.0
5406.462	0.064	78.0	445.0	168.0	760.0	335.0
5406.476	0.065	84.0	430.0	155.0	735.0	348.0
5407.427	0.172	110.0	490.0	255.0	830.0	435.0
5407.437	0.173	96.0	465.0	283.0	797.0	407.0
5408.429	0.285	76.0	487.0	382.0	753.0	396.0
5408.440	0.286	82.0	481.0	285.0	827.0	456.0
5409.448	0.399	88.0	562.0	300.0	930.0	516.0
5451.369	0.114	110.0	490.0	275.0	938.0	430.0
5451.404	0.118	102.0	475.0	262.0	900.0	415.0
5451.415	0.120	113.0	453.0	248.0	927.0	442.0
5452.325	0.222	120.0	530.0	335.0	910.0	470.0
5811.393	0.608	107.0	558.0	361.0	927.0	590.0

for the WN 7 component is about 35 $M_{\odot}$ (Stickland *et al*. 1984; Leung, Moffat & Seggewiss, 1983). Therefore, the mass ratio·in this case with a compact companion can be higher than 10. To estimate the approximate amplitude of the RV curve, we may assume q = 10 and period 6d. Then the amplitudes will be less than 30 km s^{-1}. Such small amplitudes have not been detected even with high-dispersion spectra. The polarization data does not show significant periodicity (Drissen *et al*. 1987). The polarization vector is fairly aligned with that of other stars in the area indicating that a large fraction of the polarization is interstellar.

The presence of a compact companion represents the second WR phase in the evolution of a massive binary, which in other cases, like HD 50896, has many other characteristics like the associated nebulosity. HD 151932 being a member of the relatively young cluster does not fit into this scheme.

4. Line-emitting regions in HD 151932

The violet-shifted absorptions clearly indicate an expanding envelope, following the excitation potential versus velocity relation like other systems (Seggewiss, 1974a).

Therefore, it is implied that higher excitation lines like He II, N V, N IV and C IV originate closer to the photosphere. The variations shown by the observed flux may be interpreted with this criterion. The He I lines, which are formed in the outermost regions of the atmosphere show large scatter of flux (Figs 3 and 4). Their RV curves also show a large scatter (Seggewiss 1974a) compared to other lines. Such RV variations were attributed to fluctuations in the particle density by Seggewiss & Moffat (1979). They have shown that small changes in particle density (the source for this is

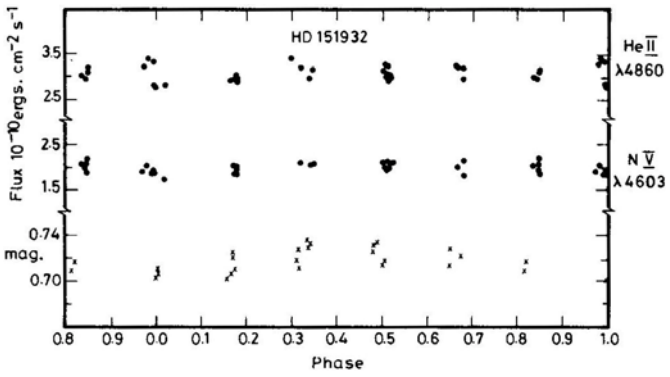

Figure 3. The photometric variations of HD 151932 at λ5560 folded over a period of 6 days, taking JD 24445068.443 as epoch. The flux variations also are included for some lines.

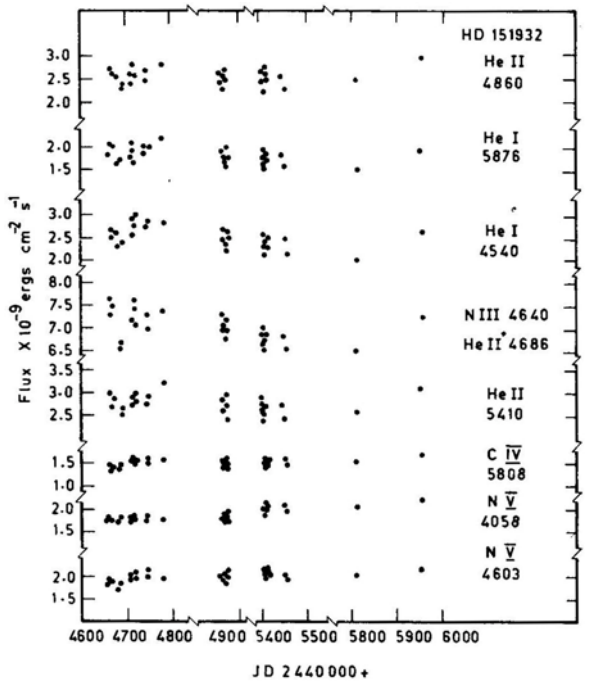

Figure 4. The variation of emission flux of HD 151932. The lines and the wavelengths of emission are indicated.

Table 3. Flux of emission lines of HD 151932.

JD 2440000+	N V λ4603	N IV λ4058	C IV λ5808	He II λ4860	He II λ5411	He II λ4686	Blend λ4540	He I λ5876
4663.430	190.0	182.0	146.0	324.0	298.0	724.0	249.0	174.0
4663.461	198.0	177.0	143.0	308.0	279.0	717.0	236.0	163.0
4664.435	182.0	174.0	135.0	318.0	272.0	769.0	268.0	212.0
4665.451	186.0	178.0	141.0	307.0	284.0	748.0	258.0	203.0
4684.467	172.0	174.0	135.0	281.0	241.0	641.0	222.0	151.0
4685.403	183.0	182.0	152.0	294.0	263.0	669.0	241.0	172.0
4685.428	180.0	177.0	143.0	286.0	256.0	658.0	236.0	164.0
4711.406	205.0	181.0	156.0	327.0	268.0	707.0	249.0	170.0
4711.436	209.0	170.0	168.0	306.0	274.0	725.0	268.0	186.0
4712.441	212.0	185.0	155.0	291.0	289.0	758.0	292.0	192.0
4713.424	196.0	174.0	141.0	308.0	275.0	741.0	297.0	214.0
4714.333	192.0	176.0	146.0	332.0	296.0	707.0	276.0	168.0
4739.383	202.0	172.0	154.0	294.0	271.0	695.0	213.0	206.0
4740.277	211.0	184.0	16[illegible]	319.0	289.0	727.0	285.0	177.0
4780.200	191.0	178.0	164.0	325.0	327.0	746.0	291.0	211.0
4780.236	206.0	162.0	147.0	341.0	311.0	728.0	276.0	237.0
5065.370	208.0	196.0	147.0	311.0	289.0	684.0	241.0	176.0
5066.353	197.0	181.0	159.0	319.0	265.0	709.0	268.0	192.0
5068.353	184.0	174.0	138.0	276.0	247.0	651.0	218.0	159.0
5069.416	194.0	170.0	149.0	309.0	275.0	674.0	231.0	172.0
5070.380	207.0	176.0	138.0	294.0	299.0	695.0	242.0	199.0
5071.454	191.0	184.0	145.0	299.0	286.0	676.0	259.0	175.0
5405.428	190.0	176.0	140.0	291.0	296.0	681.0	257.0	176.0
5406.431	207.0	199.0	154.0	315.0	280.0	694.0	232.0	195.0
5407.411	195.0	186.0	147.0	274.0	265.0	658.0	241.0	162.0
5407.419	211.0	212.0	144.0	299.0	257.0	645.0	211.0	149.0
5408.419	200.0	207.0	155.0	326.0	249.0	676.0	250.0	168.0
5409.456	217.0	195.0	149.0	311.0	274.0	668.0	227.0	184.0
5451.360	203.0	207.0	155.0	302.0	276.0	675.0	245.0	177.0
5452.317	187.0	192.0	141.0	277.0	245.0	646.0	212.0	151.0
5811.434	201.0	203.0	152.0	295.0	260.0	641.0	198.0	142.0
5964.125	212.0	215.0	163.0	342.0	311.0	717.0	257.0	185.0

not known) can lead to large changes of ion density in the outermost regions where the He I lines are formed. Any atmospheric eclipse effect is not evident on the emission lines (Fig. 3).

The observed photometric variations of period ~ 6d, which reflect the asymmetry in the envelope, also can be explained by the variable density hypothesis. Further, the intrinsic variations of WRs are not uncommon, which, in the present study, might have produced the observed apparent periodic variation. Only continuous photometry with simultaneous spectroscopic measurements can establish this aspect.

5. Possible atmospheric eclipses in HD 152270

This is one of the 6 stars with WC component, and has an established period of about 8.89d. Seggewiss (1974b) obtained the RV curves with high resolution and noticed the central absorption of the λ5696 line of C III. The absorption lines of the companion

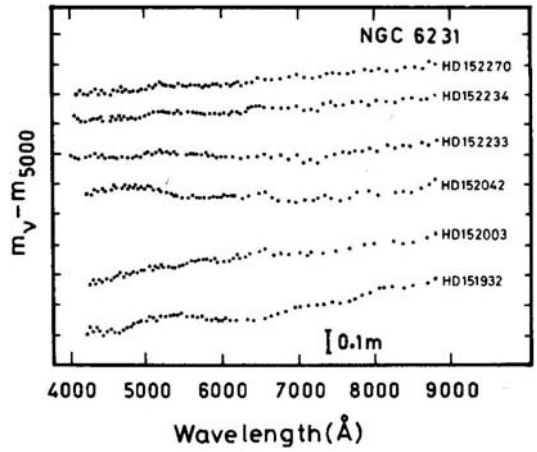

Figure 5. Observed energy distributions of some members of the cluster NGC 6231, normalized at 5000 Å.

also were easily detectable because of the phase difference of 0.5 relative to the emission lines at $\lambda\lambda$5696, 5808 and 5471. Therefore it was possible to improve the period to 8.893 d. The velocities and the amplitudes of the RV curves show different values corresponding to different emission lines. Based on the RV curve of the unblended line of C IV λ5471, which shows the systemic velocity, Seggewiss (1975b) obtained the masses of the components.

The violet-displaced absorptions have also been studied by Seggewiss (1974b); they all follow the behaviour of the emission lines. Higher excitation lines like C IV have smaller velocities compared to He I lines. However, the relation of the EP versus velocity is not as strong as in the case of WN systems. Further, the RV amplitudes of He I λ5876 and C III λ4650 are nearly same, implying that they both have similar motion in at least some binary systems.

The origin of gas streams in this star has also been discussed in detail (Seggewiss 1974b). Further detailed investigations by Schmidt & Seggewiss (1976) have clearly shown the effect of central absorption with phase. This was attributed to a 'hole' near the Lagrangian point by Neutsch & Seggewiss (1977) and Neutsch *et al*. (1985).

The polarization studies by St Louis *et al*. (1987) have improved the period to 8.8908 ± 0.0005 days and the angle of inclination to 44°.8 ±5°. Consequently the masses of the components are M(WR) = 5 ± 2$M_\odot$ and M(O) = 14 ± 5$M_\odot$. The flux measures in Fig. 3 show a dip at phase 0.1 for some lines. The zero phase corresponds to the WC in front and the angle of inclination is 45°. Therefore, one may assume that at phase 0.1 part of the line-emitting region is covered only for some lines. Then this would represent the case of an atmospheric eclipse, since at the corresponding phase there is no change in the continuum (Fig. 2).

Since it is known that the O-type companion can contribute to some line profiles (as central absorption) an effect of this may be seen on the measured total flux as well. It is a difficult task to determine this contribution because the He II and He I lines appear as blends. The brightest line λ4686 has been studied at high dispersion (Seggewiss 1974b) and no central absorption could be detected. It is also possible that this line is formed

in an extended region and therefore has a peculiar behaviour as in case of WN binaries (Shylaja 1987). In other cases, because of the line blends it is not possible to isolate the He II or He I lines. Therefore it may be assumed that such central absorptions do not contribute significantly to the total flux.

Following the type of stratification with ionization potential, we may expect to see deeper eclipses for higher excitation lines like C IV and He II compared to C III or He I. This is partly true in Fig. 2—C IV λ5808 has larger depth, which is similar to that of λ5450 (blend of He II and C IV) and λ4650 (C III/C IV and He II). The blend at λ4340 has smaller dip since the possible contributors are He II & He I. This stratification can be ascertained by individually resolving the various contributors of the blends and studying their flux variation.

5.1 *Line-Emitting Regions in HD 152270*

The masses derived by St Louis *et al.* (1987) as $14M_{\odot}$ for the O star and 5 $M_{\odot}$ for the WC star, may be used for estimating the distance of L_1, the inner Lagrangian point, following the tables of Plavec & Kratochvil (1964). For a separation of about 14 $R_{\odot}$, this will be about 9 $R_{\odot}$ from the centre of mass. Since the angle of inclination is about 45°, and since the observed eclipse is very broad, quantitative derivations are not possible. The Roche surface calculations probably may not be valid for these stars with strong winds. The eclipse effects on C IV lines imply that they are formed closer to the photosphere than the He I lines. Since the line profiles do not reflect the asymmetry directly as seen in V 444 Cyg (Ganesh, Bappu & Natarajan 1967) and θ Mus (Moffat & Seggewiss, 1977), the extension of the He II and C IV line-emitting material may be taken as the inner Roche surface itself.

From the interferometric measurements of the (WC8 + O9 I) binary γ^2 Vel (P = 78 d), Brown *et al*. (1970) found that the extension of the C III line-emitting region is five times larger than the continuum-emitting region. However, the dimensions derived by them cannot be used directly here because of the difference in the WC subgroup.

The large velocities associated with the violet absorptions of emission lines indicate that the winds in the envelopes are strong enough to complicate the structure of He I lines, which are probably formed in the outermost parts of the envelope. Very-high-dispersion spectra only can reveal this aspect, since it is known that, even in a well separated binary like γ^2 Vel the line profiles are affected by the presence of the companion (Ganesh 1966).

6. Conclusions

This spectrophotometric study of the two Wolf-Rayet members of NGC 6231 shows that the reddening is not smooth across the face of the cluster. This leads to an observable excess reddening for HD 151932. There is a variation of total flux from the emission lines which could be a consequence of variable particle density or an unseen companion. Considering that there is a variation in the continuum the latter possibility cannot be completely eliminated, because a compact companion may show barely observable RV variations less than 25 km s^{-1}. Further, the total flux of

emission lines do not show atmospheric eclipse effect. However, other characterstic features of WR + compact systems are yet to be established, which necessitates a rethinking concerning the membership to the cluster.

In the case of the established binary HD 152270, the total flux variation shows possible atmospheric eclipses of some higher excitation lines like C IV. Although C III λ5696 shows a variable line profile, the measured total flux shows atmospheric effects clearly.

Thus this study shows that the measurement of the variation of flux in binaries can be used as an effective tool to understand the atmospheric structure of binaries.

Acknowledgements

The author wishes to thank Prof. J. C. Bhattacharyya for continued encouragement, Prof. N. K. Rao for a critical reading of the manuscript and Prof. Seggewiss for very helpful discussions. Thanks are also due to Prof. A. F. J. Moffat and other referees for helpful suggestions.

References

Bappu, M. K. V. 1973, in *IAU Symp*. 49: *Wolf-Rayet Stars and High Temperature Stars*, Eds M. K. V. Bappu & J. Sahade, p. 59.
Bappu, M. K. V. 1977, *Kodaikanal Obs*. *Bull*, *Ser*. *A*, **2,** 64
Braes, L. L. E. 1967, *Bull*. *astr*. *Inst*. *Neth*. *Suppl.*, **2,** 21.
Breger, M. 1976, *Astrophys*. *J. Suppl*., **32,** 1.
Brown, R. H., Davis, J., Herbison-Evans, D., Allen, L. R. 1970, *Mon. Not. R. astr. Soc*., **148,** 103.
Crawford, D. L., Barnes, J. V., Hill G, Perry, C. L. 1971, *Astr. J*., **76,** 1948.
Drissen, L., St. Louis, N., Moffat, A. F. J., Bastien, P. 1987, *Astrophys. J*., **322,** 888.
Ganesh K. S. 1966, *Ph.D. Thesis*, Karnataka Univ.
Ganesh, K. S., Bappu, M. K. V., Natarajan, V. 1967, *Kodaikanal Obs*. *Bull Ser*. *A*., No. 184.
Garrison, R. F., Schild R. E. 1979, *Astr. J*., **84,** 1020.
Graham, J. A. 1965, *Observatory*, **85,** 196
Hayes, D. S. 1970, *Astrophys. J*., **159,** 165.
Heske, A., Wendker, H. J. 1984, *Astr. Astrophys. Suppl.*, **57,** 205.
Heske, A., Wendker, H. J. 1985, *Astr*. *Astrophys*., **151,** 309.
Hill, P. W., Kilkenny, D., Van Breda, I. G. 1974, *Mon. Not. R. astr. Soc*., **168,** 451.
Hiltner, W. 1944, *Astrophys. J*., **104,** 396
Hiltner, W., Schild, R. E. 1966, *Astrophys. J*., **143,** 770.
Kuan, P., Kuhi, L. V. 1976, *Publ. astr. Soc. Pacific*, **88,** 128.
Leung, K. C., Moffat, A. F. J., Seggewiss, W. 1983 *Astrophys. J*., **265,** 961.
Lundstrom, I., Stenholm, B. 1980, *Rep. Lund Observatory*, No. 16.
Moffat, A. F. J., Seggewiss, W. 1977, *Astr. Astrophys*., **54,** 607.
Moffat, A. F. J. Vogt, N., Paquin, G., Lamontagne, R., Barrera L. H. 1986, *Astr. J*., **91,** 1386.
Neutsch, W., Schmidt, H., Seggewiss, W. 1981, *Acta Astr*., **31,** 197.
Neutsch, W., Schmidt, H. 1985, *Astrophys. Sp. Sci*., **109,** 249.
Plavec, M., Kratochvil, P. 1964 *Bull. astr. inst. Csl*., **15,** 165.
Raveendran, A. V., Mohin, S., Mekkadan, M. V. 1982, *Mon. Not. R. astr. Soc*., **199,** 707.
Schild, R. E., Hiltner, W. A., Sanduleuk, N. 1969, *Astrophys. J*., **156,** 609.
Schild, R. E., Neugebauer, G., Westphal, J. A. 1971, *Astr. J*., **76,** 237.
Schmidt, H., Seggewiss, W. 1976, in *Multiple Periodic Variables Stars*, Ed. W. S. Fitch, Akademia Kiado, Budapest, p. 311.

Schuerman, D. W. 1972, *Astrophys. Sp. Sci*., **19,** 351.
Schumann, J. D., Seggewiss, W. 1975, in I*AU Symp.67*: *Variable Stars and Stellar Evolution*, Eds V. E. Sherwood & L. Plaut, D. Reidel, Dordrecht, p. 299.
Seggewiss, W. 1974a, *Publ. astr. Soc. Pacific*, **86,** 670.
Seggewiss, W. 1974b, *Astr. Astrophys*., **31,** 211.
Seggewiss, W., Moffat A. F. J. 1979, *Astr. Astrophys*., **72,** 332.
Shylaja B. S. 1986, *J. Astrophys. Astr*., **7,** 171.
Shylaja B. S. 1986b, *J. Astrophys. Astr*., **7,** 305.
Shylaja, B. S., 1987, *J. Astrophys. Astr*., **8,** 183.
Shylaja B. S., Bappu M. K. V., 1983, *Kodaikanal Obs. Bull*., **3,** 72.
Stickland, D. J. Bromage, G. E., Budding, E., Burton, W. M., Howrath, I. D., Jameson, R., Sherrington, M. R., Willis, A. J. 1984, *Astr. Astrophys*., **134,** 45.
St Louis, N., Drissen, L., Moffat, A. F. J., Bastien, P., Tapia S. 1987, *Astrophys. J*., **322,** 870.
Struve, O. 1944, *Astrophys. J*., **100,** 189.
Vanbeveren, D. 1977, *Astr. Astrophys*., **54,** 877
Vreux, J. M., Magain, P., Manfroid, J., Scuflaire, R. 1987, *Astr. Astrophys*., **180,** LI7.

J. Astrophys. Astr. (1988) **9,** 173–183

α^2 CVn: A comparison between Spot and Oblate Spheroid Models

Praveen Nagar & K. D. Abhyankar *Department of Astronomy, Osmania University, Hyderabad 500007*

Received 1988 February 2; revised 1988 May 27; accepted 1988 June 24

Abstract. A comparison is made between a hot-spot model and a recently proposed oblate spheroid model (Böhm-Vitense & Van Dyk 1987) to explain the spectroscopic and photometric variations of α^2 CVn. It is found that the spot model gives a better fit to the spectroscopic and photometric variations. The spot model requires five high temperature circular patches over the surface of the star. The positions of these patches agree well with those derived spectroscopically by Pyper (1969).

Key words: stars—Ap stars—spot modelling

1. Introduction

Among all the Ap stars, α^2 CVn is the brightest (m_v = 2.9) and one of the most observed peculiar stars. Its photometric variability was first reported by Guthnick & Prager (1914). α^2 CVn also shows a variable spectrum and a variable magnetic field. An extensive study of this star was carried out by Pyper (1969). Pyper found the equivalent width of rare-earth lines varying with a period of 5.5 days. Its light variations and its magnetic field followed the same period. Using a slight variation of the Deutch (1958) model, Pyper identified four patches of iron-peak elements along the magnetic equator and one patch of rare earth elements near the negative magnetic pole. The spectral variations of α^2 CVn and other Ap stars can easily be explained by Pyper's model. Various other models have been proposed, *e.g.*, the method suggested by Falk & Wehlau (1974) makes use of line profiles for harmonic analysis instead of equivalent widths as was done by Pyper. Another method was developed by Khokhlova (1975) and Khokhlova & Rjabchikova (1975). In this method the line profiles are computed by putting spots of various elements over the surface of the star. This method has been extensively used by Khokhlova and her collaborators. More recently Vogt & Penrod (1983) have developed a technique called 'doppler imaging' on similar lines and used it successfully to map the surfaces of late-type spotted stars. Vogt, Penrod & Hatzes (1986) have improved the technique by incorporating the maximum entropy method for the construction of surface images of stars. They have applied this method to Ap stars as well (Hatzes, Penrod & Vogt 1986). All these methods of mapping the stellar surfaces using spectral line profiles have clearly indicated the presence of spots on these stars.

In order to describe the photometric variations in α^2 CVn and other Ap stars, Trasco (1972) developed a model that required high temperature magnetic regions.

Trasco suggested that at least three hot spots are required to produce the observed light variations of α^2 CVn.

Recently Böhm-Vitense & Van Dyk (1987) have come out with a new model for explaining the light curves of α^2 CVn. The model suggested by them is essentially an oblique rotator but the star is an oblate spheroid with the magnetic axis being the axis of symmetry. One might call it an oblique oblate rotator. They also assume a variable surface temperature. In this model the temperature at the magnetic poles is 1000 K less than that at the magnetic equator. As the star rotates, the combined effect of the variable surface temperature and the variable projected area of the star causes the observed light variation.

We describe below the spot models we have used for α^2 CVn to explain the spectroscopic and the photometric observations of Pyper (1969) and Molnar (1973). We make a comparison between the results obtained by our models and those obtained by Pyper. We further show that the results obtained by our spot models are in better agreement with the observations than the results obtained by the oblate spheroid model of Böhm-Vitense & Van Dyk (1987).

2. The spot model for spectroscopic variations

Pyper (1969) identified a concentration of iron-peak elements in four regions along the magnetic equator of the star. She called them group 2A, 2B, 2C, and 2D, respectively. She found rare earths to be concentrated near the negative magnetic pole; she called this group 1. Longitudes and latitudes of these groups, as determined by Pyper, are listed in Table 1, where group 1 is designated as 2E. Pyper did not specify sizes of these regions. But we can consider the size of the innermost contour of the constant equivalent width curve (Figs 12 and 13 in Pyper 1969) as the approximate size of each group. We have listed these sizes as well in Table 1. Using the spot parameters listed in Table 1, we tried to model the equivalent width variations observed by Pyper. This required computation of line profiles and measurement of their equivalent widths at all the observed phases. We divide the star into several thousand small areas—specifically, 20520 area elements. This is done by dividing the projected stellar disc into 57 annuli and 360 sectors of 1 degree. We use 57 intensity profiles in all from the centre to the limb of the star. The line profile from each area is Doppler shifted according to the line-of-sight velocity of that area element. Summation of all such profiles then provides the flux profile and its area provides the equivalent width. This is done at each observed phase. This scheme of division of stellar disc into area elements is the same as described by Gray (1982).

Table 1. Spot parameters obtained by Pyper (1969).

	Spot 2A	Spot 2B	Spot 2C	Spot 2D	Spot 2E
Longitude	300	210	155	50	0
Latitude	10	−20	−25	20	−40
Radius*	20	22	15	15	25

Longitude, latitude, and radius are in degrees.
* see explanation in text.

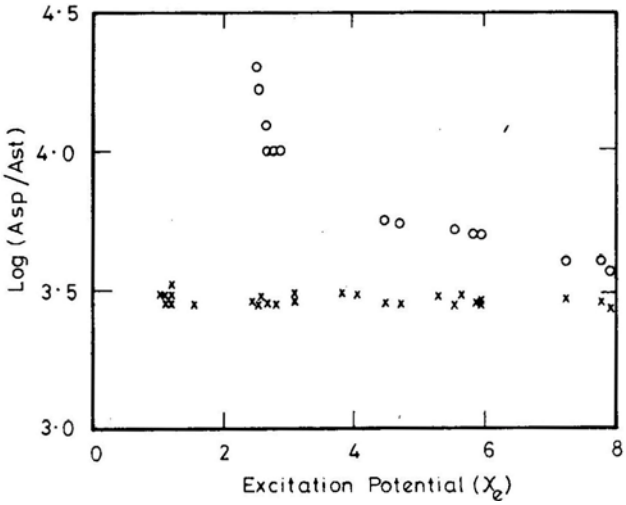

Figure 1. The spot-to-star abundance ratio is plotted against the excitation potential. The open circles refer to the case where spotted and unspotted regions are taken to be at the same temperature. The crosses are for the case where spot temperature is higher by 1000 K than the unspotted region.

In our first attempt, we used different elemental abundances for the spotted and unspotted regions, but no temperature difference between the two. This, however, did not provide us a satisfactory fit to the observations initially. But after a few trials with different abundances in spots, we arrived at a reasonably good match between the modelled equivalent width variations and the observed ones. But, here we encountered another problem. When we plotted the spot-to-star abundance ratio against the excitation potentials (χ_e) for various lines, we found that this ratio varied with χ_e. This is shown in Fig. 1 by open circles. We soon realized that our assumption of same temperature for the spotted and the unspotted regions was the cause of such behaviour of spot-to-star abundance ratio. The inverse correlation between abundance and excitation potential indicates that the higher levels have to be more populated, which means that the spots should have a higher temperature. A large abundance of elements in the spots will also increase the opacity and therefore the temperature in the spots should increase due to the backwarming. Both these reasonings made us to raise the spot temperature. After a few trials we settled for a spot temperature 1000 K higher than that of the unspotted region which was taken to be 12000 K. Once again the spot-to-star ratio was plotted against the excitation potential and was found to be reasonably constant for all the χ_e values. This is shown in Fig. 1 by crosses.

The equivalent width changes as the projected area of the spots changes due to rotation of the star. A value of $V \sin i = 23.0$ km s^{-1} was used in this model. We carried out these computations for all the lines that Pyper used in measuring the equivalent widths. Finally a mean curve was obtained for all the lines and normalized with respect to the maximum equivalent width computed. In Fig. 2 we have superimposed our model calculations on the observations of Pyper. We see that the spot model provides a good agreement with the observations. For group 2C our fit was not good at all, presumably because, according to Pyper (1969), at these phases her equivalent width

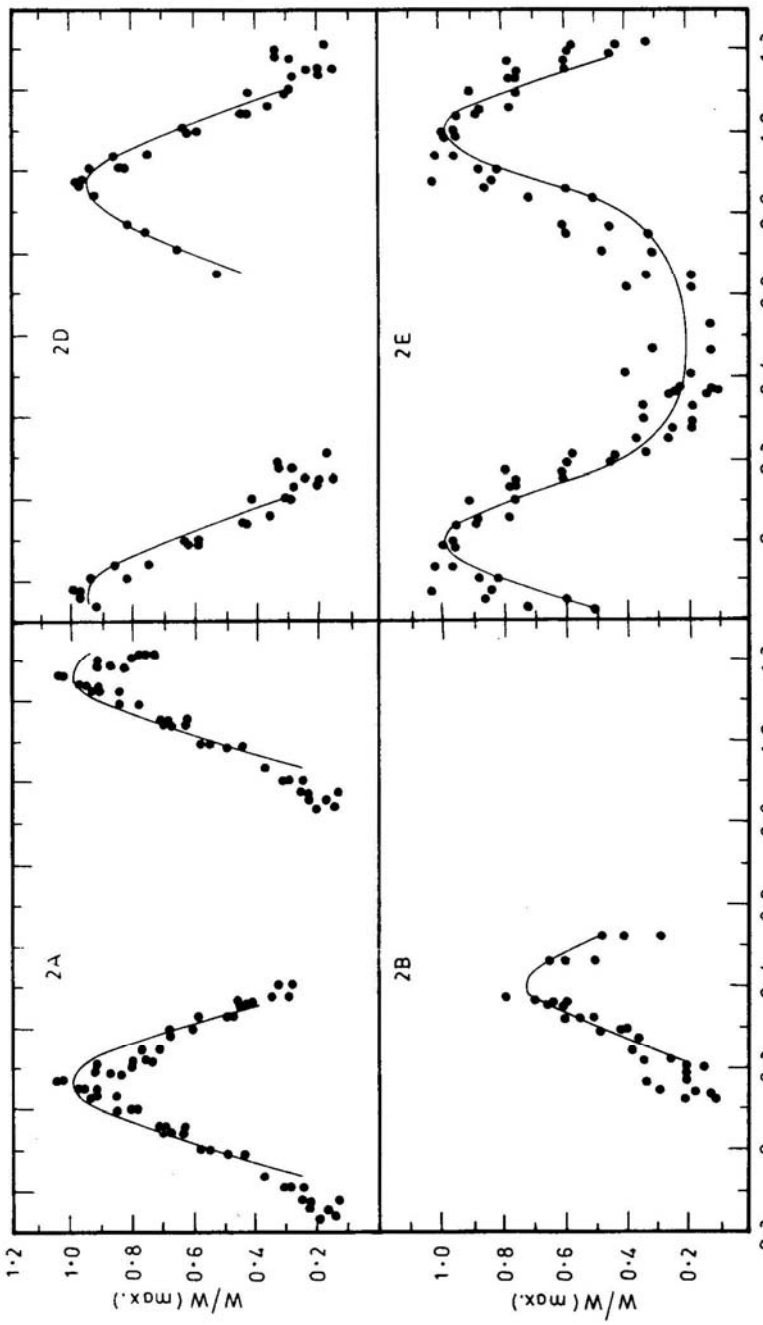

Figure 2. The top and bottom panels show the equivalent width variations observed by Pyper (1969). The solid line is the fit we obtained with our spot model.

measurements were of low accuracy. For this reason we have excluded the fit for group 2C from this figure.

In this model we consistently found a spot-to-star abundance ratio of 3×10^3 for iron peak elements (Fe, Ti, Cr) and 2×10^3 for rare earths (Eu, Gd). This means that if the unspotted region has a normal solar abundance then the spots will have a three orders of magnitude more of these elements. Such an abundance seems to be very high. Cohen (1970), by her LTE analysis of abundance determination, showed that the iron-peak elements are about two orders of magnitude more abundant in α^2 CVn. Her abundance determinations, however, refer to whole of the stellar surface, whereas our values are a ratio of abundances between the spot and the photosphere. A large spot-to-star abundance ratio, however, is not very uncommon. For HD 140160, a Sr-Ap star, an overabundance of Sr upto 10^3 was found in three spots by Khokhlova & Rjabchikova (1975). Like Cohen (1970) and Khokhlova & Rjabchikova (1975) our line profile calculations are also based on LTE approximation without taking into account the effect of magnetic field. Since atomic parameters, *e.g.*, *gf* values, for many lines are not known accurately, we take $gf = 1$ for all the lines while computing l_v. Thus, in that case

$$gfA_{\text{spot}}/gfA_{\text{star}} = A_{\text{spot}}/A_{\text{star}}.$$

Further we assume the microturbulence value of 2 km s^{-1} in spotted as well as in unspotted regions. We use Kurucz (1979) LTE model atmospheres for both the spotted and unspotted line computations. Because of these assumptions and approximations, we consider our derived values of spot-to-star abundance ratios as order of magnitude estimates only. For more accurate abundances a detailed abundance analysis, which takes into account the non-LTE effects and the effect of the presence of magnetic field, is called for. The assumptions made in our model were necessary to hold down the considerable computer time this model requires. We also notice that, even after all these approximations, a spot model can reliably reproduce the equivalent width variations observed in α^2CVn.

3. The spot model for photometric variations

The basic model is the same as that suggested by Budding (1977) and later by Poe & Eaton (1985) for late-type stars. We have made a small change in it to include a flux blocking parameter which is used in far ultraviolet region where the flux is known to be much more depressed in α^2 CVn than in a normal star of the same temperature. We have already seen in Section 2 that the spots are at higher temperature than the surrounding photosphere and have high concentration of iron-peak elements and rare earths. Therefore, we can assume that the far-ultraviolet flux-blocking takes place only in the spotted regions. Here spots are considered to be circular in shape and the star is a sphere of unit radius. The change in the light level due to the presence of the spot is given by

$$\Delta L = [\, F\,(T_{\text{star}}) - (1 - \beta)\, F\,(T_{\text{spot}})]\, \sigma_{\text{c}},$$

where $F\,(T_{\text{spot}})$ and $F\,(T_{\text{star}})$ are fluxes from the spot and surrounding photosphere at the temperatures T_{spot} and T_{star}, respectively, β is the flux-blocking parameter, and σ_{c} is

the limb-darkening-weighted projected area of the spot. It is given by

$$\sigma_c = 3/(3-u)\ \{(1-u)\,\sigma_0^0 + u\sigma_1^0\ \},$$

where u is the limb-darkening coefficient. The expressions for computing σ_0^0 and σ_1^0 are given by Budding (1977). Therefore, at a phase θ, the light from the star, normalized to unit value, becomes

$$L(\theta) = 1 - [F(T_{star}) - (1-\beta)\,F\,(T_{spot})]\,\sigma_c$$

or

$$L(\theta) = 1 - [1 - (1-\beta)\,F_{ratio}]\,\sigma_c,$$

where F_{ratio} is the spot-to-star flux ratio, $L(\theta)$ is then converted into magnitude as

$$m(\theta) = -2.5 \log L + M_{ref},$$

where M_{ref} is the reference magnitude normally chosen to be at the star's brightest phase. We have further converted these magnitudes as

$$\Delta m\ (\theta) = m\ (\theta) - m(0),$$

where $m(0)$ is the magnitude at 0 phase. This enables us to compare our results with those obtained by Böhm-Vitense & Van Dyk (1987). The limb-darkening coefficients for λ2462, λ2985, λ3317 and for U, B and V bandpasses are taken from Al-Naimy (1977) and are considered to be the same for the spots and the surrounding region. For λ1332, λ1420, and λ1554 the limb darkening coefficients are not available, therefore for these wavelengths we use $u = 1$.

4. Computation of light curves

The above model was used for generating the theoretical far-ultraviolet and *UBV* light curves. These computed light curves are then compared with the observed ones given by Molnar (1973) and Pyper (1969). We fixed the temperature of the unspotted region at 12000 K, which is the same as the one used by Böhm-Vitense & Van Dyk for the equatorial region in their model. The inclination of star's rotation axis to the line of sight is taken to be 50 degrees. We computed several light curves for each bandpass using three, four, and five spots. In every case light curves with five spots provided minimum ($O - C$)'s. Later we fixed the number of spots as five. Longitudes and latitudes of spots were determined by trial and error. Some adjustments in area and temperature of spots had to be made, as these two quantities are strongly coupled. We adjusted the spot areas such that either the temperature or the spot-to-star flux ratio was the same at least in two bandpasses. In Fig. 3a we show our computed far-ultraviolet light curves superimposed on Molnar's observations. In Fig. 3b we show the computed light curves of Böhm-Vitense & Van Dyk (1987) that they obtained by oblate spheroid model. The oblate spheroid model light curves were read off from the best fit obtained by Böhm-Vitense & Van Dyk (Fig. 8 in their paper). The far ultraviolet observations of α^2 CVn by Molnar (1973) and later by Leckrone & Snijder (1979) show large flux deficiency in this region of the spectrum. Molnar (1973) attributes this large flux deficiency to the strong line blanketing by the rare earths. For below λ1600 Å he suggests a second source of flux blocking which is a combination of continuous opacities and line blanketing from the iron-peak and rare-earth elements.

If these elements are concentrated in the spots, then the far-ultraviolet opacity will be larger for the spotted regions than for the unspotted ones. This implies that we will 'see' only top low-flux layers of spots, and deeper high-flux layers in the spot-free areas. This is where we have to make use of the flux-blocking parameter β in our model. For λ1332, λ1420, and λ1554 we use $\beta = 0.7$, for λ2462 and λ2985 the value of β is 0.5 and 0.15, respectively. For λ3317 and longward, *i.e.*, in *U*, *B*, and *V* bandpasses β is set equal to zero. These values roughly correspond to the fractional difference between Klinglesmith's (1971) hydrogen-blanketed model energy distribution and the observed energy distribution of α^2 CVn as shown in the Fig. 5 of Molnar (1973). In Table 2 we have listed the spot longitudes, latitudes and radii obtained in far-ultraviolet wavelength region. There was hardly any (or very little) change in the values of these quantities with wavelength.

On the longer-wavelength side the *U* and *B* spot temperatures (blackbody) agree well within 300 K. We get consistently a higher temperature for spots 1, 4 and 5 in the *V* bandpass. This could perhaps be due to our looking deeper in atmosphere in *V* band. One should notice that the variation in the *V* observations is almost twice as much as in *U* and *B*. In order to model this large *V* amplitude we were forced to use a higher spot-to-star flux ratio (thereby a higher spot temperature in *V* band compared to *U* and *B*). Another alternative could have been to reduce the star temperature or change

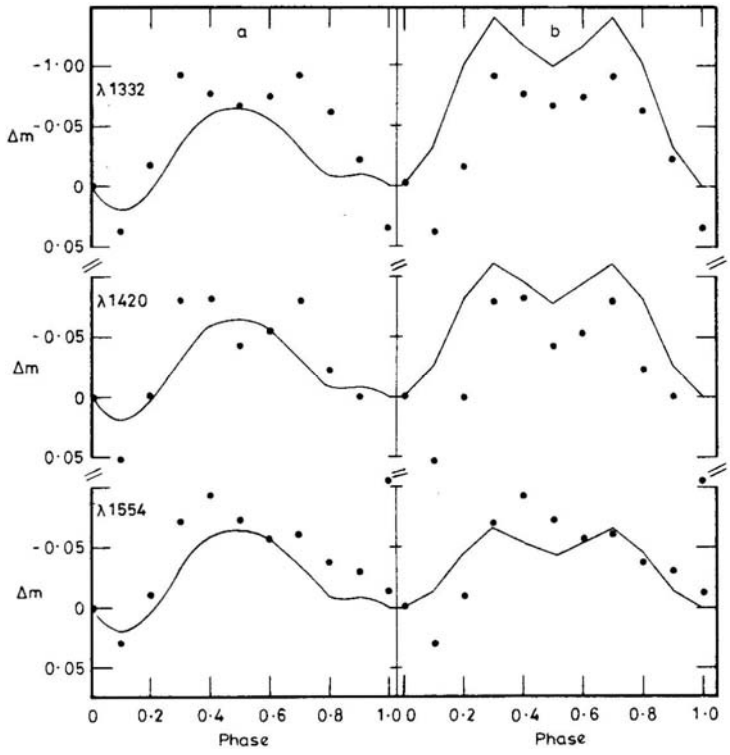

Figure 3. The calculated far-ultraviolet light curves (solid line) are superimposed on Molnar's (1973) observations (points): (a) our spot model; (b) oblate spheroid model of Böhm-Vitense & Van Dyk (1987).

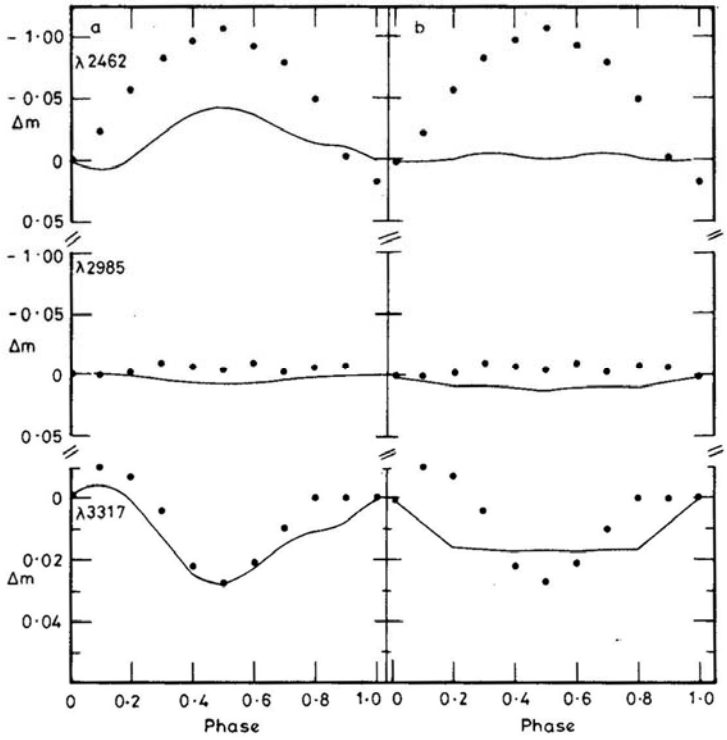

Figure 3. Continued.

Table 2. Spot parameters obtained by our spot model in far ultraviolet.

	Spot 1	Spot 2	Spot 3	Spot 4	Spot 5
Longitude	300	225	140	60	330
Latitude	10	−30	−30	20	−35
Radius	16	10	10	15	30

Longitude, latitude, and radius are in degrees.

the spot area drastically in this bandpass. None of these options seems to be reasonable when spot parameters derived from the other two bandpasses agree so well. We have listed these spot parameters for all five spots in Table 3. In Fig. 4(a) we have plotted our computed *UBV* light curves on top of Pyper's observations. In Fig. 4(b) light curves obtained by oblate spheroid model are plotted on Pyper's observations. Once again the oblate spheroid model light curves were read off from the best fit obtained by Böhm-Vitense & Van Dyk (1987; Fig. 10). It is clearly evident from Figs 2, 3 and 4 that the hot-spot model gives a far better fit to the observed data than the one suggested by Böhm-Vitense & Van Dyk.

If one looks at the observed light curves carefully, one notices an initial increase in *U* and *B* with a peak at 0.1 phase. This initial increase could not be explained by the oblate-spheroid model. But our spot model calculations do reproduce this peak in

Table 3. Spot parameters obtained by our spot model.

	Spot 1			Spot 2			Spot 3			Spot 4			Spot 5		
	V	*B*	*U*	*V*	*B*	*U*	*V*	*B*	*U*	*V*	*B*	*U*	*V*	*B*	*U*
Longitude	320	300	300	250	250	250	155	145	145	40	50	60	350	350	330
Latitude	8	10	10	−30	−30	−28	−30	−30	−28	20	20	20	−40	−40	−35
Radius	24	20	16	8	14	12	8	8	12	18	15	15	25	25	30
F_{sp}/F_{st}	1.30	1.26	1.27	1.08	1.20	1.23	1.08	1.20	1.23	1.30	1.26	1.24	1.30	1.26	1.23
T (spot)	13409	13024	12888	12386	12795	12762	12386	12795	12762	13409	13024	12793	13409	13024	12762

Longitude, latitude, and radius are in degrees. F_{sp}/F_{st} is spot-to-star flux ratio (F_{ratio}).

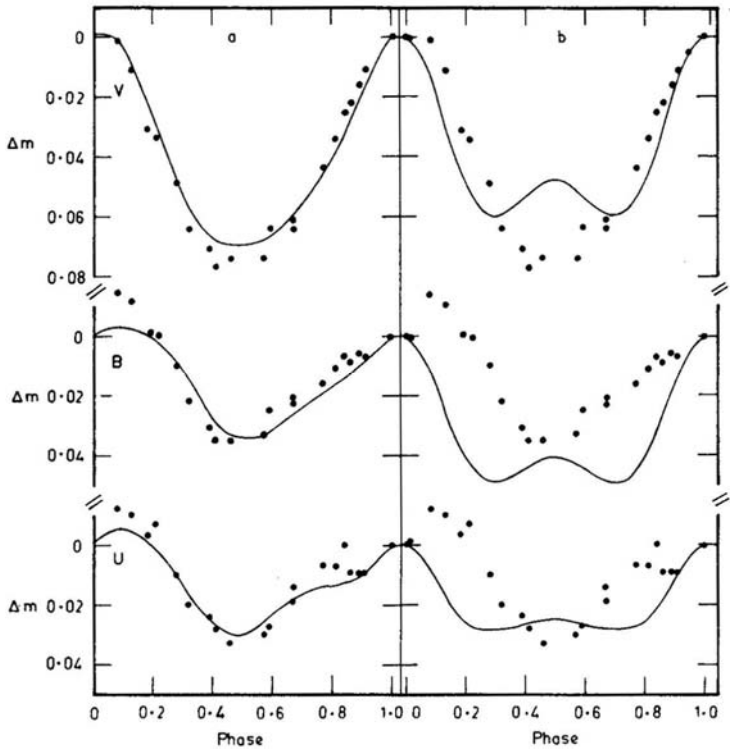

Figure 4. The model *VBU* light curves (solid line) are superimposed on Pyper's (1969) observations (points): (a) our spot model; (b) oblate spheroid model of Böhm-Vitense & Van Dyk (1987).

light satisfactorily. An exactly reverse behaviour is seen in the far-ultraviolet observations of Molnar (1973). Our model is again able to reproduce it. We find that the spot 5, which happens to be close to negative magnetic pole, is responsible for this.

A comparison between the parameters listed in Tables 1, 2 and 3 shows that there is a close agreement between the spot positions obtained by us and those given by Pyper; spot sizes, however, do not agree so well. This is because we have taken the innermost equivalent width contour as the spot size; the actual spot size and shape may differ. But the overall agreement is reasonably good.

5. Summary and conclusion

With the models described above we are able to show that, for α^2 CVn, a model consisting of five hot spots (300 to 800 K hotter than the surrounding atmosphere) can reproduce observed light curves better than the oblate-spheroid model which has a variable surface temperature as well as a variable apparent radius of the star. We also show that a spot model is needed to explain the observed equivalent-width variations. The spot positions obtained by us in our photometric model agree well with those obtained spectroscopically by Pyper (1969).

The Ap stars have fairly stable atmospheres. Such stable atmospheres are necessary if diffusion of elements is to work (Michaud 1970). However, with hot spots it becomes difficult to explain how can such hot regions survive for a long time in a cooler atmosphere. Perhaps some mechanism is at work so that there is a rapid loss of heat from these hot regions. Trasco (1972) has shown that, for magnetic stars, an equilibrium condition will exist when the temperature in the magnetic region is higher than the non-magnetic region. We believe that the spots on α^2 CVn are associated with such fields and therefore are at higher temperature than the nonmagnetic regions.

Acknowledgement

We thank the Department of Science and Technology, New Delhi for providing financial assistance, and also the Director, Indian Institute of Astrophysics, Bangalore for providing much needed computer time.

References

Al-Naimy, H. M. 1977, *Astrophys. Sp. Sc*., **53,** 181.
Böhm-Vitense, E., Van Dyk, S. D. 1987, *Astr. J*., **93,** 1527.
Budding, E. 1977, *Astrophys. Sp. Sc*., **48,** 207.
Cohen, J. G. 1970, *Astrophys. J*., **159,** 473.
Deutch, A. J. 1958, in *IAU Symp*. 6: *Electromagnetic Phenomena in Cosmical Physics*, Ed. B. Lehnert, University Press, Cambridge, p. 209.
Falk, A. E., Wehlau, W. H. 1974, *Astrophys. J*., **192,** 409.
Gray, D. F. 1982, *Astrophys. J*., **258,** 201.
Guthnick, P., Prager, R. 1914, *Veröff. Sternw*. Berlin-Babelsberg, **1,** 38.
Hatzes, A. P., Penrod, G. D., Vogt, S. S. 1986, *Bull. Am. astr. Soc*. **18,** No. 2, p. 668.
Khokhlova, V. L. 1975, *Astr. Zh*. **52,** 950.
Khokhlova, V. L., Rjabchikova, T. A. 1975, *Astrophys. Sp. Sc*., **34,** 403.
Klinglesmith, D. A. 1971, NASA SP - 3065.
Kurucz, R. L. 1979, *Astrophys. J. Suppl.*, **40,** 1.
Leckrone, D. S., Snijders, M. A. J. 1979, *Astrophys. J. Suppl.*, **39,** 549.
Michaud, G. 1972, *Astrophys. J*., **160,** 641.
Molnar, M. R. 1973, *Astrophys. J*., **179,** 527.
Poe, C. H., Eaton, J. A. 1985, *Astrophys. J*., **289,** 644.
Pyper, D. M. 1969, *Astrophys. J. Suppl*., **18,** 347.
Trasco, J. D. 1972, *Astrophys. J*., **171,** 569.
Vogt, S. S., Penrod, G. D. 1983, *Publ. astr. Soc. Pacific*, **95,** 565.
Vogt, S. S., Penrod, G. D., Hatzes, A. P. 1986, *Preprint*.

J. Astrophys. Astr. (1988) **9,** 185–192

Vortex Rings in the Working Surface of Radio Jets

Sandip K. Chakrabarti* *International Center for Theoretical Physics, Strada Costiera 11, 34000 Trieste, Italy and Theoretical Astrophysics, California Institute of Technology, Pasadena, USA*

Received 1988 February 10; accepted 1988 July 13

Abstract. We study the effects of the presence of vortex rings surrounding a supersonic radio jet inside the cocoon of a radio lobe. We show that both the jet and the shocked ambient medium are pinched. Flow speed inside the cocoon is always close to the sonic value and it stays so by successively passing through several oblique shocks. We also discuss the possibility of the non-linear growth of the instabilities of the contact surface to explain the numerical results in the literature.

Key words: radio sources, jets—shocks—vortex rings—pinch instability

1. Introduction

It is increasingly evident from the recent numerical simulations (Norman, Winkler & Smith, 1982; Williams & Gull 1984, 1985; Norman & Winkler 1985; Lind 1986) that the working surface of a radio jet is probably far more complex than the original model of Blandford & Rees (1974). In particular, periodic shedding of vortices into the cocoon which propagate upstream of the jet is common. There is yet no conclusive evidence for these features in radio jets. Recent VLA polarization data of Cyg A by Dreher, Carilli & Perley (1987) shows the rotation measure of opposite signs to be symmetrically distributed about the axis of both the east and the west lobes indicating the presence of vortical motions. To explain laboratory experiments of production of vortex rings by Baird (1987), Broadbent & Moore (1987) calculates the effect of a single vortex ring on a supersonic jet without a cocoon. No such analysis has been carried out in the context of a radio jet where the jet is surrounded by a cocoon which is in turn surrounded by the shocked ambient medium (or, *screen* for short, see Fig. 1). In this paper we present such an analysis and show that it reproduces many features which are observed in the extensive numerical simulations. A more detailed discussion is found in Chakrabarti (1988).

2. A Pair of Vortex rings in the Cocoon

We assume that the problem is strictly two-dimensional. The unperturbed boundaries between the jet and the cocoon and the cocoon and the shocked ambient medium are

* Present address: Theoretical Astrophysics, Tata Institute of Fundamental Research, Homi Bhabha Road, Colaba, Bombay 400 005.

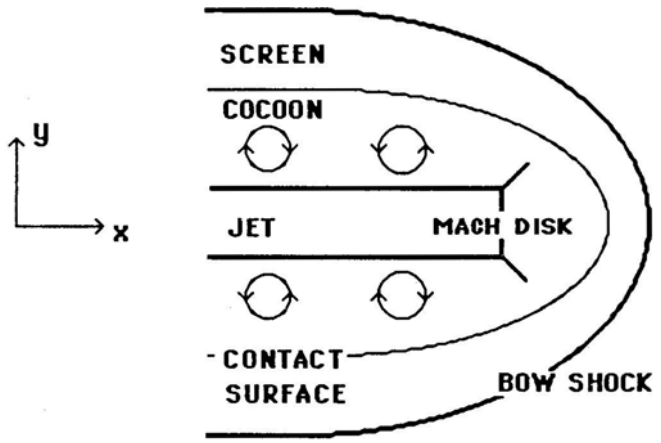

Figure 1. The schematic diagram showing the relative locatio n s of the principal components of the working surface of a radio jet.

parallel to the x-axis. The vortex rings are replaced by the line vortices which are normal to the plane of the diagram (Fig. 1). Also we assume that the strength of the vortices are small (each equal to k in analysis below) so that the perturbations can be carried out by linear analysis. The analysis is done only up to k^2 therefore ignoring the higher-order effects involving the motion of the vortex-pairs in a direction normal to the jet flow (*i.e.*, along the y-axis). All the distance scales are measured in units of the thickness of the unperturbed cocoon which is chosen to be 2π. Our coordinate system co-moves with the velocity U_r (exact number is unimportant for the present analysis) of the vortex pair with respect to infinity. Thus a pair of vortices placed at $x = \pm b$ on the $y = 0$ axis will always maintain these coordinates.

Let the subscripts s, c and j denote quantities in the screen, in the cocoon and in the jet, respectively. Also, let v_s , v_c, v_j denote the unperturbed velocities of the fluid medium in the screen, in the cocoon, and in the jet as measured in the frame of the vortices. We now expand the velocity potentials inside these three media in the following way:

$$\phi_s = v_s(x + \varepsilon_s^2 \phi_{1s} + \varepsilon_s^4 \phi_{2s} + \ldots), \tag{1}$$

$$\phi_c = v_c(x + \varepsilon_c \phi_{1c} + \varepsilon_c^3 \phi_{2c} + \ldots), \tag{2}$$

$$\phi_j = v_j(x + \varepsilon_j^2 \phi_{1j} + \varepsilon_j^4 \phi_{2j} + \ldots). \tag{3}$$

The small parameters $\varepsilon_{s,c,j}$ are defined as,

$$\varepsilon_i = \frac{\kappa}{4\pi v_i}, \tag{4}$$

where, the index i takes the values s, c and j. The quantities ϕ_1 and ϕ_2 are the correction terms due to the perturbation. Since inside the cocoon the velocity correction term must 'feel' the rotational vortex flow field, only the odd powers of ε appear in ϕ_c but since the perturbations of the flow field inside the jet and the screen are produced only via pressure (which is proportional to the square of the velocity field) variation through the boundary, only the even powers appear in ϕ_j and ϕ_s. Consequently, the equations

of the cocoon boundary and the jet boundary take the forms:

$$y_s(x)=\pi+\varepsilon_s^2\eta_{1s}(x)+\varepsilon_s^4\eta_{2s}(x)+\ \ldots\ , \tag{5}$$

and,

$$y_j(x)=-\pi+\varepsilon_j^2\eta_{1j}(x)+\varepsilon_j^4\eta_{2j}(x)+\ \ldots\ . \tag{6}$$

We use the method of images to calculate the velocity potential inside the cocoon (Lamb 1932). Thus, $\phi_{1c}=\mathrm{Re}(\omega)$, where, ω is obtained from

$$\omega\propto\log(Z\pm b)+\log(Z\pm b\pm 2\pi i)+\log(Z\pm b\pm 4\pi i)+\ \ldots\ , \tag{7}$$

Z being the complex coordinate $x + iy$. The velocity components turn out to be

$$v_x=\frac{\kappa}{4\pi}\left[\frac{\mathrm{sh}(x-b)}{\mathrm{ch}(x-b)-\cos y}\pm\frac{\mathrm{sh}(x+b)}{\mathrm{ch}(x+b)-\cos y}\right]+v_c, \tag{8}$$

and

$$v_y=\frac{\kappa}{4\pi}\left[\frac{\sin y}{\mathrm{ch}(x-b)-\cos y}\pm\frac{\sin y}{\mathrm{ch}(x+b)-\cos y}\right], \tag{9}$$

where the upper sign is to be used when both the vortices have strength $k > 0$ and the lower sign is to be used when the strengths are opposite (in the sense shown in Fig. 2a,b).

From the Bernoulli's equation the pressure variation inside the cocoon is written as,

$$\frac{P_c}{\rho_c}+\frac{1}{2}(v_x^2+v_y^2)=\frac{P_{\infty c}}{\rho_c}+\frac{1}{2}\left(\frac{\kappa^2}{16\pi^2}+v_c^2\right). \tag{10}$$

The x-component of velocity at infinity is $k/4\pi$.We have considered here the flow to be locally incompressible so that density ρ can be treated as constant. $P_{\infty c}$ is the pressure in the cocoon at infinity. We now define the pressure coefficients,

$$C_{ps}=\frac{(P_c-P_{\infty c})}{\frac{1}{2}\rho_s v_s^2}, \tag{11}$$

and

$$C_{pj}=\frac{(P_c-P_{\infty c})}{\frac{1}{2}\rho_j v_j^2}. \tag{12}$$

To the leading order, the pressure coefficients could be equated to $C_{ps} = -2\varepsilon_s^2\partial\phi_{1s}/\partial x$ and, $C_{pj} = -2\varepsilon_j^2\partial\phi_{1j}/\partial x$ (Liepman & Roshko 1956) at the screen boundary at $y= \pi$ and the jet boundary at $y = -\pi$ respectively. Substituting these partial derivatives in the wave equations for the perturbation

$$m_s^2\frac{\partial^2\phi_{1s}}{\partial x^2}=\frac{\partial^2\phi_{1s}}{\partial y^2}, \tag{13}$$

and

$$m_j^2\frac{\partial^2\phi_{1j}}{\partial x^2}=\frac{\partial^2\phi_{1j}}{\partial y^2}, \tag{14}$$

where $m_s^2 = M_{\infty s}^2 - 1$ and $m_j^2 = M_{\infty j}^2 - 1$ here M_∞ denotes the Mach number of the flow at a large distance. The equations of the screen and the jet boundary are obtained

by using the pressure balance conditions at each boundary, i.e.,

$$\frac{\partial \phi_s}{\partial y}\Big/\frac{\partial \phi_s}{\partial x} = \varepsilon_s^2 \frac{\partial \eta_{1s}}{\partial x} + \varepsilon_s^4 \frac{\partial \eta_{2s}}{\partial x} + \ldots, \tag{15}$$

$$\frac{\partial \phi_j}{\partial y}\Big/\frac{\partial \phi_j}{\partial x} = \varepsilon_j^2 \frac{\partial \eta_{1j}}{\partial x} + \varepsilon_j^4 \frac{\partial \eta_{2j}}{\partial x} + \ldots. \tag{16}$$

Substituting the expressions for ϕ_s and ϕ_j in the above equations and equating terms of order ε_s^2 and ε_j^2 one obtains,

$$\frac{\partial \eta_{1s}}{\partial x} = \frac{\partial \phi_{1s}}{\partial y}\bigg|_{y=\pi} = \pm m_s \frac{\partial \phi_{1s}}{\partial x}\bigg|_{y=\pi}, \tag{17}$$

and

$$\frac{\partial \eta_{1j}}{\partial x} = \frac{\partial \phi_{1j}}{\partial y}\bigg|_{y=-\pi} = \pm m_j \frac{\partial \phi_{1j}}{\partial x}\bigg|_{y=-\pi}. \tag{18}$$

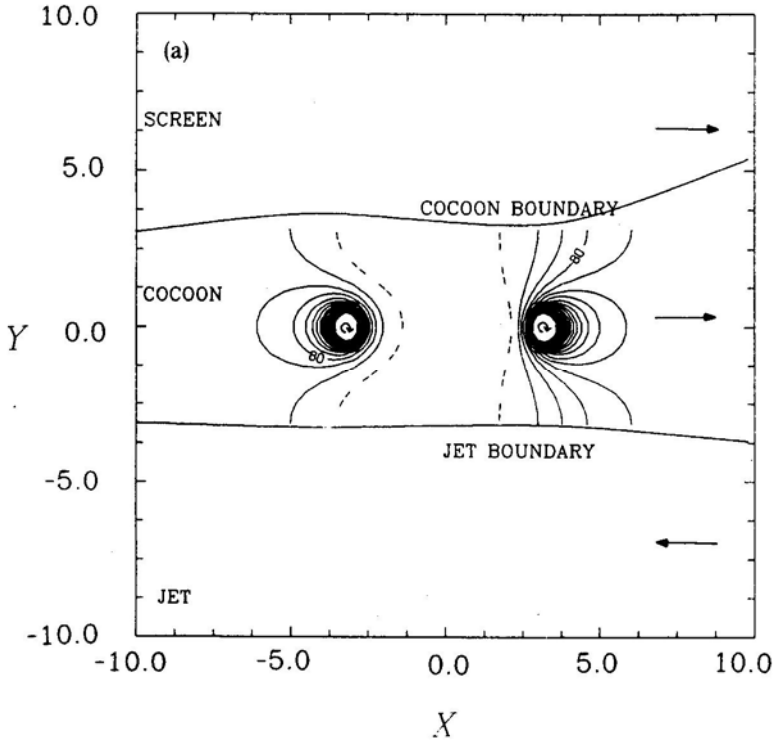

Figure 2. The nature of the perturbation of the jet boundary and the cocoon boundary are shown when a pair of vortex rings with a) same vorticity, and b) opposite vorticity are introduced in the cocoon. The fluid flows towards right both in the cocoon and in the screen and towards left in the jet. The parameters are: $4\pi\nu_c/k$ =0.4, q_s=0.16, q_j=0.04, $P_{\infty c}$ = 0.2.The contours of the constant Mach numbers are equally spaced in logarithmic scale with interval 0.003. Dashed lines correspond to subsonic motion. The contours marked 80 are for $\log_{10}(M_c) = 0.008$.

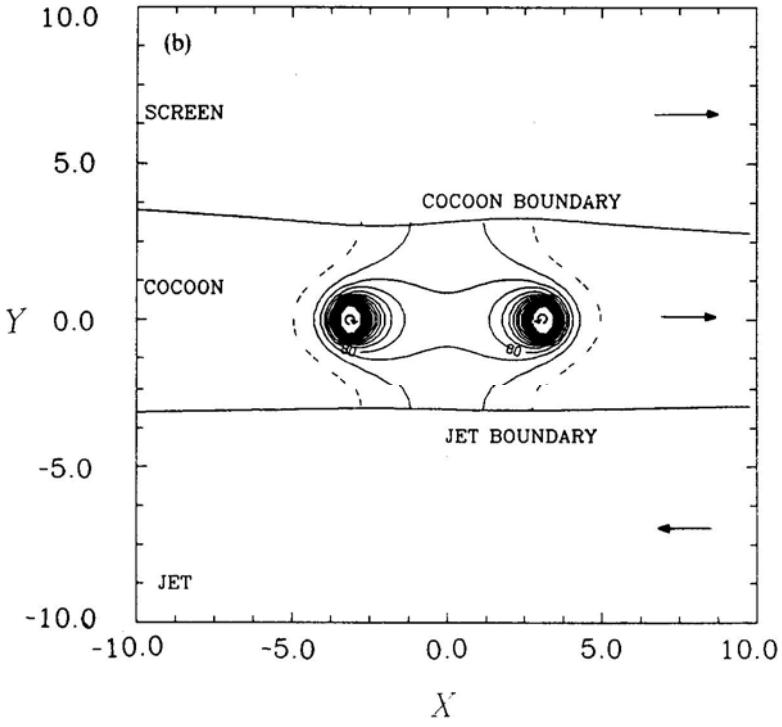

Figure 2. Continued.

Upon integration one obtains the equations for the boundary corrected up to k^2 of the screen as,

$$y_s(x)=\pi\mp q_s\left[-\left(3+\frac{16\pi^2v_c^2}{\kappa^2}\right)\frac{x}{2}+\mathrm{th}\frac{x-b}{2}+\mathrm{th}\frac{x+b}{2}\right.$$
$$\left.+2\left(\frac{1}{\mathrm{th}b}-\frac{4\pi v_c}{\kappa}\right)\log\mathrm{ch}\frac{x+b}{2}-2\left(\frac{1}{\mathrm{th}\,b}+\frac{4\pi v_c}{\kappa}\right)\log\mathrm{ch}\frac{x-b}{2}\right] \tag{19}$$

when both the vortices are of same sign and,

$$y_s(x)=\pi\mp q_s\left[\left(1-\frac{16\pi^2v_c^2}{\kappa^2}\right)\frac{x}{2}+\mathrm{th}\frac{x-b}{2}+\mathrm{th}\frac{x+b}{2}\right.$$
$$\left.-2\left(\frac{1}{\mathrm{th}\,b}-\frac{4\pi v_c}{\kappa}\right)\log\frac{\mathrm{ch}\frac{x+b}{2}}{\mathrm{ch}\frac{x-b}{2}}\right] \tag{20}$$

when the vorticities are of opposite signs Here $q_s = \varepsilon_s^2 m_s\rho_c/\rho_s$. By replacing q_s by q_j one obtains similar results for the jet boundary. The variation of the Mach number with pressure is obtained from Equation (10) as,

$$P_c[1+\tfrac{1}{2}(\gamma-1)M_c^2]^{\frac{\gamma}{\gamma-1}}=P_{\infty c}[1+\tfrac{1}{2}(\gamma-1)M_{\infty c}^2]^{\frac{\gamma}{\gamma-1}}. \tag{21}$$

The subscript ∞ refer to quantities at a large distance from the vortices. The contours of constant Mach numbers are shown in Figs 2a,b. Fig. 2a is for vortices of the same

sign and Fig. 2b is for vortices with opposite signs. The value of b was chosen to be π. Solid lines are for $M_c > 1$ and dashed lines are for $M_c < 1$. The contours are of equal logarithmic interval and the ones marked 80 are for $\log_{10}M_c = 0.008$. The ratio $q_s/q_j = 4$ is considered in this particular case.

In both the Figs 2a and b we notice that the nature of the velocity field is very much different from that of a uniform flow. Because of the large momentum flux in the jet, the pinching of the jet boundary is much smaller than that of the cocoon boundary. The magnitude of the pinching is determined by the quantities q_s and q_j which are functions of the density, velocity, Mach number of the flow and the strength of the vortices. The velocities inside the cocoon and the screen are positive towards the positive x-axis and that of the jet is along the negative x-axis. In Fig. 2a the jet expands downstream by depositing momentum in the cocoon whereas in Fig. 2b the jet is collinated (albeit very

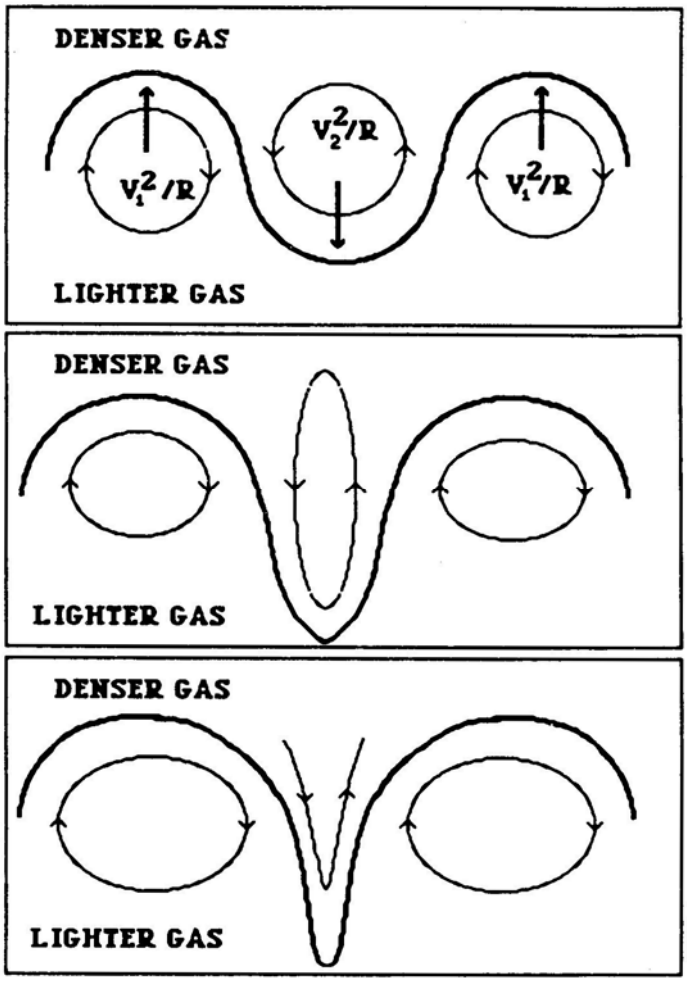

Figure 3. Plausible mechanism for production of 'spikes' on the contact discontinuity. The Rayleigh-Taylor instability is selectively turned on whenever the local gravity due to the centrifugal acceleration points from heavy fluid to the light fluid.

slowly). The perturbation propagates downstream indefinitely in this model but in reality it passes through the terminating shock called the Mach disc. The expansion and collimation of the jet show that the kinetic luminosity is affected by the vortices. In Fig. 2a the screen contracts downstream of the local flow but in Fig. 2b it expands. Through the 'de Laval' nozzles formed inside the cocoon, the flow passes successively through several weak shocks and thus it is never far away from the sonic value. The sonic surfaces are oblique. Whereas they appear very close to the vortical motions, there is little correlation between their locations and the location of the pinch in the boundary. This is because part of the kinetic energy participates in the vortical motion of the flow and the simple consideration of the nozzle flow does not hold any further. These features are observed in the numerical models (*e.g.*, Lind 1986).

3. Concluding Remarks

Although it is not obvious from our stationary model, it is quite likely that the undulations of the pinched cocoon boundary (*i.e.*, the surface of contact discontinuity)

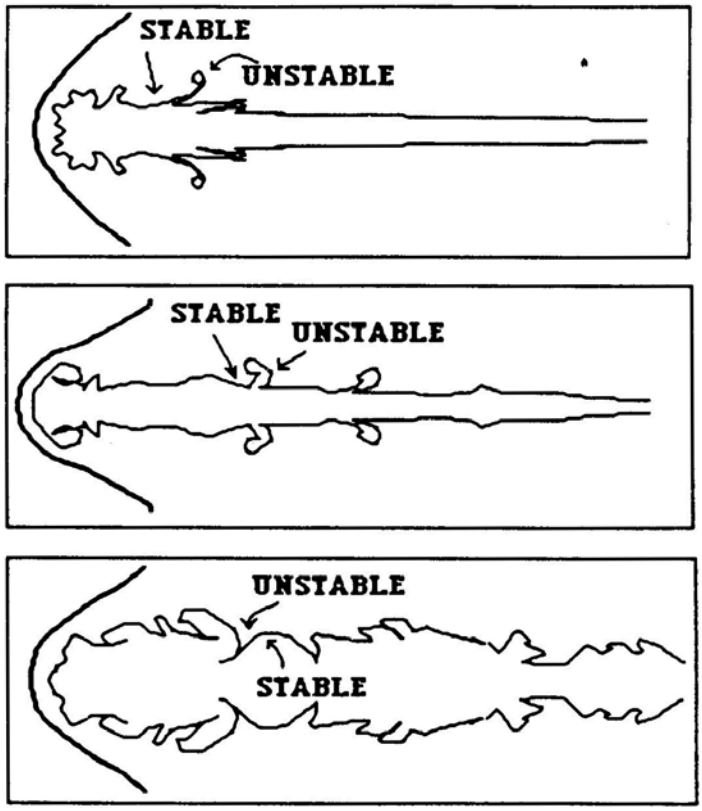

Figure 4. The contact discontinuity of M_j = 12 simulation of hydrodynamic, jets by Norman *et al.* (1985) are traced when η =10(upper panel), η = 1 (middle panel) and η= 0.1,where η is here the ratio of jet density to the external medium density. The inversion of the direction in which the spikes grow as η is varied indicates the presence of the Rayleigh-Taylor instability which may have been turned on by mechanism drawn in Fig. 3.

will grow into nonlinear regime both due to the shear of the vortex sheet and the local centrifugal acceleration of the vortical motions. Fig. 3 shows how the non-linearity due to the Rayleigh-Taylor instability may be selectively turned on depending upon whether the jet is light or heavy. The nonlinear development of the 'spikes' always takes place from the denser medium to the lighter medium. Thus, for example, for a highly supersonic jet, the spikes should point towards the jet when the jet is light and away from the jet when the jet is heavy. (For mildly supersonic jet the dissipation may wash out the effects discussed here.) In Fig. 4 we trace the contact discontinuity of some simulations of the hydrodynamic jets by Norman *et al.* (1985), to show that our conjecture is probably correct. Simulations of Lind (1986) also show similar features. In all the simulations one observes the oblique shocks and the Mach number of the flow inside the cocoon is very close to the unity, exactly as is derived in this paper. Although this implies that the instabilities will grow indefinitely, in reality the presence of dissipation and magnetic field may inhibit such growth to a finite amplitude. In the radio lobes the oblique shocks inside the cocoon could be the site of the electron accelerations powering the radio sources. The repeated reconnection of the magnetic field lines at the locations of the nonlinear growth may also supply sufficient power. The latter assertions could only be verified by the numerical simulation of hydromagnetic jets with dissipation taken into account.

Acknowledgement

The author acknowledges the NSF grants AST86-15325 and AST85-19411 and a Tolman fellowship with Caltech and the financial support from the International Atomic Energy Agency.

References

Baird, J. P. 1987 *Proc. R. Soc. London*, Ser.A, **409,** 59.
Blandford, R., Rees, M. 1974, *Mon. Not. R. astr. Soc*, **169,** 395.
Broadbent, E. G., Moore, D. W. 1987, *Proc. R. Soc. London*, Ser.A, **409,** 47.
Chakrabarti, S. K. 1988, *Mon. Not. R. astr. Soc.*, (In press).
Clarke, D. A., Norman, M. L., Burns, J. O., 1986, *Astrophys. J.* (Lett.), **311,** L63.
Dreher, J. W., Carilli, C. L., Perley, R. A. 1987, *Astrophys. J.*, **316,** 611.
Lamb, H., 1932, *Hydrodynamics*, Cambridge University Press.
Liepmann, H. W., Roshko, A., 1956, *Elements Of Gas Dynamics*, Wiley, New York.
Lind, K. 1986, *Ph.D. Dissertation*, Calif. Inst, of Technology.
Norman, M. L., Winkler, K.-H. A., 1985, *Bull. Los Alamos Lab.*, **12**, 38.
Norman, M. L., Winkler, K.-H. A, Smith, M. D., 1982, *Astr. Astrophys.*, **113,** 285.
William, A. G., Gull, S. F., 1984, *Nature*, **310,** 33.
William, A. G., Gull, S. F., 1985, *Nature*, **313,** 33.

J. Astrophys. Astr. (1988) **9,** 193–203

Composite Spectra
Paper 2: HD 88021/2

R. & R. Griffin *The Observatories, Madingley Road, Cambridge CB3 0HA, England; Visiting Associates, Mount Wilson & Las Campanas Observatories, Carnegie Institution of Washington*

Received 1988 July 1; accepted 1988 August 3

Abstract. HD 88021/2 (ADS 7662) is a very close visual binary. The accepted visual orbit, which is of very high eccentricity and graded "reliable", led to the expectation of a periastron passage in 1981, when there should have been a large difference in radial velocity between the components. No such event took place, and there is little indication that it is likely to occur in the near future. A new interpretation of the visual orbital data leads to an orbit of a different character from those hitherto proposed. A decision between the competing orbits should be possible within a very few years. Meanwhile, the method of spectral subtraction developed in Paper 1 has enabled us to separate the spectra of the two components and to show that their spectral types are K0 III and A2m.

Key words: composite spectra—visual binaries—stars, individual

1. Introduction

In Paper 1 (Griffin 1986) we showed how, by a technique of spectral subtraction, it is possible to disentangle the contributions of the individual component stars to a composite spectrum. Such a spectrum is frequently encountered when a binary star system has an angular separation that is too small to permit the components to be resolved on the spectrograph slit. The system treated in Paper 1 (HR 6902) must have an angular separation of only a few milliseconds of arc and has never been resolved directly. The one treated in the present paper has been known as a difficult visual double star since 1910; its maximum separation is less than 0″.25 and there has been no possibility of observing the spectra of the components separately. Indeed, the measurements simply of its position angle and separation have created such uncertainties that six different orbits have been proposed; even the accepted one is grossly erroneous, as we show from radial-velocity observations.

2. Existing knowledge concerning HD 88021/2

Miss Cannon, in the course of compiling the *Henry Draper Catalogue*, was the first person to examine the spectrum of the object with which we are concerned in this paper. She recognized it as composite, and accordingly invested it with two HD

numbers—HD 88021, type F5, and HD 88022, type A2 (Cannon & Pickering 1919). Not many years previously, Aitken (1910) had discovered the duplicity of the system by direct visual observation with the Lick 36-inch refractor; he saw the object as consisting of two equally bright stars only 0".15 apart, and gave it the discoverer's designation A 2145.

Photoelectric *UBV* photometry of the system has been carried out by Häggkvist (1965), Eggen (1965) and Sanders (1966), with results near $V = 6^{m}.66$, $(B - V) = 0^{m}.54$, $(U - B) = 0^{m}.32$.

The comprehensive study of composite spectra by Hynek (1938) included HD 88021/2 as no. 304. Curiously, Hynek classified the system as belonging to his Class I, whose definition is "Composite spectrum arising from a physical binary whose component stars are not resolvable even with the largest instruments . . .", rather than Class III ("Very close physical pair, observable as a binary, but whose component spectra cannot be obtained separately"); and he did so notwithstanding that Aitken (1932) had explicitly pointed out the seemingly obvious fact that "The composite spectrum doubtless is due to the two components of the visual pair .". Hynek also noted that the system was on the radial-velocity programme at Mount Wilson; the interest in it there proved to be rather short-lived, but the results of the four spectrograms taken at Mount Wilson have been published by Wilson & Joy (1950) as a mean velocity and by Abt (1970) with individual details. Radial velocities have also been published by Heintz (1981) from three Kitt Peak spectrograms taken in 1979, and by Beavers & Eitter (1986) from four photoelectric measurements taken in 1977/8. All the published radial velocities are consistent with the hypothesis that HD 88021/2 shows a constant velocity of about +12 km s^{-1}.

Several attempts have been made to classify the spectra of HD 88021 and 88022 from observations of the composite spectrum. Stephenson & Sanwal (1969) and Markowitz (1969) gave the types as G2 III and A2 V; the former authors also derived for the system, from a now-discredited visual orbit (Baize 1957), the improbable total mass of 15.52 $M_{\odot}$. The types gG5 + A2 are quoted in the catalogue of Finsen & Worley (1970), but we have not located the original source. More recently, Abt (1981) has recognized HD 88022 as being a metallic-lined A star: he classified the system as Am + F5 III, and gave the calcium and hydrogen-line types of the early component as A2 and F1 respectively. We shall show below that the Am nature of HD 88022 is confirmed, but that all classifications of the cooler star (HD 88021) have placed it at much too early a type. That is a general tendency in the classification of composite spectra: it seems that the classifier, confronted with a spectrum in which the late-type lines are heavily veiled by the superposition of the more muted spectrum of the early-type component, cannot bring himself to accept that such weak lines could originate from a star of such a late type as is actually the case.

Abt & Cardona (1984), who give the same types as Abt (1981), make a clear (if implicit) claim to have taken classification spectrograms of the two stars separately. We feel that that claim must be either inadvertent or mistaken, not merely because of its manifest improbability but also because expert classifiers would never make such a gross error as Abt & Cardona do in respect of the type of HD 88021 if they could see its spectrum in isolation from that of its companion.

2.1 The Visual Orbit

Double-star observers have long known HD 88021/2 as ADS 7662, its number in Aitken's (1932) catalogue, and we shall so designate it in this section. Nobody except Aitken measured the pair between 1910, when he discovered it, and 1937, after he had retired. It has subsequently turned out that the Aitken era was a more interesting and critical time, as far as the orbit is concerned, than the ensuing half-century has been.

A serious difficulty arises in the interpretation of double-star measurements of ADS 7662, inasmuch as the components are so comparable in magnitude as not to be certainly distinguishable from one another. Although the two stars must be of considerably dissimilar colours, observers seem not to have commented upon the fact, and it has not even been known which spectrum is associated with which star. Thus all measured position angles are subject to a 180° ambiguity. (These remarks are not to be construed as any criticism of the double-star observers: it seems amazing to us that anyone can measure pairs of such extreme difficulty. As mere spectroscopists, we have observed the object more than 50 times ourselves and seen it as a single star every time!)

The discovery observation, averaged with two others made shortly afterwards, was reported as giving a separation of 0″.15 in position angle 195°.3 (Aitken 1910). In view of the fact that the components were attributed identical magnitudes, we are at a loss to know why the position angle should have been assigned to the third quadrant and not, as would seem more natural, to the first. The next observations, in 1918 and 1919, are simply reported by Aitken (1932) as "Too close". Although he occasionally recorded objects as "single", "round" and "no elongation" (*cf.* the entries in the ADS for ADS 3264,2178 and 7107), Aitken used the expression "too close" so regularly that we think it must imply that the relevant binary was unresolved on that occasion and not that it was visibly double but so close as not to be measureable.

Aitken subsequently measured our object in 1921, 1923 and 1925 (Aitken 1932) at separations of rather more than 0″.l and position angles of 89°.2, 77°.0 and 66°.6, thereby establishing that the motion is retrograde, *i.e.* in the direction of decreasing position angle (clockwise on the sky). His final observation (Aitken 1937) was made in 1933 and gave the position angle as 240°.5.

Between 1937 and 1975 several observers measured ADS 7662. The position angle was generally considered to lie in the third quadrant, but to what extent that became merely a matter of convention is not clear; some observers saw a small difference of magnitude, ranging up to $0^{m}.4$ (Worley 1962), between the components. During that whole 40-year interval the separation of the system was near 0″.2 and the position angle declined only very slowly, from about 230° to 200°. In 1975 the age of speckle interferometry dawned for ADS 7662 (McAlister 1977); it is no disparagement of the filar-micrometer heroes to say that since then, with much larger telescopes and much more complicated equipment, the system has been well observed with a new degree of reliability. The position angle has continued to decrease slowly, and the system has at last been closing in separation. The observations are plotted in Fig. 1 to give an impression of the material available for determining the orbit.

As the data of Fig. 1 have unfolded, ADS 7662 has provided embarrassment to a succession of orbit computers, as may be seen from Table 1. The first three orbits (Eggen 1946, Baize 1956, 1957) accepted the 1921–1925 observations as being in the first quadrant, and in order to fulfil Kepler's (1609) second law (equal areas in equal

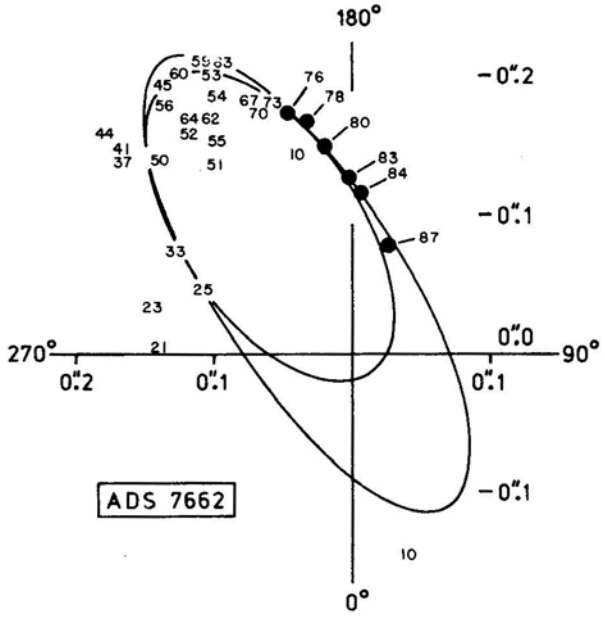

Figure 1. The relative angular positions of the components of ADS 7662 as a function of time The origin of the coördinate system represents the constant position of the primary star, which we shall show in Section 4 to be likely to be the cooler star in the system. The mean position angle and angular distance of the secondary is represented by the last two digits of the year of observation (observations made at the end of a calendar year have been attributed to the following year). Aitken's observations of 1921, 1923 and 1925 are plotted with the quadrdrant reversed. The speckle-interferometry measures made since late 1975 by McAlister and his colleagues (McAlister 1977, McAlister & Fekel 1980, McAlister & Hendry 1982, McAlister *et al.* 1983, McAlister (private communication 1988)) appear to us to be of such reliability that we have elected to portray them differently, as large dots with the year noted beside them. The orbit ellipse must pass very close to them, but it obviously cannot pass equally close to all of the other measurements, and the form of the orbit is still uncertain. The most recent published orbit (Tokovinin 1987) is shown as the smaller ellipse. It accepts the discovery observation of 1910 in its published quadrant at position angle 195°, and demands a very high eccentricity in order to achieve a change of nearly 300° in angle by the time of the next observation in 1921, which however it cannot match in distance at all. We think that another type of possible orbit, which has only moderate eccentricity and therefore requires no special assumption to avoid predicting large radial-velocity changes, is that shown schematically by the larger ellipse. The quadrant of the discovery observation has then to be reversed, to position angle 15° where it is shown near the bottom of the Figure.

times) they necessarily predicted angular motions of several degrees a year. When such motions failed to materialize, such orbits became progressively more untenable, until Baize (1957) proposed an alternative interpretation by transposing the components for the measurements of 1921–1925, placing the position angles in the third quadrant. A more plausible orbit resulted, and the subsequ ent one by Finsen (1977) represented an attempt to improve on it in detail while retaining the same principle. Even so, the orbital motion continued to fall behind expectation, with Finsen's orbit just as with its predecessors, and it seemed certain that the upward trend in periods assigned to ADS 7662 (*cf.* Table 1) must continue. Recently this has in fact happened, with a new

Table 1. Orbital elements successively attributed to ADS 7662.

Element	Eggen 1946	Baize 1956	Baize I 1957	Baize II 1957	Finsen 1977	Tokovinin 1987
P (years)	43.0	48.0	53.73	60.0	64.7	71.1
T (date)	1973.10	1976.5	1981.23	1976.88	1981.75	1990.0
e	0.61	0.54	0.60	0.94	0.949	0.86
a (arcsec)	0.25	0.215	0.21	0.19	0.240	0.129
i (degrees)	103.8	108.5	107.6	124.1	115.8	180.0
ω (degrees)	71.4	54.9	54.9	104.8	104.5	87.9
Ω (degrees)	57.4	58.4	57.8	157.0	161.2	122.1

orbit published by Tokovinin (1987), which has managed to put off the periastron passage until 1990. Recent speckle measurements kindly communicated to us in advance of publication by Dr H. A. McAlister suggest that the orbital motion is already lagging about one year behind Tokovinin's one-year-old prediction.

3. Radial velocities, and the light they shed on the orbit

In 1976 Dr J. Dommanget was kind enough to send us an early draft of his second *Catalogue d' Éphémérides* that was eventually published in 1982 (Dommanget & Nys 1982). It showed the expected variations, as functions of time, of the relative radial velocities of the components of visual binary stars whose orbits had been computed. We noticed that HD 88021/2 was a case where alternative orbits—those of Baize (1957)—led to entirely different radial-velocity behaviours, which would readily be distinguished by just a few measurements. It was an exceptionally good time, just then, to make such radial-velocity measurements, inasmuch as the dramatic periastron passage predicted on the basis of orbit II (eccentricity 0.94) was due to take place at epoch 1976.9 and involved a sudden change of more than $60 kms^{-1}$ in relative velocity.

We therefore placed the system immediately upon our observing programme with the Cambridge radial-velocity spectrometer (Griffin 1967). The first observation was made at just about the time predicted for periastron. It soon became apparent that little, if any, change was occurring in the radial velocity of the giant component of the system, which was presumed to be the only one to which the spectrometer would respond.

Meanwhile, Baize's (1957) orbits were superseded by Finsen's (1977); by that time 'Baize I' was completely untenable on the evidence of the continuing visual observations alone, and the new orbit was of much the same form as 'Baize II' but even more extreme and with the dramatic periastron passage postponed until 1981.75. Van Dessel (1979) drew attention to the urgent need for radial-velocity coverage, but again the predicted event failed to materialize.

The object has continued under systematic observation right up to the time of writing, and we present in Table 2 the 54 radial-velocity measurements that we have made of it photoelectrically in 1976–1988. A graph of them (Fig. 2) shows a very slight downward trend; a straight line fitted by least squares to the observations has a slope

Table 2. Photoelectric radial velocities of HD 88021, observed at Cambridge except where otherwise noted.

Date	Velocity km s^{-1}	Date	Velocity km s^{-1}
1976 Nov 29.18	+11.3	1982 Apr 14.90	+12.0
1977 Jan 30.08	12.2	May 11.88	11.5
Mar 14.98	12.6	Oct 27.24	11.2
Apr 13.93	13.1	Nov 24.56*	12.2
May 24.90	13.6	1983 Jan 19.09	12.3
June 1.91	13.7	Feb 10.25†	13.2
Nov 1.19	12.2	Apr 15.87	12.7
1978 Jan 23.07	12.5	May 6.88	12.7
Mar 13.07	11.6	Dec 3.14	11.0
Apr 15.93	14.8	1984 Jan 2.14	12.1
Oct 12.22	12.5	Apr 15.92	11.0
Nov 16.19	13.2	1985 Jan 14.12	11.9
1979 Jan 3.15	12.6	Feb 24.00	13.3
Mar 1.04	11.8	1986 Jan 4.46*	12.1
Apr 28.89	13.8	Feb 27.01	11.2
May 13.90	13.5	Apr 10.86‡	12.4
June 7.15*	13.6	May 5.87	13.1
Nov 24.18	13.2	Dec 12.18	11.8
Dec 31.10	11.3	1987 Jan 31.10	11.1
1980 Jan 23.11	11.9	Feb 21.01	10.5
May 4.89	13.3	Mar 20.92	11.2
Dec 7.21	12.9	May 4.86	11.4
1981 Jan 15.08	13.2	Nov 8.38§	11.3
Apr 20.91	12.3	Dec 8.22	11.5
May 19.17*	13.4	1988 Jan 8.14	10.1
1982 Jan 11.10	12.6	Feb 1.40†	10.5
Mar 5.02	+11.7	May 21.90	+12.5

* Observed with 200-inch telescope (Griffin & Gunn 1974).
† Observed with DAO 48-inch telescope (Fletcher *et al.* 1982).
‡ Observed with 'Coravel' (Baranne, Mayor & Poncet 1979) at OHP.
§ Observed with 'Coravel' at ESO.

of –0.14 ± 0.03 km s^{-1} per annum, so the trend may certainly be regarded as significant. If the assumption is made that the trend is satisfactorily represented by the linear relationship whose slope has been calculated, the total change of radial velocity during the $11\frac{1}{2}$ years covered by the observations is approximately 1.6 km s^{-1}.

We are not alone in failing to see a periastron passage: it is evident from Fig. 1 that the 'visual' (actually speckle) measurements have not shown one either. It would be somewhat presumptuous of spectroscopists to put forward a new visual orbit; but we may perhaps be allowed to offer some qualitative remarks on the present situation, as we see it, concerning the orbit.

The speckle observations of the last decade show the system to be following a path not very different from that expected on the basis of Finsen's (1977) orbit but far too slowly. If the real orbit is basically similar to Finsen's and simply requires minor

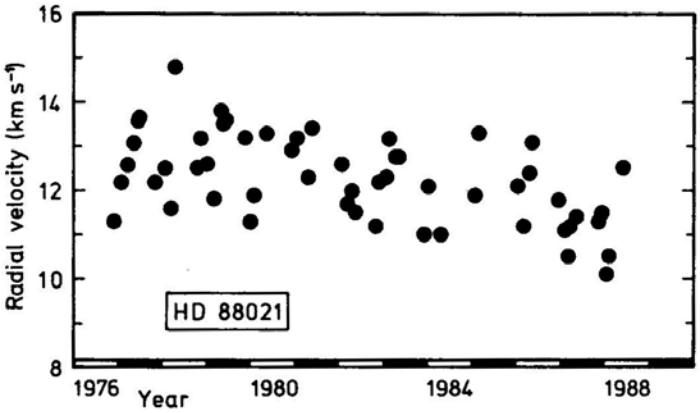

Figure 2. Radial-velocity measurements of HD 88021 plotted as a function of time.

refinement, the latest date which can reasonably be held to correspond to one complete revolution from Aitken's discovery observation is about 1983. Periastron supposedly took place less than seven years after discovery: no plausible modification to the orbit can delay it much beyond 1990, and therefore we must now be within about two years (at most) of the periastron passage which Finsen regarded as due in 1981. Reference to the radial-velocity ephemeris (Dommanget & Nys 1982) shows that in the decade from 12 to 2 years before periastron the relative radial velocities should have changed by about l0 kms^{-1}. If a reasonable assumption is made about the relative masses, the velocity of the late-type component should have shown a steady change amounting to at least 4 km s^{-1} during the last decade. That simply has not happened. It should be mentioned that Tokovinin (1987) has avoided any embarrassment over the lack of radial-velocity change by adopting an orbital inclination of exactly 180°, so no change at all would ever be expected; but there would seem to be an element of artificiality in such a choice of inclination, and in any case *some* change of velocity has in fact been witnessed.

Summarizing the above evidence, we may say that the abrupt periastron passage that was due to take place in 1981, only four years after the prediction of it was made, has manifestly failed to take place even within eleven years; and the radial velocities have changed very slowly, offering little support to the idea that a sudden periastron passage is imminent now. Despite the grading of Finsen's (1977) orbit in the recent catalogue of visual binary orbits (Worley & Heintz 1983) as "reliable", we think that there is a possibility of re-interpreting the visual data in terms of a quite different orbit of no more than modest eccentricity.

The slowness of the motion in position angle during the last 50 years admits of no uncertainty in the continuity of the quadrant. That same slowness obliges us to agree with the reversal, first proposed in orbit II of Baize (1957), of the published quadrant of Aitken's (1932) observations in 1921–1925. We now suggest reversing the quadrant of the discovery observation (Aitken 1910) as well. The necessity for a very rapid change of position angle and a very high eccentricity then disappears, and a relatively sober orbit with a period of about 110 years results. We cannot make it fit Aitken's first three measurements very well in distance: the position angles can be matched, but then the distances need to be even smaller than Aitken measured, especially for the 1921

observation. That observation is only a single night's measure; Aitken himself (1935, p. 74) says that such a measure "deserves small weight", and in an illustration of an orbit computation he rather sportingly chooses an example (*loc. cit.*, p. 103) in which he is obliged to reject two such measures made by himself. It is only too apparent that no orbit solution can fit perfectly all the observations. In fact, we should point out that the new orbit by Tokovinin (1987) fits the 1921 and 1923 measures even worse than ours does: it gives a computed separation of less than 0″.06 in 1921, so the binary should then have been completely unresolved and the observation (although it gives an acceptable position angle) would have to be dismissed as imaginary.

Baize (1957) noted that the negative residuals in angular separation in the 1950s were "irreducible", whatever orbit one adopted; the same remains true today. On the other hand, most of the pre-1950 measurements equally obstinately give positive residuals. An open-minded consideration of the data shown in Fig. 1 would lead to the conclusion that the ellipse representing the orbit ought to be shorter and fatter than those drawn there. Unfortunately, such an orbit would violate the discovery observation. Rejection of that particular observation is far too radical a proposition to be seriously put forward by us; but Tokovinin's rejection of Aitken's next two measurements is to be seen as a resort only one degree less desperate. Fortunately, it seems almost certain that we shall not have to wait very long for a definite resolution of this whole problem: the angular separation is now very small, so the angular motion must be correspondingly rapid. Within a very few years a final decision between the various orbits should become possible, especially if improved processing of speckle-interferometry measures removes the ambiguity in sign of the position angles.

4. Spectroscopy

When it became clear that there was little prospect that HD 88021/2 could be observed at a time when there would be a large difference in radial velocity between the components, we were obliged to abandon the hope of determining a mass ratio by the spectroscopic method put forward in Paper 1 (Griffin 1986). Nevertheless, it remained worth while to observe the spectrum of the system in order to determine the spectral types of the components, and to that end we took a spectrogram with the coudé spectrograph of the Mount Wilson 100-inch reflector on 1984 March 23. Details of the equipment and procedures are given in Paper 1; suffice it to say here that the spectrogram is on IIa-O emulsion, covers the nominal wavelength range 3650-4650 Å, and has a reciprocal dispersion of 10 Å $mm^{-1}$and a trailed width of 1.7mm.A small part of the spectrogram is illustrated in Fig. 3. The Figure also shows the corresponding regions of the spectra of other stars which we have identified as being spectroscopically similar to the individual components of the binary.

By the methods, at once naïve and refined, developed in Paper 1 we discovered that the most accurate match for the late-type component, HD 88021, is provided by the spectrum of β Gem (K0 III). When appropriate fractions of the spectrum of β Gem are subtracted from that of HD 88021/2, the spectrum of HD 88022 which is thus uncovered bears the unmistakeable hallmarks (Conti 1970) of a metallic-lined A star: in relation to the general metallic-line spectral type, the Ca II K line is too weak and the Balmer lines are too strong, *i.e.* both are too early in type. The subtraction process for the wavelength region 3850–4050 Å is depicted in Fig. 4, in which the metallic-line star

ε Ser, which has been classified (Cowley *et al.*, 1969) as A2m, is compared with HD 88022. Fig. 5 shows the spectrum of HD 88022 over the whole wavelength range (3650–4650 Å) for which we have recovered it.

In HD 88022 the Balmer-line profiles and the weakness of the Ca II K line match those in ε Ser well, though the other metallic lines are systematically less enhanced than they are in the spectrum of ε Ser. We therefore propose the classification of A2m for the spectrum of HD 88022. Comparisons with other spectra similarly classified prompt us to comment that ε Ser shows a particularly late metallicline type. The fact that HD 88022 should prove to be metallic-lined causes little surprise, since we have already remarked (Paper 1) on the rather high frequency of Am secondaries in composite systems—an observation based on preliminary investigations of some of the systems on our composite-star programme. Of course, not all the secondaries of those stars have sufficiently narrow-lined spectra for the condition to be instantly recognizable.

A by-product of the subtraction procedure is the ratio of fluxes of the K-and A-type components, which is conveniently expressed in the sense K/A and is of interest for comparison with the flux ratios computed for single stars of known spectral types. The comparison is performed automatically: lists of fluxes measured in 50-Å bands by Willstrop (1965), and necessarily restricted to the wavelength interval 4000–4650 Å which is common to our own work and Willstrop's, in sample K giants and A dwarfs

Table 3. Relative fluxes of ε Phe (K0 III) and 1 Cen (A2 V) in 50-Å bands, compared with the ratios between HD 88021 and HD 88022. The ε Phe/1 Cen ratios have all been multiplied by the empirical factor 1.34, which represents the relative visual luminosity of HD 88021 in comparison with HD 88022.

λ (Å)	From Willstrop (1965) ε Phe	1 Cen	Ratio	HD 88021/2 (observed)
3650	---	---	---	0.63
3700	---	---	---	0.37
3750	---	---	---	0.30
3800	---	---	---	0.16
3850	---	---	---	0.21
3900	---	---	---	0.19
3950	---	---	---	0.30
4000	196	842	0.31	0.29
4050	193	704	0.37	0.40
4100	193	637	0.41	0.41
4150	183	763	0.32	0.33
4200	205	736	0.37	0.38
4250	207	717	0.39	0.41
4300	226	523	0.58	0.60
4350	252	599	0.56	0.53
4400	271	665	0.55	0.55
4450	298	650	0.62	0.65
4500	317	624	0.68	0.68
4550	325	606	0.72	0.70
4600	340	597	0.76	0.74
4650				

are fed into a computer, which then selects pairs of K and A stars whose flux ratios are most nearly similar to the observed flux ratios in HD 88021/2. Since no two Am stars seem to be identical it is doubtful whether Willstrop's list contains an adequate variety of standard stars; but at least the computer was able to confirm our classification of early K giant and early A dwarf. The observed fluxes, and the corresponding ratios between a suitable pair of stars selected from Willstrop's list, are shown in Table 3.

In order to match the observed flux ratios in Table 3, it has been necessary to multiply those calculated from Willstrop's (1965) data by the constant factor 1.34, which is tantamount to adopting that factor as representing the difference in luminosity between the two stars in the *V* band. Thus we expect the components of ADS 7662 to differ by that factor, which is just over $0^{m}.3$ in magnitude terms, in the sense that the late-type component (HD 88021) is the brighter.

Acknowledgements

We are very grateful for the privilege of having worked at the Mount Wilson Observatory and for the assistance of the staff there, and to the SERC for paying the costs of our visits to Mount Wilson. One of us is pleased to acknowledge financial support successively from SERC, St John's College, Cambridge, and the Leverhulme Trust. We offer our warm thanks to Dr H. A, McAlister for informing us of his recent interferometric measures of ADS 7662 in advance of publication. We are also pleased to acknowledge the kindness of the Palomar, Dominion Astrophysical, Geneva, and European Southern observatories in allowing us to make radial-velocity observations, some of which appear in Table 2, with their equipment.

Errata in Paper 1. We apologize for having omitted the reference to Willstrop (1965) in the bibliography of Paper 1; it is given in the bibliography of the present paper. A few errors unfortunately crept into Paper 1 after we had seen the proofs. The first line on p. 206 should be restored to the foot of p. 207, and the word 'respectively' should be deleted from the fourth line up from the foot of p. 218. The half-tone plate (Fig. 3) appears to have suffered abrasion in the printing process and hardly does justice to the pristine cosmetic quality of the Mount Wilson spectrograms.

References

Abt, H. A. 1970, *Astrophys. J. Suppl.,* **19,** 387.
Abt, H. A. 1981, *Astrophys. J. Suppl.*, **45**, 437.
Abt, H. A., Cardona, O. 1984, *Astrophys. J.*, **276,** 266.
Aitken, R. G. 1910, *Lick Obs. Bull.*, **6**, 62:
Aitken, R. G. 1932, *New General Catalogue of Double Stars Within 120° of the North Pole*, Carnegie Institution of Washington, Washington, D.C.
Aitken, R. G. 1935, *The Binary Stars,* second edition, McGraw-Hill, London.
Aitken, R. G. 1937, *Lick Obs. Bull.*, **18**, 109.
Baize, P. 1956, J. *Obs.*, **39**, 82.
Baize, P. 1957, *J. Obs.*, **40**, 17.
Baranne, A., Mayor, M., Poncet, J. L. 1979, *Vistas Astr.*, **23**, 279.
Beavers, W. I., Eitter, J. J. 1986, *Astrophys. J. Suppl.*, **62,** 147.
Cannon, A. J., Pickering, E. C. 1919, *Ann. Harv. Coll. Obs.*, **94**, 118 & 290.

Conti, P. S. 1970, *Publ. astr. Soc. Pacific*, **82,** 781.
Cowley, A., Cowley, C., Jaschek, M., Jaschek, C. 1969, *Astr. J.*, **74**, 375.
Dommanget, J., Nys, O.1982, *Second Catalogue d' Éphémérides des vitesses radiales relatives des composantes des étoiles doubles visuelles dont l' orbite est connue*, Observatoire Royal de Belgique, Brussels.
Eggen, O. J. 1946, *Astr. J.*, **52,** 82.
Eggen, O. J. 1965, *Astr. J.*, **70**, 19.
Finsen, W. S., Worley, C. E. 1970, *Rep. Obs. Johannesburg Circ.*, **7**, 201.
Finsen, W. S. 1977, IAU Comm. 26 *Circ. d' Inf.*, no. 71.
Fletcher, J.M,Harris, H.C, McClure, R.D.,Scarfe, C.D. 1982, *Publ. astr. Soc. Pacific*, **94**, 1017.
Griffin, R. F. 1967, *Astrophys.* J., **148,** 465.
Griffin, R. & R. 1986, *J. Astrophys. Astr.*, **7**, 195 (Paper 1).
Griffin, R. F., Gunn, J. E. 1974, *Astrophys. J.*, **191,** 545.
Haggkvist, L. 1965, *Ark. Astr.*, **4**, 165.
Heintz, W. D. 1981, *Astrophys. J. Suppl.*, **46**, 247.
Hynek, J. A. 1938, *Contr. Perkins Obs.*, **1**, 185.
Kepler, J. 1609, *Astronomia Nova*, Vogelin, Heidelberg.
Markowitz, A. H. 1969, *A Study of Stars Exhibiting Composite Spectra*, Ohio State Univ., Columbus.
McAlister, H. A. 1977, *Astrophys. J.*, **215,** 159.
McAlister, H. A., Fekel, F. C. 1980. *Astrophys. J. Suppl.*, **43**, 327.
McAlister, H. A., Hendry, E. M. 1982, *Astrophys. J. Suppl.*, **48**, 273.
McAlister, H. A., Hendry, E. M., Hartkopf, W. I., Campbell, B. G., Fekel, F. C. 1983, *Astrophys. J. Suppl.*, **51,** 309.
Sanders, W. L. 1966, *Astr. J.*, **71**, 719.
Stephenson, C. B., Sanwal, N. B. 1969, *Astr. J.*, **74**, 689.
Tokovinin, A. A. 1987, *Pis'ma Astr. Zh.*, **13**, 1065.
Van Dessel, E. 1979, *Obs. R. de Belg. Commun.*, Ser. B, No. 109.
Willstrop, R. V. 1965, *Mem. R. astr. Soc.*, **69**, 83.
Wilson, R. E., Joy, A. H. 1950, *Astrophys. J.*, **111,** 221.
Worley, C. E. 1962, *Astr. J.*, **67**, 403.
Worley, C. E., Heintz, W. D. 1983, *Publ. U.S. Naval Obs.*, **24,** Part 7.

J. Astrophys. Astr. (1988) **9,** 205–211

Spectroscopic Binaries near the North Galactic Pole
Paper 16: HD 116093

R. F. Griffin *The Observatories, Madingley Road, Cambridge, England CB3 0HA*

Received 1988 July 13; accepted 1988 August 23

Abstract. Photoelectric radial-velocity measurements show that HD 116093 is a double-lined spectroscopic binary in a very eccentric 53-day orbit. Very little else is known about the system, but circumstantial evidence is consistent with the hypothesis that the components' types are near to F3 V and F8 V. If that is so, the orbit must be seen very nearly edge-on; a search for eclipses is warranted and an ephemeris for them is given.

Key words: radial velocities—spectroscopic binaries—stars, individual

1. Introduction

The last two papers in this series have dealt with spectroscopic binaries having periods of 59 days. The object treated in the present paper, HD 116093, has a very similar period, and (like the subject of Paper 15) is double-lined. It is situated in the eastern part of Coma Berenices in a region lacking conspicuous stars, and is hitherto totally undistinguished in the literature. Apart from positional data, and the approximate magnitude given in the *Henry Draper Catalogue* (Cannon & Pickering 1920), the only information (*mis*information, as will be shown below to be probable) that we have on it is its *HD* spectral type of G5.

2. Observations

Some of the fainter stars of the earliest *HD* type (G5) included in the Cambridge Galactic-Pole observing programme were not observed until rather late in the project, and so it came about that the first observation of HD 116093 was not made until 1980. The object proved to give such a weak and elusive dip on the trace made with the original radial-velocity spectrometer at Cambridge that it was noted for observation at Palomar, where it was at once discovered to be double-lined. A subsequent observation at the Dominion Astrophysical Observatory revealed the two dips to be separated by as much as 120 km s^{-1}, and led to the expectation that the period would be much shorter than it actually proved to be. Although the system was then observed frequently at Cambridge it is right at the limit of the capability of the original instrument, so every opportunity has been taken to observe it with newer spectrometers, and when in 1986 the period became apparent the Cambridge efforts were discontinued altogether. Fortunate timing of a recent observing run on the Geneva Observatory's 'Coravel' at Haute-Provence at last permitted good coverage of the

abrupt periastron passage in the very eccentric orbit ($e \simeq 0.7$). Altogether, measurements have been made on 62 occasions; they are set out in Table 1. Several additional traces were made at Cambridge during the long intervals when the components have a velocity separation such as to produce a broad blend, but they had to be discarded because it proved impossible to read them. One other Cambridge observation was

Table 1. Photoelectric radial-velocity measurements of HD 116093.

Date		MJD	Velocity			$(O-C)$	
			Prim. km s^{-1}	Sec. km s^{-1}	Phase	Prim. km s^{-1}	Sec. km s^{-1}
1980 May	14.91	44373.91	+16.4		0.262	+1.4	
1981 May	17.40*	44741.40	+25.1	−42.8	7.171	+0.4	+1.4
1982 Nov	23.57*	45296.57	−14.5	−1.6	17.609	−0.1	−0.1
	24.58*	297.58	−15.2	+1.4	.628	+0.8	+1.0
	25.56*	298.56	−16.8	+1.4	.647	+0.9	−0.8
1983 Feb	3.53†	45368.53	−67.3	+56.3	18.962	−0.8	+0.7
	4.50†	369.50	−58.5	+49.1	.980	+0.6	+1.6
	23.13	388.13	+12.1	−31.8:	19.331	+3.4	−5.1
	28.12	393.12	−0.3:		.425		
Mar	15.11	408.11	−24.0		.706	−0.3	
1984 Apr	14.03	45804.03	+27.9	−44.2	27.150	+0.7	+2.8
	17.04	807.04	+21.2	−39.0	.207	+0.6	+0.8
	21.01	811.01	+16.3	−28.6:	.282	+3.2	+2.9
	23.97	813.97	+12.5	−22.8:	.337	+4.4	+3.3
	24.97	814.97	+5.5	−30.9::	.356	−1.0	−6.6
	25.90	815.90	+6.6	−27.6:	.373	+1.5	−4.9
May	9.00	829.00	−11.0		.620		
	10.97	830.97	−13.6:		.657		
	12.93	832.93	−20.9		.694		
Nov	29.57*	46033.57	−2.0	−17.4	31.466	+0.5	−2.9
	30.54*	034.54	−4.7	−11.2	.484	−0.8	+1.7
Dec	2.55*	036.55	−8.3	−8.3	.522	−1.3	+1.2
1985 Feb	7.51†	46103.51	−33.5:	+21.8:	32.781	−1.1	+3.5
	8.56†	104.56	−34.9	+21.7	.801	+0.3	+0.4
	16.45†	112.45	−62.8	+54.6:	.949	+2.6	+0.3
	17.40†	113.40	−65.7	+54.5	.967	+0.3	−0.6
	18.35†	114.35	−53.7	+43.1	.985	+0.5	+1.0
Mar	2.08	126.08	+59.5:	−35.2:	33.205	+38.7	+4.7
	6.04	130.04	+7.4	−27.5:	.280	−5.9	+4.2
	17.99	141.99	−6.9		.504		
May	31.96	216.96	−58.0	+45.5	34.914	−1.0	+0.3
June	1.92	217.92	−58.3	+49.4	.932	+3.3	−0.8
1986 Jan	4.54*	46434.54	−14.5	−6.9	39.005	−1.7	−3.7
	17.20	447.20	+17.0	−31.6	.243	+0.1	+4.0
	25.16	455.16	−0.1:		.393		
Mar	6.07	495.07	+29.0	−44.9:	.143	+0.8	+3.1
April	4.98‡	524.98	−24.1	+7.9	.705	−0.6	−0.7
	9.97‡	529.97	−35.3	+21.3	.799	−0.4	+0.3
	11.06‡	531.06	−38.8	+23.7	.820	−0.8	−0.7

Table 1. Continued

Date		MJD	Velocity Prim. km s^{-1}	Velocity Sec. km s^{-1}	Phase	(O−C) Prim. km s^{-1}	(O−C) Sec. km s^{-1}
May	5.98	555.98	+13.8	−31.4	41.288	+1.3	−0.5
	13.96	563.96	−7.4:		.438		
	15.93	565.93	−7.9		.475		
	18.93	568.93	−8.0		.532		
	25.91	575.91	−14.3:		.663		
June	3.93	584.93	−40.2	+31.6	.832	−0.1	+4.9
	10.92	591.92	−60.0		.964	+6.4	
	11.92	592.92	−57.8	+43.6:	.983	−1.0	−1.3
	14.94	595.94	+34.0	−50.4	42.039	+0.8	+3.2
Aug	28.81†	670.81	−8.8		43.447		
Nov	23.55*	757.55	+35.1	−57.9	45.078	−0.9	−1.3
	25.55*	759.55	+31.8	−51.2	.116	+0.1	+0.7
1987 Mar	1.18‡	46855.18	−56.7	+44.7	46.914	+0.2	−0.3
	3.02‡	857.02	−67.9	+52.8	.948	−2.7	−1.4
1988 Jan	23.55‡	47183.55	+35.5	−56.4	53.087	+0.4	−0.8
	31.47‡	191.47	+16.9	−37.0	.236	−0.6	−0.6
Mar	11.15‡	231.15	−57.4	+46.6	.982	−0.3	+1.4
	12.02‡	232.02	−28.2	+10.5	.999	−0.7	−2.4
	12.97‡	232.97	+11.1	−28.4	54.017	−0.7	+1.7
	13.18‡	233.18	+18.4	−37.0	.021	+0.6	−0.3
	13.95‡	233.95	+32.3	−49.8	.035	+1.1	+1.5
	14.98‡	234.98	+35.8	−57.7	.054	−0.7	−0.6

* Observed, in collaboration with Dr J. E. Gunn, with the 200-inch telescope (Griffin & Gunn 1974).

† Observed with the Dominion Astrophysical Observatory 48-inch telescope (Fletcher *et al.* 1982).

‡ Observed with 'Coravel' at Haute-Provence (Baranne, Mayor & Poncet 1979).

rejected: it gave such a wild residual ($\simeq$40 km s^{-1}) that the feature measured on the trace must have been illusory.

3. Orbit

Once the general nature of the orbit was established, the best determination of the elements required the observations to be suitably weighted. By iterative trials it was found that the standard errors of the Palomar, DAO and Coravel measurements were comparable with one another and averaged nearly $2\frac{1}{2}$ times smaller than those of the Cambridge velocities, which were accordingly weighted one-sixth ($\simeq(2\frac{1}{2})^{-2}$) in the final solution. Additionally, observations of the secondary star needed to be weighted 0.6 to obtain a weighted variance similar to that found for the primary. Some unexpectedly bad residuals are given by each of the sources of velocities, and (with one possible exception discussed below) it is probably fruitless to try to identify the cause of each one with a view to finding an excuse to reject the corresponding observation. The fairest thing to do is to leave all the observations in the solution and to allow the

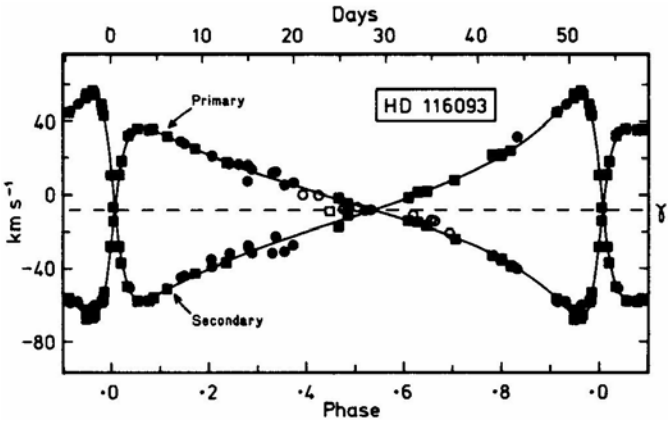

Figure 1. The computed radial-velocity curve for HD 116093, with the measured radial velocities plotted. Palomar, Dominion Astrophysical Observatory and Coravel observations, which were accorded weight 6 in the orbital solution, are plotted as squares; Cambridge observations are represented by circles. Open symbols indicate data which are (or may be) affected by blending between the two components and were not used in the solution.

standard errors of the orbital elements to reflect the real uncertainties of the data. On that basis the orbit plotted in Fig. 1 was determined; its elements are:

$P = 53.1870 \pm 0.0011$ days	$(T)_{37} = \text{MJD } 46327.907 \pm 0.022$
$\gamma = -8.21 + 0.15$ km s^{-1}	$a_1 \sin i = 27.35 \pm 0.17$ Gm
$K_1 = 51.7 \pm 0.3$ km s^{-1}	$a_2 \sin i = 29.93 \pm 0.31$ Gm
$K_2 = 56.5 \pm 0.6$ km s^{-1}	$f(m_1) = 0.289 \pm 0.005\ M_\odot$
$q = 1.094 \pm 0.009\ (= m_1/m_2)$	$f(m_2) = 0.378 \pm 0.012\ M_\odot$
$e = 0.690 \pm 0.002$	$m_1 \sin^3 i = 1.39 \pm 0.03\ M_\odot$
$\omega = 259.2 \pm 0.4$ degrees	$m_2 \sin^3 i = 1.27 \pm 0.03\ M_\odot$

R.m.s. residuals (km s^{-1}):	Primary	Secondary
Palomar, DAO, Coravel	1.0	1.5
Cambridge	2.7	3.2

4. Discussion

An interesting feature of the orbital elements shown above is the size of the minimum masses: the values of 1.39 and 1.27 $M_\odot$ are too large to belong to main-sequence stars of the type (G5) attributed in the *Henry Draper Catalogue* to the system. The dips seen on radial-velocity traces are also incompatible with an origin in normal G5 stars, being much too shallow. In this section, therefore, we shall disregard the *HD* classification and, unfettered by any other published data about the system, explore the consequences of supposing that we are dealing with a pair of F-dwarfs.

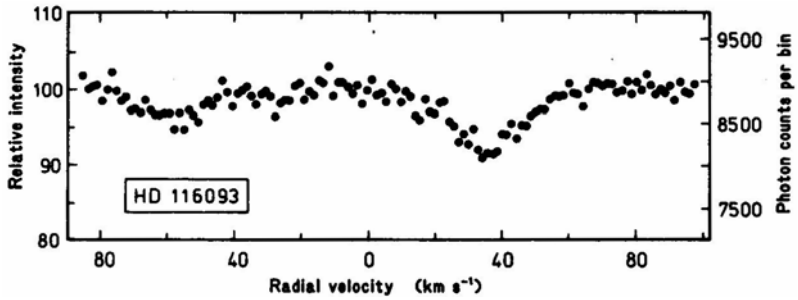

Figure 2. Palomar radial-velocity trace of HD 116093, obtained on 1986 November 23 and illustrating the double-lined nature of the object.

First we present such astrophysical information as may be gleaned from the Palomar radial-velocity traces. It is unfortunate that seven of the ten Palomar traces show closely blended dips, only three being truly double-lined; one of those three is shown in Fig. 2. The sum of the equivalent widths of the two dips is in all cases close to 3.2 km s^{-1} , and the ratio between the two is approximately 1:0.6 in the three cases in which it is independently determinable. The first number can be used to estimate the mean spectral type, and the second indicates the difference in types between the twin components. The three double-lined traces are in fair mutual agreement that the projected rotational velocity of the primary star is 9km s^{-1}; with much more uncertainty the secondary has a mean of 5 km s^{-1}.

Not having any significant experience of observing normal F-dwarf field stars with the Palomar spectrometer, we use the Hyades ((*B* – *V*), equivalent width) relationship to estimate that the observed total equivalent width corresponds to a (*B* – *V)* colour of $0^m.42$. From Allen (1973) we find that such a colour belongs to stars of type F5 V. To obtain the desired ratio of dip areas the best types to choose are F3 V and F8 V. The properties of that combination, again according to Allen (1973), are shown in Table 2.

The difference in *B* magnitude is 1.08, corresponding to a ratio of luminosities in the *B* band of 2.7:1 or (expressed in percentage terms) 73:27. The equivalent widths of the dips given by single Hyades stars having the colours of the stars in the model are 2.7 and 4.1 km s^{-1} respectively (the former value represents an extrapolation of the observed relationship). When the two stars are observed simultaneously, each dip area is reduced in the same proportion as the light of the respective component is diluted by the light of the other, so the equivalent widths become73% of 2.7 and 27% of 4.1, or 1.97 and 1.11 km s^{-1} , respectively—close to the observed values.

Table 2. Model for HD 116093.

Spectral Type	Absolute Mag. *V* m	*B* m	Colour (*B*−*V*) m	Mass $M_\odot$
F3 V	3.08	3.44	0.36	1.43
F8 V	4.00	4.52	0.52	1.17
F3 V + F8 V	2.69	3.10	0.41	2.60

The masses of both the stars in the model are close to the minimum masses $m \sin^3 i$ demanded by the orbit; the mass ratio in the model is however rather too high, and a compromise with the ratio of dip areas would warrant a choice of components somewhat closer to one another in spectral type. A significant fact is that the observed *minimum* total mass is marginally greater than the mass of the model system, indicating that $\sin^3 i$ must be close to unity and implying the possibility of eclipses.

One of the times of conjunction in this very eccentric orbit is very close to periastron, when the separation of the stars is $(a_1 + a_2)(1 - e)$, or about 17.7/sin i Gm. The sum of the radii of the model stars is about 1.65 Gm, so there will be an eclipse if tan $i > 17.7/1.65$ or $i > 84°.7$. The orbital elements allow the time of conjunction to be predicted within about an hour for several years ahead: it occurs 0.212 days after periastron, so the ephemeris for it is $t_{conj} = T + 0.212 + nP$, = MJD 46328.12 + 53.187n, where n is any integer. Favourable dates during the next three observing seasons (though only near appropriate longitudes, of course) are 1989 Jan 25.42, Mar 19.61, May 11.79; 1990 Feb 1.72, Mar 26.91, May 19.10; 1991 Feb 9.03, Apr 3.21. At those conjunctions the eclipse (if any) would be of the secondary star. The relative transverse velocity is about 180 km s^{-1}, so the maximum duration of an eclipse would be $2(R_1 + R_2)/180$ seconds (where the radii are expressed in kilometres), or about 5 hours.

An indication that there may indeed be an eclipse is afforded by the Palomar radial-velocity observation of 1986 Jan 4, which was made one hour after conjunction and therefore possibly during an eclipse. The trace on that occasion shows the dips closely blended together, with the secondary on the positive-velocity side of the blend. Although in Section 3 above we affected to a view all disconcerting residuals with an air of lofty detachment, we did suffer a good deal of private pain at the incredible negative residuals (particularly the secondary's) given by that observation. An eclipse would explain them. If half the secondary star were eclipsed, half of the share of the dip that is attributed to it would really belong to the primary, whose velocity would then be found to be more positive than before. As for the secondary velocity, of course that *would* be found far too negative during egress from eclipse because we would only be seeing the approaching limb of the star.

If the rotational velocities of the stars are pseudo-synchronized (Hut 1981) with the orbit, the rotation periods are about 0.13 times the orbital period or about 7 days, corresponding to $v \sin i \simeq 9$ km s^{-1} for the primary (in exact agreement with the observed value) and 8km s^{-1} for the secondary (in reasonable agreement with the weakly determined observational value).

Although the model developed in this section fits the few known facts rather attractively, it is only fair to recall that such basis as it may have is largely circumstantial and in fact the only previously published datum has in effect been rejected. Even if the model proves to be broadly correct it may still require some adjustment to take account of the inaccuracies of assumptions such as the use of the Hyades relationship between colour and radial-velocity dip areas. The probable direction of the adjustment needed on that particular account is easily assessed: the average field star is likely to have smaller line-strengths in relation to its spectral type and therefore will need to be of later type than we have suggested in order to match the observed dip areas. Since the expected masses will then be smaller, such an adjustment further strengthens the likelihood of eclipses; it also tends to reduce the discrepancy with the *HD* type. Clearly, the next steps that need to be taken concerning HD 116093

are to watch for eclipses at the known times of conjunction and to obtain good spectra for classification purposes,

Acknowledgements

I am most grateful to the Palomar, Dominion Astrophysical and Geneva observatories for the use of their equipment, and to Dr R. E. M. Griffin for her assistance in using it.

Errata in Paper 15. Owing to an elementary arithmetical mistake, for which I apologize, the distance modulus of HD 106947 according to the model given in Table 3 of the paper was quoted as $4^m.44$ when it should have been $5^m.44$; the correction impairs the correspondence between the properties of the Coma star cluster and HD 106947, whose membership is now much less conclusive than the paper made it appear. The date of the reference to Trumpler in the bibliography should have been 1938.

References

Allen, C. W. 1973, *Astrophysical Quantities*, Athlone, London, pp. 206, 209.
Baranne, A., Mayor, M., Poncet, J. L. 1979, *Vistas Astr.*, **23**, 279.
Cannon, A. J., Pickering, E. C. 1920, *Ann. Harv. Coll. Obs.*, **95**, 127.
Fletcher, J. M., Harris, H. C., McClure, R. D., Scarfe, C. D. 1982, *Publ. astr. Soc. Pacific*, **94**, 1017.
Griffin, R. F., Gunn, J. E. 1974, *Astrophys. J.*, **191**, 545.
Hut,P.1981, *Astr.Astrophys.*, **99**,126.

J. Astrophys. Astr.(1988) **9,** 213–224

HD 115781 and HD 116204—Two RS CVn Binaries

R. F. Griffin† *The Observatories, Madingley Road, Cambridge, England CB3 0HA;*

Francis C. Fekel‡ *Dyer Observatory, Vanderbilt University, Nashville, Tennessee 37235, U.S.A.*

Received 1988 July 1; accepted 1988 August 29

Abstract. HD 115781 and HD 116204 (BL CVn and BM CVn) are shown to be RS CVn binaries with periods near 20 days. HD 115781 is double-lined; the primary type is about K1 III, while the secondary is probably a late-type subgiant. The masses of the two components are equal within observational error. There is substantial photometric variability with a period half the orbital period; it is attributed to ellipsoidal variation. HD 116204 is also of type K1 III. It shows exceptionally strong Ca II H and K emission, together with an emission-line spectrum typical of RS CVn stars in the *IUE* ultraviolet region, but Hα is an absorption line. The secondary star in the HD 116204 system has not been detected. The primary shows photometric variations, presumably due to starspots, with a period 5 per cent longer than the orbital period.

Key words: spectroscopic binaries—RS CVn stars—stars, individual

1. Introduction: Radial velocities and orbits

HD 115781 and HD 116204 were discovered to be RS CVn binaries as a result of their inclusion in a radial-velocity survey of late-type stars in the field surrounding the North Galactic Pole. All stars listed in the *Henry Draper Catalogue* (Cannon & Pickering 1920) as having spectral types of G5 or later and positions within 15° of the Galactic Pole were placed on the survey programme in 1968, for observation with the prototype photoelectric radial-velocity spectrometer (Griffin 1967) at Cambridge. Because of the size of the programme in relation to the observing time available for it, an interval of the order of a decade elapsed after the first observation of each of the stars discussed here before the second measurements—coincidentally made on the same date, 1980 May 14—revealed the binary natures of both objects.

In 1981–1984 the radial velocities of the two systems were monitored at Cambridge frequently and also, when opportunity arose, at other observatories equipped with

† *Guest Investigator, Palomar Observatory; Visiting Associate, Mount Wilson & Las Campanas Observatories, Carnegie Institution of Washington; Visiting Observer, Dominion Astrophysical Observatory, Victoria*

‡ *Guest Observer with the International Ultraviolet Explorer satellite; Visiting Astronomer, Kitt Peak National Observatory, [U.S.] National Optical Astronomy Observatories, operated by the Association of Universities for Research in Astronomy, Inc., under contract with the [U.S.] National Science Foundation*

photoelectric radial-velocity spectrometers. Altogether, 46 measurements were made of HD 115781 and 51 of HD 116204. They show that both systems have quite short periods, 18.692 and 20.625 days respectively, and both orbits have eccentricities that are indistinguishable from zero. In the case of HD 115781, six traces obtained at Palomar Observatory with the radial-velocity spectrometer on the 200-inch telescope (Griffin & Gunn 1974) near the nodes of the orbit showed a measurable secondary feature which has permitted the amplitude of the radial-velocity variation of the secondary star to be obtained as well as that of the primary. The journals of

Table 1. Radial-velocity observations of HD 115781, made at Cambridge except where otherwise noted.

Date	MJD	Velocity km s^{-1}	Phase	$(O-C)$ km s^{-1}
1971 Feb 16.16	40998.16	+23.9	0.934	−6.2
1980 May 14.00	44373.00	−57.5	181.487	−2.9
1981 Mar 13.11	44676.11	−20.0	197.703	+3.4
May 17.39*	741.39	+4.0	201.195	−0.5
31.96	755.96	+32.2:	.975	−1.1
Dec 4.56*	942.56	+32.0	211.958	−0.3
4.56*S	942.56	−51.8	.958	+1.8
6.56*	944.56	+31.0	212.065	+0.7
6.56*S	944.56	−49.8	.065	+1.7
1982 Jan 10.23	44979.23	+26.2	213.920	−2.1
11.12	980.12	+30.2	.967	−2.7
21.13	990.13	−58.8:	214.503	−4.0
21.25	990.25	−56.1	.509	−1.4
22.22	991.22	−52.2	.561	−0.6
Mar 2.08	45030.08	−35.0	216.640	+3.7
4.01	032.01	−8.9	.743	+3.4
5.04	033.04	+2.7	.798	−0.1
5.15	033.15	+3.1	.804	−1.3
6.02	034.02	+19.2	.851	+3.4
6.09	034.09	+22.1	.855	+5.5
6.17	034.17	+20.2	.859	+2.6
7.97	035.97	+27.6	.955	−4.5
8.07	036.07	+30.2	.961	−2.3
8.19	036.19	+34.5	.967	+1.6
13.04	041.04	−5.4	217.226	−1.5
16.12	044.12	−46.1	.391	−1.3
Apr 7.91	066.91	−43.3	218.610	+1.3
15.00	074.00	+33.9	.990	+0.1
May 5.02	094.02	+32.8	220.061	+2.1
25.96	114.96	+10.3	221.181	+2.2
29.93	118.93	−43.9	.394	+1.3
Nov 23.58*	296.58	+24.7	230.898	−0.3
23.58*S	296.58	−45.2	.898	+1.1
24.58*	297.58	+31.2	.951	−0.6
24.58*S	297.58	−52.9	.951	+0.2
25.57*	298.57	+34.8	231.004	+0.9
25.57*S	298.57	−58.2	.004	−3.0

Table 1. Continued.

Date	MJD	Velocity km s^{-1}	Phase	$(O-C)$ km s^{-1}
1983 Feb 3.54†	45368.54	−9.3	234.748	+1.8
4.47†	369.47	−3.4	.797	−5.9
23.14	388.14	−5.1	235.796	−7.3
28.15	393.15	+32.9:	236.064	+2.6
1984 Jan 22.56‡	45721.56	−40.0	253.634	0.0
22.56‡S	721.56	+19.1	.634	−0.2
Apr 3.02	793.02	−55.5	257.457	−2.3
15.97	805.97	+18.4	258.150	+2.8
17.05	807.05	−1.9	.208	−3.1
21.03	811.03	−48.9	.421	+0.5
25.91	815.91	−26.8	.682	+2.1
May 9.01	829.01	−41.8	259.383	+1.5
11.01	831.01	−53.8	.490	+0.9
11.96	831.96	−53.8	.540	−0.4
Nov 29.58*	46033.58	−31.1	270.327	0.0
Dec 2.54*	036.54	−55.0	.485	−0.4
2.54*S	036.54	+35.6	.485	+1.5

* Observed with 200-inch telescope.
† Observed with DAO 48-inch telescope.
‡ Observed with Kitt Peak coudé feed telescope.
S Velocity of secondary component.

Table 2. Photoelectric radial-velocity observations of HD 116204, made at Cambridge except where otherwise noted.

Date	MJD	Velocity km s^{-1}	Phase	$(O-C)$ km s^{-1}
1968 Apr 24.05	39970.05	+17.8	0.926	−0.5
1980 May 14.92	44373.92	−3.0	214.445	+0.2
1981 Jan 17.24	44621.24	−3.0	226.436	0.0
Mar 13.11	676.11	+15.9	229.097	−1.5
Apr 28.01	722.01	+1.3	231.322	−1.4
May 5.01	729.01	+1.3	.662	−0.3
July 18.91	803.91	+3.1	235.293	−1.6
1982 Jan 10.22	44979.22	+10.9	243.793	0.0
21.16	990.16	+3.1	244.323	+0.5
Mar 4.12	45032.12	+1.0	246.358	+0.5
8.10	036.10	−3.0	.551	+0.3
13.06	041.06	+11.0	.791	+0.2
Apr 14.99	073.99	−0.1	248.388	+1.0
May 4.02	093.02	+4.1	249.310	+0.6
11.93	100.93	+2.9	.694	−0.9
25.96	114.96	0.0	250.374	+0.4
June 29.94	149.94	+17.5	252.070	−0.9
July 19.89	169.89	+17.9	253.037	−1.3
28.89	178.89	−3.4	.474	+0.4
Nov 23.58*	296.58	+13.1	259.180	+0.3
25.58*	298.58	+6.3	.277	+0.5

Table 2. Continued

Date	MJD	Velocity km s^{-1}	Phase	$(O-C)$ km s^{-1}
1983 Jan 19.13	45353.13	+18.3	261.922	+0.2
Feb 3.51†	368.51	+2.8	262.667	+0.8
4.46†	369.46	+5.6	.713	+0.5
10.41†	375.41	+20.5	263.002	+1.0
13.47†	378.47	+14.1	.150	−0.6
15.35†	380.35	+8.6	.241	+0.2
16.39†	381.39	+3.9	.292	−0.9
18.47†	383.47	−1.6	.393	−0.2
23.09	388.09	−0.9	.617	0.0
28.12	393.12	+16.6	.861	+1.3
Mar 7.10	400.10	+12.3	264.199	+0.8
11.13	404.13	−1.1	.394	+0.3
15.07	408.07	−3.1	.585	−0.8
Apr 16.01	440.01	+18.9	266.134	+3.3
May 9.96	463.96	+4.3	267.295	−0.2
1984 Apr 3.03	45793.03	+8.4	283.250	+0.6
14.02	804.02	+8.3	.783	−1.9
15.98	805.98	+16.0	.878	−0.2
17.03	807.03	+18.4	.929	0.0
20.98	810.98	+16.2	284.120	−0.1
23.96	813.96	+5.8	.265	−0.9
24.96	814.96	+1.7	.313	−1.6
25.99	815.99	−0.3	.363	−0.5
26.93	816.93	−1.0	.409	+1.0
May 8.98	828.98	+19.5	.993	0.0
11.02	831.02	+16.7	285.092	−0.9
11.92	831.92	+15.3	.135	−0.2
12.96	832.96	+13.0	.186	+0.6
13.93	833.93	+9.0	.233	0.0
Nov 30.52*	46034.52	+20.7	294.958	+1.6

* Observed with 200-inch telescope.
† Observed with DAO 48-inch telescope.

observations are set out in Tables 1 and 2 and the orbital elements derived from them appear in Table 3. The orbits are illustrated in Fig. 1.

2. Spectral types and RS CVn characteristics

Both the stars of interest are giants. The only MK classification from a slit spectrogram is that of K1– III given by Keenan (1940) for HD 116204. An objective-prism classification of G8 III published for the same star by Zaytseva (1973) is less accordant with the $(B-V)$ colour of about $1^{m}.16$ (Walker 1971, Häggkvist & Oja 1973, Oja 1985). There is an Abastumani type of K1 V for HD 115781 (Tchipashvili 1973), but we are inclined to doubt the luminosity class. Unpublished photometry in the Copenhagen system, obtained by Dr G. A. Radford and one of the present authors (R. F. G.) at

Table 3. Circular orbital elements for HD 115781 and HD 116204.

	HD 115781	HD 116204
P (days)	18.6917 ± 0.0011	20.6252 ± 0.0018
γ (km s^{-1})	-10.46 ± 0.28	$+7.80 \pm 0.14$
K_1 (km s^{-1})	44.3 ± 0.4	11.71 ± 0.21
K_2 (km s^{-1})	44.7 ± 1.0	
q [mass ratio]	1.009 ± 0.021	
T_0(MJD)	45279.80 ± 0.03	45251.62 ± 0.05
$a_1 \sin i$ (Gm)	11.40 ± 0.10	3.32 ± 0.06
$a_2 \sin i$ (Gm)	11.50 ± 0.26	
$f(m_1)$ ($M_\odot$)	0.169 ± 0.004	0.00344 ± 0.00018
$f(m_2)$ ($M_\odot$)	0.174 ± 0.012	
$M_1 \sin i$ ($M_\odot$)	0.69 ± 0.05	
$M_2 \sin i$ ($M_\odot$)	0.68 ± 0.02	
*R.m.s. residual (km s^{-1})	2.6	0.9

*The value for HD 115781 is for Cambridge observations. Palomar observations of the primary (weight 8) have r.m.s. errors of 0.9 km s^{-1}; those of the secondary have errors of 1.8 km s^{-1}.

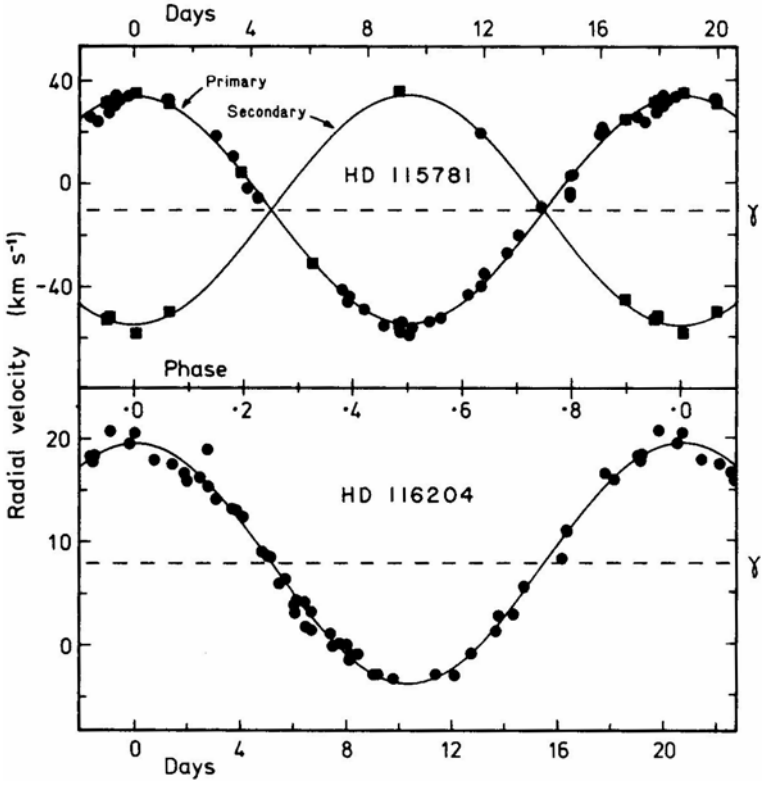

Figure 1. The computed radial-velocity curves of HD 115781 and HD 116204, with the observed radial velocities plotted. In the case of HD 115781, the Palomar observations are distinguished by being plotted as squares.

Palomar Observatory in 1976 and reduced by Dr L. Hansen shows that HD 115781, like HD 116204, is a giant.

Late-type giant stars in orbits with periods as short as about 20 days generally show peculiarities of the RS CVn type, arising from rapid rotation (usually more or less synchronized with the orbital motion) and from the heavily spotted surfaces and extraordinary chromospheric activity which seem to be corollaries of such rotation. The gross observable characteristics engendered by those peculiarities include rotational modulation of the apparent magnitude, rotational broadening of the spectral lines, and unusually strong emission lines in the spectra all the way from Hα and H and K down into the X-ray region.

A certain amount of evidence for all three of these characteristics was already available for HD 116204 without the need for special observations, although it has been amplified by the investigations reported below. The discordance between the V magnitude of 7.21 found by Walker (1971) and the 7.14 given by Häggkvist & Oja (1973) is surely too great to be ascribed to observational error and could well be interpreted as evidence of the small-amplitude variability typical of an RS CVn binary. Clear evidence of rotational broadening is present in radial-velocity traces of HD 116204. Moderate broadening was noticed in Cambridge traces; Palomar observations allow it to be quantified. All of the three Palomar traces available give $v \sin i$ values within half a km s^{-1} of 15 km s^{-1}; Fekel, Moffett & Henry (1986) found a value of 15 ± 2kms^{-1} from spectroscopy at Kitt Peak. When we were already actively observing the star, Bidelman (1983) noted HD 116204 as having the most extreme H and K emission among all the G-and K-type emission objects that he discovered in the first 100 fields surveyed with the then new 10° objective prism on the Burrell Schmidt. The emission is illustrated in Fig. 2, which is reproduced from a spectrogram obtained with the coudé spectrograph of the Mount Wilson 100-inch reflector at 10 Å mm^{-1} on 1985 June 12. The spectrum, and the tremendous strength of the H ánd K emission, is remarkably similar to that of the extreme RS CVn star HR 1099. A reproduction of a spectrogram of that star, taken with the same equipment as Fig. 2 and identified by its alias ADS 2644 A, has been published by Wilson (1963).

HD 115781 is a magnitude fainter than HD 116204 and has been mentioned less frequently in the literature. Häggkvist & Oja (1973) gave its magnitudes as $V = 8.13$, $(B - V) = 1.14$, $(U - B) = 0.94$, and since they only observed it on a single night they did not discover its variability. Palomar radial-velocity traces, of which an example is seen in Fig. 3, show an extraordinary rotational broadening, amounting to nearly 40 km s^{-1}. That broadening is only too apparent on traces made at Cambridge also: it creates considerable difficulty there in measuring a velocity at all, and is responsible for the unusual raggedness of the orbit illustrated in Fig. 1. It was necessary in the orbital solution to attribute Palomar observations 8 times the weight of the Cambridge ones to obtain reasonable equality in the weighted variances.

Fig. 3 shows that the secondary component of HD 115781 does not by any means share the great rotational broadening of the primary; in fact it is not clear that there is any broadening at all, although the secondary feature is so weak (2 per cent of the 'continuum') that we prefer not to attempt from the Palomar observations to set a stringent upper limit to the rotation that might be present. The relative areas of the two 'dips' are approximately 19:1. Thus, on the purely arbitrary assumption that the two stars have the same surface brightness, the ratio of radii would be about $4\frac{1}{2}$:1; and on the further assumption of equal rotation periods the value of $v \sin i$ for the secondary

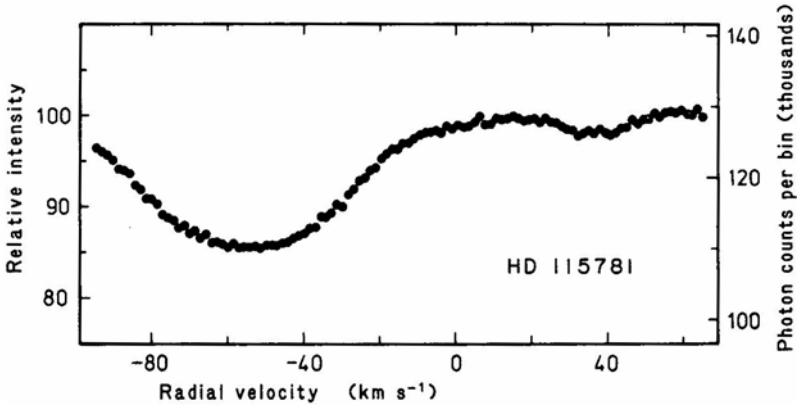

Figure 3. Palomar radial-velocity trace of HD 115781, obtained on 1984 December 2, showing the small secondary feature and the great rotational broadening of the primary. The FWHM of an unbroadened dip is about 20 km s^{-1}.

would be between 8 and 9 km s^{-1}, a value which is not inconsistent with Palomar radial-velocity traces such as that shown in Fig. 3 or with the Kitt Peak spectroscopy referred to in Section 4. It is noteworthy that, despite the disparity in their respective signatures on radial-velocity traces, the two components of HD 115781 have masses that are identical within the observational uncertainty of about 2 per cent.

The fit of a computed profile to the trace of HD 115781 in Fig. 3 leaves something to be desired. If a small discrepancy near the middle of the trace is ascribed to a third component in the system, a beautiful match between the computed and observed traces can be obtained. However, it is axiomatic that the more degrees of freedom one permits oneself the more accurately one can model anything; and in this case the "third component" turns out to have a radial velocity that is considerably (9kms^{-1}) removed from the γ-velocity of the binary system, so it is not an obviously attractive proposition. We would need substantially more evidence than is provided by Fig. 3 before we would seriously propose HD 115781 as a triple system. Our other Palomar radial-velocity traces have appreciably lower signal/noise ratios and offer little assistance in this matter.

The Copenhagen photometry referred to above gives large values of the quantity res (k) for both stars, $0^m.17$ for HD 115781 and ($0^m.19$ for HD 116204. Those values would normally be associated with a substantial degree of compositeness in the spectra of the objects concerned, *i.e.* with significant contributions from two or more sources at very different temperatures. The two observed components of HD 115781 might account for the photometric compositeness of that object, but the secondary of HD 116204 has not been detected. Of course a heavily spotted star has different areas of its surface at substantially differing temperatures and might be able, on its own, to mimic the photometric pecularities to which a large value of res (k) alerts us.

3. Photometry

At our suggestion, photometric observers have made intensive measurements of the two systems in order to search for variations associated with the rotation of the

primaries. Such variations have indeed been demonstrated in both systems. Heiser (1985) reported Hall and his collaborators as finding HD 115781 to show a variation of $0^m.20$—a very large amplitude—with a period of 18.7 days. That was presumably the same work as was published by Lines *et al.* (1985), which indicates that the magnitude variation is sinusoidal with a period of 9.31 ± 0.06 days—half the orbital period, within observational error—phased in such a way that maximum brightness is reached at times of quadrature. Lines *et al.* accordingly considered HD 115781 to be an ellipsoidal variable, in which the changing brightness arises from the changing areas presented to the observers' view of a star which is considerably elongated along the direction towards its companion. However, v sin i measurements from Palomar radial-velocity traces do not show a clear correlation with orbital phase. For HD 116204, Boyd, Genet & Hall (1984) found an amplitude of $0^m.06$ and a period of 21.7 ± 0.2 days; more extensive photometry has been published by Mohin & Raveendran (1987). In the case of HD 116204 there is a definite difference of 5 ± 1 per cent between the rotational and orbital periods, the rotational period being the longer of the two.

It is quite appropriate that both of our new RS CVn stars are in the constellation of Canes Venatici; they have taken the variable-star designations BL and BM CVn (Kholopov *et al.* 1987).

4. Spectroscopic observations

4.1 *HD 115781*

Because the rapid rotation of HD 115781, in relation to its spectral type, suggested that it is an RS CVn binary, spectroscopic observations were obtained at Hα and in a wavelength region centred on λ6430 Å to search for evidence of chromospheric activity. The Hα observations were obtained with the McDonald Observatory 2.1-m reflector, coudé spectrograph, and 1728-element reticon detector. The wavelength range covered was 235 Å at a resolution of 0.55 Å. The Hα line was not centred in the field but was positioned so that lines near λ6400 Å were included. Several observations were also obtained with the Kitt Peak coudé feed telescope and TI CCD detector centred on a wavelength of 6430 Å; those observations have a wavelength range of 90 Å and a resolution of 0.23 Å. From the one double-lined Kitt Peak observation v sin i values of 35 ± 2 and 7 ± 2km s^{-1} were determined for the primary and secondary, respectively (Fekel, Moffett & Henry 1986).

Smith & Bopp (1982) found that the Hα absorption feature of chromospherically active systems is weaker than that of stars which are not chromospherically active but are otherwise of similar type. Fig. 4 shows the Hα line of HD 115781 in comparison with that of α Ari. The equivalent width of the line in HD 115781 is 1.1 Å, several tenths of an Ångström less than that of α Ari, thus indirectly supporting our belief that HD 115781 is an RS CVn binary.

4.2 *HD 116204*

Spectroscopic observations were obtained at Hα, at λ6430 Å, and at far-ultraviolet wavelengths, to search for evidence both of a secondary component and of chromospheric activity. The ultraviolet observation (Simon & Fekel 1987) was obtained with

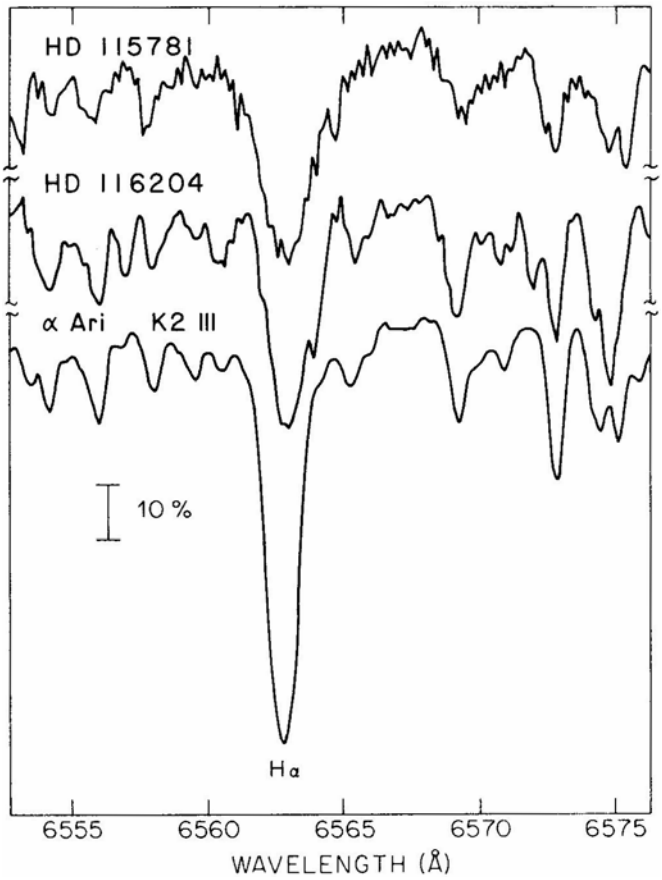

Figure 4. The Hα region of the spectra of HD 115781 and 116204, compared with α Ari, an inactive K2 III star. The bar shows the intensity corresponding to 10 per cent of the continuum.

the *International Ultraviolet Explorer* satellite in the short-wavelength region, λλ1200–2000 Å, with the SWP camera; the mid-exposure epoch was MJD 45692.118. This low-resolution observation (6 Å resolution) was obtained through the large aperture and was absolutely calibrated. Fig. 5 shows the far-ultraviolet emission-line spectrum, which is typical of chromospherically active stars. We have converted the emission-line fluxes tabulated by Simon & Fekel (1987) to surface fluxes (Table 4) on the basis of an estimated stellar angular diameter of 6.98×10^{-4} arcsec. For the 1983/4 observing season, Strassmeier *et al.* (1989) found the photometric period and an epoch of minimum light to be 21.13 ± 0.21 days and MJD 45691.0 ± 0.4 respectively. Thus the ultraviolet fluxes correspond to a rotational phase of 0.05 after spot maximum. Rodonò *et al.* (1987) have shown that the surface fluxes of active RS CVn stars are strongly phase-dependent, with ratios of active to quiescent fluxes ranging from about 2 to 9 for the systems they observed. They found that that ratio is generally largest for the higher-excitation lines such as C IV and He II. Table 5 compares the surface fluxes of HD 116204 with the ranges of fluxes found for V711 Tau, II Peg and AR Lac (Rodonò *et al.* 1987). The lines fluxes for II Peg show strong enhancements at the time of spot

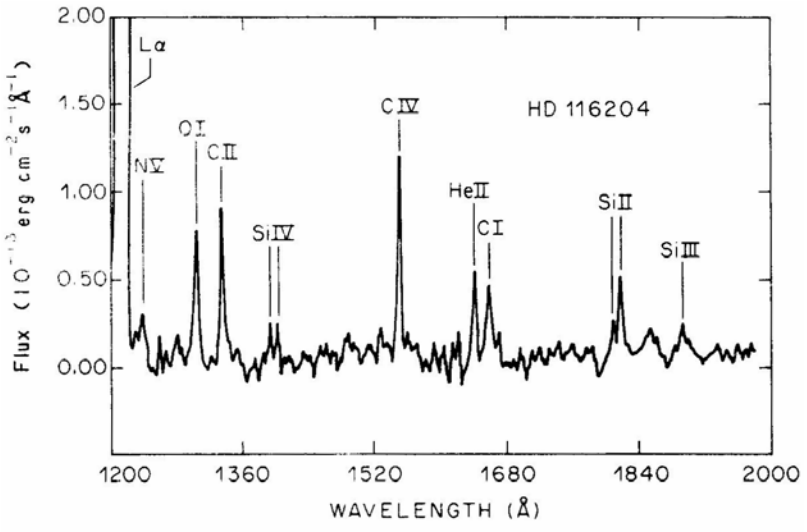

Figure 5. Spectrum SWP 21859 of HD 1162.04, obtained with the short-wavelength camera of *IUE*. The observed flux at the Earth is plotted as a function of wavelength. The Lyman-α emission is geocoronal in origin.

Table 4. Ultraviolet emission-line fluxes of HD 116204.

Line	Wavelength Å	Observed flux 10^{-13} erg cm^{-2} s^{-1}	Surface flux 10^{4} erg cm^{-2} s^{-1}
N v	1240	2.6	9.1
O i	1305	6.6	23.0
C ii	1335	6.0	20.9
Si iv	1393, 1402	2.3	8.0
C iv	1550	8.2	28.6
He ii	1640	3.8	13.3
C i	1657	4.1	14.3
Si ii	1807, 1818	4.3	15.0
Si iii	1892	1.0	3.5

Table 5. Surface fluxes (10^{4} erg cm^{-2} s^{-1})

Star	O i	C ii	C iv	He ii
HD 116204	23.0	20.9	28.6	13.3
V711 Tau*	16.6–29.9	25.5–37.0	36.7–49.1	11.2–19.3
II Peg*	7.6–15.3	9.7–27.9	21.4–98.3	10.1–25.5
AR Lac*	7.2–20.2	9.6–25.5	18.0–76.2	7.2–22.7

* Extreme observed values at different phases for the combined system, *i.e.* by using the first conversion factor (F/f) between surface and observed fluxes in Table 7 of Rodonò *et al.* (1987).

maximum, and the higher-excitation lines of the Kl IV component of V711 Tau show a similar although more modest correlation with phase. Whether that is also the case for HD 116204 remains to be determined.

In very few of the RS CVn binaries is the Hα feature in emission above the continuum. The few RS CVn systems with Hα in emission, such as HR 1099, UX Ari and II Peg, have very strong Ca II H and K lines. Thus, the fact that HD 116204 has very strong Ca II emission suggested the possibility that Hα might also be in emission. As Fig. 4 shows, this is not the case for HD 116204, although the absorption feature does appear to be weaker than in α Ari; its equivalent width is approximately 0.8 Å. No features attributable to the secondary star are apparent in the observations obtained in the red.

5. Line broadening and stellar dimensions

The great line broadening of HD 115781 and the ellipsoidal light variations might suggest that the K giant star is close to filling its Roche lobe. The extreme range of the values that we have obtained for v sin i is from 34 to 41 km s^{-1}, with a mean of 37.6 ± 0.7 km s^{-1}, although no doubt the standard error of the mean is an optimistic value of the true error in view of the systematic effects of the assumptions that go into the estimation of the rotational velocity from the observed line-width. There is no convincing relationship between the observed widths and the orbital phases of the observations. With a rotation period of 18.7 days, a v sin i value of 37.6 km s^{-1} corresponds to a radius R_1 of approximately 14/sin i $R_\odot$. The separation (a_1 + a_2) of the stars is known from the orbit to be 22.9/sin i Gm, = 32.9/sin i $R_\odot$; that separation and a mass ratio of unity lead to a minimum Roche-lobe radius of 12.5/sin i $R_\odot$ (Plavec 1968). The true Roche-lobe radius will be greater than that minimum in the direction between the centres of the two stars. However, the comparison certainly suggests that if the primary does not fill its Roche lobe—and we have no spectroscopic evidence that mass transfer is occurring—it is extremely close to doing so.

The absence of eclipses (Lines *et al.* 1985) shows that cos $i > (R_1 + R_2)/(a_1 + a_2)$ or $i \lesssim 63°$. The masses of 0.7/sin i $M_\odot$ found for each component from the orbit suggest that sin $i \gtrsim 0.7$ ($i \gtrsim 45°$). The implied range of R_1 of 11 to 15 Gm (about 15 to 20 $R_\odot$) is very much what would be expected for a normal giant of the type (K1 III) attributed to the integrated light of the system. The radius of the secondary cannot be much less than 3 $R_\odot$—much larger than any late-type main-sequence star—so the secondary itself must be an evolved object. In HD 155638 and HD 158393 (Fekel, Moffett & Henry 1986; Lloyd Evans, Balona & Fekel 1987), chromospherically active systems which share most of the known characteristics of HD 115781, the secondary is an F-type subgiant.

The rotational velocity of HD 116204 leads to a primary radius of 4.5/sin i Gm (6.5/sin i $R_\odot$). In the absence of any information on the secondary or on sin i this result is less significant than that obtained for HD 115781, but since the radius of the primary orbit is only 3.32/sin i Gm it does show that the centre of gravity of the system lies well within the primary star. Mohin & Raveendran (1987) give photometric reasons for believing that the system is seen at a low inclination, as indeed the smallness of the mass function also indicates; however, they also think that the mass ratio is near unity

and consequently expect the secondary star to be detectable spectroscopically, which (at least by us) it is not.

Acknowledgements

We are very grateful for the use of facilities at the Palomar, Kitt Peak, Mount Wilson, Dominion Astrophysical and *IUE* observatories. We wish to thank Drs G. Henry and G. Sonneborn for obtaining several of the spectroscopic observations, and Dr M. Rodonò for his helpful referee's report. This research was in part supported by the UK SERC and by NASA grant NAG5–397.

References

Bidelman, W. P. 1983, *Astr. J.*, **88,** 1182.
Boyd, L. J., Genet, R. M., Hall, D. S. 1984, *Inf. Bull. var. Stars*, no. 2546.
Cannon, A. J., Pickering, E. C. 1920, *Ann. Harv. Coll. Obs.*, **95**.
Fekel, F. C., Moffett, T. J., Henry, G. W. 1986, *Astrophys. J. Suppl.*, **60**, 551.
Griffin, R. F. 1967, *Astrophys. J.*, **148,** 465.
Griffin, R. F., Gunn, J. E. 1974, *Astrophys. J.*, **191,** 545.
Häggkvist, L., Oja, T. 1973, *Astr. Astrophys. Suppl.*, **12,** 381.
Heiser, A. M. 1985, *Bull. Amer. astr. Soc.*, **17,** 145.
Keenan, P. C. 1940, *Astrophys. J.*, **91,** 506.
Kholopov, P. N., Samus, N. N., Kazarovets, E. V., Kireeva, N. N. 1987, *Inf. Bull. var. Stars*, no. 3058.
Lines, R. D., Barksdale, W. S., Stelzer, H. J., Hall, D. S. 1985, *Inf. Bull. var. Stars*, no. 2728.
Lloyd Evans, T., Balona, L. A., Fekel, F. C. 1987, *Mon. Not. R. astr. Soc.*, **226,** 813.
Mohin, S., Raveendran, A. V. 1987, *J. Astrophys. Astr.*, **8**, 389.
Oja, T. 1985, *Astr. Astrophys. Suppl.*, **61,** 331.
Plavec, M. 1968, in *Adv. Astr. Astrophys.* (Academic Press, New York), **6**, 220.
Rodonò, M. Byrne, P. B., Neff, J. E., Linsky, J.L., Simon, T., Butler, C. J., Catalano, S., Cutispoto, S., Doyle, J. G, Andrews, A. D. Gibson, D. M. 1987, *Astr. Astrophys.*, **176,** 267.
Simon, T., Fekel, F. C, Jr., 1987, *Astrophys. J.*, **316,** 434.
Smith, S. E., Bopp, B. W. 1982, *Astrophys. Lett.*, **22,** 127.
Strassmeier, K. G, Hall, D. S., Boyd, L. J., Genet, R. M. 1989, *Astrophys. J. Suppl.*, **69,** in press.
Tchipashvili, D. G. 1973, *Abast. Bull,* **44,** 3.
Walker, R. L. 1971, *Publ astr. Soc. Pacific*, **83,** 177.
Wilson, O. C 1963, *Astrophys. J.*, **138,** 832.
Zaytseva, E. I. 1973, *Abast. Bull.*, **44,** 55.

J. Astrophys. Astr. (1988) **9,** 225–229

The Low-Frequency Radio Spectrum of the Continuum Emission from the undisturbed Sun

K. R. Subramanian & Ch. V. Sastry *Indian Institute of Astrophysics, Bangalore 560034,* and *Raman Research Institute, Bangalore 560034*

Received 1988 June 29; accepted 1988 September 6

Abstract. The low-frequency radio spectrum of the continuum emission from the undisturbed Sun is determined for 24 days during the period 1985 May-September. It is found that the spectral index varied from + 1.6 to +3.6 during this period. It is suggested that the large positive spectral indices are due to the existence of temperature gradients in the outer corona.

Key words: Sun, low-frequency radio observations—Sun, corona

1. Introduction

Very few measurements of the flux densities and spectra of the low frequency ($\leqslant$100 MHz) radio emission from the undisturbed Sun have been made, on a synoptic basis. The difficulties in making such measurements were pointed out by Aubier Leblanc & Boischot (1971) and Erickson *et al.* (1977). Briefly, the problems deal with accurate calibration, and base-line determination due to the low contrast between the solar brightness and the sky background temperature. The only measurements available, are due to (1) Aubier, Leblanc & Boischot (1971) who published only one set of flux densities at three low frequencies in the range 60 to 29 MHz and (2) Erickson *et al.* (1977) who reported two sets of flux densities in the frequency range 109 to 19 MHz, and computed the spectral index. The variations of the spectral index were not investigated.

We have used a broad-band antenna system to measure the flux densities of the undisturbed Sun at four low frequencies in the range 64 to 36 MHz. We report here on a series of measurements made, during the solar minimum period 1985 May-September, when the transient burst activity of the Sun was absent.

2. Observations

The antenna system consists of 64 bi-conical dipoles placed in corner reflectors. The dipoles are designed for operation in the frequency range 70 to 30 MHz, with a VSWR$\leqslant$2. The antenna is divided into two groups of 32 elements in the NS direction. Diode delay shifters are used to steer the beam of each group to ± 45° in zenith angle instantaneously. The EW and NS beamwidths of the array at various frequencies are listed in Table 1. The collecting area is approximately 2500 m^2. The signals collected

Table 1. Antenna parameters and measured maximum, minimum and average flux densities of the Sun at various frequencies during the period 1985 May-September.

Frequency MHz	Flux Density (Jy)			HPBW (Degrees)	
	Maximum	Minimum	Average	E−W	N−S
36.25	4212	1011	2436	12.27	7.60
45.70	6135	2402	3615	9.55	5.96
55.50	10616	3598	5878	7.80	4.88
64.25	18686	5513	11784	6.61	4.13

by the two groups are split into four frequency channels and the corresponding channels are correlated in four separate receivers. The bandwidth and time constant used were 1 MHz and 1 s respectively. The sensitivity of the system is better than 100 Jy at 64 MHz and $\leqslant$ 200 Jy at 36 MHz and so it is possible to detect extremely weak radio bursts from the Sun. We have monitored the Sun continuously during the period 1985 May-September and selected about 24 days on which there was no transient burst activity on the Sun. The radio sources Tau A, and Virgo A, were used as calibrators since their spectra are accurately known (Viner 1973) and their positions were close to the Sun during the above period. The following corrections were applied to the measured flux densities of the Sun at various frequencies:

(1) During the entire observing period the Sun's declination was within 5 degrees of the calibrating radio source, and on a majority of days the difference in declination was less than 2 degrees. Corrections ($\simeq$ 1 per cent) were applied for the change in the gain of the antenna with declination.

(2) Due to the incremental nature of the delay shifters there was in general a difference between the setting of the beam and the actual position of the source in the sky. The maximum difference was about 0.25 degrees and the correction due to this effect is $\leqslant$2 per cent.

(3) The distance between the two phase centres of the antennas in the NS direction is 32 metres. Therefore the visibility is slightly less than unity at all the four frequencies. The correction factors were calculated on the basis of uniform brightness distribution of the Sun.

(4) The major factor contributing to the error in the flux density measurement is the baseline determination. In our case the uncertainity due to this amounts to about 5 per cent at 65 MHz and 10 per cent at 35 MHz.

After taking into account all the above individual errors the total error in the measurement of flux densities is estimated to be about ±15 per cent. The maximum and minimum values of the measured flux densities at various frequencies are listed in Table 1. The minimum values agree well with the spectrum given by Erickson *et al* (1977).

The spectral index α (defined as in the expression $S \propto \cdot \nu^{\alpha}$) is calculated for each day using the observed flux densities at the four frequencies. It is found that the spectral index varied from +1.6 ± 0.4 to 3.9 ± 0.7. Out of a total number of 24 days for which spectral index measurements are available, on 18 days its value was > 2.5 and on 6

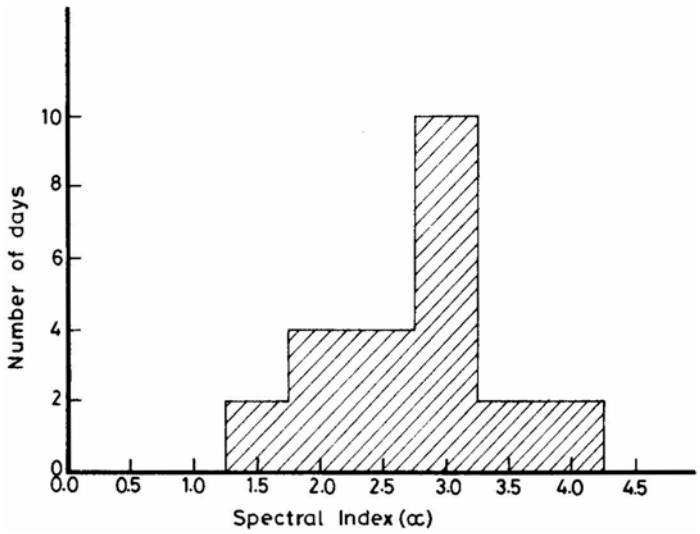

Figure 1. Distribution of spectral indices of the solar radio flux in the frequency range 64 to 36 MHz during the period 1985 May-September.

days value was < 2.3. Fig. 1 shows the distribution of spectral indexes during the period 1985 May-September.

3. Discussion

The solar radio emission in the frequency range 65 to 35 MHz originates entirely in the corona. The total flux density of the undisturbed Sun is the sum of the flux densities due to quiet Sun and the contributions due to bright regions. Kundu, Gergeley & Erickson (1977) measured the peak brightness temperatures of the quiet Sun and some sources of slowly varying component (SVC). According to Sastry, Shevgaonkar & Ramanuja (1981) the continuum emission from bright regions, identified as SVC at 34.5 MHz, can be explained on the basis of thermal emission from regions of enhanced density and temperature. Erickson *et al.* (1977) derived a spectral index of +2.3 based on observed flux densities of the quiet Sun in the range 109 to 19 MHz. We have computed the total flux of the quiet Sun at several frequencies in the range 65 to 35 MHz by determining the brightness temperature (T_B) distribution using the equation:

$$T_B(\nu) = T_e\,(1-e^{-\tau(\nu)})$$

and integrating over the solid angle subtended by the Sun at each frequency. Here $\tau(\nu)$ is the optical depth at any frequency ν. A spherically symmetric corona with an uniform temperature (T_e) of 10^6K and density distribution of Newkirk (1961) is assumed. The derived spectral index is $\simeq +2.3$ in good agreement with the observed value of Erickson *et al.* (1977). We found that it is not possible to increase the spectral index to values $\geqslant +3$ either by varying the density gradient or uniformly increasing the temperature and density over the entire corona. The possibility of nonthermal

contribution to the observed flux densities is then considered. This contribution at any frequency must originate at or above the corresponding plasma level. If it originates at the plasma level then one can consider, to a first approximation, that the thermal and nonthermal contributions are mixed along the line of sight. This is because the major contribution to the optical depth comes from a thin region located near the plasma level. The solution of the transfer equation in this case is:

$$T_B(\nu) = \left[T_e + \frac{T_N \nu^{\beta}}{\tau(\nu)} \right] [1 - e^{-\tau(\nu)}].$$

If the nonthermal radiation originates in front of the region of origin of thermal radiation then the equation describing the frequency dependence of the brightness temperature is

$$T_B(\nu) = T_e [1 - e^{-\tau(\nu)}] + T_N \nu^{\beta}.$$

Here T_N is the nonthermal brightness temperature and β is its spectral index. In the direction of the centre of the Sun the corona is optically thick ($\tau \geqslant 1$) in the frequency range 65 to 35 MHz for an uniform temperature of 10^6 K and Newkirk (1961) density distribution. Therefore the factor $(1–e^{-\tau(\nu)})$ is approximately equal to unity in the above equations. Generally, the nonthermal spectral index, β, is < 0 and can be < -3 for some processes like the plasma emission (Kaplan & Tsytovitch 1968). It is therefore clear from the above equations that the observed flux density should increase with decreasing frequency in the presence of nonthermal emission, for both cases discussed above. The sspectral index is not likely to attain large ($> +2.3$) positive values. This will not be the case if the nonthermal emission is confined to frequencies around 65 MHz only either due to the bandwidth of the emission process or the radial extent of the source. However, such a situation is most unlikely since the measured sizes of bright regions are $\simeq$20 arcmin and the bandwidth of the emission $\geqslant$100 MHz (Kundu, Gergeley & Erickson 1977). Another possibility is the existence of temperature gradients in the corona. We have assumed a temperature of 10^6K at the 65 MHz plasma level and decreasing to 0.5×10^6 K at the 35 MHz plasma level, and computed the expected flux densities from the quiet Sun, In this case the spectral index turns out to be $\simeq +3$ and will further increase if the density gradient is steeper than that given by Newkirk (1961). The existence of such gradients in the coronal temperature distribution can be inferred from arguements based on the constancy of the conducted energy flux. According to Athay (1976) the gradient would be about –0.4 K km^{-1} at 1.5 $R_\odot$ in the case of a hydrostatic conduction model and –0.8 K km^{-1} if coronal expansion is taken into account. It should also be pointed out here that Aubier, Leblanc & Boischot (1971) measured brightness temperatures of 0.60, 0.50 and 0.36 ($\times 10^6$ K)at 60, 37 and 29 MHz respectively and Erickson *et al.* (1977) measured brightness temperatures of 0.7 and 0.2 ($\times$ 10^6 K) at 74 and 26 MHz. Sastry, Shevgaonkar & Ramanuja (1983) measured peak brightness temperatures in the range 0.2 to 0.5 ($\times$ 10^6 K) at 34.5 MHz. These measurements also imply the existence of temperature gradients since the corona is optically thick at these frequencies and so the measured brightness temperatures are equal to the electron kinetic temperatures. It is therefore possible that temperature gradients of the order of – 1 K km^{-1} do exist at distances of the order of 1.5 $R_\odot$ in the solar corona, on some occasions.

It should however be pointed out that the density models of Newkirk (1961) and others may not be applicable to the corona on some occassions. If the densities in the

height range 1 to 2 $R_{\odot}$ are reduced by more than an order of magnitude then the corona might become optically thin at lower frequencies leading to steeper positive spectral indexes. Another possibility is the scattering of radiation by density inhomogeneities in the corona, (Aubier, Leblanc & Boischot 1971). The effect of scattering, if it exists, is to raise the level of reflection above the plasma level leading to smaller optical depths at lower frequencies. The resulting decrease in the brightness temperature, of the order of twenty to thirty per cent, is not sufficient to explain temperatures of about 0.2×10^6 K sometimes observed at 34.5 MHz by us (Sastry, Shevgaonkar & Ramanuja 1983). Also, according to McLean & Melrose (1985) the scattering hypothesis fails to account for the observed sizes and directivity of Type I solar radio bursts although it should offer a plausible explanation for these features. On this basis, the effect of scattering to explain coronal phenomena, is not favoured by many authors.

Acknowledgement

We would like to thank Mr. Nanje Gowda for his help in the construction and operation of the broadband antenna system.

References

Athay, R. G. 1976, *The Solar Chromosphere and Corona*: *Quiet Sun*, D. Reidel, Dordrecht.

Aubier, M., Leblanc, Y., Boischot, A. 1971, *Astr. Astrophys.*, **12**, 435

Erickson, W. C, Gergeley, T. E., Kundu, M. R., Mahoney, M. J. 1977, *Solar Phys.*, **54**, 57.

Kaplan, S. A., Tsytovitch, V. N. 1968, *Sov. Astr.* **11**, 956.

Kundu, M. R., Gergeley, T. E., Erickson, W. C. 1977, *Solar Phys.*, **53**, 489.

McLean, D. J., Melrose, D. B. 1985, *Solar Radiophysics*, Eds D. J. McLean & N. R. Labrum, Cambridge Univ. Press.

Newkirk, G. 1961, *Astrophys. J.*, **133**,983.

Viner, M. R. 1973, *Ph D Thesis*, Univ. of Maryland.

Sastry, Ch. V., Dwarakanath, K. S., Shevgaonkar, R. K., Krishan, V. 1981, *Solar Phys.*, **73**, 363.

Sastry, Ch. V., Shevgaonkar, R. K., Ramanuja, M. N. 1983 *Solar Phys.*, **87**, 391.

J. Astrophys. Astr. (1988) **9,** 231–236

One more Explanation of Superluminal Motion

V. Krishan *Indian Institute of Astrophysics, Bangalore 560034*

Received 1988 July 11; accepted 1988 October 14

Abstract. The occurrence of superluminal motion in extragalactic radio sources is believed to be quite common. Among others, the geometrical scattering of radio radiation can also cause superluminal expansion and or motion and halo formation, In this paper, the effectiveness of the stimulated Raman scattering in producing these features is investigated. The scattering medium is a plasma whose position, density and temperature decide the rate and angle of scattering. When the radiation from a stationary and constant source gets scattered from a stationary plasma, a halo is formed around the source. However, the scattering of a rotating radiation beam does produce superluminal motion of the virtual source. It is found that the plasma should have the characteristics of the emission-line regions and the intercloud medium in order to Raman scatter the radiation. Since the scattering is polarization dependent, it is possible to estimate the rotation of the electric vector along the direction of the apparent motion of a radio source.

Key words: extragalactic radio sources—superluminal motion—Raman scattering

1. Introduction

The several explanations of superluminal motion include: (i) a light house model in which a small change in the direction of electromagnetic beam causes a large traversal on a distant screen, exciting it in the process; (ii) relativistic beaming in which the source moving at a small angle to the line of sight with a speed slightly less than the speed of light, appears to move with superluminal speeds perpendicular to the line of sight due to light travel time effects (Blandford, McKee & Rees 1977; Blandford & Königl 1979); (iii) gravitational lensing which can magnify the real motion and the observed flux (Barnothy 1965). A critical discussion of these processes can be found in Scheuer (1984). Sanders (1974) used geometrical effects of a strong dipole magnetic field to account for superluminal expansion, though it is infested with the fast fall of flux with separation as pointed out by Blandford, McKee & Rees (1977). Wilson (1982) considered induced Compton scattering which though can give rise to light-echo effects and therefore superluminal motion but the strong frequency dependence of the motion is in contradiction with the observations. Here, we consider stimulated Raman scattering of radio radiation in a plasma such that the apparent motion of the source is actually the scattered radiation at increasing scattering angles. The advantages of this coherent scattering process are the preservation of the flux and its spectral characteristics after the scattering, provided the plasma parameters are chosen appropriately.

2. Stimulated Raman scattering in superluminal sources

Consider a large-amplitude plane-polarized electromagnetic wave $\mathbf{E}_0 = 2E_0\hat{\mathbf{e}}_0 \cos(\mathbf{K}_0 \cdot\mathbf{x} - \omega_0 t)$ incident on a plasma of electron density n and temperature T. Stimulated Raman scattering takes place when the incident wave (ω_0, $\mathbf{K}_0$) decays into a scattered wave (ω_s, $\mathbf{k}_s$) and an electron plasma wave (ω_e, $\mathbf{K}_e$) such that

$$\omega_0 = \omega_s + \omega_e,$$
$$\mathbf{K}_0 = \mathbf{K}_s + \mathbf{K}_e. \tag{1}$$

The equilibrium consists of electrons oscillating with velocity $V_0 = eE_0/m\omega_0$ in the field of the incident wave. Ions form a stationary background. Raman scattering is a nonlinear process and occurs when the incident radiation satisfies a threshold condition (Krishan 1988; Drake *et al.* 1974):

$$\left(\frac{V_0}{c}\right)^2 \geqslant \frac{1}{\psi^2}\left(\frac{\Gamma_p}{\omega_p}\right)\left(\frac{\Gamma_-}{\omega_0}\right) \tag{2}$$

Where

$$\psi = |\sin\phi|\cos\theta_e,$$
$$\sin^2\phi = \frac{\mathbf{E}_0 \cdot \mathbf{E}_s}{|E_0||E_s|},$$

and $\phi = \pi/2$ when the incident $\mathbf{E}_0$ and scattered $\mathbf{E}_s$ waves are polarized in the same direction; θ_e is the angle between $\mathbf{K}_0$ and $\mathbf{K}_e$,

$$\Gamma_p = \frac{\sqrt{\pi}}{2}\frac{\omega_p}{K_e^3\lambda_D^3}\exp\left[-\frac{1}{2K_e^2\lambda_D^2} - \frac{3}{4}\right] + \gamma_{ei} \tag{3}$$

is the damping rate of the electron plasma wave, and

$$\gamma_{ei} = (3\omega_p^3/4\pi n\lambda_D^3)$$

is the electron-ion collision frequency; $\Gamma_- = (\omega_p^2 y_{ei}/2\omega_s^2)$ is the collisional damping rate of the electromagnetic wave of frequency ω_s; $\omega_p = (4\pi ne^2/m)^{1/2}$ is the electron plasma frequency, λ_D is the Debye length. The maximum growth rate for stimulated Raman scattering is found to be:

$$\gamma_{sR} = \frac{V_0}{c}\psi(\omega_0\omega_p)^{1/2}$$

for $\omega_p \gg y_{sR} \gg \Gamma_p$ and $V_0/c > \Gamma_p/(\psi\omega_0\omega_p)^{1/2}$. In the above analysis $\omega_0 \gg \omega_e \simeq \omega_p$ and therefore $\omega_0 \simeq \omega_s$; $\omega_0 = K_0 c$, $K_e = 2K_0\cos\theta_e$ and $K_e\lambda_D < 1$ so that the electron plasma wave is only weakly damped. The threshold condition (2) is rewritten as:

$$(\omega_0)\left(\frac{L_{47}}{r_{pc}^2}\right) \geqslant \frac{2.85\times10^7 n_{10}^{1/2}(\omega_0/\omega_R)^{\alpha-1}}{\cos^2\theta_e\sin^2\phi\, T_4^3} \times$$
$$\times\left[\frac{2.67\times10^{39}n_{10}^3}{\cos^3\theta_e\,\omega_0^3}\exp\left\{-\frac{1.19\times10^{24}n_{10}}{\omega_0^2\cos^2\theta_e T_4} - \frac{3}{4}\right\} + 2.31\times10^{-2}n_{10}^2\right]. \tag{4}$$

The conditions $K_e\lambda_D < 1$ and $\omega_0 \gg \omega_p$ translate to

$$5.46 \times 10^9 n_{10}^{1/2} \ll \omega_0 < \frac{1.54 \times 10^{12}}{\cos\theta_e} n_{10}^{1/2} T_4^{-1/2}. \tag{5}$$

Here, $L = L_{47} \times 10^{47}$ erg s^{-1} is the luminosity of radio radiation and $R = r_{pc} \times 3 \times 10^{18}$ cm is the position of the scattering plasma of density $n = n_{10} \times 10^{10}$ cm^{-3} and temperature $T = T_4 \times 10_4$ K. α is the radiation spectral index such that the flux $F_\omega \propto \omega^{-\alpha}$, then the spectral variation of the luminosity $L_{47}(\omega)$ is given as:

$$L_{47}(\omega_0) = L_{47}(\omega_R)\left(\frac{\omega_0}{\omega_R}\right)^{-\alpha+1}$$

and the energy density $E_0^2(\omega_0)$ can be expressed as:

$$E_0^2(\omega_0) = \frac{0.37\, L_{47}(\omega_0)}{r_{pc}^2} = \frac{0.37}{r_{pc}^2} L_{47}(\omega_R)\left(\frac{\omega_0}{\omega_R}\right)^{-\alpha+1}$$

where ω_R is a reference frequency. Equation (4) describes the variation of luminosity as a function of the angle θ_e which is related to the scattering angle $\theta_s = \cos^{-1}[\mathbf{K_0} \cdot \mathbf{K_s}/(|\mathbf{K_0}|\,|\mathbf{K_s}|)]$ as, $\cos\theta_s = 1 - 2\cos^2\theta_e$, for given plasma parameters, when the incident radiation has attained a steady state with the plasma. It is known that the maximum allowed value of $K_e\lambda_D \sim 0.4$ for Raman scattering to remain valid. This gives the highest allowed frequency of the incident radiation as:

$$\omega_0|_{max} = \frac{6.17 \times 10^{11} n_{10}^{1/2} T_4^{-1/2}}{\cos\theta_e}\ s^{-1} \tag{6}$$

3. Superluminal motion

The superluminal sources generally show a core and jet configuration. The jet and features in it like knots show superluminal motion with respect to the core. In the case of radiation from a stationary source scattered by stationary plasma surrounding the source, since one does not observe a time delay between the direct and the scattered paths of the radiation, the formation of virtual images for different angles of incidence results in a halo around the source. Motion may appear to take place if the source is a delta function in time and the plasma is localized along a line perpendicular to the line of sight. The apparent superluminal motion of the jet can result if source radiation beam, the fixed end of which is in the core is rotating. Let us imagine a ring of plasma ($P_1\ P_2 \ldots$) at a distance of about one pc from the core A. The rotating radiation beam intercepts plasma at increasing angles ($P_1\ P_2 \ldots$) as it rotates (say anticlockwise in Fig. 1). To an observer at M the Raman scattered radiation appears to come from $A_1\ A_2 \ldots$ at successive times. The observed motion of a few milliarcseconds per year of ($A_1\ A_2 \ldots$) corresponds to a rotation rate $\frac{d\theta}{dt} = \left(\frac{mas}{yr}\right)\frac{PM}{AP} \simeq 10^3$ arcsee yr^{-1} of the beam ($AP_1, AP_2 \ldots$). The apparent motion takes place with a uniform speed if the beam rotates at a uniform rate. From Fig. 1, the scattering angle θ_s is given as $\theta_s \simeq 180 - \theta$ and recall that $\cos\theta_s = 1 - 2\cos^2\theta_e$.

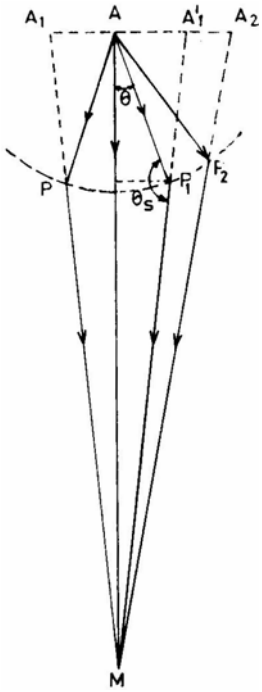

Figure 1. Apparent superluminal motion of radio source A through geometrical scattering.

As θ increases, θ_s decreases and so does cos θ_e. The variation with cos θ_e of threshold for Raman scattering is shown in Fig. 2. The threshold is found to be the lowest for θ_e between 30°–60° which corresponds to θ between 64°–127°. Thus for a given value of θ and θ_S, θ_e can be calculated and so can be the steady state value of (L_{47}/r_{pc}^2). In Fig. (3) (ω_0) (L_{47}/r_{pc}^2) is plotted against frequency for two values of θ for different sets of fixed

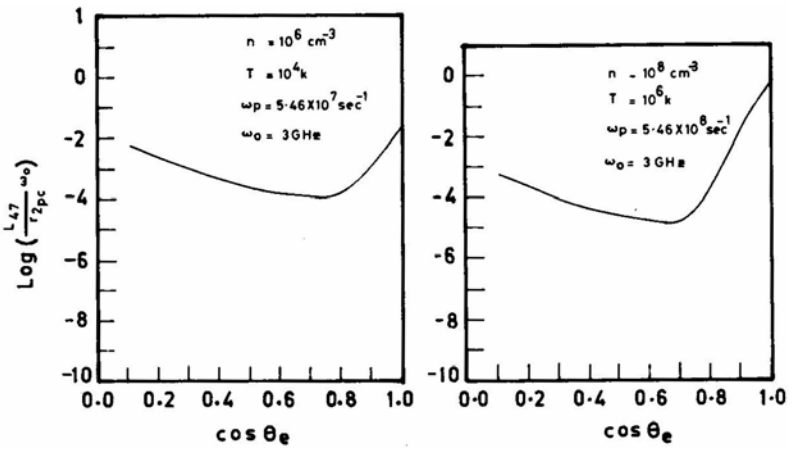

Figure 2. Variation of threshold luminosity with cos θ_e at a fixed frequency ω_0 = 3 GHz.

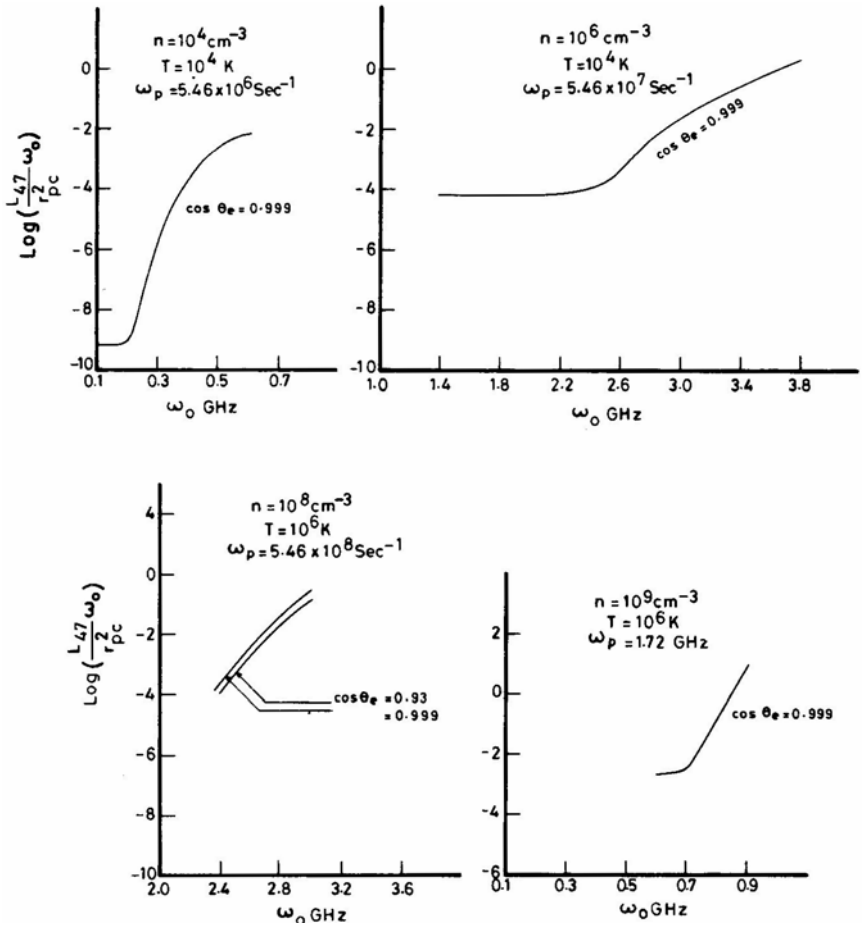

Figure 3. A plot of $(L_{47}\omega_0/r_{pc}^2)$ *vs* frequency ω_0 of the incident radiation for different parameters of the scattering plasma and α =1.

plasma parameters, It is seen that the Raman scattering can occur over a range of frequencies decided by the plasma parameters and the scattering angle for very reasonable values of the radio luminosity L. However, Raman scattering may not take place for very large and very small values of θ. The superluminal motion may appear to stop due to the increasing inefficiency of the Raman scattering to produce a virtual image. Raman scattering again becomes operative when the jet is about to complete a revolution and makes appropriate angles to the line of sight. But now, the resulting apparent motion will be towards the core, which has been reported though not yet confirmed in a couple of cases. In this scenario, the jet swings from one side of the core to the opposite side in about a rotation period of the radiation beam.

In reality, the scattering plasma may be in the form of clouds floating around the rotating radiation beam in the core, instead of being a continuous ring. The distribution may have different geometries: annular, disc, shell or filled sphere. Different perspectives of the plane of symmetry and the plane of the rotating beam are also possible. A choice of these can result in virtual images with several components,

possibly with diffuse haloes around them, exhibiting subluminal or superluminal motion. Sporadic increase in the incident luminosity would result in the brightening of different components at different times.

An attempt to fit observations with a two-component model leads to a large scatter in the plot of angular size of the source against time (Cohen & Unwin 1982). This has led to the suggestion that the observed source has several components. A model with several discrete clouds can give rise to a multi-component virtual image.

The stimulated Raman scattering is also a function of the angle between the electric vectors of the incident and scattered radiation. So, for a fixed value of the luminosity parameter (L_{47}/r_{pc}^2) and plasma parameters, one can calculate the amount of rotation that the electric vector of the scattered radiation had undergone with respect to the incident radiation.

4. Conclusion

The advantages of Raman scattering over any other incoherent process are (i) the scattered radiation has an intensity almost comparable to that of the incident because under the condition $\omega_0 \gg \omega_p$ very small amount of energy goes to the plasma waves (Figueroa *et al.* 1984), and thus the source does not diminish very much as it undergoes this apparent motion; and (ii) again because of $\omega_0 \gg \omega_p$ there is no significant spectral modification of the scattered radiation, and thus the characteristics of the real source are reproduced faithfully in the virtual source generated due to Raman scattering. Observations of the polarization differences between the core and the superluminally moving components will provide a test of the model.

Acknowledgements

The author is grateful to Prof. R. D. Blandford for suggesting this problem, to Prof. R. K. Varma, the referee, for pointing out that in the unrevised version a halo was produced instead of motion, and to Dr T. P. Prabhu for many very useful discussions during the revision of this paper.

References

Barnothy, J.M.1965, *Astr. J.*, **70,** 666.
Blandford, R. D., McKee, C. F., Rees, M. J. 1977, *Nature*, **267,** 211.
Blandford, R.D., Konigl, A.1979, *Astrophys. J.*, **232,** 34.
Cohen, M. H., Unwin, S. C. 1982, in *IAU Symp*. 97: *Extragalactic Radio Sources*, Eds D. S. Heeschen & C. M. Wade, D. Reidel, Dordrecht, p. 345.
Drake, J. F, Kaw, P. K, Lee, Y. C, Schmidt, G. 1974, *Phys. Fluids*, **17,** 778.
Figueroa, H., Joshi, C., Azechi, H., Ebrahim, N. A., Estabrook, K. 1984, *Phys. Fluids*, **27,**1887
Krishan, V.1988, *Mon. Not. R. astr. Soc.* **230,** 183.
Sanders, R. H. 1974, *Nature*, **248,** 390.
Scheuer, P. A. G. 1984, in *I A U Symp*. 110: *VLBI and Compact Sources*, Eds R. Fanti, K. Kellermann & G. Setti, D. Reidel, Dordrecht, p. 197.
Wilson, D. B. 1982, *Mon. Not R. astr. Soc.*, **200,** 881.

J. Astrophys. Astr. (1988) **9,** 237–241

The O III 52 μm/88 μm Emission-Line Ratio in Planetary Nebulae

F. P. Keenan *Department of Pure and Applied Physics, Queen's University of Belfast, Belfast BT7 1NN, N. Ireland*

K. M. Aggarwal *Department of Physics and Astrophysics, University of Delhi, Delhi 110007*

Received 1988 July 12; accepted 1988 October 20

Abstract. *R*-matrix calculations of electron impact excitation rates in O III are used to derive the electron-density-sensitive emission-line ratio $R = I\,(2s^2\,2p^{2\,3}P_2 - 2_S{}^2 2p^{2\,3}P_1)/I\,(2s^2 2p^{2\,3}P_1 - 2s^2 2p^{2\,3}P_0) = I\,(52\mu\text{m})/I\,(88\mu\text{m})$ for a range of electron temperatures (T_e = 5000–20000 K) and densities (N_e= 10–10^5 cm^{-3}) applicable to planetary nebulae. Electron densities deduced from the observed values of *R* in several planetary nebulae are in excellent agreement with those deduced from C1 III and Ar IV, which provides support for the accuracy of the atomic data adopted in the calculations.

Key words: emission-line diagnostics—electron densities—planetary nebulae

1. Introduction

Emission lines arising from transitions in ions of the carbon isoelectronic sequence have been frequently observed in the spectra of astronomical and laboratory plasmas (Keenan, Aggarwal & Berrington 1988; Keenan *et al.* 1988a; Davé *et al.* 1987; Stratton *et al.* 1987). Of particular interest are lines from O III, which have been detected in a wide variety of astronomical objects, including planetary nebulae (Aller & Keyes 1987), Seyfert galaxies (De Robertis 1987), QSOs (Filippenko 1985), H II regions (Evans & Dopita 1985), late-type stars (Basri, Linsky & Eriksson 1981) and the Sun (Widing, Feldman & Bhatia 1986). These transitions may be used to infer the electron temperature and density of the emitting region through diagnostic line ratios, although to calculate these reliably accurate atomic data must be employed, especially for electron impact excitation rates and oscillator strengths (Dufton & Kingston 1981), Several diagnostics have been developed over the past few years involving optical and ultraviolet lines in O III, probably the most accurate being those of Aggarwal (1985), Keenan & Aggarwal (1987) and Keenan *et al.* (1988b), which employ the electron impact excitation rates of Aggarwal (1983, 1985) calculated with the *R*-matrix code (Burke & Robb 1975; Berrington *et al.* 1978).

Emission lines of O III have also been observed in the far-infrared region of the spectra of gaseous nebulae (Lester *et al.* 1987; Rubin *et al.* 1988; Watson *et al.* 1981) at wavelengths of 52 μm ($2s^2 2p^{2\,3}P_2 - 2s^2 2p^{2\,3}P_1$) and 88 μm ($2s^2 2p^{2\,3}P_1 - 2s^2 2p^{2\,3}P_0$). In this paper we use the Aggarwal (1983, 1985) electron excitation rate calculations to

derive the emission line ratio $R = I(52\mu\text{m})/I(88\mu\text{m})$, and show that it is a useful density diagnostic for planetary nebulae.

2. Atomic data

The model ion adopted for O III was similar to those for other carbon-like ions such as Ca XV and Ne V discussed by Keenan and his co-workers (see, for example, Keenan, Aggarwal & Berrington 1988; Keenan *et al.* 1986, 1988a). Briefly, the 9 energetically lowest LS states were included in the calculation *viz.* $2s^2 2p^2\ ^3P$, ^1D, ^1S; $2s2p^3\ ^5S$, ^3D, ^3P, ^1D, ^3S and ^1P, making a total of 15 levels when the fine-structure splitting in the triplet terms was taken into account. Energies of all the ionic levels were taken from Moore (1971).

Electron impact excitation rates in O III were obtained from Aggarwal (1983,1985), while for Einstein A-coefficients the results of Froese Fischer & Saha (1985) were adopted. As noted by, for example, Seaton (1964), proton excitation may be important for transitions with small excitation energies, *i.e.* fine-structure transitions such as that in the $2s^2 2p^5\ ^2P$ ground term of Fe XVIII (Keenan & Reid 1987). However at the temperatures we are interested in excitation by protons is negligible and hence was not included in the calculations. For example, at T_e = 20000 K, protons add only 1–2 percent to the total excitation rates of the $^3P_0$–$^3P_1$, $^3P_0$–$^3P_2$ and $^3P_1$–$^3P_2$ transitions in the $2s^2 2p^2\ ^3P$ ground term of O III (Aggarwal, Baluja & Tully 1982).

3. Results and discussion

Using the atomic data discussed in Section 2 in conjunction with the statistical equilibrium code of Dufton (1977), relative O III line strengths were deduced for a range of electron temperatures (T_e= 5000–20000 K) and densities (N_e = 10–10^5 cm $^{-3}$) applicable to planetary nebulae (Kaler 1586; Barlow 1987). The following assumptions were made in the calculations: (i) that ionization to and recombination from other ionic levels is slow compared with bound-bound rates, (ii) that photoexcitation and de-excitation are negligible in comparison with the corresponding collisional rates, (iii) that all transitions are optically thin. Further details of the procedures involved may be found in Dufton (1977) and Dufton *et al.* (1978).

In Fig. 1 we plot the emission line ratio $R = I(52\ \mu\text{m})/I(88\ \mu\text{m})$ as a function of electron density at three electron temperatures, namely T_e = 5000,10000 and 20000 K; the results are also given in Table 1. It may be seen that the density sensitivity of the ratio is quite large, with R varying by a factor of approximately 16 between N_e = 10 and 10^5 cm^{-3}. However the temperature sensitivity is small with, for example, a factor of 2 change in T_e resulting in a 12 per cent or less variation in R. We note that our line ratios differ by up to 20 per cent from those calculated by Dinerstein, Lester & Werner (1985). These discrepancies are principally due to the adoption of improved electron impact excitation rates in the present analysis (see Aggarwal 1985 and Keenan & Aggarwal 1987 for more details).

The R ratios in several planetary nebulae have been obtained by Dinerstein, Lester & Werner (1985) using the 91-cm telescope of NASA's Kuiper Airborne Observatory

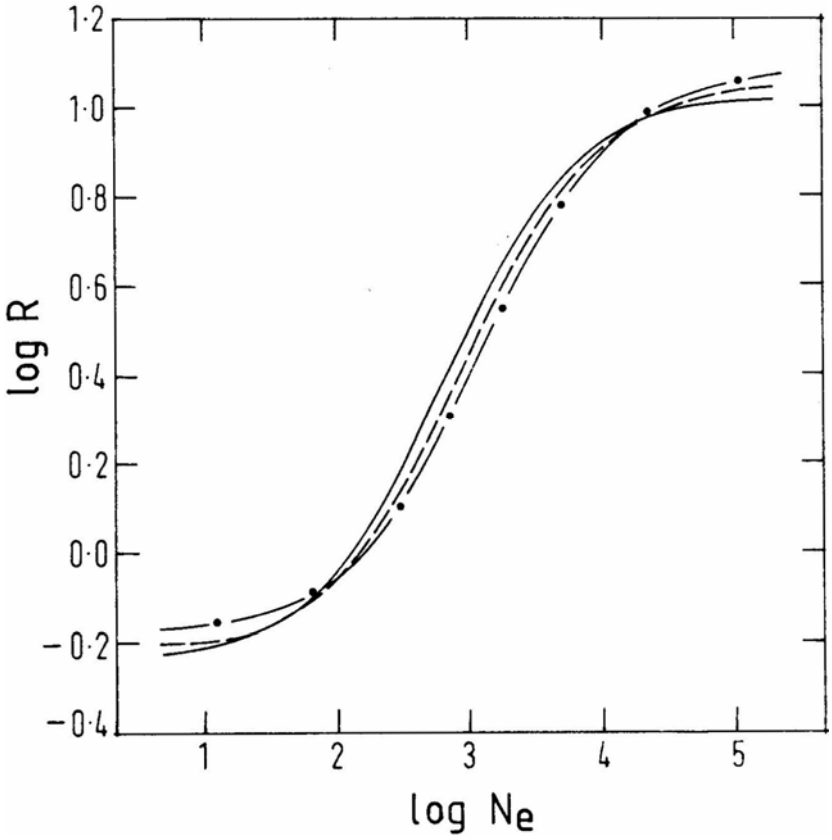

Figure 1. The theoretical O III emission line ratio $R = I(2s^2 2p^{23}P_2 - 2s^2 2p^{23}\ P_1)\ /\ I(2s^2 2p^{2\ 3}P_1 - 2s^2 2p^{2\ 3}P_0) = I(52\ \mu\text{m})/I(88\ \mu m)$, where I is in energy units, plotted as a function of electron density at electron temperatures of 5000 K (*solid line*), 10000 K (*dashed line*) and 20000 K (*dash-dot line*).

Table 1. The theoretical OIII emission line ratio $R = I(52\ \mu\text{m})/I(88\ \mu\text{m})$, where I is in energy units.

	T_e(K)		
$\log N_e$	5000	10000	20000
1.0	6.10−1	6.30−1	6.84−1
1.5	6.84−1	6.88−1	7.32−1
2.0	9.13−1	8.69−1	8.80−1
2.5	1.57+0	1.40+0	1.32+0
3.0	3.16+0	2.77+0	2.51+0
3.5	5.82+0	5.32+0	4.94+0
4.0	8.34+0	8.13+0	7.99+0
4.5	9.74+0	9.88+0	1.01+1
5.0	1.03+1	1.06+1	1.10+1

$A \pm B$ implies $A \times 10^{\pm B}$

Table 2. Observed values of the emission line ratio R = I(52 μm)/I(88 μm) in planetary nebulae (taken from Dinerstein, Lester & Werner 1985) and the derived electron densities.

Planetary nebula	T_e K	log R	log $N_e(R)$	log N_e(Cl III, Ar IV)
NGC 2440	13500[a]	0.55	3.2	3.5[c]
NGC 3242	11300[b]	0.43	3.0	3.2[d]
NGC 6543	8100[b]	0.90	3.9	3.9[e]
NGC 6826	11200[b]	0.58	3.2	3.4[f]

[a] from Keenan & Aggarwal (1987)
[b] from Kaler (1986)
[c] observational data from Shields *et al.,* (1981)
[d] observational data from Barker (1978)
[e] observational data from Saraph & Seaton(1970)
[f] observational data from Aller & Czyzak (1983)

(KAO) in conjunction with a Fabry-Perot spectrometer. These observations are summarized in Table 2, along with the electron temperatures of the O III emitting regions in the nebulae, and the electron densities derived from R. Also listed in the table are the average values of log N_e estimated from line ratios in ions that have similar ionization potentials and spatial distributions to OIII, namely Cl III I(5518Å)/I(5538Å) and Ar IV I(4711Å)/I(4740Å). The sources of the Cl III and Ar IV observational data are given in the footnotes to the table. However the line ratio calculations used for these ions are those discussed by De Robertis, Dufour & Hunt (1987), as these employ the most accurate atomic physics data currently available.

We should point out that Keenan & Aggarwal (1987) found log N_e = 4.1 for NGC 2440 from the O III line ratio R_2 = $I(2s2p^3\ ^5S - 2s^22p^2\ ^3P_{1,2})/I(2s^22p^2\ ^1D - 2s^22p^2\ ^3P_{1,2})$ = I(1661Å + 1667Å)/I(4960Å + 5009Å), which is approximately a factor of 8 larger than log $N_e(R)$ in Table 2. However as the observed value of R_2 in NGC 2440 (R_2 = 0.023, Shields *et al.* 1981) is close to the theoretical low density limit (R_2 = 0.020 for $N_e \leqslant 10^4 cm^{-3}$, Keenan & Aggarwal 1987), the value of log N_e estimated from R_2 is probably unreliable.

An inspection of Table 2 reveals that the densities deduced from R and from CI III and Ar IV are in excellent agreement, with discrepancies of typically less than 0.2 dex. This provides observational support for the accuracy of the atomic data adopted in the present analysis, and also for the methods employed to derive the theoretical line strengths.

Acknowledgements

We would like to thank Professor H. B. Gilbody for his continued interest in this work, and an anonymous referee for several useful comments on an earlier version of this paper. FPK is grateful to the United Kingdom Science and Engineering Research Council for financial support.

References

Aggarwal, K. M. 1983, *Astrophys. J. SuppL.*, **52,** 387.
Aggarwal, K. M. 1985, *Astron. Astrophys.*, **146,** 149.
Aggarwal, K. M., Baluja, K. L., Tully, J. A. 1982, *Mon. Not. R. Astr. Soc.*, **201,** 923.
Aller, L. H., Czyzak, S. J. 1983, *Astrophys. J. Suppl.*, **51,** 211.
Aller, L. H., Keyes, C. D. 1987, *Astrophys. J. Suppl.*, **65,** 403.
Barker, T. 1978, *Astrophys. J.*, **219,** 914.
Barlow, M. J. 1987, *Mon. Not. R. Astr. Soc.*, **227,** 161.
Basri, G. S., Linsky, J. L., Eriksson, K. 1981, *Astrophys. J.*, **251,** 162.
Berrington, K. A., Burke, P. G., Le Dourneuf, M., Robb, W. D., Taylor, K. T., Lan, V. K. 1978, *Comp. Phys. Comm.*,**14,** 367.
Burke, P. G., Robb, W. D. 1975, *Adv. At. Mol. Phys.*, **11,** 143.
Davé, J. H., Feldman, U., Seely, J. F., Wouters, A., Suckewer, S., Hinnov, E., Schwob, J. L. 1987, *J. Opt. Soc. Am.*, **B4,** 635.
De Robertis, M. M. 1987, *Astrophys. J.*, **316,** 597.
De Robertis, M. M., Dufour, R. J., Hunt, R. W. 1987, *J. R. Astr. Soc. Canada,* **81,** 195.
Dinerstein, H. L., Lester, D. F., Werner, M. W. 1985, *Astrophys. J.*, **291,** 561.
Dufton, P. L. 1977, *Comp. Phys. Comm.*, **13,** 25.
Dufton, P. L., Berrington, K. A., Burke, P. G., Kingston, A. E. 1978, *Astr. Astrophys.*, **62,** 111.
Dufton, P. L., Kingston, A. E. 1981, *Adv. At. Mol. Phys.*, **17,** 355.
Evans, I. N., Dopita, M. A. 1985, *Astrophys. J. Suppl.*, **58,** 125.
Filippenko, A. V. 1985, *Astrophys. J.*, **289,** 475.
Froese Fischer, C., Saha, H. P. 1985, *Phys. Scripta*, **32,** 181.
Kaier, J. B., 1986, *Astrophys. J.*, **308,** 322.
Keenan, F. P., Aggarwal, K. M. 1987, *Astrophys. J.*, **319,** 403.
Keenan, F. P., Aggarwal, K. M., Berrington, K. A. 1988, *J. Phys.*, **B21,** L89.
Keenan, F. P., Aggarwal, K. M., Berrington, K. A., Widing, K. G. 1988a, *Astrophys. J.,* **327,** 473.
Keenan, F. P., Dufton, P. L., Aggarwal, K. M., Kingston, A. E. 1988b, *Astrophys. J.*, **324,** 1068.
Keenan, F. P., Kingston, A. E., Aggarwal, K. M., Widing, K. G. 1986, *Solar Phys.*, **103,** 225.
Keenan, F. P., Reid, R. H. G. 1987, *J. Phys.*, **B20,** L753.
Lester, D. F., Dinerstein, H. L. Werner, M. W., Watson, D. M., Genzel, R. L., Storey, J. W. V. 1987,*Astrophys. J.*,**320,** 573.
Moore, C. E. 1971, *Atomic Energy Levels*, NSRDS-NBS 35.
Rubin, R. H., Simpson, J. P., Erickson, E. F., Haas, M. R. 1988, *Astrophys. J.*, **327,** 377.
Saraph, H. E., Seaton, M. J. 1970, *Mon. Not. R. Astr. Soc.*, **148,** 367.
Seaton, M. J. 1964, *Mon. Not. R. Astr. Soc.*, **127,** 191.
Shields, G. A., Aller, L. H., Keyes, C. D., Czyzak, S. J. 1981, *Astrophys. J.*, **248,** 569.
Stratton, B. C., Moos, H. W., Suckewer, S, Feldman, U., Seely, J. F., Bhatia, A. K. 1987, *Phys. Rev.*, **A31,** 2534.
Watson, D. M., Storey, J. W. V., Townes, C. H., Haller, E. E. 1981, *Astrophys. J.*, **250,** 605.
Widing, K. G., Feldman, U., Bhatia, A. K. 1986, *Astrophys. J.*, **308,** 982.

J. Astrophys. Astr. (1988) **9,** 243–248

On the Damping of the Bending Waves in Saturn's Ring

Sandip K. Chakrabarti* *International Center of Theoretical Physics, Trieste, Italy* and *Theoretical Astrophysics, California Institute of Technology, Pasadena, USA*

Received 1988 August 26; accepted 1988 November 21

Abstract. We study numerically the motion of a single particle in the bending wave of finite thickness in Saturn's ring. We include the forcing due to the planet, a moon, the coriolis force and the self gravity of the ring. In particular, we compute the variation of the velocity arising due to the variation of the amplitude and the phase of the epicyclic motion across the local vertical height of the ring. We suggest that the dissipation of energy due to the collision of ring particles in this shear layer damps out the bending wave of Saturn's ring at the 5:3 vertical resonance of Mimas within a distance of 150 km from the site of its launching as is observed in Voyager data.

Key words: planetary rings, Saturn

Recently, through the analysis of the Voyager data it is discovered that the particulate Saturn's rings show varieties of the collective effects such as the spiral density waves and the spiral bending waves (Smith *et al.* 1981; Cuzzi, Lissauer & Shu 1981; Lane *et al.* 1982; Holberg, Forrester & Lissauer 1982; Shu, Cuzzi & Lissauer 1983; Shu 1984; Gresh *et al.* 1986). Spiral bending waves in Saturn's ring launched at the inner vertical resonance propagate radially inwards and the spiral density waves launched at the inner horizontal resonance propagate radially outwards (Shu 1984). In the case of the 5:3 vertical resonance of Mimas, the wave amplitude at the launch is about 1 km and within a distance of about 150 km from the site of the launching, the wave is almost completely damped.

In this paper, we provide an explanation for the rapid attenuation of the bending wave. We show that there is a significant variation of the radial component of the velocity across the vertical height of the ring. The energy of such a shearing motion is dissipated through collisions. Since the collisional frequency is about twice per orbit, the particle picture may be more suitable. Furthermore, the frequencies of the different forces acting on the particle being incommensurate, the particle trajectories in the phase space is expected to be ergodic, and therefore the time averaged behaviour of a single particle should be similar to the instantaneous behaviour of the whole disc. The analysis of the damping length is done in two parts: in the first part we study the motion of a single particle in the warped self-gravitating ring of finite thickness by numerically integrating the equations of motion of the particle. This provides a

* Present address: Theoretical Astrophysics, Tata Institute of Fundamental Research, Homi Bhabha Road, Colaba, Bombay 400005.

reasonable estimate for the vertical shear component σ_{xz}. In the second part we estimate the kinematic viscosity coefficient ν_k by using the amplitude of the epicyclic motion. Using this we calculate the damping length of the bending wave. Although, the work is applied to the problem of Saturn's ring, as far as the mathematical part goes, it is completely general, and therefore can have much broader application. Details will be discussed elsewhere (Chakrabarti 1989).

We choose a right-handed Cartesian coordinate system (X, Y, Z) at a radial distance r from the centre of the planet (See Fig. 1). The X axis points radially outwards, the Y axis points toward the azimuthal direction, and the Z axis points vertically upwards, normal to the equatorial plane of the planet. The frame is rotating around the planet with the local Keplerian velocity $\Omega(r)$. The frame is also oscillating vertically with an amplitude ε and frequency ω, the frequency of perturbation due to the moon as seen from the rotating frame. In general, the frequency n at which the perturbation is launched at the inner vertical resonance as seen from the inertial frame is given by (Shu, Cuzzi & Lissauer 1983),

$$n = m\Omega_{\rm M} \pm \eta\mu_{\rm M} \pm p\kappa_{\rm M}. \tag{1}$$

Here, $\Omega_{\rm M}$ denotes the angular velocity of the moon, $\mu_{\rm M}$ denotes the vertical frequency, $^{K}_{\rm M}$ denotes the epicyclic frequency and m, η and p are integers. At the vertical resonance radius $r_{\rm v}$, one has (Brahic 1977),

$$n - m\Omega(r_{\rm v}) = \pm\mu(r_{\rm v}). \tag{2}$$

Assuming the planet to be spherically symmetric, $\Omega(r) = \mu(r) = k(r)$. In the case of the 5:3 vertical resonance of Mimas, for example, $m = 4$, and $n_{\rm v} = 3\Omega(r_{\rm v}) = 5\Omega_{\rm M}$.The

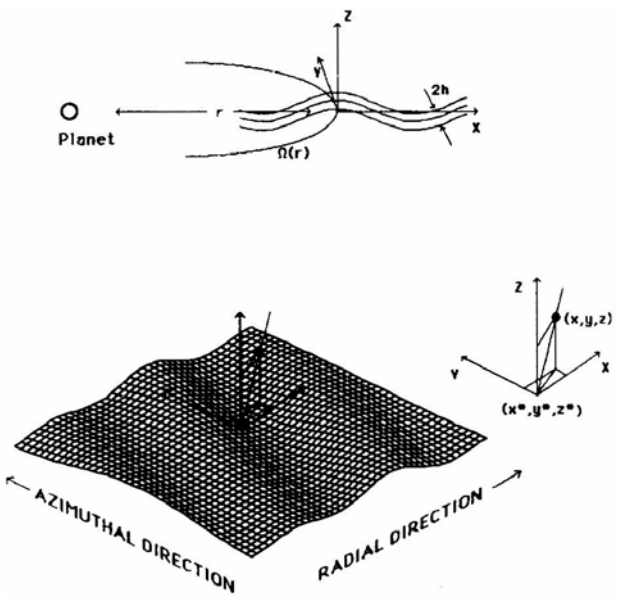

Figure 1. Geometry and coordinates of the problem are schematically shown. Rotating frame (X, Y, Z) also oscillates vertically with frequency ω of the perturbation due to the moon. Equation of the midplane is $z^* = \varepsilon \cos(k_x x^* + K_y y^* \omega t) \cdot (x^*, y^*, z^*)$ is the coordinate on the midplane where the local normal drawn from the particle at (x, y, z) intersects.

perturbation frequency ω as seen from the rotating frame is given by, $\omega = n - 4\Omega(r)$, which is exactly equal to $\Omega(r_V)$ at the vertical resonance. Since the bending wave is launched inwards, the Keplerian frequency $\Omega(r)$ at the radius r that we are considering, is somewhat higher than $\Omega(r_V)$. We let k_x and k_y denote the radial and the azimuthal wave numbers of the perturbation. The midplane of the warped ring is assumed to be of the form,

$$z^* = \varepsilon \cos (k_x x^* + k_y y^* - \omega t). \tag{3}$$

To the zeroth order, this represents the first Fourier component of the bending wave form (see, *e.g.* Shu 1984). By a star ($*$) symbol we denote the coordinates on the midplane of the ring. Denoting the phase of the wave by ϕ^* ($= k_x x^* + k_y y^* - \omega t$) and that of the particle by ϕ ($= k_x x + k_y y - \omega t$) the equations of motion are given by (Chakrabarti 1989),

$$\frac{d^2x}{dt^2} = -2\Omega\frac{dy}{dt} + 3\Omega^2 x - v^2 x_1 - (\Omega^2 - \omega^2)\varepsilon^2\kappa_x \cos\phi \sin\phi^*/(1 + \varepsilon^2\kappa^2 \sin^2\phi^*)^{1/2}, \tag{4a}$$

$$\frac{d^2y}{dt^2} = 2\Omega\frac{dx}{dt} - v^2 y_1 - (\Omega^2 - \omega^2)\varepsilon^2\kappa_y \cos\phi \sin\phi^*/(1 + \varepsilon^2\kappa^2 \sin^2\phi^*)^{1/2}, \tag{4b}$$

and,

$$\frac{d^2z}{dt^2} = -\Omega^2 z - v^2 z_1 + (\Omega^2 - \omega^2)\varepsilon \cos\phi/(1 + \varepsilon^2\kappa^2 \sin^2\phi^*)^{1/2}. \tag{4c}$$

Here x_1, y_1, and z_1 are the projection of the local normal to the ring drawn from the particle position on our local frame of reference. Also, $k^2 = k_x^2 + k_y^2$. The first two terms of Equation (4a) and the first term of Equations (4b) and (4c) are due to the distant planet and the coriolis force. The terms proportional to v^2 are due to the self-gravity effect assumed to be arising due to the flat ring of uniform density ρ, so that $v^2 = 4\pi G\rho$. In the absence of the self-gravity and forcing due to the moon, the solution is given by,

$$y - y_0 = -v_g(t - t_0) - 2A \cos[(t - t_0)\Omega + \psi], \tag{5a}$$

$$x = -\frac{2v_g}{3\Omega} + A \sin[(t - t_0)\Omega + \psi], \tag{5b}$$

and

$$z = h \cos(\Omega t + \zeta). \tag{5c}$$

Here, A is the amplitude of the epicyclic motion, ψ and ζ are arbitrary phases, v_g is the speed of the guiding centre, t_0 is the origin of time for the problem, h is the half thickness of the ring.

Numerical solution of the above equations (4a–c) are obtained by using fourth order Runge-Kutta method. The dynamical timescale in the problem is of the order of 5.0×10^4 s. We take the time step of the integration dt = 1s, and perform the integration up to about 100 orbits. The simulation is carried out for h = 10 metres. The vertical frequencies in this case is μ =1.948 $\times$ 10^{-4}. Eight different initial phases ($\psi = n\pi/4$, $0 \leqslant n$ 7) are used for averaging purposes. Since the local vertical motion is very nearly sinusoidal, ζ of Equation (5c) is always chosen to be 0 so that the particle starts from the midplane in every simulation. Other parameters include: ε = 1 km, $k_x = 5.0\times10^{-6}$, k_y= 3.077 $\times$ 10^{-10} cm^{-1}, σ = 50 g cm^{-2} appropriate for the 5:3 vertical resonance of Mimas. To obtain the variation of the velocity and the shear in the ring, the

configuration space at each phase ϕ^* of the wave in the ring is divided into 729 bins with 9 equal bins along each of the x_1, y_1 and z_1 directions. Such divisions are made at eight phases of the wave centred around $\phi^* = n\pi/4, 0 \leqslant n \leqslant 7$. In each of the 729 zones at each ϕ^*, the peculiar velocity components are calculated from the number of times the particle visited that particular zone and the velocity it carried during each such visit. Such processes are carried out for each of the eight initial intrinsic phases (ψ) of the particle, over which the final average of the velocity is computed assuming each ψ is equally probable. Analytic functions are fit through average velocities as a function of the vertical zone co-ordinates at each phase of the wave, upon differentiating which,

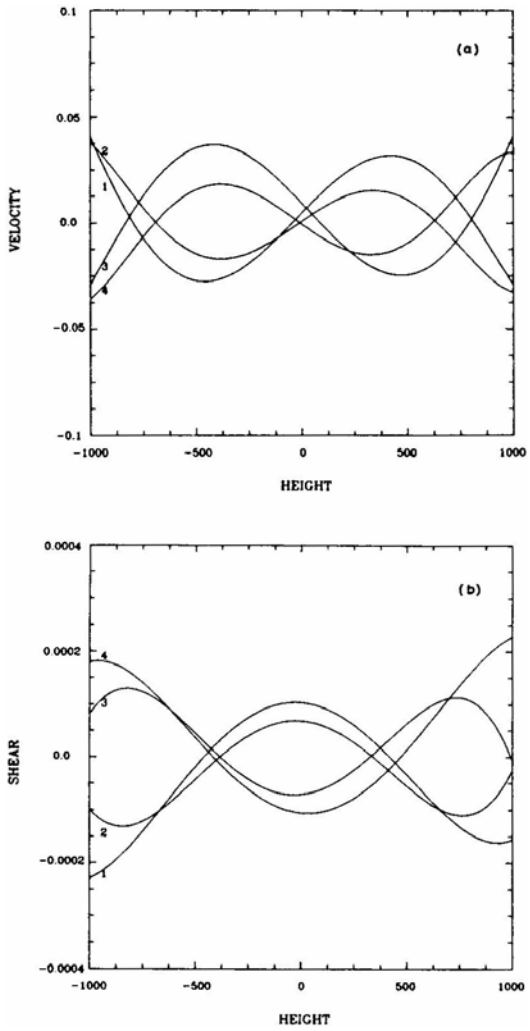

Figure 2. Variation of (a) $\langle v_x \rangle$ and (b) shear component $\partial\langle \upsilon_\chi \rangle/\partial z_1$ as a function of local height as obtained from numerical solution at phases: (1) $\phi^* = 0$, (2) $\phi^* = \pi/4$, (3) $\phi^* = 3\pi/4$, and (4) $\phi^* = \pi$. Half thickness of the ring = 10 m.

the shears are obtained. The analytic functions are found to be very smoothly fitting through the numerical data indicating that random fluctuations are virtually absent The 'shear' in our particle-dynamical model retains the micro-physical definition and is understood to be arising due to the variation of the particle velocities when they are colliding at the same instant of time (*i.e.*, at same phase ϕ^*). The results of our simulation are shown in Fig. 2. Fig. 2a illustrates $\langle v_x \rangle$ in cm s^{-1} as a function of the local height of the ring, and Fig. 2b shows the corresponding values of $\partial\langle v_x\rangle/\partial z_1$ in s^{-1} (the value of $\partial\langle v_x\rangle/\partial x_1$ is very small in our analysis.). The four curves denoted by the numbers 1, 2, 3, and 4 in each of the diagrams are for $\phi^* = 0$, $\pi/4$, $3\pi/4$ and π respectively. The average shear is about 7×10^{-5} s^{-1} (Fig. 2a).

One can do an order of magnitude estimate for the damping length of the bending wave assuming this to be the only source of shear. The energy density of the wave is given by, $\frac{1}{2}\varepsilon^2\Omega^2$ which is about 85 erg g^{-1}. This energy is transferred to the particles through infrequent collisions (about twice per orbit). In the absence of a proper model, we assume that the coefficient of the kinematic viscosity ν_k is roughly given by (Brahic 1977; Goldreich & Tremaine 1978, 1982),

$$\nu_k = \Omega\tau \max(R, R_{\rm epi}), \tag{6}$$

where R is the size of the largest particles (about 5 m for 'A' ring of Saturn) and $R_{\rm epi}$ is the amplitude of the epicyclic motion which is similar to the half thickness of the ring. The coefficient ν_k calculated in this manner probably provides the upper limit. With the optical depth $\tau \simeq 0.5$, one obtains $\nu_k = \Omega\tau h^2 \approx 64 \text{cm}^2\ s^{-1}$ for h =10 m. The rate of dissipation of energy density is $\nu_k(\partial\langle v_x\rangle/\partial z_1)^2$. Substituting the values mentioned above, one obtains the time period for dissipation as 2.6×10^8 seconds. The group velocity is $c_g = -\pi G\sigma/(\omega - 4\Omega) \simeq 0.026$ cm s^{-1}. This provides the damping length $\lambda_d \approx 70$ km—roughly half of the observed length of about 150 km. It is observed that for simulation with higher half thickness shear remains very similar but ν_k goes up reducing the damping length even further. We therefore conclude that, considering uncertainties in ν_k, the total thickness of the disc is no more than 20 metres and probably closer to 15 metres is consistent with the other theoretical considerations that ring could be only tens of metres thick (Goldreich & Tremaine 1982).

Acknowledgements

The author thanks Prof. Peter Goldreich for suggesting the problem and making valuable comments at various stages. This work was supported by NASA grant No. AST 86-15325 and AST 85-19411, and a Tolman Fellowship with Caltech.

References

Brahic, A. 1977, *Astr. Astrophys.*, **54,** 895.
Chakrabarti, S.K.1989, *Mon. Not. R. astr. Soc.* (in press).
Cuzzi, J. N., Lissauer, J. J., Shu, F. H. 1981, *Nature*, **292,** 703.
Goldreich, P., Tremaine, S. 1978, *Icraus*, **34,** 227.

Goldreich, P., Tremaine, S. 1982, *A. Rev. Astr. Astrophys.*, **20,** 249.
Gresh, D. L., Rosen, P. A., Tyler, G. L., Lissauer, J. J. 1986, *Icarus*, **68,** 481.
Holberg, J. B., Forrester, W. T., Lissauer, J. J. 1982, *Nature*, **297,** 115.
Lane, A. L. *et al.* 1982, *Science*, **215,** 537.
Shu, F. H. 1984 in *Planetary Rings*, Eds A. Brahic & R. Greenberg, Univ. Arizona Press, Tucson, p. 513.
Shu, F. H., Cuzzi, J. N., Lissauer, J. J. 1983, *Icarus*, **53,** 185.
Smith, B. A. *et al.* 1981, *Science,* **212,** 163.